THE EFFECT OF PLASTIC DEFORMATION ON THE ELECTRICAL PROPERTIES OF INDIUM ANTIMONIDE

Thesis submitted for the degree of
Doctor of Philosophy
in the University of London

by

Arthur Frank Wesley Willoughby

June, 1965.

Department of Metallurgy,
Imperial College of Science and Technology,
University of London.

Abstract

A study was made of the effect of plastic deformation on the electrical properties of indium antimonide. Single crystal specimens oriented for single slip were plastically bent to introduce an excess of dislocations having either In-atoms at the edge of their extra half-planes (In-dislocations) or having Sb-atoms there (Sb-dislocations).

Plastic bending at a constant strain rate was characterised by a sharp yield point followed by a region of constant stress where single slip predominated. The lower yield stress for bending at 270° C was dependent on the direction of bend, being greater when specimens were bent to produce an excess of Sb-dislocations than when they were bent to produce an excess of In-dislocations. This may be due either to the glide mobility of In-dislocations being greater than that of Sb-dislocations, or to the more rapid climb of the former.

The reliability of etching reagents in revealing dislocations as etch-pits was tested by a series of bending and annealing experiments. It was shown that one type of etchant attacks In-dislocations preferentially. Another etchant was found to give a reliable estimate of the total density of dislocations present.

The electrical properties of dislocations were investigated by Hall coefficient and electrical conductivity measurements on bent samples. It was found that both In- and Sb-dislocations act as acceptor centres in n-type material. The conductivity of bent samples was highly anisotropic indicating that the dislocations were lying predominantly parallel to the bend axis. The results were analysed in terms of two models, and, in each case, an energy level in the forbidden gap was assigned to each type of dislocation.

CONTENTS

Page No.

Page No.

Page No.

CHAPTER 1.

INTRODUCTION.

The industrial applications of indium antimonide, for example in infra-red detectors and Hall effect devices, render it a very important electronic material. For Hall effect devices an important feature is its extremely high electron mobility which, in samples with low impurity concentrations, is about 70,000 cm^2/volt sec at room temperature and about 500,000 cm^2/volt sec at $80^{\circ}K$. It is therefore important to have under control all those factors which influence this mobility. The effects of impurities are well understood and purification techniques have been developed which have reduced the concentration of electrically active impurities to very low levels. The importance of crystal defects is not nearly so well understood although preliminary experiments have indicated that dislocations are very effective in reducing the mobility.

In semiconductors, dislocations influence not only the mobility of the current carriers, but also the number of current carriers. From this viewpoint, indium antimonide presents some interesting possibilities since the carrier-trapping properties of an edge dislocation with indium atoms at the edge of its extra half plane (an 'In-dislocation') are expected to be different from

those of a dislocation with Sb-atoms at the edge of its extra half-plane (an 'Sb-dislocation'). Highly perfect crystals of indium antimonide are available, and thus a study of the electrical effects of plastic deformation should not be unduly complicated by the presence of impurities and grown-in dislocations.

In order to introduce an excess of In- or Sb-dislocations, high temperature plastic bending was adopted as the method of deformation. Although etchants have been developed which can reveal dislocations as surface pits it was not known whether all the dislocations could be revealed in this way. Furthermore, there was a possibility that some etchants revealed In-dislocations but not Sb-dislocations. In order to investigate the reliability of certain etchants in revealing dislocations a series of bending and annealing experiments was carried out. The etch-pit densities were then compared directly with the theoretical dislocation densities calculated from the radii of bend.

The major part of the work, however, was concerned with the electrical effects of plastic deformation. In the first series of experiments, specimens which had been deformed by R. Latkowski by a three-point bending technique, were measured electrically. This series of experiments yielded interesting qualitative results about the effects of bending, but measurements were limited

because of the non-uniformity of samples. In order to produce uniform specimens, four-point bending was adopted. These results were analysed in detail in terms of two models and, in each case, an energy level in the forbidden gap was assigned to each type of dislocation. It was found that the electrical properties of In-dislocations are different from those of Sb-dislocations in n-type material. The plastic bending experiments indicated that In-dislocations and Sb-dislocations have different dynamical properties also.

The results presented here enable one to assess the extent to which dislocations can limit the electron mobility in indium antimonide. For instance, the maximum dislocation density which can be present without significantly reducing the electron mobility in n-type material at 80^{o}K is estimated as $5 \times 10^{5}/cm^{2}$ for a sample of extrinsic carrier concentration $\sim 10^{14}$ cm^{-3}.

The thesis is divided into two parts. Part I contains a review of previous work and Part II contains an account of the present experimental programme, the results and discussion. The extent of Part I is mainly due to the long Chapter 4, which deals with the electrical properties of dislocations in germanium. However, the material contained there is of extreme importance to the present work, and for this reason it was felt necessary

to treat it in some detail. Chapter 4 contains some original contributions by the author, viz., alternative analyses of results obtained by previous workers, and these too have contributed to the length of the chapter.

PART I

REVIEW OF LITERATURE.

The following literature review is divided into four chapters. Chapter 2 is concerned with the structure of dislocations, their movement during plastic bending, and with etching techniques to reveal them. In Chapter 3 a summary of the electrical properties of undeformed indium antimonide is given. Chapters 4 and 5 deal with the electrical properties of dislocations in semiconductors, Chapter 4 being concerned with germanium and Chapter 5 with indium antimonide.

CHAPTER 2.

DISLOCATIONS IN SEMICONDUCTORS.

2.1. Geometrical properties of dislocations in the diamond and sphalerite structure.

The semiconducting compound indium antimonide crystallises in the sphalerite structure, which is similar to the diamond cubic structure (of group IV semiconductors) except that it has In and Sb atoms on alternate sites. The diamond lattice can be visualised as two interpenetrating face centred cubic lattices with origins at (0, 0, 0) and $(\frac{1}{4}, \frac{1}{4}, \frac{1}{4})$. The sphalerite structure can also be visualised in this way but the face centred cubic lattice with origin at (0, 0, 0) is composed of a different type of atom from that with origin at $(\frac{1}{4}, \frac{1}{4}, \frac{1}{4})$. The glide plane and glide direction in germanium, silicon and indium antimonide have been identified as $\{111\}$ and $\langle 110 \rangle$ respectively.

Fig.2.1(a) illustrates the diamond lattice as a series of (111) planes with alternate large and small spacings between them. Slip most probably occurs between the widely spaced pairs of (111) planes, i.e. between planes A and α, not α and B. This type of slip is favoured both by the larger interplanar spacing and by the breakage of bonds (slip between planes A and α will

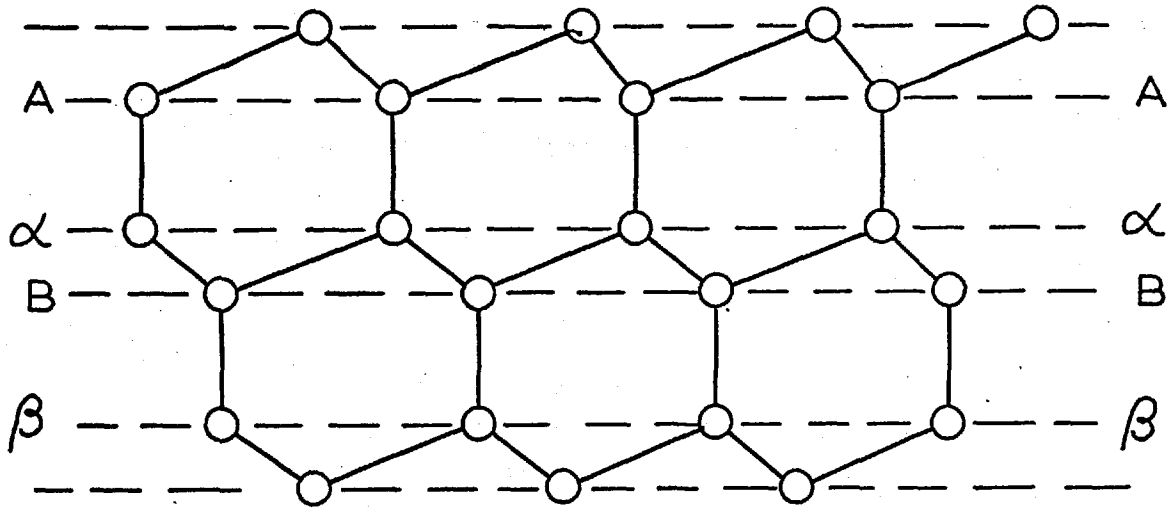

FIG. 2.1.(a) Projection of diamond structure on (1$\bar{1}$0) plane. A, α, B and β, mark the traces of (111) planes.

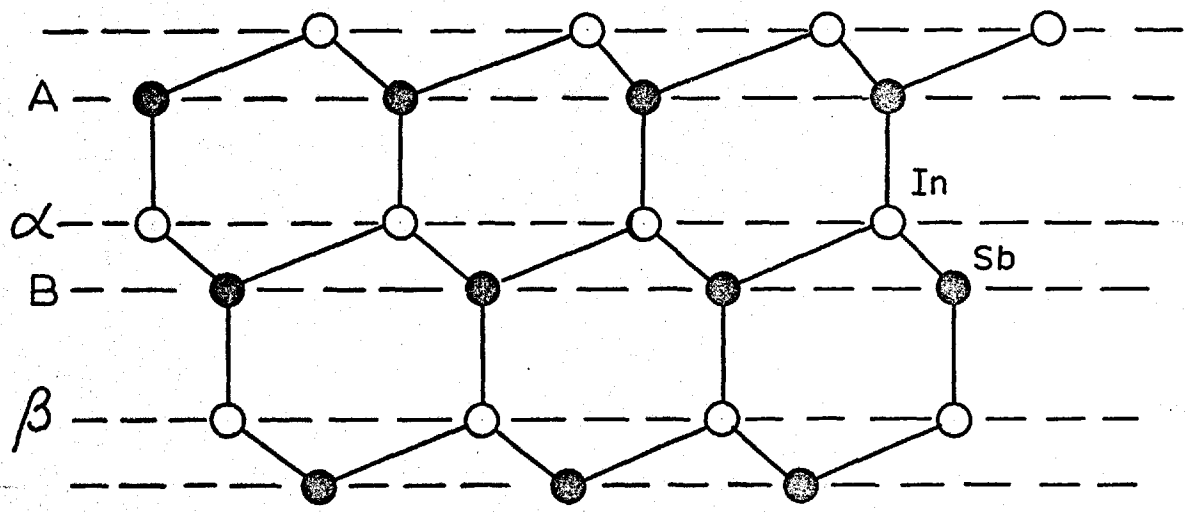

FIG. 2.1.(b) Projection of In Sb structure on (1$\bar{1}$0) plane. A, α, B and β, mark the traces of (111) planes.

break one third as many bonds as slip between α and B). Hornstra (1958) has discussed possible dislocation core structures in the diamond lattice. For slip between the widely spaced (111) planes the simplest dislocation is the "60° dislocation" shown in Fig.2.2(a). This dislocation runs in the $[0\bar{1}\bar{1}]$ direction in the $(\bar{1}\bar{1}1)$ plane, and the Burgers Vector, $^1/_2a\ [\bar{1}10]$, is at 60° to the line direction. The atoms at the edge of the extra half-plane have free or 'dangling' bonds as there are no neighbouring atoms in the plane above. Hornstra found that all slip dislocations with an edge component required 'dangling bonds'. Screw dislocations, however, could be drawn in two forms, neither of which required 'dangling bonds'.

In the sphalerite structure the $\{111\}$ sheets are occupied alternately by group III and group V atoms as shown in Fig.2.1(b). Because of the polar nature of this structure, positive and negative edge dislocations will have different core structures. Considering slip between planes A and α in Fig.2.1(b), we will define a positive edge dislocation as that formed by inserting an extra half-plane from <u>above</u> the slip plane. Thus a positive edge dislocation will have a row of Sb atoms at the edge of its extra half-plane, and a negative edge dislocation will have a row of In atoms there. We will refer to

(a)

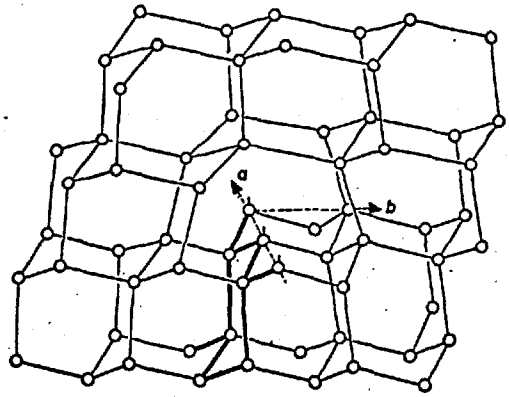

(b)

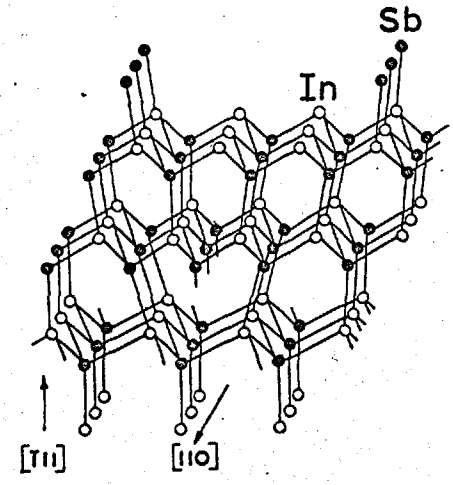

(c)

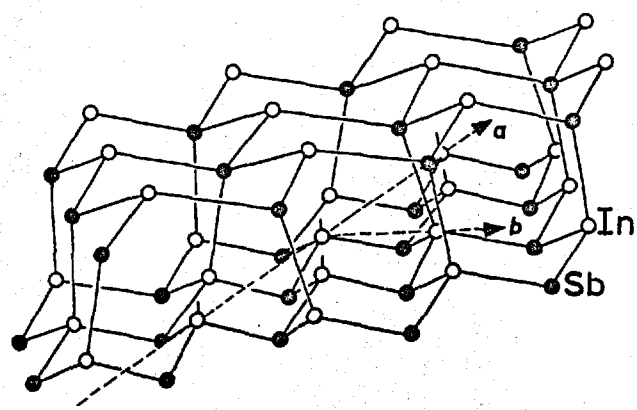

FIG. 2.2. Dislocations lying in the {111} slip plane

these as Sb-dislocations and In-dislocations respectively. Fig.2.2(b) shows an Sb-dislocation corresponding to the 60° dislocation in the diamond lattice. Holt (1962) has shown that most simple dislocations in the sphalerite structure can be envisaged in two forms. For example, the pure edge dislocation which runs in the <112> direction (perpendicular to the <110> slip vector) is shown in Fig.2.2(c).with a double row of In atoms at the edge of its two extra half-planes. The dislocation of similar character but opposite sign would have a double row of Sb atoms there. Holt also drew the core structure of screw dislocations lying in the <110> direction. When the Burgers vector is parallel to the positive line direction the screw is right-handed and Holt found that the minimum Burgers circuit had only one step with a component antiparallel to the Burgers vector. This step could occur either in the sequence In→Sb or Sb→In. and hence there are two types of right-handed screw dislocation. Similarly the minimum Burgers circuit round a left handed screw had only one step with a component antiparallel to the Burgers vector and this could occur in two sequences giving rise to two types of left-handed screw dislocations. Holt found that none of these screw dislocations required 'dangling bonds'.

Hornstra (1958) and Holt (1962) emphasised that the dislocations in Fig.2.2 are not necessarily the

lowest energy structures. They suggested that, in all the dislocations, rearrangements of the bonds were possible if these would lower the energy. Bond rearrangements which eliminated broken bonds could be envisaged, and in the case of certain types of dislocation, the number of broken bonds could be reduced by diffusion of atoms away from the core. As will be discussed in Chapter 4, measurements of the electrical properties of dislocations in germanium provide some indication that all the broken bonds in their cores have not been eliminated by rearrangement.

A second type of process which may lower the energy of dislocations is dissociation. Hornstra showed that it was possible for a 60^{o} dislocation to split into two partial dislocations separated by a stacking fault. Aerts, Delavignette, Siems and Amelinkx (1962) examined hexagonal networks of dislocations in silicon by transmission electron microscopy and reported that the dislocations were separated into partials. The stacking fault energy measured from the geometry of the extended nodes was about 50 ergs/cm^2. Later, Art, Aerts, Delavignette and Amelinckx (1963) reported extended nodes in germanium and gave the stacking fault energy as about 90 ergs/cm^2. From similar measurements Siethoff and Alexander (1964) obtained stacking fault energy values of 66 ergs/cm^2 for germanium, and 31 ergs/cm^2 for indium antimonide. Recently, however, the experiments of

Booker (private communication) have thrown doubt on the interpretations of Aerts et al., Art et al. and Siethoff and Alexander, and Booker's results indicate no dissociation of dislocations in silicon.

Summarising, there is a possibility that bond rearrangement could occur in the simple dislocation core structures drawn by Hornstra (1958) and Holt (1962), but there is no evidence at present to suggest that dissociation occurs.

2.2. Plastic deformation of semiconductors.

The semiconductors germanium, silicon, and indium antimonide have the same slip systems as the face centred cubic metals. However, there are considerable differences in their plastic behaviour. Materials with the diamond and sphalerite structure are very brittle at room temperature but become plastic above a temperature T_1, where in general

$$T_1/T_m \simeq 0.45 - 0.65$$

if T_m is the melting point. Alexander (1961) carried out constant strain-rate tensile tests on germanium single crystals and showed that, after a large yield drop, the stress-strain curve shows three stages of work-hardening rather similar to those of face centred cubic metals.

The yielding phenomenon, which is most unlike that in face centred cubic metals, has been studied extensively and will be discussed in greater detail.

Treuting (1955) and Carreker (1956) noted sharp yield points when deforming germanium specimens in tensile loading. The yield point was not observed on unloading and immediate reloading of the specimen, nor did it return after annealing. Treuting and Carreker suggested that these yield points could be explained in terms of the impurity locking of dislocations, while noting that the yield point did not return after annealing. This theory seemed unsatisfactory since one would expect a recoverable yield point with impurity locking (Cottrell, 1958).

Early experiments employing constant loading were also interpreted in terms of the locking of dislocations by impurities. Gallagher (1952), and subsequently Patel (1956) and Treuting (1955), in constant load tests of germanium, observed a 'delay time' before deformation was detected, which indicated the existence of a yield stress to be overcome by thermal fluctuations. Seitz (1952) associated this delay time with the freeing of edge dislocations locked by impurity atoms. Delay times were also observed in creep of indium antimonide (Allen 1957).

More recent work has indicated that the yield point

in constant strain rate tests, and the delay time in constant load tests, is not due to impurity locking of dislocations but to the multiplication of the originally small number of dislocations. This idea was first suggested by Johnston and Gilman (1959) in connection with the plastic behaviour of lithium fluoride. It is summarised in two equations

$$\bar{v} = \frac{\dot{a}}{\rho b} \qquad \ldots\ldots\ldots\ldots\ldots\ldots \quad (2.1)$$

$\bar{v}$ is the average velocity of ρ mobile dislocations per cm^2 when the glide strain rate is $\dot{a}$. Thus an increase in ρ by dislocation multiplication will produce a reduction in $\bar{v}$ at constant $\dot{a}$. If the relation between the stress and dislocation velocity is of the form

$$\bar{v} \propto s^m \qquad \ldots\ldots\ldots\ldots\ldots\ldots \quad (2.2)$$

then a reduction in $\bar{v}$ will produce a significant drop in stress s, provided m is not too large. The exponent m has been determined for a range of semiconducting materials by the direct measurements of dislocation velocity of Chauduri et al. (1962), and for germanium, silicon, indium antimonide and gallium antimonide the value of m lies between 1.3 and 1.9. This may be contrasted with $m = 44$ for silicon-iron (Stein and Low 1960), and $m = 25$ for LiF (Johnston and Gilman 1959). Thus one important condition for the Johnston-Gilman

yield point is fulfilled in diamond structure materials.

Alexander (1961) explained the large yield points, which he had observed, in terms of this dislocation velocity mechanism. The experiments of Dew-Hughes (1961) also supported the idea of the Johnston-Gilman yield point and his direct measurements of dislocation velocity were in agreement with those of Chauduri et al (1962). Bell and Bonfield (1964) investigated the yielding of germanium single crystals as a function of initial dislocation density, temperature and strain rate. They observed large increases in the dislocation density on yielding (for a typical specimen it increased from 1×10^3 cm^{-2} to 7×10^6 cm^{-2}). This large increase would favour the Johnston-Gilman yield point since, according to (2.1), a large decrease in dislocation velocity would result. Bell and Bonfield noted a critical initial dislocation density above which no yield point was observed. There was a strong dependence of upper yield stress on initial dislocation density and generally the yield point was not recoverable by ageing. All these measurements led to the conclusion that the yield point in germanium is produced by the Johnston-Gilman mechanism rather than by the impurity locking mechanism. Patel and Chauduri (1962) made similar deductions for silicon. When silicon crystals containing oxygen were heated to precipitate the oxygen as a second phase, dislocation loops were created

to accommodate the volume change. These extra dislocations reduced the magnitude of the yield point in a subsequent test. This oxygen effect was thus readily explained in terms of the Johnston-Gilman model of yielding. Subsequently Patel and Chauduri (1963) observed large yield drops in tensile deformation of germanium, silicon, indium antimonide and gallium antimonide and obtained results which indicated that the Johnston-Gilman mechanism is applicable to all these materials.

Chauduri et al. (1962) obtained the following empirical relation between dislocation velocity and stress

$$\bar{v} = B_o \left(s/s_o \right)^m \exp\left(-U/kT \right) \quad \ldots\ldots\ldots\ldots \quad (2.3)$$

Haasen (1957) proposed a model of dislocations in the diamond lattice which predicted an expression for the dislocation velocity similar to (2.3). He suggested that, in the 60° dislocation, certain saturated bonds beneath the edge of the extra half plane could not accommodate the strong distortions occurring there, and an atomic rupture would occur as in Fig.2.3.

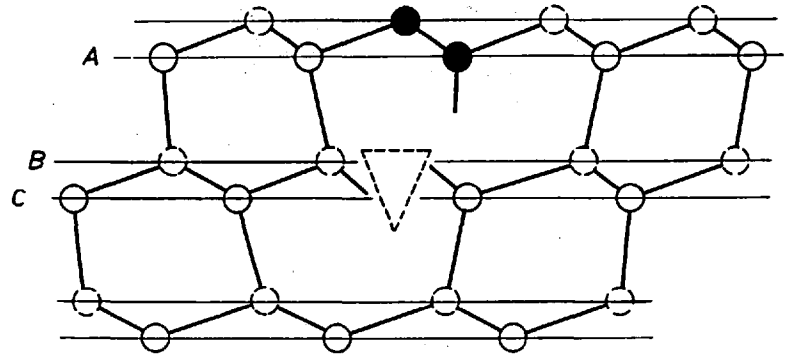

A 60° dislocation in the diamond lattice (schematic). Slip on (111) planes probably occurs between those marked *A* and *B* (not *B* and *C*). The triangle marks the "crack" at the dislocation.

Fig. 2.3.

If this dislocation moves the rupture must diffuse with it, and this led to the following expression for the velocity $\bar{v}$ of the 'cracked' dislocation.

$$\bar{v} = \frac{D}{kT} \cdot F = \frac{D_o}{kT} sb^2 \exp\left(-U/kT\right) \ldots\ldots\ldots (2.4)$$

where s is the shear stress,

$F = sb^2$ is the force on a dislocation of length b,

D is the 'diffusion constant' of the crack,

U is the activation energy for diffusion of the crack.

Equation (2.4) agrees quite well with (2.3) except that the value of the activation energy U obtained by Chauduri et al. is about half that for self-diffusion. The predicted $m = 1$, however, is close to the

experimental m = 1.5 value.

Haasen (1964) has developed a technique which calculates macroscopic plastic properties (such as stress-strain curves for constant strain rate tests, and strain-time curves for constant load tests) from measurements of dislocation velocity and dislocation density. He used the empirical relation (2.3) between dislocation velocity and stress.

In his analysis, Haasen allowed for the work hardening contribution to the stress s. He pointed out that, during yield, the dislocation distribution was very inhomogeneous over the length of a specimen. When a certain limiting dislocation density, ρ, was reached in a particular region dislocation multiplication ceased, and subsequently this region did not contribute to the strain. He wrote the relation between the limiting dislocation density and the stress as

$$s = A\rho^{\frac{1}{2}} \qquad \ldots\ldots\ldots\ldots\ldots\ldots (2.5)$$

which is Taylor's expression for the mean internal stress of a distribution of positive and negative dislocations where $A = \alpha_0 G^* b$ and $\alpha_0 \simeq 0.3$ for germanium (G^* is the shear modulus). Thus this model assumed that dislocation multiplication would stop when the mean internal stress of the dislocations balanced the applied stress. In calculating the total strain rate, therefore, Haasen

left out all the 'dead' regions with $\rho^{\frac{1}{2}} \geqslant s/A$. He introduced an 'effective' stress S_{eff}, where

$$S_{eff} = s - A\rho^{\frac{1}{2}} \quad \ldots\ldots\ldots\ldots\ldots\ldots\ldots\ldots (2.6)$$

Haasen (1964) assumed a mechanism of dislocation multiplication which had been suggested by Alexander (private communication quoted by Haasen (1964)). This mechanism led to an exponential dependence of dislocation density on time. Alexander had concluded from electron transmission microscopy that edge dislocation dipoles, formed at long jogs in screws, constitute potential sources for dislocation multiplication. The partners of a dipole might pass each other and develop into a loop. This led to the relation

$$d\rho = \delta\rho \, v \, dt \quad \ldots\ldots\ldots\ldots\ldots\ldots\ldots\ldots (2.7)$$

where the multiplication constant δ, determined by the process of two edge dislocations passing each other, is proportional to stress and is written

$$\delta = Y \cdot S_{eff} \quad \ldots\ldots\ldots\ldots\ldots\ldots\ldots\ldots (2.8)$$

Now, substituting (2.3), (2.6), (2.7) and (2.8) into (2.1) Haasen obtained the plastic strain rate $\dot{a}_p$

$$\dot{a}_p = b \, B\rho \left(s - A\rho^{\frac{1}{2}}\right)^m$$

where $B = B_o \, s_o^{-m} \exp\left(- U/kT\right)$

Adding the elastic strain rate $\dot{a}_c = \dot{s}/G^*$

he obtained the total strain rate $\dot{a}$

$$\left.\begin{aligned} \dot{a} &= b B \rho \left(s - A\rho^{\frac{1}{2}} \right)^m + \dot{s}/_{G^*} \\ \text{and, from (2.7)} \qquad & \\ \dot{\rho} &= Y B \rho \left(s - A\rho^{\frac{1}{2}} \right)^{m+1} \end{aligned}\right\} \quad (2.9)$$

Solutions of equations (2.9) could then be compared with experimental results. It is obvious that, for a constant strain rate test, (2.9) will predict a yield point since these equations are only an extension of (2.1) and (2.2). For the lower yield stress s_{ly}, Haasen neglected the elastic term $\dot{s}/_{G^*}$ in (2.9) and, using the criterion $ds/_{da} = 0$, he obtained

$$s_{ly} = s_o \left(A^2 C_m/_{b B_o} \right)^{1/(2+m)} \dot{a}^{1/(2+m)} \exp \left\{ \frac{U}{(2+m)kT} \right\} \quad (2.10)$$

where $C_m = \left(1 + \frac{2}{m} \right)^{m+2} \left(\frac{m}{2} \right)^2$

Haasen showed that his experimental values of $s_{ly}(\dot{a}, T)$ for compression of germanium, were best described by (2.10) with $m = 1.1$, $U = 1.64$ e.V. and $\alpha_o = 0.3$. These values are close to those obtained by the dislocation velocity measurements of Chauduri et al. which gave for germanium $U = 1.6$ e.V. and $m \simeq 1.5$. For compression of InSb the results of Schafer, Alexander and Haasen (1964) could also be described by (2.10) with values of m, U and α_o in good agreement with

independently measured values.

Haasen also used equations (2.9) to analyse creep tests. The lower yield stress in a constant strain-rate test corresponds to steady state creep under constant load conditions. The constant creep rate $\dot{a}_w$ follows by inversion of (2.10)

$$\dot{a}_w = \frac{b\,B_o}{A^2\,C_m}\left(\frac{s}{s_o}\right)^{m+2} \exp\left(-U/kT\right) \quad \ldots\ldots (2.11)$$

The values of $\dot{a}_w$ predicted by (2.11) were in good agreement with experimental values for compression of germanium when $U = 1.75$ e.V. and $m \simeq 1.2$ and for bending of InSb when $U = 0.88$ e.V., $m = 1.5$. Thus the main features of both constant strain-rate and creep tests could be calculated from independent measurements of dislocation density and velocity.

Peissker, Haasen and Alexander (1961) applied this analysis to some interesting results obtained for indium antimonide. Specimens oriented for single slip were plastically bent under creep conditions. In order to introduce an excess of either In- or Sb-dislocations, samples were plastically bent in opposite directions (The direction of bending was determined by an etching technique similar to that described in Section 6). The measured values of the constant creep rate $(\dot{a}_w)$ depended on the bending direction and indicated a higher

mobility for In- than for Sb-dislocations. The average values of $\dot{a}_w$ obtained for In- bending were about 1.5 times larger than those for Sb- bending. Peissker et al. deduced that Sb-dislocations are on the average 1.5 times slower than In-dislocations. The measurements of $\dot{a}_w$ could be accommodated by (2.11) if the activation energy U for Sb-bending was 1 - 2% higher than that for In-bending. Peissker et al. suggested, by analogy with Haasen's 'crack-diffusion' model, that this was in agreement with the measurements of the self-diffusion of In and Sb in InSb by Eisen and Birchenall (1957), which gave a higher activation energy for diffusion of Sb than for diffusion of In. However, the relative difference in activation energies for diffusion is greater than for dislocation movement and Peissker et al. suggested that this was due to the motion of minority sign dislocations in the bend test.

From measurements of the dependence of the incubation time on the specimen dimensions, Peissker deduced that dislocation multiplication was not markedly influenced by sources at the surface. The height of the specimens was varied but the breadth and thus the upper and lower surface areas, which presumably would act as sources, was held constant. The incubation time was found to be shorter for thick specimens and Peissker et al.

deduced that dislocation sources must exist in the interior of the crystal.

2.3. Observation of dislocations by the etch-pit technique.

2.3.1. Dislocation distributions in bent crystals - general.

Cahn (1949) first suggested that plastic bending of a single crystal produces an array of edge dislocations which are all of the same sign. Fig.2.4 shows how the curvature can be accommodated by such an array. For a bent crystal with its glide plane parallel to the neutral plane, and glide direction perpendicular to the bend axis, Cahn showed that the density of edge dislocations is given by

$$\rho = \frac{1}{R\,\underline{b}}$$

where R = radius of curvature,

$\underline{b}$ = Burgers Vector.

In any real case plastic bending will produce dislocations of both signs, but there must always be an excess of the one or the other to maintain the curvature of the bent sample. The dislocations which are required to maintain the curvature will be termed the "majority" dislocations and the ones of opposite sign the "minority" dislocations.

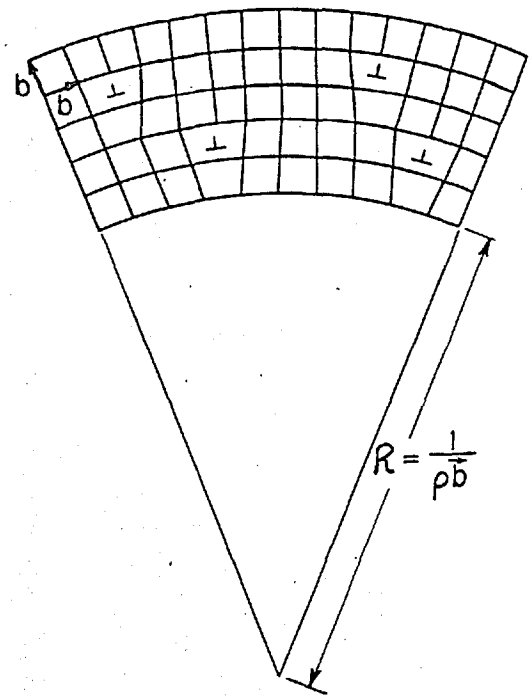

FIG. 2.4

Bending produced in simple cubic lattice by edge dislocations: ρ = density of edge dislocations, R = radius of curvature of slip plane, and $\vec{b}$ = Burgers vector.

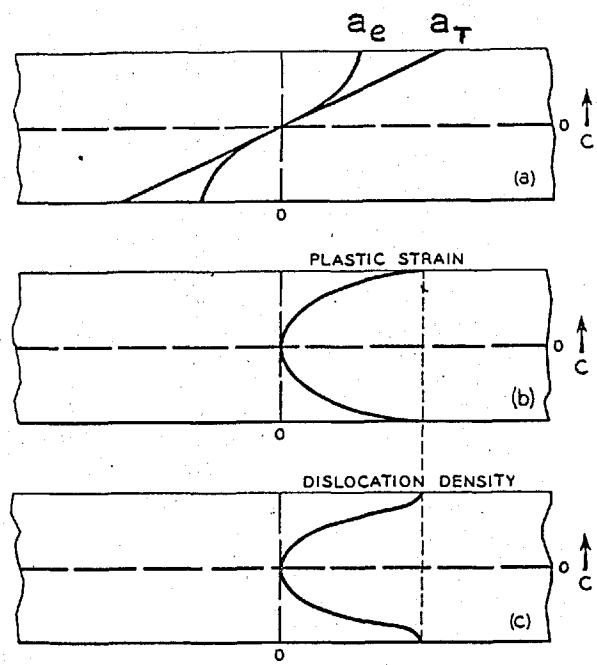

Schematic representation of several parameters in bent crystal beam: a) total strain, a_T and elastic strain, a_e as a function of distance normal to neutral axis, C; b) plastic strain, a_p as a function of distance from neutral axis, C; and c) dislocation density, ρ, as a function of distance from neutral axis, C.

FIG. 2.5

Assuming single glide and the absence of macroscopic elastic stresses, Nye (1953) derived an expression for the excess density of majority dislocations

$$\rho_{MAJ} - \rho_{MIN} = \frac{1}{Rb \cos \omega} \quad \ldots\ldots\ldots\ldots (2.12)$$

which is a general form of Cahn's relation where ω = angle between slip plane and neutral plane. Nye predicted that, for a bar bent to a radius which is large compared with its thickness, the dislocation density should be uniform across the bar.

Vogel (1956) tested (2.12) by bending germanium samples to various radii, annealing to remove macroscopic elastic stresses, and measuring the resulting etch-pit densities. Specimens oriented to favour single slip were bent about a <112> bend axis. After bending, the etch-pit density was very small at the neutral axis but increased towards the upper and lower surfaces. This was explained by Vogel in terms of the stress distribution in a bent bar. The total strain, a_T was assumed to be roughly proportional to the distance from the neutral plane as shown in Fig.2.5(a). (There appears to be no theoretical reason for this assumption). Vogel also estimated the elastic strain a_e as shown in Fig.2.5(a). The difference between these two curves, $a_T - a_e$, is the plastic strain curve, which is shown in Fig.2.5(b).

Assuming the dislocations to be all of the same sign, the plastic strain at any point is proportional to the number of dislocations which have glided through that point. Therefore the slope of the plastic strain curve at a particular point is proportional to the dislocation density there. The dislocation distribution was thus obtained from Fig.2.5(b) by differentiation. This distribution is the same as that observed experimentally by Vogel, but it is evident that the theory is qualitative and only gives a general picture of the dislocation distribution. A quantitative treatment would require accurate estimates of a_T and a_e and would be a more complex problem.

Average etch-pit densities in the bent bars were consistently higher than the dislocation densities predicted from (2.12). This discrepancy was attributed to the presence of dislocations of the minority sign trapped inside the crystal but, since the specimens had not been annealed to remove macroscopic elastic stresses, one would not expect (2.12) to hold. Vogel suggested that, at the earliest stage of bending, dislocation sources at the surface of the beam operate because the stress is greatest there. As the material at the outside deforms, sources further in become active when their critical stresses are exceeded. Minority sign dislocations nearer the neutral axis have greater distances to

travel and are more likely to be trapped in the bar.

After annealing, the distribution of etch-pits became uniform across the bar, presumably by dislocation migration from the high density outside regions to the low density neutral axis region. Also the pits became aligned into walls perpendicular to the slip plane, a process which is known as 'polygonisation' (Cahn, 1949). Furthermore, the average etch-pit densities of the bent crystals were reduced to values which were in good agreement with those predicted by (2.12) from the bend radius. Vogel suggested that this reduction occurred by annihilation of dislocations of opposite sign until only those of the majority sign remained.

Vogel proposed a mechanism of plastic bending which would produce an array of edge dislocations of one sign. When a bending couple is applied to a single crystal bar a critical stress is reached for the operation of dislocation sources. Fig.2.6(a) shows two sources, one above and one below the neutral plane, which have emitted dislocation rings such as a and b. Each ring expands under the applied stress, the screw orientations of both signs moving to the surfaces of the bar where they are rejected. Now when a crystal is bent the shear stress on a given slip plane is opposite in sense on opposite sides of the neutral plane. Thus, like sign

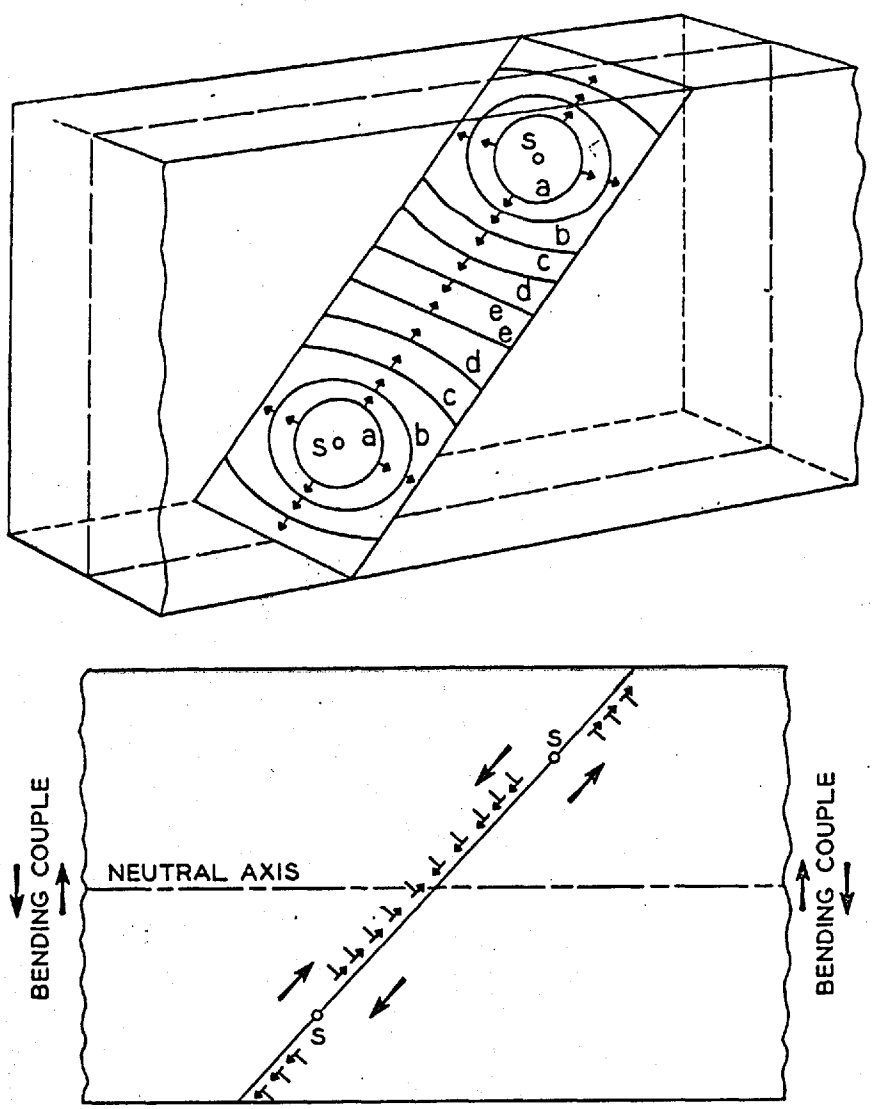

Formation of excess edge dislocations on bending by expansion of dislocation rings and rejection of certain orientations: a) slip plane is shown in perspective; b) section cutting dislocation rings is shown in edge orientation. Lettering in diagram, *a*, *b*, *c*, etc., represents successive positions of dislocations coming from source, *S*.

FIG. 2.6.

dislocations on opposite sides of the neutral plane will be moved in opposite directions. Therefore, as shown in Fig.2.6(b), edge segments of one sign from the two sources will move to the surface, while edge segments of the opposite sign (from both sources) will move inwards towards the neutral axis until the stress can no longer support their motion. Thus, an excess of edge dislocations of the sign which accommodates the bending can be produced.

The application of (2.12) has also been tested in silver single crystals by Hendrickson and Machlin (1955), in silicon-iron by Hibbard and Dunn (1956) and in silicon by Patel (1958). In each case the etch-pit densities in bent - and - annealed samples were in agreement with the dislocation densities predicted by (2.12) from the bend radii. This verification appears to be good statistical proof that the etch-pits occur at individual edge dislocations. In these materials (germanium, silicon, silicon-iron and silver) the average etch-pit density of the as-bent samples (before annealing) was about two or three times higher than the calculated dislocation density. The distribution of etch-pits in the as-bent germanium samples of Vogel, however, was very different from that observed by Patel in as-bent silicon samples. Fig.2.7 shows the etch-pit density as a function of the distance from the neutral axis for a silicon and a

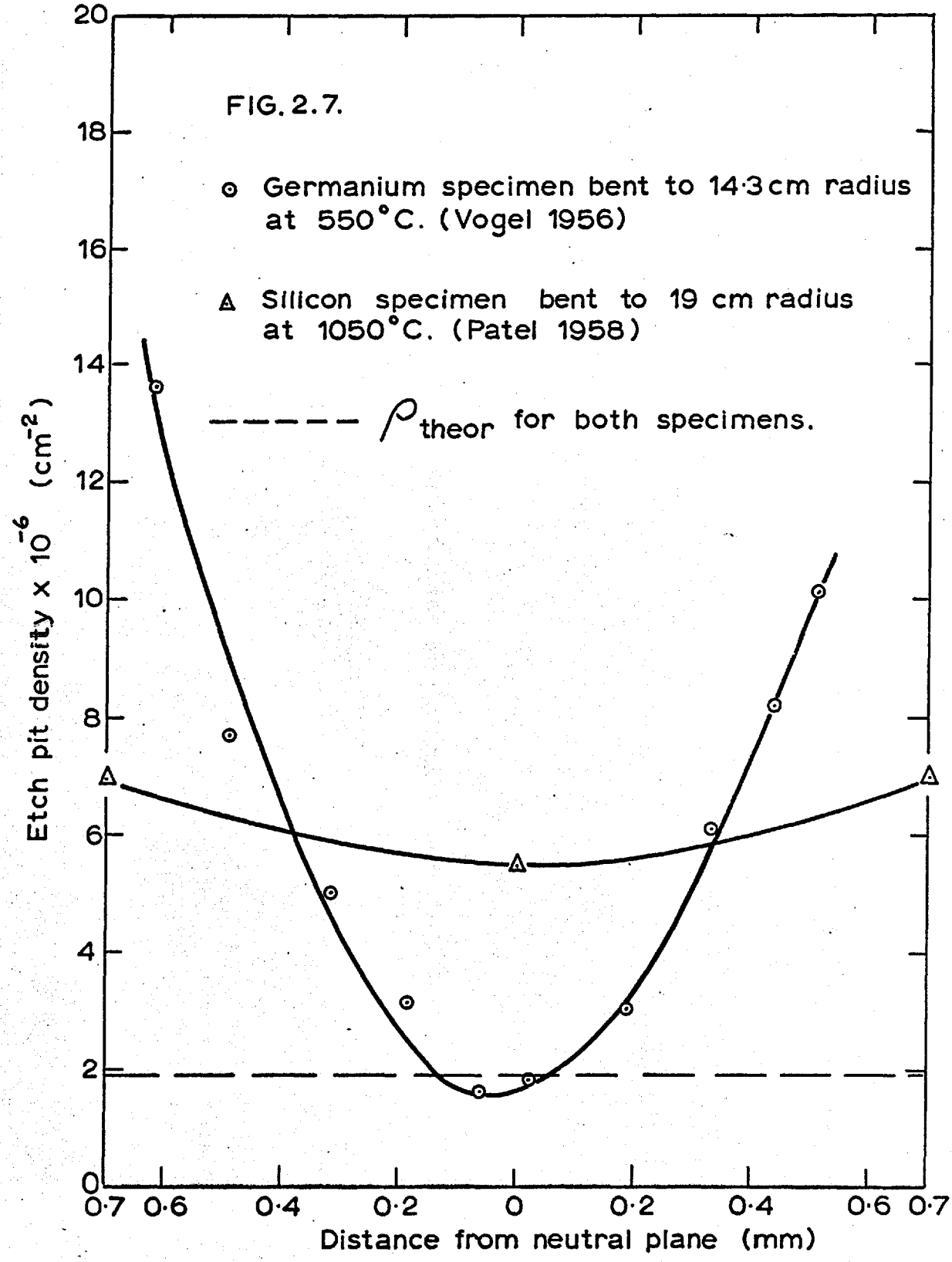
FIG. 2.7.
⊙ Germanium specimen bent to 14·3 cm radius at 550°C. (Vogel 1956)
△ Silicon specimen bent to 19 cm radius at 1050°C. (Patel 1958)
ρtheor for both specimens.
Etch pit density x 10⁻⁶ (cm⁻²)
0
2
4
6
8
10
12
14
16
18
20
0·7 0·6 0·4 0·2 0 0·2 0·4 0·6 0·7
Distance from neutral plane (mm)

germanium sample bent to radii of 19 cms and 14.3 cms respectively. These radii have been chosen because the dislocation density predicted by (2.12) is 1.9×10^6 cm^{-2} for both samples (the different radii compensating for the different Burgers vectors of germanium and silicon). Fig.2.7 shows that the distribution of etch-pits in the silicon sample is more uniform than in the germanium sample. It is very probable that this difference (which occurred in samples bent to other radii) is due to a difference in the temperatures of deformation, since the silicon sample was deformed at $1050^{\circ}C = 0.77\ T_m$, a relatively higher temperature than that of the germanium sample ($550^{\circ}C = 0.67\ T_m$). Now, the measurements of dislocation velocity by Chauduri et al (1962) indicated that, as the temperature was raised, the dislocation mobility increased very rapidly. Thus at the higher temperature one would expect dislocations to be able to move farther toward the neutral axis in a bent sample and hence produce a more uniform distribution than at the lower temperature.

Livingston (1963) showed that the sign of individual edge dislocations in copper single crystals could be determined by an etch-pitting technique. The application of this technique indicated that 95% of the edge dislocations in bent crystals were of the majority sign, although no quantitative comparison with Nye's relation was made.

Livingston suggested, in accordance with Vogel's deduction for germanium, that in copper nearly all the dislocations were generated at or near the surface and moved in without further multiplication. The multiplication mechanism of double cross slip, which continually creates new dislocations of both signs, was thought not to be important in copper.

The only attempt at a quantitative test of the Nye relation in indium antimonide has been made by Duga (1962). Specimens were bent at 300°C to radii of bend from 15 cms to 200 cms. He found that the etch-pit densities (with an unspecified etchant) of as-bent samples were in good agreement with dislocation densities which he calculated from the Nye relation (2.12). There is some ambiguity concerning the precise orientation of the samples since the only information given is that specimens with bounding planes $\{111\}$, $\{110\}$ and $\{211\}$ were bent about a $\langle 211 \rangle$ axis. If $\{111\}$ were the neutral plane, three $\{111\}$ slip planes would be favourably oriented for slip, while if $\{110\}$ were the neutral plane, two slip planes would be favourably oriented. There is further uncertainty concerning the calculation of the theoretical dislocation density, since the dislocations could not lie parallel to the bend axis and one must make some assumption about their line direction in order to apply the general Nye relation for multiple glide. In view of these ambiguities,

therefore, it is not possible to check Duga's calculation of the theoretical dislocation density. However, the agreement between etch-pit densities and theoretical dislocation densities in the as-bent samples is quite unlike the measurements on silicon and germanium, where the etch-pit densities in as-bent samples were two or three times higher than the theoretical densities, after bending at temperatures which were a similar fraction of the absolute melting temperature. The measurements of Peissker et al. (1961) which indicated that internal sources were important in indium antimonide, suggest the presence of minority sign dislocations in bent samples. Furthermore, Duga's specimens were oriented to favour double or multiple slip and the intersection of slip planes would be expected to result in work-hardening and a high density of dislocations. Therefore, it is probable either that the etch used by Duga did not reveal all the dislocations present, or that the calculation of the theoretical dislocation density was in error.

Patel (1958) presented some direct evidence concerning the orientation of dislocation lines in silicon samples bent in the single slip orientation (as used by Vogel, 1956). Lightly bent samples were 'decorated' with copper and examined by infra-red transmission microscopy which revealed long straight dislocations lying parallel to the $[112]$ bend axis. This observation has important

implications when considering the electrical properties of dislocations in bent samples, as will be discussed in Chapter 4.

Dislocation etching in indium antimonide presents some interesting possibilities which were not envisaged by Duga. These will be discussed more fully in the next section.

2.3.2 Dislocations in indium antimonide.

Bardsley and Bell (1957) observed etch-pits on a $\{111\}$ surface of a single crystal of InSb using CP_4 type etches. The alignment of the pits suggested that they were formed at polygonised walls of dislocations. The geometry of the pit arrangement was consistent with the dislocations being pure edges corresponding to slip on $\{111\}$ in a $\langle 110 \rangle$ direction; the slip system in germanium. Subsequently Bell (1957) examined indium antimonide single crystals by the Guinier-Tennevin x-ray technique. The dislocation densities deduced from line-broadening were in order-of-magnitude agreement with the etch-pit density. A closer comparison was not possible using this technique.

It was noted in section 2.1., that, in the crystallographic structure of indium antimonide, $\langle 111 \rangle$ is not equivalent to $\langle \bar{1}\bar{1}\bar{1} \rangle$. Dewald (1957) found that the kinetics of formation of anodic films on $\{111\}$ and

$\{\bar{1}\bar{1}\bar{1}\}$ surfaces were different and he assigned the index (111) to the face which formed the thicker oxide film under the same conditions. The results could be understood most easily if it were assumed that the (111) face terminated in antimony atoms triply bonded to the lattice, or indium atoms singly bonded to the lattice. Furthermore, it seems reasonable to assume that $\{111\}$ faces terminate with atoms triply bonded to the lattice, since this would minimise the number of broken bonds. Thus it is likely that the (111) face forming the thicker oxide film terminated with antimony atoms.

Allen (1957) stated that his CP_4A etch produced pits on faces of the form $\{\bar{1}\bar{1}\bar{1}\}$ but not on faces of the form $\{111\}$, using Dewald's sign convention for the crystallographic directions. (Strictly, however, Allen could not label the faces in this way unless he had repeated Dewald's experiments on these faces). By successive grinding and etching of the same sample, Allen confirmed that the pits were formed at line imperfections. Experiments on bent bars showed that the etch-pit density was of the same order of magnitude as the dislocation density predicted by (2.12).

Maringer (1958) etched a single crystal sphere with a mixture of lactic and nitric acids. He observed etch-pits on four equivalent octahedral faces but it was

not determined whether these were the four $\{111\}$ or the four $\{\bar{1}\bar{1}\bar{1}\}$ faces as defined by Dewald. The shape of the etch-pits was conical on an octahedral face, but became elongated as the surface departed from this orientation. On the etched sphere two different types of elongation were observed. Allen had previously observed elongated pits on $\{112\}$ faces while Maringer observed pits up to 20° away from the octahedral face. Venables and Broudy (1958) produced etch-pits on a $\{110\}$ surface (35° away from $\{111\}$) with a 1 : 1 mixture of HF and HNO_3. These pits were only observable with dark field microscopy and were elongated in <001> directions. By successive grinding and etching, Venables and Broudy traced dislocations through the crystal, both in as-grown material and in samples which had been bent at 400 - 450°C around a <110> bend axis in an orientation which favoured slip on two slip planes at 55° to the neutral plane. In all cases the dislocations lay in <110> directions. The authors pointed out that it was strange for pits to be elongated when dislocations ran perpendicular to the $\{110\}$ surface, since elongated pits can often be associated with dislocations meeting the surface at a shallow angle. It appears that, in indium antimonide, the elongation of a pit is determined by the crystallographic orientation of the etched plane as well as by the direction of the dislocation line relative to

the surface. By etching a single crystal cylinder, Venables and Broudy confirmed previous observations of the characteristic etching properties of $\{111\}$ planes. However, they observed that pits formed on all $\{110\}$ planes. This is consistent with the sphalerite structure in which the $[110]$ direction is equivalent to the $[\bar{1}\bar{1}0]$ direction. The direction of elongation of the pits on $\{110\}$ surfaces, however, was found to depend on the polarity of the specimen. Pits on opposite $\{110\}$ faces pointed in the same direction, but pits on, say, a (110) plane pointed in an opposite direction to those on a $(1\bar{1}0)$ plane. As the pits pointed in an $[001]$ direction, Venables and Broudy suggested that this experiment distinguished $[001]$ from $[00\bar{1}]$. However, $[001]$ and $[00\bar{1}]$ are crystallographically equivalent directions and it should therefore be impossible to distinguish them. The results can be understood qualitatively with reference to Fig.2.8. The (110) plane is unlike a $(1\bar{1}0)$ plane when viewed along an $[001]$ direction. It therefore seems reasonable that pits point, say, towards $[001]$ in a (110) plane and towards $[00\bar{1}]$ in a $(1\bar{1}0)$ plane.

From observation of slip lines on bent specimens, Venables and Broudy deduced that the slip plane in InSb was $\{111\}$ and they suggested that $\langle 110 \rangle$ was the slip direction, since it is the shortest translation direction. This slip system had previously been suggested by Bardsley

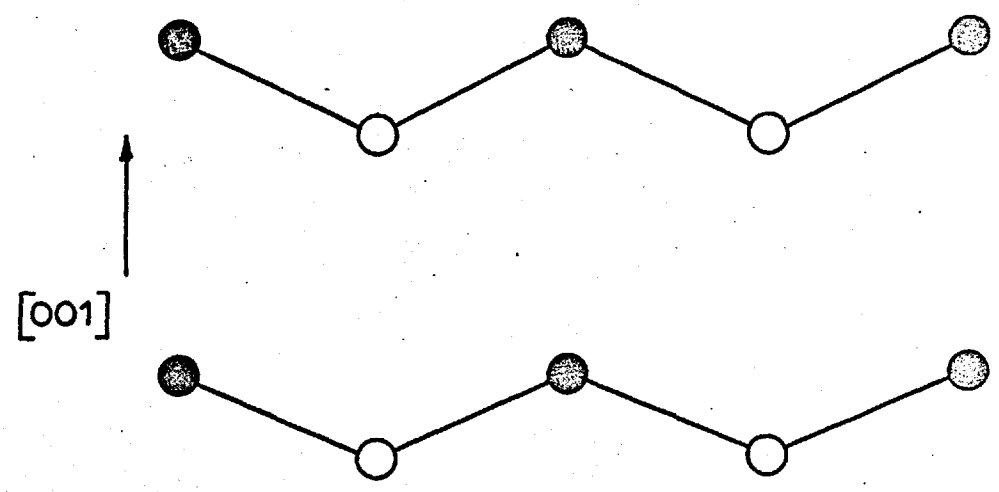

(a) (110) plane

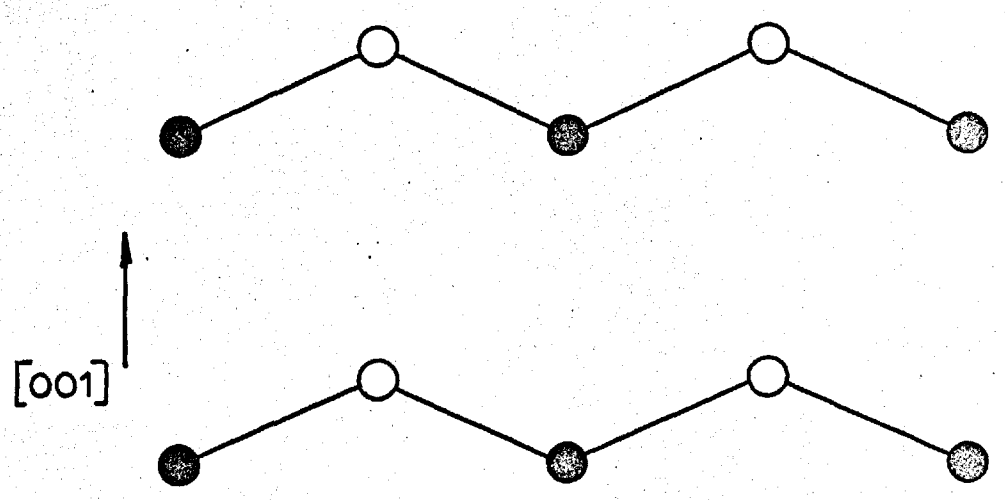

(b) $(1\bar{1}0)$ plane

FIG. 2.8. Atomic arrangement on {110} planes of InSb.

and Bell (1957) and by Allen (1957). In Section 2.1 it was noted that edge dislocations in indium antimonide could exist in two forms, which were called In-dislocations and Sb-dislocations. It was also noted that, in Fig.2.1(b), positive edge dislocations would always be In-dislocations and negative edge dislocations would always be Sb-dislocations (if slip only occurred between the widely spaced pairs of $\{111\}$ planes). Plastic bending, therefore, should produce dislocations of one sort or the other in excess.

Venables and Broudy plastically bent specimens to introduce an excess of In- or Sb-dislocations, the relative polarity of the specimens having been determined from the direction of elongation of the etch-pits on $\{110\}$ planes. Sample A was bent in one direction and sample B was bent in the opposite direction. After bending, the etch-pit density on $\{110\}$ in sample A was higher than in sample B. Also etch-pits extended far into the neutral axis region in A, whereas in B they did not, B having a much more clearly defined neutral axis region. After annealing the etch-pit density decreased for both samples. For sample B the etch-pit density became very small, while sample A had a higher density of pits than sample B. The pits in sample A were more uniformly distributed after the annealing treatment than before it. Venables and Broudy concluded that only one type of dislocation was

revealed by their etchant; that type in excess in sample A. According to their model this type of dislocation should be almost eliminated in sample B by annihilation of opposite signs during annealing. It was not possible to say whether the dislocations revealed were Sb-type or In-type since the absolute polarity of the specimens was not known. Venables and Broudy also found that etching of octahedral planes of as-bent samples showed similar differences in etch-pit distribution. The neutral axis was well defined for sample B but not well defined for sample A. From this they deduced that only one type of dislocation was responsible for etch-pits on $\{110\}$ and octahedral faces of InSb.

Warekois (1959), using an x-ray technique developed by Koster, Knol and Prins (1930), was able to distinguish the $\{111\}$ surface from the $\{\bar{1}\bar{1}\bar{1}\}$ surface. Because of the polarity of the structure the moduli of the structure factors $F(hkl)$ and $F(\bar{h}\bar{k}\bar{l})$, and hence the intensities of these reflections $I(hkl)$ and $I(\bar{h}\bar{k}\bar{l})$, have different magnitudes. This difference only becomes important, however, when the frequency of the incident radiation approaches the critical absorption frequency of one type of atom in the material. A technique based on this phenomenon was used to identify $\{111\}$ and $\{\bar{1}\bar{1}\bar{1}\}$ surfaces in InAs by Warekois and Metzger (1959) and in

GaAs by White and Roth (1959). For indium antimonide Warekois derived $\frac{I(hkl)}{I(\bar{h}\bar{k}\bar{l})}$ for several reflections and for several wavelengths of incident radiation. Defining the $(\bar{1}\bar{1}\bar{1})$ surface as that terminating in indium atoms triply bonded to the lattice or antimony atoms singly bonded to the lattice, he found that for iodine radiation, the theoretical value of $\frac{I(333)}{I(\bar{3}\bar{3}\bar{3})}$ was 1.27 while for tellurium radiation this ratio was almost unity. Using the fluorescent radiation from a tellurium-iodine target he measured intensities for both wavelengths irradiating opposite $\{111\}$ faces of a crystal. The measured intensity ratios of the iodine and tellurium reflections were in good agreement with the predicted values and he found that the surface which showed etch-pits (using an etchant containing equal parts HNO_3 , HF , H_2O) corresponded to the $(\bar{1}\bar{1}\bar{1})$ surface. Thus the etching properties of $\{111\}$ planes, in conjunction with the calibration of Warekois, can be used to determine the polarity of any sample of indium antimonide. It is not necessary to know what the surface atoms are if the polarity only is required, but to discuss the detailed mechanism of the etching process it is usually assumed that the surface developing etch-pits (the $(\bar{1}\bar{1}\bar{1})$ surface) terminates in triply bonded indium atoms. For the rest of this thesis we will adopt the convention of

Warekois (1959) for labelling the crystallographic directions in indium antimonide, as shown in Fig.2.9.

Gatos and Lavine (1960a) used Warekois' calibration of the etching properties to interpret Venables and Broudy's results. They deduced that the dislocation etch-pits observed by Venables and Broudy occurred at In-dislocations only. This deduction, however, is only possible if one assumes that the etch used by Venables and Broudy for $\{110\}$ surfaces also produces pits on $\{\bar{1}\bar{1}\bar{1}\}$ surfaces rather than $\{111\}$ surfaces. It is also necessary to assume a model for $\{110\}$ etch-pit formation since it is not obvious how to determine the type of dislocation in excess knowing only the direction in which $\{110\}$ pits are elongated. Venables and Broudy's experiment, therefore, does not unambiguously show that In-dislocations rather than Sb-dislocations are revealed as pits.

Gatos and Lavine (1960 a) found that the etching behaviour of the $\{111\}$ and $\{\bar{1}\bar{1}\bar{1}\}$ surfaces of indium antimonide was typical of other III - V compounds. In all of the six compounds investigated (InSb , GaSb , AlSb , InAs , GaAs and InP) etch-pits formed on the $\{\bar{1}\bar{1}\bar{1}\}$ surface and not on the $\{111\}$ surface, using a variety of etchants. The authors proposed an interpretation of these results assuming that the group V

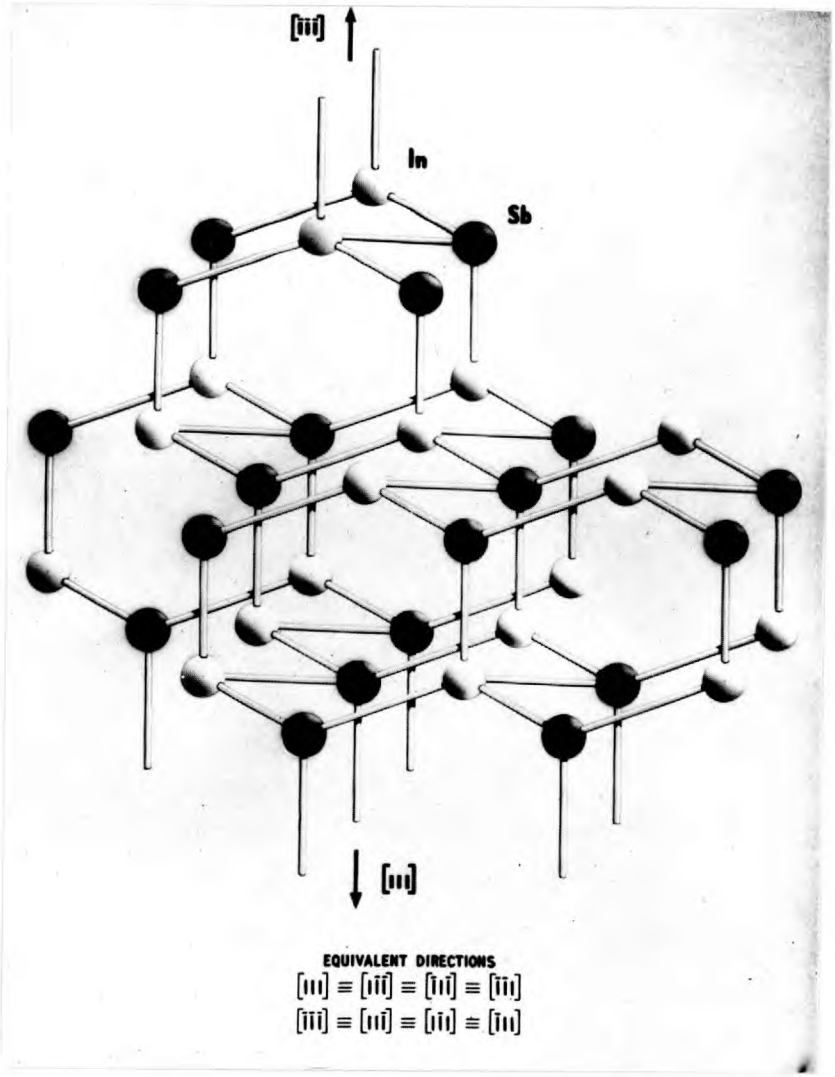

FIG. 2.9. The InSb crystal structure showing the convention used for labelling the crystallographic directions.

surface atoms are more reactive (chemically) than the group LII surface atoms. Considering each type of 60° dislocation intersecting $\{\bar{1}\bar{1}\bar{1}\}$ and $\{111\}$ surfaces they deduced that only In-dislocations intersecting a $\{\bar{1}\bar{1}\bar{1}\}$ surface should produce etch-pits. They concluded that the formation of dislocation etch-pits was controlled by the specific chemical differences between the group III and group V atoms at the dislocation core.

Gatos and Lavine (1960 b and c) obtained etch-pits on the $\{111\}$ surface as well as on the $\{\bar{1}\bar{1}\bar{1}\}$ surface by adding 'inhibitors', such as stearic acid or primary amines, to the CP_4 etch used previously. The pits on $\{111\}$ surfaces, however, are shown by the micrographs to be very poorly defined. Gatos and Lavine noted that the pits ordinarily appearing on the $\{\bar{1}\bar{1}\bar{1}\}$ surface appeared also in the presence of inhibitors, and the authors associated the new pits on the $\{\bar{1}\bar{1}\bar{1}\}$ surface with Sb-dislocations. They suggested that the pits on the $\{111\}$ surface occurred at In-dislocations, Sb-dislocations, or possibly screw dislocations. They suggested that the formation of the new pits was connected with adsorption of positively charged ammonium ions (from the amine inhibitors), which caused a change in reactivity of the Sb-surface atoms.

More recently, Lavine, Gatos and Finn (1961) have

developed another etchant which, they suggested, revealed only Sb-dislocations. Using an etchant known as the 'base-etchant', the same pits as obtained with the CP_4 etch were observed, and these were similarly associated with In-dislocations. When an inhibitor, n-butylthiobutane, was added to the base etchant, pits appeared on both $\{111\}$ and $\{\bar{1}\bar{1}\bar{1}\}$ surfaces. These pits did not correspond to the pits developed by the uninhibited base-etchant and it was suggested that these new pits corresponded to Sb-dislocations. The authors proposed an explanation of this behaviour in terms of adsorption of an oxidation product of butylthiobutane.

In order to test the selectivity of various etchants, samples were plastically bent in a double slip orientation at 300°C to a radius of about 30 cm, to produce an excess of In-dislocations in one case (In-bending) and Sb-dislocations in the other (Sb-bending). After In-bending, the base etchant on a $\{\bar{1}\bar{1}\bar{1}\}$ surface and the CP_4 + amylamine etchant on a $\{111\}$ surface both showed an increase in etch-pit density. Etching in the base etchant + n-butylthiobutane on $\{\bar{1}\bar{1}\bar{1}\}$ or $\{111\}$ surfaces showed no increase in etch-pit density after In-bending. After Sb-bending, the base etchant on a $\{\bar{1}\bar{1}\bar{1}\}$ surface showed no increase in etch-pit density. However, the CP_4 + amylamine etchant on a $\{111\}$ or $\{\bar{1}\bar{1}\bar{1}\}$

surface did show an increase in the etch-pit density. With the butylthiobutane etchant the density of pits on both $\{111\}$ and $\{\bar{1}\bar{1}\bar{1}\}$ surfaces increased after Sb-bending. The above results led to the deduction that the base etchant revealed only In-dislocations on $\{\bar{1}\bar{1}\bar{1}\}$ surfaces, that the CP_4 + amylamine etchant revealed both types of dislocation on $\{\bar{1}\bar{1}\bar{1}\}$ and $\{111\}$ surfaces, and that the base etchant + n-butylthiobutane revealed only Sb-dislocations on $\{\bar{1}\bar{1}\bar{1}\}$ and $\{111\}$ surfaces.

The evidence presented in support of these arguments, however, is not conclusive. The micrographs show only very small fields containing very few pits and, in some cases, only one pit. There is no indication that these fields are representative of the whole specimens. Furthermore, it is possible that the results were dominated by minority sign dislocations since no attempt was made to allow for their presence. Minority sign dislocations could produce quite misleading results when examining very small fields.

CHAPTER 3.

ELECTRICAL PROPERTIES OF UNDEFORMED INDIUM ANTIMONIDE.

Before discussing the effect of plastic deformation on the electrical properties of germanium and indium antimonide, the electrical properties of undeformed indium antimonide will be summarised.

3.1. Preparation of single crystals.

Techniques have been developed for purification and growth of InSb single crystals (see for example Hulme 1959, Hulme and Mullin 1962). The compound was prepared from the elements of nominal purities better than 99.99%. Troublesome impurities zinc and cadmium were removed by a volatilization technique which, when followed by zone-refining, produced n-type material with an electron concentration $\left(1/R_{Hq}\right)$ at 77°K near 10^{14} cm^{-3}. Single crystals were grown from this material by the Czochralski vertical pulling technique and the horizontal zone-melting technique, and had mobilities $\left(R_H\sigma\right)$ of over 5×10^5 $cm^2/V.sec$ at 77°K. The density of etch-pits in vertically grown crystals (as revealed by a CP_4 etchant) was generally about 10^3 cm^{-2}, and etch-pit densities of less than $10cm^{-2}$ occurred quite frequently. Growth twins, in large scale

or 'lamellar' form were often encountered in such crystals. The formation of twins was found to be favoured by using seeds of certain orientations such as $[\bar{1}\bar{1}\bar{1}]$ or $[110]$, while twin-free crystals were obtained more easily with $[111]$ oriented seeds. Freedom from twins with seeds of $[\bar{1}\bar{1}\bar{1}]$ and $[110]$ orientations could only be obtained with a highly developed technique.

3.2. Band structure.

Fig.3.1 shows the variation of electron energy in indium antimonide with the wave vector $\underline{k}$.

Experiments have shown that the minimum of the upper $E(\underline{k})$ curve (the conduction band) occurs at $\underline{k} = 0$. It has also been shown from cyclotron resonance experiments (Dresselhaus et al. 1955) that, in the conduction band, surfaces of constant energy in $\underline{k}$ - space are spherical. Dresselhaus et al. showed that the effective mass of electrons at the bottom of the band is only $0.013\ m_o$. This very small effective mass means that the band has a high curvature at its minimum and a very low density of states there. As a result a small number of electrons fills the band to a high level. The band is non-parabolic, the curvature decreasing rapidly with increasing energy.

The form of the valence band is not certain, but

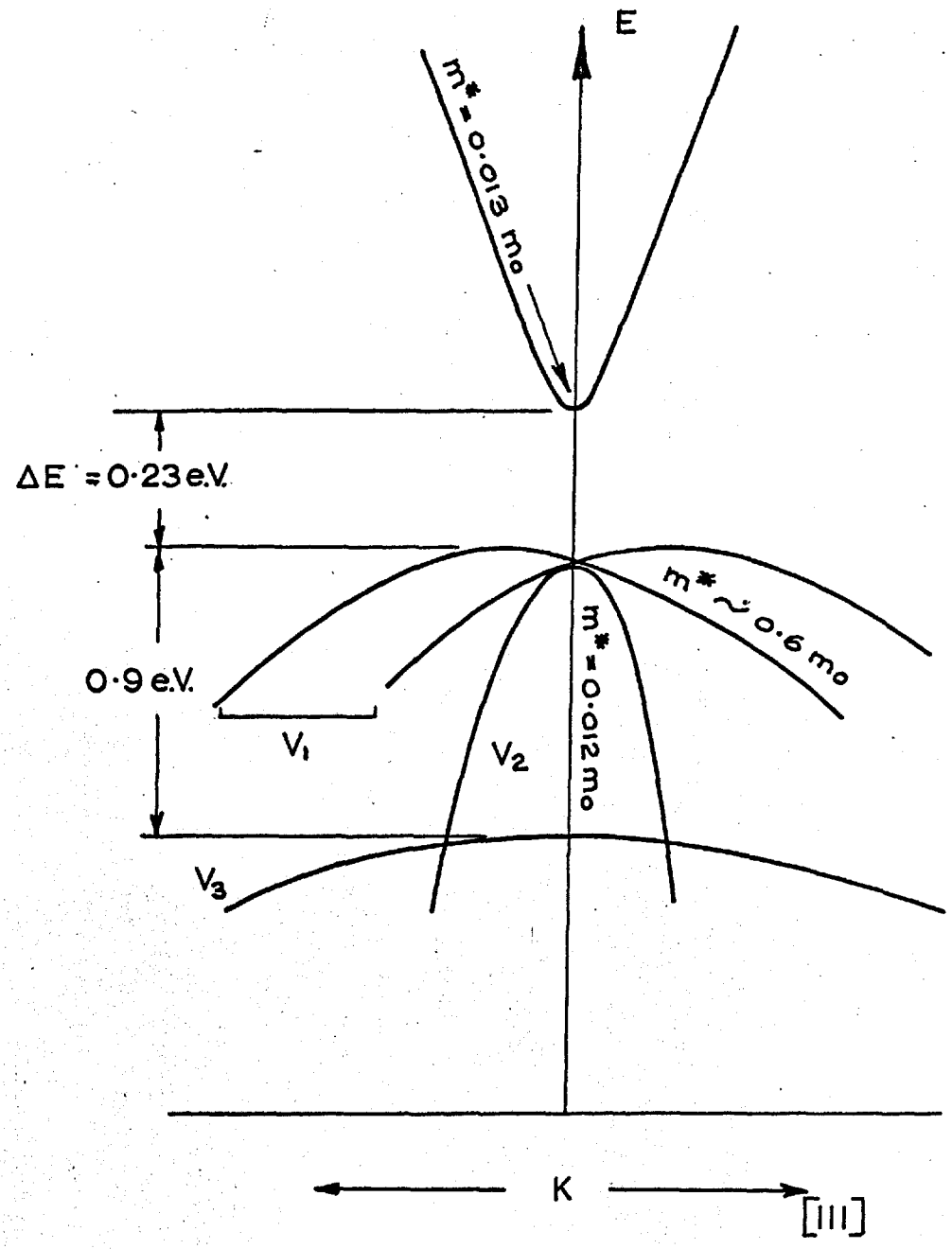

FIG. 3.1. The electron energy, E, as a function of the wave vector $\underline{k}$, in indium antimonide.

the experimental results appear to be consistent with a valence band structure consisting of three bands, a 'heavy-hole' band V_1, a 'light-hole' band V_2 degenerate with V_1 at $\underline{k} = 0$, and a band V_3 split off by spin orbit coupling. Fig.3.1 shows the form of the $E(\underline{k})$ curves near $\underline{k} = 0$. There is some doubt about the effective mass of holes in InSb. Hilsum and Rose-Innes (1961) suggest that 0.6 m_o is the most probable value for the heavy holes. The effective mass of the light holes was estimated as 0.0120 m_o from infra red spectra by Fan and Gobeli (1960). However, the most abundant type of carriers in the valence band are the heavy holes.

The forbidden energy gap ($\triangle E$) obtained by optical methods is 0.23 e.V. at $0^{\circ}K$ and 0.18 e.V. at $300^{\circ}K$, and its variation with temperature is nearly linear above $100^{\circ}K$. The value at $0^{\circ}K$ extrapolated from the linear section is $\triangle E = 0.25$ e.V. which is in fair agreement with that obtained by electrical measurements (also by extrapolation). Thus the value of the energy gap is confirmed by independent measurements, and the good agreement adds confidence to the result.

3.3. Hall coefficient measurements.

3.3.1. Intrinsic range of temperature.

Because of the small energy gap, indium antimonide is intrinsic at room temperature and, in some cases, intrinsic conduction dominates down to 150°K. Putley (1959) calculated intrinsic carrier concentrations from the Hall coefficient by the relation

$$R_H = \frac{3\pi}{8 n_i q}$$

neglecting hole conduction since the mobility of holes is so much less than that of electrons in InSb. He obtained the empirical expression

$$n_i = 5.7 \times 10^{14} T^{3/2} \exp\left(-\frac{0.125}{kT}\right)$$

which describes his results from 180°K to 300°K.

3.3.2. Extrinsic range of temperature.

The Hall coefficient of n-type material varies little with temperature in the extrinsic range (below about 150°K) and there is no evidence for a donor ionisation energy. This behaviour was predicted on the basis of the hydrogen-like model of impurity states which indicated a zero-field ionisation energy of donors of about 7×10^{-4} e.V. This low value is a result of the very low value of the effective mass of electrons in the conduction band.

We turn now to material which is p-type at low temperatures. As the holes are much less mobile than the electrons, the conductivity can be dominated by electrons even when the number of holes exceeds the number of electrons. Thus the Hall coefficient is negative down to quite low temperatures. In the extrinsic region evidence for deep and shallow levels has been obtained.

Table 3.1 summarises the behaviour of impurities in InSb and their estimated energy levels.

3.4. Hall mobility measurements.

Hall mobility ($R_H\sigma$) values, obtained from Hall coefficient and conductivity measurements on n-type material, were found to obey the following relation above 200°K.

$$\mu_n = 7 \times 10^8 \, T^{-1.6} \quad cm^2/Volt.\,sec.$$

Since this temperature dependence is close to the $T^{-1.5}$ law of acoustic scattering, many early workers assumed that this was in fact the dominant lattice scattering process. However, Ehrenreich (1957, 1959) has shown that a combination of polar scattering and electron-hole scattering gives a $T^{-1.7}$ dependence, and his theoretical values of mobility were in close agreement with experimental values between 200°K and 700°K. According to Ehrenreich, electron-hole scattering is not important

Element	Electrical effect	Energy level (e.V.)
Na, Li	Donor ?	
Cu	Double Acceptor	0.023 e.V. (V.B.)
Ag	Double Acceptor	0.022 e.V. (V.B.)
Au	Double Acceptor	0.032 e.V. (V.B.)
Mg, Zn, Cd	Acceptor	0.0075 e.V. (V.B.)
Al	Acceptor ?	
Ga, As	Neutral	
Si, Ge	Acceptor	
Sn	Donor	
Pb	Donor or Neutral	
S, Se, Te	Donor	Apparently Zero ionisation energy
Mn	Acceptor	
F	Donor	

Table 3.1: Impurity levels in InSb.

V.B. = measured from top of Valence band.

below 500°K, when polar scattering is the dominant scattering mechanism. He calculated the scattering factor, r, for InSb where

$$R_H = \frac{r}{nq}$$

and obtained values of 1.07 at 200°K, 1.01 at 300°K and 1.09 at 700°K. The mobility at temperatures below 200°K often begins to show effects of impurity scattering and at low temperatures tends to the $T^{+1.5}$ law of impurity scattering. Hrostowski et al. (1955), Putley (1959) and Bate, Willardson and Beer (1959) analysed their results in terms of combined acoustic and impurity scattering, for which the scattering factor, r, lies between 1 and $315\,\pi/512$ ($\simeq 1.9$). However, no complete calculation of the combined effects of polar scattering and impurity scattering has yet appeared. For the purposes of analysing Hall coefficients of undeformed material from 300°K to 80°K it will be assumed, in the present experiments, that $r = 1$.

The variation of hole mobility with temperature above 100°K has been given as

$$\mu_p = 1.1 \times 10^8 \; T^{-2.1} \; cm^2/Volt.\,sec.$$

No explanation has yet been given for this dependence.

Hilsum and Rose-Innes (1961) have summarised mobility results for InSb obtained by a number of

workers. Fig.3.2 shows the dependence of electron mobility ($R_H\sigma$) on impurity concentration, for n- and p-type samples at 77°K.

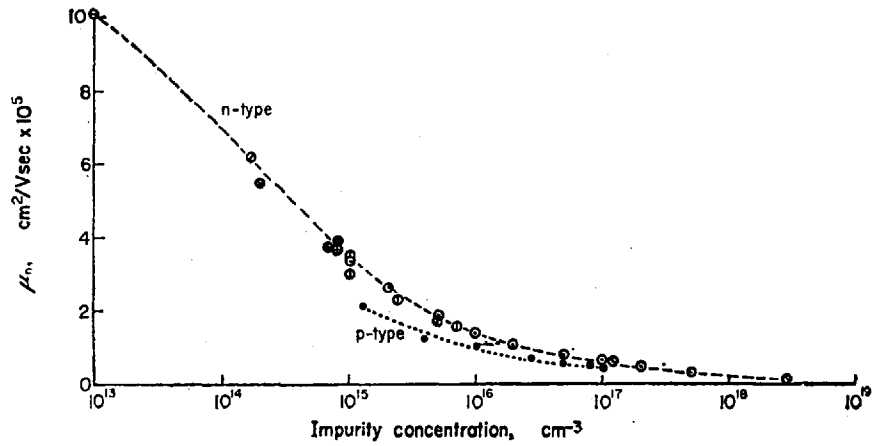

Dependence of electron mobility on impurity concentration for *n*- and *p*-type samples of InSb at 77°K.

Fig. 3.2.

It can be seen that about 10^{15} impurities/cm^3 are needed to reduce the electron mobility from 5.5×10^5 $cm^2/V.sec.$ to 3.5×10^5 $cm^2/V.sec.$

3.5. Summary.

It is important to note that the Hall coefficient of undeformed n-type samples is temperature independent in the extrinsic range. The deionisation of any centres introduced by deformation can thus be easily detected in indium antimonide. It is also important to note the magnitude of impurity scattering effects. The measurements of the effects of dislocations in germanium (discussed in Section 4) indicate that a given number of donors and acceptors are more effective in reducing the mobility when arranged along a line than they are when randomly distributed. When arranged along a line there is the necessity for a cylinder of opposite charge, screening the line, and this cylinder is very effective in reducing the mobility. The change in mobility after deformation is thus an indication of the distribution of the centres introduced.

CHAPTER 4.

ELECTRICAL PROPERTIES OF DISLOCATIONS IN GERMANIUM.

The conductivity of homogeneous n-type material can be expressed in the following form

$$\sigma = nq\mu \qquad \ldots\ldots (4.1)$$

where σ = electrical conductivity ($ohm^{-1}\ cm^{-1}$)

n = concentration of conduction electrons (cm^{-3})

q = electronic charge (coulombs)

μ = electron mobility (cm^2/volt sec.)

The electron concentration in such material can be calculated from the Hall coefficient (R_H) by the relation

$$R_H = \frac{r}{nq} \quad cm^3/Coulomb \qquad .. (4.2)$$

where r is a numerical factor which lies between about 1 and 2. (The value of r depends on the type of scattering which predominates and the degree of degeneracy of the electron gas). Similar equations apply to p-type material, the sign of the Hall coefficient indicating whether it is an n- or a p-type semiconductor. An estimate of the carrier mobility can thus be obtained from the measured conductivity and Hall coefficient.

Plastically deformed material, however, may be inhomogeneous, and consequently the carrier concentration

may not be directly obtainable from the Hall coefficient as in (4.2). It is therefore more convenient to discuss the effect of dislocations on the measurable parameters, the Hall coefficient and conductivity, rather than on calculated quantities like the carrier concentration and mobility. The effect of dislocations on the Hall coefficient and the conductivity will therefore be discussed throughout.

In this chapter the effects of dislocations in n-type material are discussed before their effects in p-type material, since previous work has concentrated mainly on the former. In the review on n-type germanium the early work is briefly discussed, and then a summary of Read's theory of dislocation-acceptors is given, followed by a description of the application of this model to later experimental measurements. The modification to the Read model, introduced by Broudy, is discussed and the Read and Broudy models are compared in relation to the experimental results. The work on p-type germanium is next reviewed followed by a survey of the effects of dislocations on the properties of minority carriers. Finally, the electrical effects of dislocations in germanium are summarised.

Work in this field up to 1959 has been reviewed by Bardsley (1959).

4.1. n-type germanium.

4.1.1. Effect of dislocations on the Hall coefficient.

Early experimental work.

The first observations concerning the effect of plastic deformation on the electrical properties of semiconductors were made by Gallagher (1952) who noted an increase in the resistivity of n-type germanium after plastic bending. A similar result was obtained by Ellis and Greiner (1953) for compression of n-type silicon and germanium. The measurements of Pearson, Read and Morin (1953), who found changes in Hall coefficient as well as resistivity after bending n-type germanium samples, indicated that, although the carrier mobility was lowered, the carrier density was also changed by deformation. They suggested from their measurements that edge dislocations in germanium are associated with acceptor centres. In p-type material, deformation had a negligible effect on the Hall coefficient and consequently they deduced that the dislocation energy level must lie in the upper half of the forbidden gap. The measurements of Tweet (1955) also indicated that dislocations act as acceptors in n-type germanium.

Read's theory of dislocation-acceptors.

a) The basic model.

Following an idea of Shockley's, Read (1954 a) postulated a simple model of dislocation-acceptors. Fig.2.2(a) shows a 60° dislocation in the diamond lattice, which, as was noted in Section 2.1., has a row of 'dangling-bonds' at the edge of its extra half-plane. Read associated dislocation acceptors with these 'dangling bonds'. In the 60° dislocation the spacing between 'dangling bonds' is equal to the spacing, b, of neighbouring atoms in a $\langle 110 \rangle$ direction in a $\{111\}$ plane. Read derived a general expression for the spacing, c, between dangling bonds as a function of the angle, χ, between the dislocation line and its Burgers Vector

$$c = 0.866\, b \ \mathrm{cosec}\, \chi$$

The spacing c is a minimum for the edge orientation ($\chi = 90^{\circ}$) and infinite for the screw orientation ($\chi = 0^{\circ}$) when there are no 'dangling bonds'. If d, the spacing between accepted electrons, is small compared with the mean spacing between chemical donors and acceptors then the dislocation will act as a charged line. This negatively charged line will repel conduction electrons and a cylindrical space charge region of positively charged ions will form around the dislocation. The radius of this cylinder (R_s) is defined such that

it contains an amount of fixed positive charge (in the form of ionised donors) equal to the negative charge on the dislocation. The positive charge per unit length in the space charge cylinder is therefore $\pi R_s^2 (N_D - N_A) q$. If d is the spacing of accepted electrons the negative charge on the dislocation line per unit length is q/d, and

$$\therefore \pi R_s^2 (N_D - N_A) = \frac{1}{d} = \frac{f}{c} \qquad \ldots (4.3)$$

where $N_D - N_A$ = excess donor concentration in the bulk of the material (cm^{-3})

and f = fraction of dislocation sites occupied.

Read showed that it is probable that the dislocation acceptor level in germanium lies within the energy gap, and hence in n-type material some of the acceptor sites will be occupied. If a dislocation is introduced into n-type material, therefore, the acceptors will begin to fill up. The free energy will initially decrease as electrons drop from the conduction band into the dislocation acceptors. However, the electrostatic energy of the negatively charged line will increase as each electron is added, because the average spacing between electrons will decrease. At a certain spacing, d, between electrons the increase in electrostatic energy will make it unfavourable, from the viewpoint of free energy, to add any more electrons to the

dislocation. Read used this thermodynamic argument to calculate the equilibrium spacing, d, and the corresponding value of f, the fraction of sites occupied at a given temperature.

b) Read's 'Minimum Energy' Approximation.

Firstly, Read derived an expression for f, neglecting the configurational entropy of the accepted electrons. In this model the electrons were assumed to be evenly spaced along the dislocation and the entropy vanishes, there being only one configuration of even spacing. The model of energy band structure around the dislocation is shown in Fig.4.1. The negatively charged line increases the electrostatic energy of any electron in the neighbourhood and this is represented by the change in position of the bottom of the conduction band and the top of the valence band near to the dislocation line. Measuring energies from the top of the valence band, E_D is the dislocation energy level measured at the dislocation and E_F is the Fermi level in the normal n-type material (as shown in Fig.4.1).

The decrease in energy when one electron drops into the dislocation level is thus $(E_F - E_D)$. If $\varepsilon_s(f)$ is the electrostatic energy per electron added to the line, the total increase in energy per unit electron on the dislocation $U_e(f)$, is :

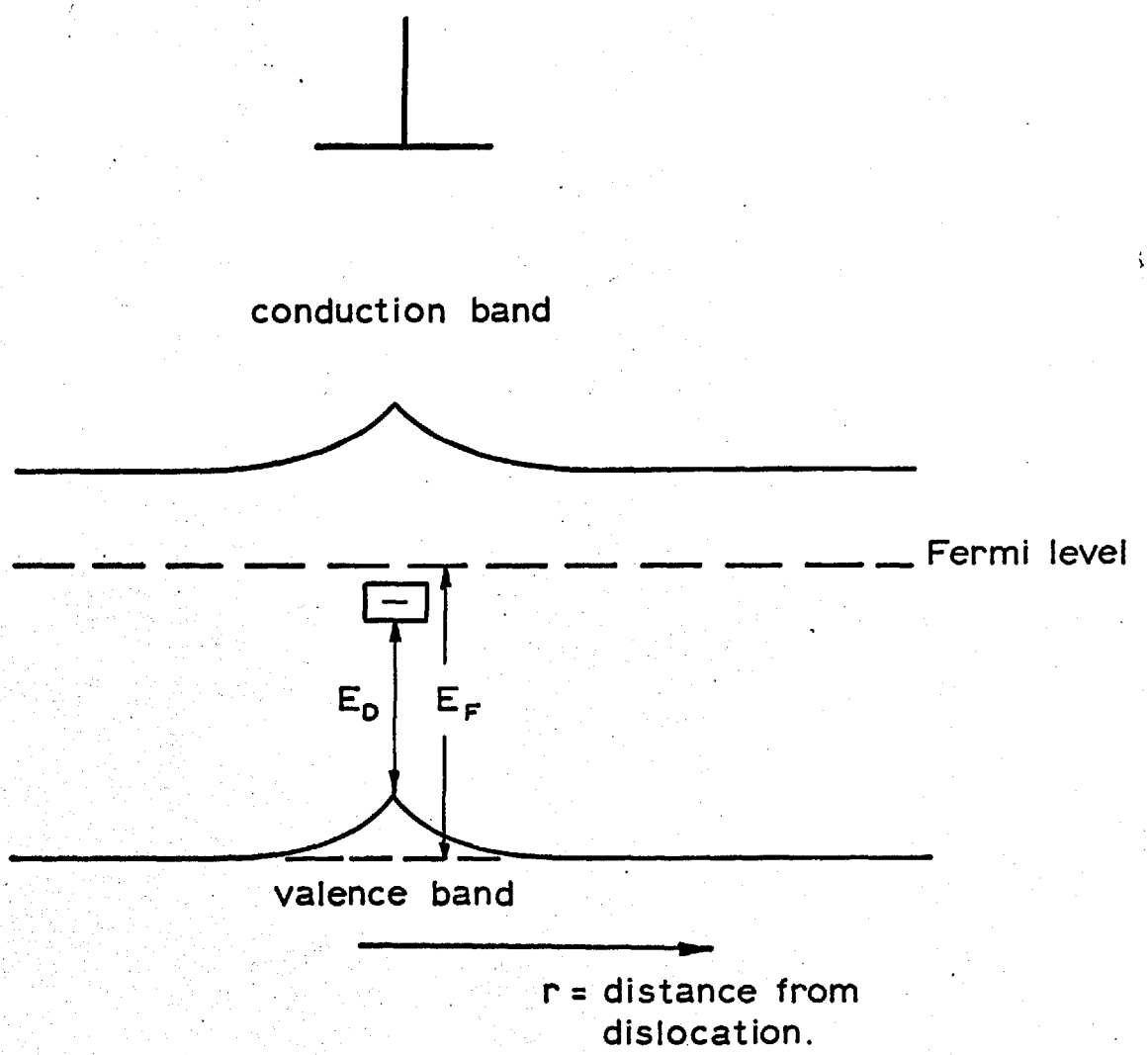

FIG. 4.1 Energy band structure around dislocation.

$$U_e(f) = E_D - E_F + \mathcal{E}_S(f)$$

For a constant spacing d ($= c/f$) of accepted electrons, the energy per site is $f U_e$

$$f U_e = f \left\{ E_D - E_F + \mathcal{E}_S(f) \right\}$$

Minimising $f U_e$ we have

$$E_F - E_D = \mathcal{E}^*(f) \qquad \ldots \quad (4.4)$$

where $$\mathcal{E}^*(f) = \frac{d}{df} f \mathcal{E}_S(f)$$

Read derived $\mathcal{E}_S(f)$ for a row of evenly spaced electrons running along the axis of a cylinder of positive space charge. The calculations were made on the basis of the general expressions for the electrostatic energy of an array of charges. By Coulomb's law, the potential at the ith charge due to all the other charges is

$$\psi_i = \sum \frac{q_j}{\varkappa r_{ij}} \qquad \ldots \quad (4.5)$$

where r_{ij} is the distance between the ith and jth charges, q_j is the charge on the jth charge and the sum is taken over all j's except $i = j$.

The expression

$$\sum \psi_i q_i$$

is twice the total electrostatic energy since every term

such as $\frac{q_i q_j}{\kappa r_{ij}}$

will be repeated as $\frac{q_j q_i}{\kappa r_{ji}}$

in the sum. The interaction energy between each pair of charges will thus be considered twice. Thus the total electrostatic energy is

$$\tfrac{1}{2} \sum \psi_i q_i \qquad \ldots\ldots (4.6)$$

The calculation was simplified by calculating ψ_e, the potential of the row of electrons, and ψ_c, the potential of the positive space charge. ψ_e and ψ_c were calculated for the section of cylinder in the centre of the length Nd of the cylinder (where N = number of electrons in the row), since ψ_e and ψ_c have a simpler form in the central section. Combining ψ_c and ψ_e with the two charge distributions, according to (4.6), gave four terms in the energy $\mathcal{E}_s$. Two terms are self energies and involve the potentials and corresponding charge distributions; the other two terms involve the potential of one distribution and the charge of the other. $\mathcal{E}_s$ was then given by

$$\mathcal{E}_s = \mathcal{E}_e + \mathcal{E}_c + \mathcal{E}_{ce} + \mathcal{E}_{ec} \qquad \ldots\ldots (4.7)$$

where $\mathcal{E}_e$ is the energy of the row of electrons

$\mathcal{E}_c$ is the energy of the positive space charge

and $\mathcal{E}_{ce}$ and $\mathcal{E}_{ec}$ are the energies of interaction of the electrons and the positive space charge. Read calculated the four terms in (4.7) and obtained

$$\mathcal{E}_s = f\mathcal{E}_o\left\{{}^3/_2 \ln(f/f_c) - 0.866\right\}$$

where $\mathcal{E}_o = q^2/\varkappa c$

and $f_c = c\pi^{1/3}(N_D - N_A)^{1/3}$

also $$\mathcal{E}^*(f) = {}^d/_{df}(f\mathcal{E}_s)$$
$$= \mathcal{E}_o f\left[3\ln(f/f_c) - 0.232\right] \quad (4.8)$$

Substituting (4.8) in (4.4) one obtains

$$E_F - E_D = \mathcal{E}_o f\left\{3\ln(f/f_c) - 0.232\right\} \quad \ldots\ldots (4.9)$$

Now, for a particular specimen, $N_D - N_A$ can be measured before the dislocations are introduced and c can be calculated provided the orientation of the dislocations is known. Also the Fermi level in the normal n-type material, $E_F(T)$, can usually be calculated from the Hall coefficient of the undeformed material. Thus equation (4.9) can be solved for f at any temperature, T, for a range of values of the dislocation acceptor level, E_D. It will be shown below that the experimental temperature dependence of f can be compared with this theoretical dependence to determine the acceptor level.

The expression (4.9) is known as Read's 'Minimum Energy' Approximation.

c) Read's 'Fermi' Approximation.

In the second approximation Read took into account non-uniform spacing of electrons along the dislocation. However, it was assumed that all configurations have the same energy. This assumption is not always a good approximation since the energy will be a maximum if all the electrons are crowded together in one part of the dislocation and a minimum if equally spaced. However, if the interaction energy between neighbouring electrons vanishes then most of the arrangements will have approximately the same energy. Assuming that all configurations have the same energy, the occurrence of any one arrangement of electrons is as probable as the occurrence of any other arrangement, and thus the configurational entropy is a maximum. Now, the total number of ways of putting N electrons on M sites is $W = M!/N!\,M-N!$
If $S_e(f)$ is the entropy per electron on the dislocation, the entropy per site is thus

$$f S_e(f) = -k \ln W/M$$
$$= -k[f \ln f + (1-f)\ln(1-f)]$$

If $G_e(f)$ is the free energy per accepted electron, the free energy per site is

$$f G_e(f) = f\{E_D - E_F + \varepsilon_s(f) - T S_e\}$$

and, minimising, one obtains

$$\varepsilon^*(f) = E_F - E_D + kT \ln\left(\frac{1-f}{f}\right) \quad \ldots(4.10)$$

where $\varepsilon^*(f) = d/df\,(f\varepsilon_s)$

Substituting $\varepsilon^*(f)$ from (4.8) in (4.10) one obtains

$$E_F - E_D + kT \ln\left(\frac{1-f}{f}\right) = \varepsilon_0 f \left\{3 \ln(f/f_c) - 0.232\right\} \quad \ldots\ldots (4.11)$$

Equation (4.11) is known as Read's 'Fermi' approximation and can be solved to obtain f as a function of temperature for a range of values of E_D. This theoretical temperature dependence of f could be used in a similar way to that described for the Minimum Energy approximation to estimate the acceptor level E_D from experimental measurements. Bliek (1964), however, suggested that Read's Fermi approximation was in error since electron spins were not considered in the calculation of the entropy. Bliek modified the calculation to take account of electron spins, as will be described in Section 4.2.

The only difference between the two approximations (4.11) and (4.9) is that the Fermi approximation considers maximum entropy while the Minimum Energy approximation considers zero entropy, the internal energy being the same for both. The Fermi approximation thus gives a lower limit for G_e (the free energy increase per accepted electron) while the Minimum Energy approximation gives an upper limit. The correct value of f, therefore, lies somewhere between these two limits. In a later paper (1954 b) Read derived other approximations to take account of the effect of the non-uniform spacing

of electrons along the dislocation and also for the dislocation acceptors having a range of levels rather than a single level. The f versus T curves for these approximations lay between the 'minimum energy' and 'Fermi' approximations given above.

Read calculated f versus T curves for germanium on both the 'minimum energy' and 'Fermi' approximations for a typical set of values, viz. $E_c - E_D = 0.225$ e.V. and $N_D - N_A = 10^{15}/cm^3$. The Fermi level measured from the conduction band ($E_c - E_F$) was calculated in the usual way. He obtained values of f of the order of 0.1, being a maximum at $0^\circ K$ and decreasing with rise in temperature. The Fermi approximation curve lay above the 'minimum energy' curve at all temperatures except $0^\circ K$, when the two estimates of f coincided.

d) Interpretation of Hall coefficient measurements on Read's theory.

To make possible a comparison of experimental results with the theory given above, Read considered conduction in material containing a parallel array of dislocations.

Firstly, Read considered current flow perpendicular to the dislocation direction, as in Fig.4.2(a), where the applied electric field is in the x-direction. Read argued that, since the conduction electrons have to follow curved paths that wind around the space charge cylinders, the mobility should be reduced. He obtained

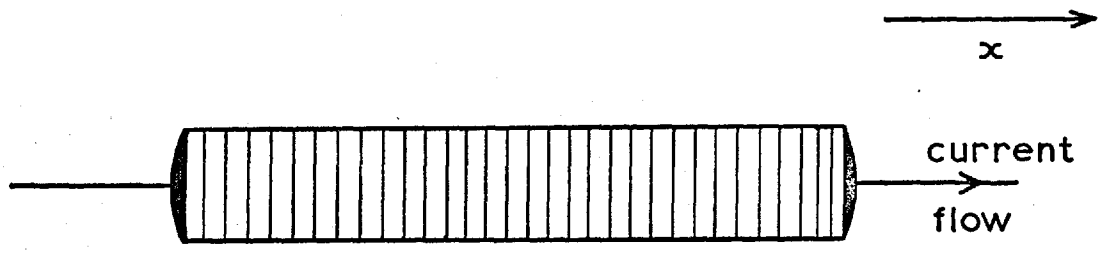

FIG.4.2.a $I \perp D$, $H = 0$.

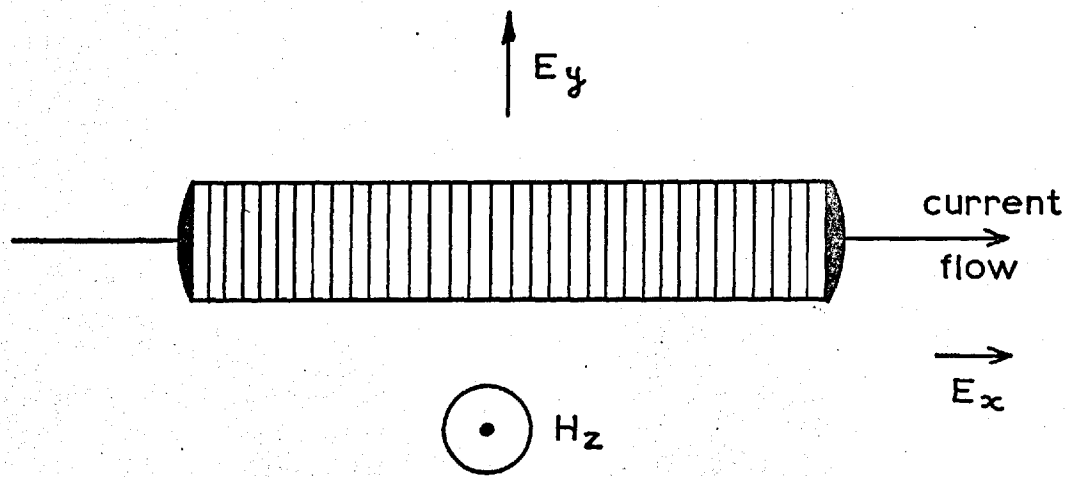

FIG.4.2b. $I \perp D$, $H \perp D$, $I \perp H$.

the following expression for the average current density $\langle I_x \rangle$ (where $\langle\ \rangle$ refers to an average over the whole specimen) in terms of the average density of conduction electrons $\langle n \rangle$, and the average electric field $\langle E_x \rangle$

$$\langle I_x \rangle = q \mu \langle n \rangle \langle E_x \rangle g(\epsilon) \qquad \ldots\ (4.12)$$

where $g(\epsilon) = \langle E_x \rangle_n / \langle E_x \rangle$ is known as the 'distortion parameter' and $\langle E_x \rangle_n$ is E_x averaged just over the normal n-type material (the space charge tubes assumed to be insulating).

Secondly, Read considered conduction with current flow again in the x-direction but with a magnetic field in the z-direction (normal to the dislocations) as in Fig.4.2(b). The Hall field is thus in the y-direction, parallel to the dislocations. Read considered the variation of the electric field $\overline{E}$ throughout the sample. $\overline{E}$ is constant in the y-direction and therefore the component E_y must be constant at all values of x and z also. Now the current density at any point is given by

$$\overline{I} = nq\mu \overline{E} - \mu_H \overline{I} \times \overline{H} \qquad \ldots\ (4.13)$$

Read took averages in (4.13) for the y-components and obtained

$$\langle n \rangle q \mu E_y = \mu_H \langle I_x \rangle H_z \qquad \ldots\ (4.14)$$

Now, since the Hall coefficient is given by the relation

$$R_H = \frac{E_y}{\langle I_x \rangle H_z} \qquad \ldots\ (4.15)$$

substitution of $\langle I_x \rangle$ from (4.14) into (4.15) gives

$$R_H = \frac{\mu_H}{\mu \langle n \rangle q} \quad \ldots\ldots (4.16)$$

Thus the average carrier concentration $\langle n \rangle$ can be calculated, according to this theory, directly from the Hall coefficient of the deformed sample.

e) Comparison of theory with experiment.

Now, in the space-charge model there are no conduction electrons inside a cylinder of cross sectional area πR_s^2 around each dislocation. Thus, with a parallel array of dislocations of density ρ (cm^{-2}), the fraction of volume occupied by the space-charge cylinders is given by $\epsilon = \pi R_s^2 \rho$, and the average density of conduction electrons $\langle n \rangle$, is given by

$$\langle n \rangle = n(1-\epsilon)$$

where n was the electron concentration in the material before the dislocations were introduced. Now, the change in electron concentration $n - \langle n \rangle$ for a dislocation density ρ is $f\rho/c$, so that one obtains

$$\epsilon = \frac{n - \langle n \rangle}{n} = \frac{f\rho}{cn} \quad \text{or} \quad \frac{f\rho}{c(N_D - N_A)} \quad \ldots\ldots (4.17)$$

After introducing a known density of dislocations (ρ cm^{-2}) into a sample of original carrier concentration $N_D - N_A$ (cm^{-3}), the average carrier concentration in the deformed sample $\langle n \rangle$ may be calculated from the Hall

coefficient via (4.16) and, in principle, one can calculate an experimental value of f, the fraction of occupied sites, from (4.17), assuming a reasonable value for c, the spacing of sites. This experimental value of f (and its temperature dependence) may then be compared with the theoretical estimates of Read's theory to obtain E_D, the dislocation acceptor level.

Experimental test of the Read model.

Read's approach was followed by Logan, Pearson and Kleinman (1959) when analysing their experimental results on bent n-type germanium samples. Specimens oriented to favour single slip were deformed by four point bending at 800°C to a radius of about 5 cms. L-shaped samples were cut from the bent samples such that one leg was parallel to the bend axis and the other perpendicular to it. Now the observations of Patel (1958) on silicon samples bent in the same orientation, indicated that the dislocations lay parallel to the bend axis, and, if this occurred also in Logan's samples, the current would flow parallel to the dislocations in one limb and perpendicular to the dislocations in the other. Properties obtained with these two directions of current flow will be called 'parallel' and 'perpendicular' properties respectively, e.g. $R_{\parallel}$, $R_{\perp}$. A magnetic field was applied in the direction perpendicular to both

limbs of the L-shaped sample, and thus the orientation of the 'perpendicular' limb was equivalent to Fig.4.2(b) of Read's treatment. From a theoretical analysis, similar to that of Read, Logan et al. confirmed Read's expression (4.16) for $R_\perp$. They extended this analysis to the 'parallel' limb, and obtained

$$R_{//} = \frac{\mu_H}{\mu \langle n \rangle q}$$

Now, since the work of Morin (1954) indicated that the ratio of the Hall mobility to the drift mobility was close to unity, Logan et al. wrote

$$R_\perp = R_{//} = \frac{1}{\langle n \rangle q} \qquad \ldots\ldots (4.18)$$

Using (4.18), the carrier concentration in the deformed samples was calculated directly from the Hall coefficient.

Now, if $R_o = 1/nq$ is the Hall coefficient of the undeformed sample

then $$\frac{R_{//}}{R_o} \left(= \frac{R_\perp}{R_o} \right) = \frac{n}{\langle n \rangle} = \frac{1}{1-\epsilon} \qquad \ldots\ldots (4.19)$$

Juretschke et alia (1956) have obtained this result for material containing cylindrical voids by deriving the fields due to the voids. A similar derivation by Broudy (1963) confirmed (4.19) for $R_{//}/R_o$. These independent calculations increase confidence in the validity of (4.19).

Logan et al. measured the Hall coefficients of deformed and 'control' samples over a range of temperature from 4°K to 300°K, 'control' samples being undeformed

specimens which had been kept close to the deformed samples during the heat treatment. Values of

$\epsilon \left(= \frac{n - \langle n \rangle}{n} = 1 - \frac{R_0}{R_{II}} \right)$ were then calculated from the measured Hall coefficients at each temperature. Because of uncertainty in ρ and c in (4.17) Logan et al. did not calculate f directly from that equation. Instead, the basic relation (4.17) between ϵ and f was written

$$\epsilon(T) = \lambda f(T) \qquad \ldots (4.20)$$

where $\lambda = \frac{\rho}{c(N_D - N_A)}$ was used as an adjustable parameter.

A family of $f(T)$ curves was calculated for several values of the dislocation energy level using the 'Fermi' approximation, equation (4.11). These curves are shown in Fig.4.3(a). $\epsilon(T)$ curves were then obtained from these $f(T)$ curves using (4.20). The following is a typical example of the method.

Consider the $f(T)$ curve calculated for $E_c - E_D = 0.35$ e.V. (Fig.4.3(a)). First, relation (4.20) is used to obtain λ from the measured value of ϵ and the computed value of f, at a particular temperature.

For example $f(0^\circ K) = 0.123$ (Fig.4.3(a)).

and $\epsilon(0^\circ K) = 0.565$ (extrapolated from experimental results in Fig.4.3(b)).

Thus $\lambda = \frac{\epsilon(0^\circ K)}{f(0^\circ K)} = \frac{0.565}{0.123} = \underline{4.593}$

Then, using this value of λ (4.593) and the $f(T)$ curve shown in Fig.4.3(a), the theoretical $\epsilon(T)$ curve was calculated by the relation (4.20). This is shown in Fig.4.3(b) and labelled $E_c - E_D = 0.35$ e.V. This curve is not in agreement with the experimental points having too shallow a slope.

It can be seen from Fig.4.3(a) that, since $\epsilon(0^\circ K)$ is extrapolated from experimental results and therefore constant, the value of $\lambda = \frac{\epsilon(0^\circ K)}{f(0^\circ K)}$ will be different for each $f(T)$ curve (i.e. for each value of $(E_c - E_D)$ tried). Furthermore, since all the $f(T)$ curves are nearly parallel, i.e. $\frac{df}{dT} \simeq$ constant

then, since $\frac{d\epsilon}{dT} = \lambda \frac{df}{dT}$ (by differentiation of equation (4.20)), $\frac{d\epsilon}{dT} \propto \lambda$.

The quality of fit between the experimental points and the theoretical $\epsilon(T)$ curve is determined by the choice of $(E_c - E_D)$, but effectively this only fixes the magnitude of f , the slope of the theoretical $\epsilon(T)$ curve is governed by λ . For the experimental points shown in Fig.4.3(b) the best fit is bracketed by values of 0.179 and 0.225 e.V. for $(E_c - E_D)$. Logan et al.

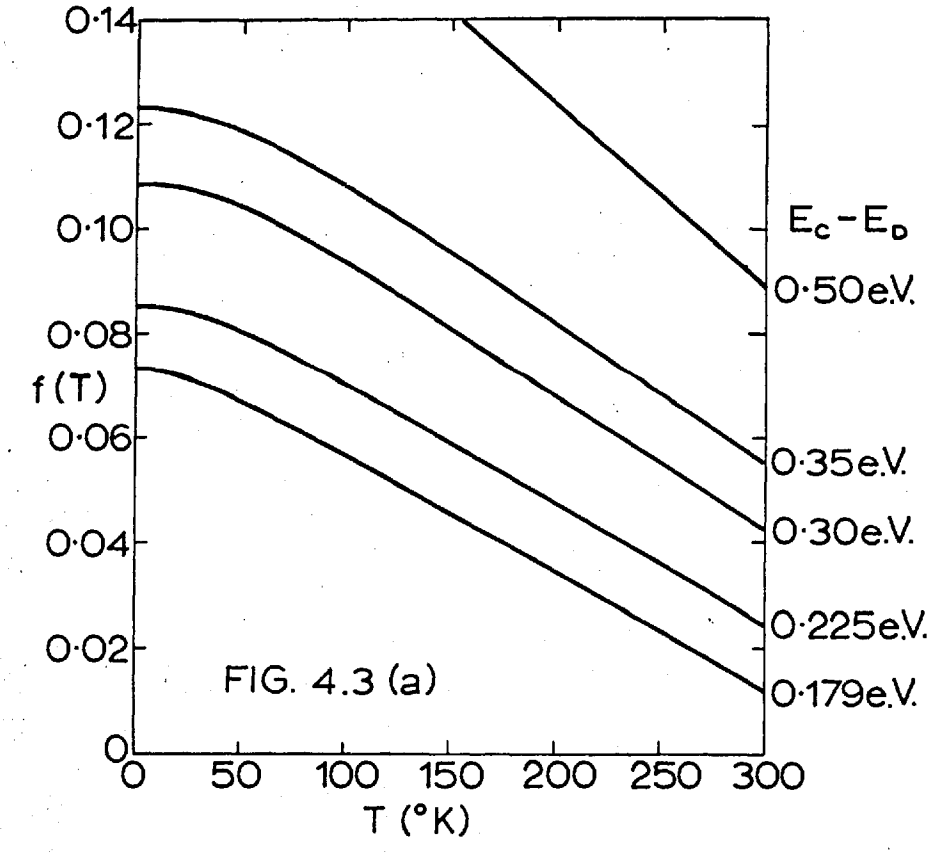

FIG. 4.3 (a)

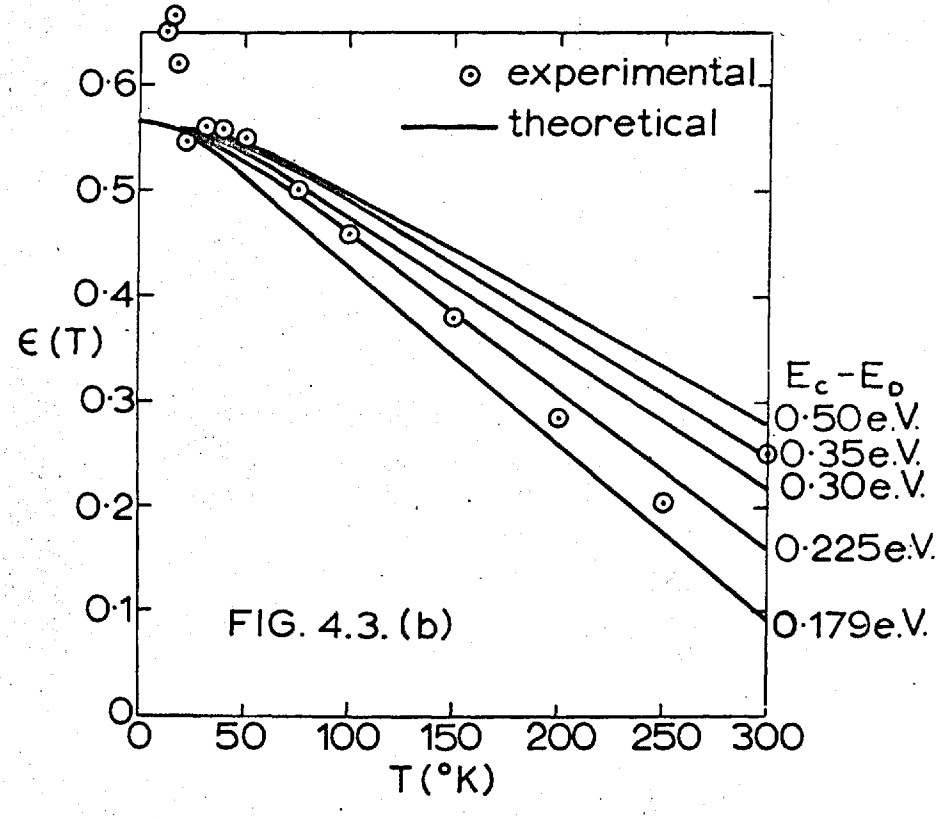

FIG. 4.3. (b)

neglected the lowest temperature points which were subject to a considerable experimental uncertainty. The discrepancy at 300°K they attributed to the onset of intrinsic conductivity.

From the value of λ involved with the best fit the dislocation density was calculated using the relation

$$\lambda = \frac{\rho}{c(N_D - N_A)},$$

and, assuming $c = 3.5\,\text{Å}$

$$\rho = 5.4 \times 10^7 \text{ cm}^{-2}$$

Logan et al. considered two possible dislocation arrangements in their computation of c, the 'dangling-bond' spacing. They suggested that either the dislocations lay parallel to the $\langle 112 \rangle$ bend axis, or that they were in the form of zig-zags extending in the $\langle 112 \rangle$ direction with line segments lying along $[\bar{1}01]$ and $[01\bar{1}]$ directions. The former behaviour was found experimentally in silicon specimens bent in the same orientation by Patel (1958), while Dash (1956) has observed dislocations lying in $\langle 110 \rangle$ directions in bent silicon samples. Logan et al's computation of the dangling-bond spacing on the first model was in error. They state incorrectly that the number of dangling bonds per unit length measured in the $\langle 112 \rangle$ direction would be doubled by the zig-zag arrangement. They overlooked the fact that the $\langle 112 \rangle$ edge dislocation has a pair

of half-planes (see Fig.2.2(c)) and that the straight dislocation has, therefore, the same number of dangling-bonds as the zig-zag one. Logan's recalculation using $c = 6.9$ Å was therefore unnecessary.

The value obtained for ρ was about eight times the equilibrium dislocation density one would expect from the radius of bend of 5 cms. It was also higher than that found by Vogel from etch-pit measurements on specimens bent at a lower temperature (A specimen bent at 550°C to 5 cms radius exhibited an average etch-pit density $\simeq 1 \times 10^7$ cm^{-2}). Logan et alia suggested that the etch-pit method badly underestimates dislocation density for $\rho > 10^7$ cm^{-2} due to overlapping of etch-pits. However, measurements by Rezek and Rosenberg (1963) which compare the etch-pit densities with dislocation densities observed by transmission electron microscopy, indicate that this discrepancy may be too large to be explained by overlapping of pits.

The value of E_D obtained is sensitive to the occupation statistics chosen. Read's calculated curves show that, for the same value of E_D, the minimum energy approximation gives a steeper $f(T)$ curve than the 'Fermi' approximation. In order to obtain a fit to the experimental points with the minimum energy curve, therefore, a smaller value of λ and consequently a

larger value of $f(0^{\circ}K)$ is needed. The required curve would therefore have E_D lower in the forbidden gap. Also, it was noted above that the correct Fermi approximation is that of Bliek (1964) who took into account electron spins. Bliek's Fermi approximation gives a steeper $f(T)$ curve than Read's Fermi approximation (see Section 8.3.2.) and if used in the analysis would result in a value of E_D lower in the forbidden gap than 0.20 e.V. from the conduction band (but not as low as the minimum energy level). An acceptor level of 0.20 e.V. below the conduction band, therefore, is not the only value which could accommodate Logan's results.

The Broudy model.

Broudy (1963) made an important modification to Read's theory to accommodate his experimental results on plastically bent germanium. Since he introduced some important modifications to Logan et al's bending and measurement techniques, a description of his experiments will be given first, and then the application of his analysis to his results will be described.

n-type samples oriented for double slip were deformed by four-point bending. Specimens were gold plated before deformation since a preliminary experiment had indicated that deformed specimens, if not plated, could be contaminated during heating whilst undeformed

specimens, which were not plated, were not contaminated by the same heat treatment. Broudy concluded that an undeformed control sample is not a reliable check of impurity effects. The first measurements were made on unsectioned bent samples, but measurements on sub-sections of these samples indicated that the electrical properties varied considerably throughout each bent specimen, presumably because of a corresponding variation in dislocation density. In order to obtain uniform samples for electrical measurements, therefore, extremely small samples (about 0.05 x 0.05 x 0.11 cms) were cut from the bent beams.

The electrical properties of these small samples did not agree with the requirements of the Read theory in certain respects. In his treatment of the effect of dislocations on conductivity (discussed in Section 4.1.2.), Read considered the scattering of carriers at the space charge cylinders to be purely specular. This led to the prediction that for current flow parallel to an array of dislocations the mobility should be unchanged from that in the undeformed material. This behaviour was found by Logan (1959), but his experiments were confined to a single specimen. In all of Broudy's measurements, the mobility of 'parallel' specimens was less than the 'undeformed' mobility. To accommodate this result Broudy proposed, as a modification to Read's theory, that the

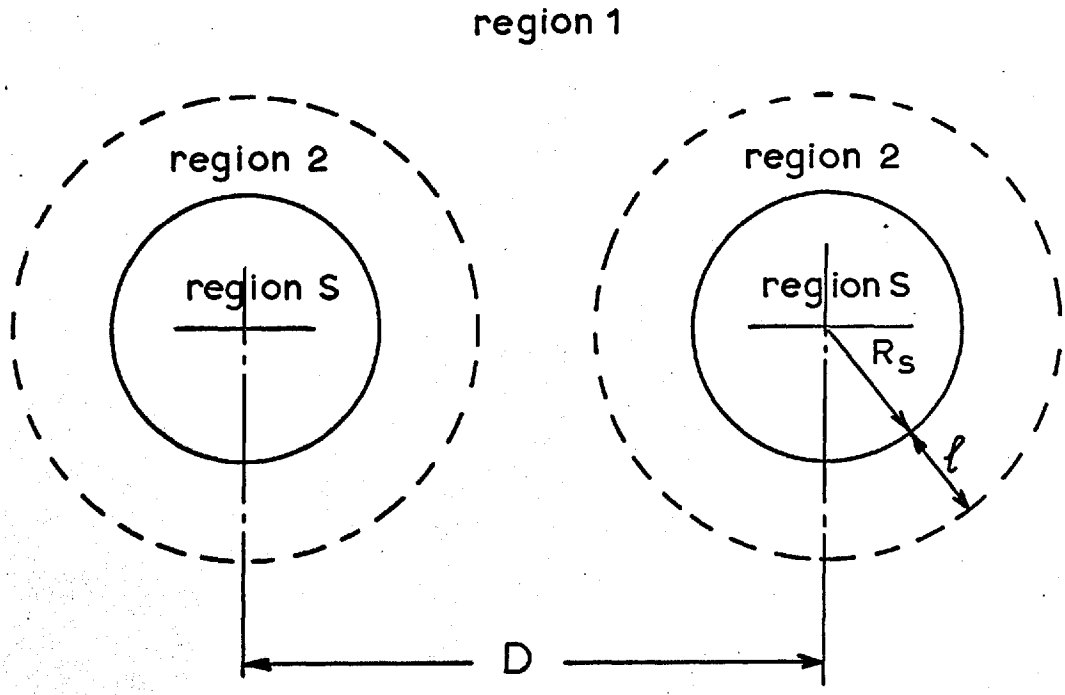

FIG.4.4. The Broudy model.

R_s is the radius of the space charge cylinders.
ℓ is the mean free path of electrons.
D Is the distance between dislocations.

scattering at the space charge cylinders is non specular. This leads to a two-region model for electron scattering at dislocations, shown in Fig.4.4. Region S (also known as the ϵ-region) is the space-charge cylinder of radius R_s. Region 2 (also known as the ϕ-region) is a hollow cylindrical shell of inner radius R_s, and outer radius $(R_s + l)$ where l is the mean free path of the carriers. Within this region the mobility is reduced to a value μ_2, which is less than the value μ_1 outside this region. In this outer region, Region 1, the mobility μ_1 is unchanged from the undeformed mobility.

When the current flows parallel to the dislocations a parallel arrangement of these three regions exists. Broudy applied to this situation a simple model of two conductors in parallel as shown in Fig.4.5.

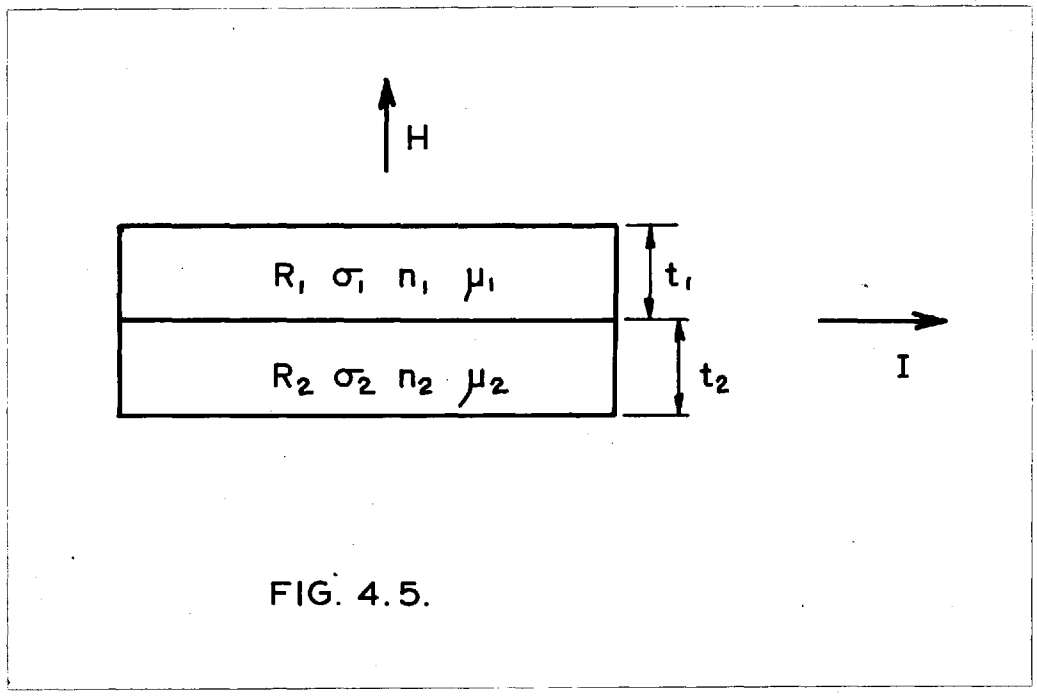

FIG. 4.5.

For this arrangement he obtained

$$R_H = \frac{1}{n_2 q} \frac{[1+\beta_1][1+\beta_1\mu_1\sigma_1/\mu_2\sigma_2]}{[1+\beta_1\sigma_1/\sigma_2]^2} \quad \ldots\ldots (4.21)$$

and

$$\sigma = \frac{(\sigma_2 + \beta_1\sigma_1)}{(1+\beta_1)} \quad \ldots\ldots (4.22)$$

where $\beta_1 = t_1/t_2$

In Broudy's dislocation model there are three rather than two regions, but the properties, R_{S2} and σ_{S2}, of a parallel arrangement of regions S and 2 were first calculated (by (4.21) and (4.22)) and then these properties (R_{S2} and σ_{S2}) were treated as those of a single region which was in parallel with Region 1, in order to calculate the properties of the three-region arrangement. This procedure gave

$$\frac{R_{//}}{R_o} = \frac{1-\epsilon-(1-\theta^2)\phi}{[1-\epsilon-(1-\theta)\phi]^2} \quad \ldots\ldots (4.23)$$

and

$$\frac{\sigma_{//}}{\sigma_o} = [1-\epsilon-\phi(1-\theta)] \quad \ldots\ldots (4.24)$$

where $\theta = \mu_2/\mu_1$

and ϵ = fraction of material in Region S

ϕ = fraction of material in Region 2

Solving (4.23) for ϵ, one obtains

$$\epsilon = 1-\phi(1-\theta) - \frac{1}{2}\frac{R_o}{R_{//}}\left[1+\sqrt{1-\frac{4\phi\theta(1-\theta)}{R_o/R_{//}}}\right] \quad \ldots\ldots (4.25)$$

In this equation, $R_o/R_{//}$ is a measurable quantity, Θ is treated as an adjustable parameter (taken by Broudy to be 0.30 by an a posteriori argument), and from the geometry of the model it is seen that ϕ is given by

$$\phi = \rho\pi(l^2 + 2R_s l) \qquad \ldots\ldots (4.26)$$

where l (the mean free path) was taken to be

$$l = 1.2 \times 10^{-10} \mu(T) T^{1/2}$$

as derived by Logan (1959).

Since this model modifies Read's theory only with respect to scattering, the occupation statistics are not affected. Thus the basic equations (4.3) and (4.17) still hold. Substituting ρ from (4.17) and R_s from (4.3) in (4.26) gives

$$\phi = \frac{\pi\epsilon c(N_D - N_A)}{f}\left\{l^2 + 2l\sqrt{\frac{f}{c\pi(N_D - N_A)}}\right\} \ldots (4.27)$$

Equations (4.25) and (4.27) contain 3 unknowns ϵ, ϕ, f, and so can be combined to give a relation between the unknowns ϵ and f in terms of the measured quantity $R_o/R_{//}$. The following calculation procedure was used.

Application of the Broudy model to experimental results.

First, a value of the dislocation acceptor

level was chosen, say

$$E_c - E_D = 0.520 \text{ e.V.}$$

Then an $f(T)$ curve was calculated by Read's Fermi approximation as before. This is shown for sample G 14 in Fig.4.6(a).

Next, a particular temperature was chosen, say 298°K. At this temperature f (298°K) = 0.123 (from Fig.4.6(a)) and R_o/R_{II}(298°K) = 0.623 (from experiment). Substituting in (4.25) and (4.27) one obtains two equations connecting ϵ and ϕ from which, by elimination of ϕ , ϵ may be obtained.

Similarly, another temperature was chosen, say 250°K, and ϵ(250°K) was calculated as above. In this way a set of $\epsilon(T)$ values was computed. These are shown as circles in Fig.4.6(b)).

Having obtained $\epsilon(T)$ values for this specimen it remains to test the basic relation (4.17) between $\epsilon(T)$ and $f(T)$. (This $f(T)$ is, of course, that originally calculated and shown in Fig.4.6(a)). Again, (4.17) was written as

$$\epsilon(T) = \lambda f(T)$$

and λ was obtained by substituting values for a particular temperature, say 298°K

$$\lambda = \frac{\epsilon(298°K)}{f(298°K)} = \frac{0.325}{0.123} = 2.643$$

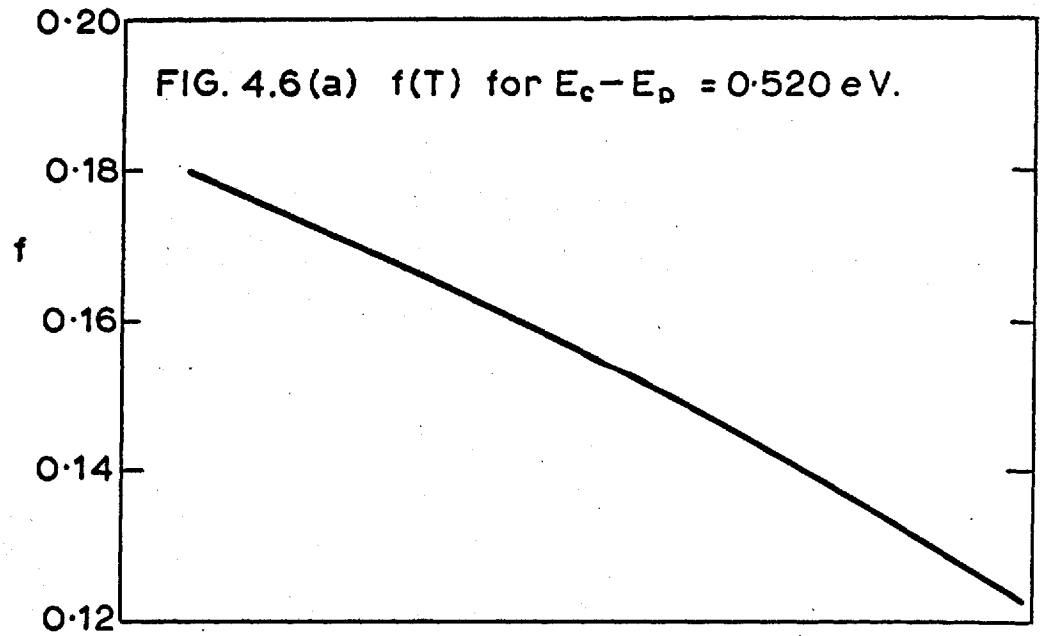

FIG. 4.6(a) f(T) for $E_c - E_D$ = 0·520 eV.

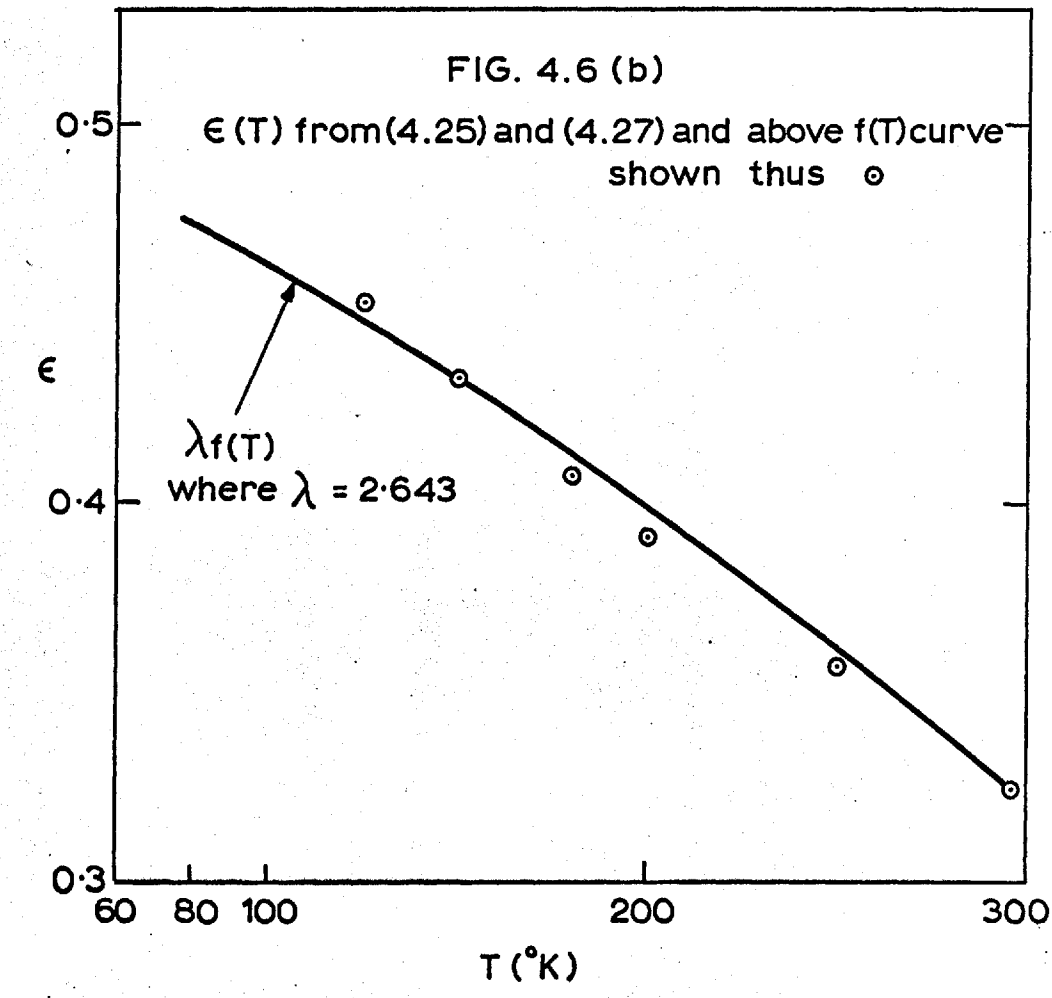

FIG. 4.6 (b)

ϵ (T) from (4.25) and (4.27) and above f(T) curve shown thus ⊙

The curve $\epsilon(T) = \lambda f(T)$ was then calculated from Fig.4.6(a). This is shown as the smooth curve in Fig.4.6(b).

The agreement between the results of the two calculations, shown in Fig.4.6(b), is quite close and it was concluded that the original choice of energy level, $E_c - E_D = 0.520$ e.V., was an accurate one. However, if agreement were not obtained one would repeat the calculation with other choices of acceptor level until reasonable agreement was obtained.

Results obtained from the other deformed specimens could be accommodated by the model with values of $E_c - E_D$ from 0.480 to 0.520 e.V. Agreement with experiment was poor below 125°K, presumably because the ϕ-regions overlapped such that equation (4.26) was not valid. For each specimen ρ, the dislocation density, was calculated from λ as in Logan's calculation above. The dependence of this calculated ρ on distance from the neutral axis, strain rate, temperature of deformation and time and temperature of annealing was qualitatively reasonable. However, the dislocation densities obtained were a factor of three larger than the etch-pit densities obtained by Vogel on samples bent at the same temperature. Both Broudy and Vogel employed constant load deformation. The load used was not given in either

case but the strain rate in Vogel's experiments was much higher than in Broudy's experiments. However, Vogel used a single slip orientation while Broudy's specimens were deformed in double slip. It is therefore impossible to make any detailed comparison with Broudy's calculated dislocation densities.

Comparison of the Read and Broudy models.

Theories of the Hall coefficient in deformed n-type germanium are compared in Table 4.1. On the Read model, in which dislocation space-charge tubes are treated as cylindrical voids, Read, Logan and Broudy are essentially in agreement. The modification introduced later by Broudy can more easily be seen in the approximate value of R_{II}/R_o.

On Read's model $$\frac{R_{II}}{R_o} = \frac{1}{1-\epsilon}$$

on Broudy's model $$\frac{R_{II}}{R_o} \simeq \frac{1}{1-\epsilon-\phi(1-\theta)^2}$$

Thus $$\left(\frac{R_{II}}{R_o}\right)_{Broudy} > \left(\frac{R_{II}}{R_o}\right)_{Read}$$

Broudy's model thus predicts bigger increases in the Hall coefficient of n-type samples on deformation. When $\theta = 0$, this is simply due to the extension of the space charge volume fraction ϵ by a further volume fraction ϕ, the volume of Region 2.

Experimental results on the effect of dislocations

Table 4.1: Theory of Hall effect and conductivity in n-type Germanium containing a parallel array of dislocations.

Author	$R_{\parallel}/R_0$	$R_{\perp}/R_0$	$\sigma_{\parallel}/\sigma_0$	$\sigma_{\perp}/\sigma_0$	$(R\sigma)_{\parallel}/(R\sigma)_0$	$\frac{(R\sigma)_{\perp}}{(R\sigma)_0}$
Read (1955)	Not calculated	$\frac{1}{(1-\epsilon)}$	$(1-\epsilon)$	(1) Distortion $\frac{}{(1-\epsilon)g(\epsilon)}$ (2) Scattering $\frac{1}{\tau}=\frac{1}{\tau_t}+\frac{1}{\tau_D}$	1	$g(\epsilon)$
Logan (1959)	$\frac{1}{(1-\epsilon)}$	$\frac{1}{(1-\epsilon)}$	$(1-\epsilon)$	$(1-\epsilon)g(\epsilon)F(X)$	1	$g(\epsilon)F(X)$
Broudy (1963) Specular Reflection Model	$\frac{1}{(1-\epsilon)}$	Not Calculated	$(1-\epsilon)$	$\frac{(1-\epsilon)}{(1+\epsilon)}$	1	Not calculated
Broudy (1963) Non-Specular Reflection Model	$\frac{1-\epsilon-(1-\theta^2)\phi}{[1-\epsilon-(1-\theta)\phi]^2} \simeq \frac{1}{[1-\epsilon-\phi(1-\theta)^2]}$	Not Calculated	$[1-\epsilon-\phi(1-\theta)]$	$\simeq \frac{[1-\epsilon-\phi(1-\theta)]}{[1+\epsilon+\phi(1-\theta)]}$	$\frac{[1-\epsilon-(1-\theta^2)\phi]}{[1-\epsilon-(1-\theta)\phi]}$	Not calculated

on the Hall coefficient of n-type germanium are compared in Table 4.2. For ease of comparison, carrier concentrations of deformed samples have been calculated using the relation

$$R_H = \frac{1}{\langle n \rangle q}$$

Now, from (4.17), $\frac{n-\langle n \rangle}{\rho/c} = f$, and so values of $\frac{n-\langle n \rangle}{\rho/c}$ were calculated from the Hall coefficient results at $77^{\circ}K$. To compute these values, the dislocation densities were calculated by substituting the measured radii in (2.12) for in none of these experiments were the etch-pit densities given. As expected, the values of $\frac{n-\langle n \rangle}{\rho/c}$ are highest for specimens deformed at lower temperatures, when one would expect the true dislocation density to be much greater than that predicted by (2.12). Specimens deformed at higher temperatures, however, still have $\frac{n-\langle n \rangle}{\rho/c}$ significantly greater than the theoretical value of f ($\simeq 0.1$). This can be accommodated in two ways

1) By analysing the results on the Read model and assuming that the dislocation density is seriously underestimated (as Logan).
2) By postulating a model which predicts higher Hall coefficients in deformed samples (as Broudy).

The values of $\frac{n-\langle n \rangle}{\rho/c}$ found in Logan's specimen and in Broudy's specimens G 15A, B and C (which had been

Table 4.2: Electrical effects of bending N-type Germanium.

Author	Slip systems	Bending temp(^{o}C)	ρ_{theor}	Original $(N_D-N_A)cm^{-3}$	$n-\langle n\rangle$ (77^{o}K)	$\frac{n-\langle n\rangle}{\rho_{theor}/c}$
Pearson,) Read,) Morin)	Double slip	650^{o}C	7×10^{6}	9.5×10^{13}	6.3×10^{13}	0.32
Logan et al.	Single slip	800^{o}C	7×10^{6}	2×10^{14}	1.1×10^{14}	0.55
Broudy G13,	Double slip	550^{o}C	3.5×10^{6}	4.15×10^{14}	2.83×10^{14}	2.84
G13A.	Double slip	550^{o}C	3.5×10^{6}	3.47×10^{14}	2.61×10^{14}	2.61
G13C.	Double slip	550^{o}C	3.5×10^{6}	3.47×10^{14}	1.16×10^{14}	1.16
G14.	Double slip	550^{o}C	3.5×10^{6}	3.67×10^{14}	2.11×10^{14}	2.12
G14A	Double slip	550^{o}C	3.5×10^{6}	3.67×10^{14}	2.53×10^{14}	2.43
G15A.	Double slip	800^{o}C	3.5×10^{6}	3.9×10^{14}	0.9×10^{14}	0.9
G15B.	Double slip	800^{o}C	3.5×10^{6}	3.9×10^{14}	1.2×10^{14}	1.2
G15C.	Double slip	800^{o}C	3.5×10^{6}	3.9×10^{14}	0.4×10^{14}	0.4
G16C.	Double slip	550^{o}C	3.5×10^{6}	3.9×10^{14}	1.1×10^{14}	1.1
G17C	Double slip	550^{o}C	3.5×10^{6}	3.9×10^{14}	1.6×10^{14}	1.62

deformed at the same temperature as Logan's specimen) are in reasonable agreement, being within a factor of two. It is therefore interesting to compare the temperature dependence of the Hall coefficient obtained by the two authors. In order to make this comparison, the results obtained by Broudy for specimens G 14A and G 15B have been analysed on the Read model. G 15 B was almost directly comparable to Logan's specimen since it was deformed at the same temperature (800°C). Now, on the Read model, Logan obtained

$$R_{II}/R_o = 1/(1-\epsilon)$$

$$\therefore \quad \epsilon = 1 - (R_o/R_{II}) \qquad \ldots\ldots (4.28)$$

Values of $\epsilon(T)$ were calculated directly from Broudy's Hall coefficient data using (4.28). These $\epsilon(T)$ values are shown as circles in Fig.4.7. Using $f(T)$ curves computed for these specimens by Read's 'Fermi' approximation (as described in Appendix 1), the curve-fitting procedure was applied to this data exactly as described for Logan's results. Fig.4.7 shows that good agreement can be obtained in both cases when

$$E_c - E_D = 0.30 \text{ e.V.}$$

The discrepancy at high temperatures is attributed to the onset of intrinsic conduction. This value of the dislocation energy level is probably within experimental error of Logan's value of 0.20 e.V.

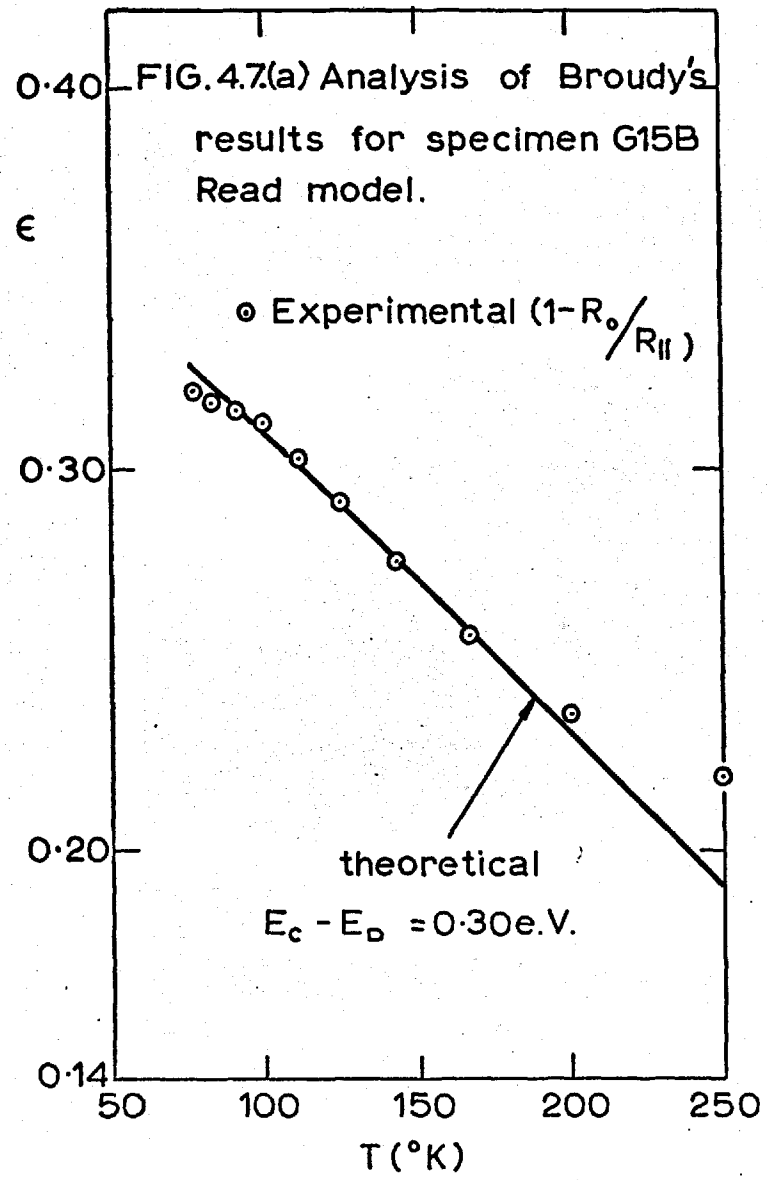

FIG. 4.7.(a) Analysis of Broudy's results for specimen G15B Read model.

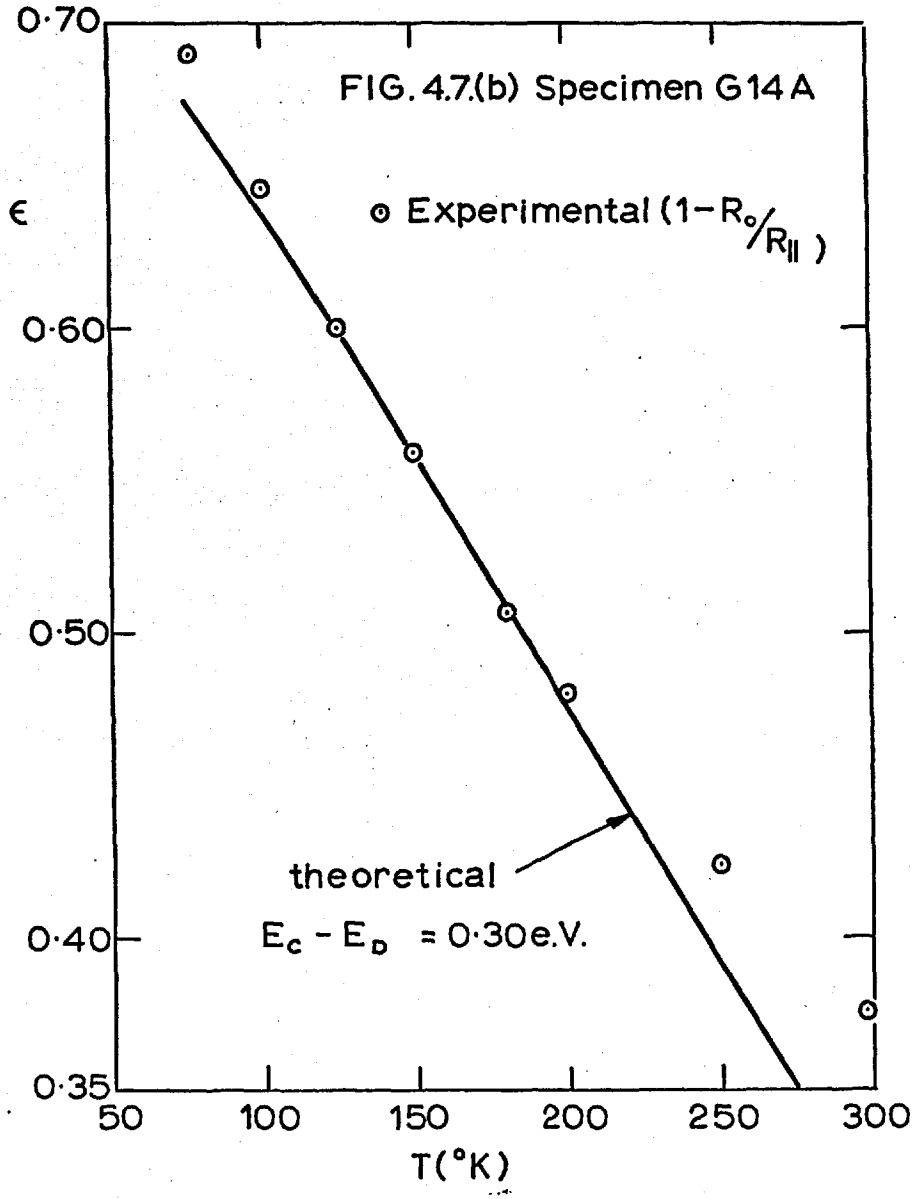

FIG. 4.7.(b) Specimen G14A

From the values of λ obtained in the analysis, dislocation densities were calculated. These are compared in Table 4.3 with ρ_{theor}, the value predicted from the bend radius, and with the dislocation density obtained on the Broudy model (the units being cm^{-2}).

TABLE 4.3

Specimen	ρ_{theor}	ρ Read Model	ρ Broudy Model
G 14A	$3.5 \cdot 10^{6}$	$6.37 \cdot 10^{7}$	$3.9 \cdot 10^{7}$
G 15B	$3.5 \cdot 10^{6}$	$4.13 \cdot 10^{7}$	$2.4 \cdot 10^{7}$

In each case the Read analysis indicates dislocation densities more than an order of magnitude higher than ρ_{theor}, the value predicted from the bend radius. For Logan's specimen the corresponding discrepancy was a factor of eight and thus there is no wide disagreement between Broudy's and Logan's results in this respect.

It has been shown that the Hall coefficient data obtained by Broudy and Logan are not widely in disagreement. Both can be accommodated on the Read model with the dislocation energy level from 0.20 to 0.30 e.V. below the conduction band, and with dislocation densities about an order of magnitude higher than ρ_{theor}. The results of Broudy, however, could also be accommodated on the

Broudy model with the dislocation acceptor level at about 0.50 e.V. below the conduction band, and presumably a Broudy analysis of Logan's results would give a similar level. As shown in Table 4.3, the Broudy analysis gives a dislocation density which is closer to ρ_{theor} than the value given by the Read analysis. Thus, considering the Hall coefficient measurements, the Broudy model is preferred since it predicts more reasonable dislocation densities.

4.1.2. Effect of dislocations on conductivity.

Read's theory.

The measurements of Pearson, Read and Morin, who noted a reduction of conductivity after bending n-type germanium samples, led to a theoretical treatment by Read (1955). For a parallel array of dislocations Read suggested that the conductivity should be highly anisotropic with maximum conductivity parallel to the dislocations and minimum conductivity perpendicular to them. Read considered that the scattering due to dislocations would have only a small effect on mobility for current flow parallel to the dislocations, since the dislocations would be relatively ineffective in scattering the component of momentum parallel to their length. For current flow normal to the dislocations, however, the mobility should be reduced by two factors.

Firstly, the current streamlines would be distorted by the space charge cylinders since the carriers have to follow curved paths winding between the cylinders. Secondly, the conduction electrons would be scattered by the space charge cylinders reducing the mean free time.

Considering the distortion effect, the conductivity for current flow perpendicular to the dislocations follows from (4.12)

$$\sigma_\perp = \frac{\langle I_x \rangle}{\langle E_x \rangle} = q \mu \langle n \rangle g(\epsilon)$$

$$\text{Now } \langle n \rangle = n(1-\epsilon)$$

$$\therefore \quad \sigma_\perp = \sigma_o (1-\epsilon) g(\epsilon) \qquad \ldots\ (4.29)$$

where $g(\epsilon) \left(= \langle E_x \rangle_n / \langle E_x \rangle\right)$ is known as the 'distortion parameter'. ($\langle E_x \rangle_n$ is E_x averaged just over the normal n-type material). Morgan (private communication quoted by Read, 1955) showed that, for small ϵ, $g(\epsilon) = 1 - \epsilon$. For larger values of ϵ he found $g(\epsilon)$ experimentally by cutting circular holes in strips of resistance paper. Juretschke et al. (1956) derived $g(\epsilon) = \frac{1}{(1+\epsilon)}$ theoretically. This agrees with Morgan's experimental values up to $\epsilon \simeq 0.7$. For values of ϵ greater than 0.7, Juretschke's theoretical value of $g(\epsilon)$ was greater than Morgan's experimental value.

Considering the scattering of electrons by the space

charge cylinders, Read calculated the mean free path for dislocation scattering by considering elastic collisions with rigid cylinders. He obtained

$$l_D = \frac{2}{3 R_s \rho} \quad \ldots\ldots (4.30)$$

This derivation, however, contained arithmetical errors. The corrected expression is

$$l_D = \frac{3}{8 R_s \rho} \quad \ldots\ldots (4.31)$$

Logan (1959) confirmed (4.31) by a different method. Read then showed that dislocation and thermal scattering could be combined by adding reciprocal mean free times,

$$\frac{1}{\tau} = \frac{1}{\tau_t} + \frac{1}{\tau_D} \quad \ldots\ldots (4.32)$$

where τ_t and τ_D are the mean free times for thermal and dislocation scattering respectively when each acts alone. However, Read stated that if there were impurity as well as dislocation and thermal scattering then the reciprocal mean free times would not be additive. Using (4.32) he derived expressions for the Hall and drift mobilities in terms of the mean free paths for dislocation and thermal scattering when acting independently. In this paper, (1955), Read did not suggest any method for combining the distortion and scattering contributions to the reduction in mobility.

Application of Read's theory to experimental results.

Logan, Pearson and Kleinman (1959) suggested that the distortion effect is not equivalent to a scattering mechanism but rather represents a redistribution of the electric field. They suggested therefore that the distortion and scattering effects could not be combined by adding reciprocal mobilities as is usual for two scattering mechanisms, but that it would be more appropriate to obtain the resultant mobility reduction by multiplying together the separate reduction factors for the distortion and scattering effects. Logan obtained, for current flow normal to the dislocations

$$\mu_\perp = \mu_o \, g(\epsilon) \, F(X) \qquad \ldots\ldots (4.33)$$

where $g(\epsilon)$ is the distortion factor,

$F(X)$ is the scattering factor,

$$= \frac{3}{2} \int_0^{\pi/2} \frac{\sin^3\varphi \, d\varphi}{1 + X \sin\varphi}$$

where φ = angle between electron direction and dislocation axis.

and $$X = \frac{l}{l_D} = \frac{\text{mean free path in undeformed material}}{\text{mean free path for dislocation scattering.}}$$

Now $$\sigma_\perp = \langle n \rangle q \mu_\perp$$

$$= \langle n \rangle q \mu_o \, g(\epsilon) \, F(X)$$

and $$\langle n \rangle = n(1-\epsilon)$$

$$\therefore \quad \sigma_\perp = \sigma_0 (1-\epsilon)\, g(\epsilon)\, F(X) \quad \ldots\ldots (4.34)$$

Equation (4.34) is equivalent to Read's result (4.29) multiplied by $F(X)$, the scattering factor. Logan found that the mobility predicted by (4.33) was in good agreement with his measured mobility $(R_\perp \sigma_\perp)$ for temperatures above 50°K. It was suggested that the error below 50°K was in the function $g(\epsilon)$ since distortion was the dominant effect at this temperature range. The value of $g(\epsilon)$ may be sensitive to the arrangement of dislocations and a non-regular array of dislocations could have a smaller value of $g(\epsilon)$ than that computed by Morgan for regular arrays. Logan et al. found that the mobility measured parallel to the bending axis was equal to the undeformed mobility. The authors suggested that this was evidence that the dislocations lay parallel to the bend axis and were "smooth". If the dislocations preferred to lie in <110> directions they must have zig-zagged with an amplitude of less than the radius of the space charge cylinders, which on this theory is about $\frac{1}{2}$ micron.

The only adjustable parameter in Logan's mobility analysis is the dislocation density ρ. For this specimen, Logan took

$$\rho = 5.4 \times 10^7 \text{ cm}^{-2}$$

the value obtained in the Hall coefficient analysis. As discussed above this is rather higher than the etch-pit densities of similar specimens. Thus, on this model a high dislocation density is needed to accommodate both Hall coefficient and conductivity results.

The Broudy model.

Broudy (1963) obtained conductivity results which did not agree with those obtained by Logan et alia. Values of $(R\sigma)_{\parallel}/(R\sigma)_0$ were consistently less than unity contrary to Read's prediction that the parallel mobility would be practically unchanged. This deviation from the prediction of the Read theory was a major reason for the development of the two-region model (as described in Section 4.1.1.). This model led to the following relation for the "parallel" conductivity.

$$\frac{\sigma_{\parallel}}{\sigma_0} = \left[1 - \epsilon - \phi(1-\theta)\right] \qquad \ldots\ldots (4.35)$$

This can be compared with the Read relation

$$\frac{\sigma_{\parallel}}{\sigma_0} = \left[1 - \epsilon\right] \qquad \ldots\ldots (4.36)$$

The "parallel" conductivity is therefore reduced by the factor $\phi(1-\theta)$ on the Broudy model. Broudy also calculated $\sigma_{\perp}/\sigma_{\parallel}$ on the Read model using

$$g(\epsilon) = \frac{1}{1+\epsilon} \quad \text{(Juretschke, 1956)}$$

and neglecting scattering.

He obtained

$$\frac{\sigma_\perp}{\sigma_{//}}\left(\begin{matrix}\text{Read}\\ \text{Model}\end{matrix}\right) = \frac{1}{1+\epsilon}$$

By analogy with the transition from (4.35) to (4.36) he wrote

$$\frac{\sigma_\perp}{\sigma_{//}}\left(\begin{matrix}\text{Broudy}\\ \text{Model}\end{matrix}\right) = \frac{1}{[1+\epsilon+\phi(1-\theta)]} \quad \ldots (4.37)$$

After obtaining ϵ and ϕ from the Hall coefficient data (as described in Section 4.1.1.), Broudy used (4.35) and (4.37) to predict the conductivity results. Reasonable agreement between experimental and predicted values of $\sigma_{//}/\sigma_o$ above 125°K was found. Below 125°K the agreement was not so good but, as $(\epsilon+\phi)$ was calculated to be greater than 0.9 in this range of temperature, equation (4.26) would not be valid because of overlap of ϕ regions. Values of $\sigma_\perp/\sigma_{//}$ were overestimated for large ϵ but this is not surprising since Juretschke's relation does not hold in this range.

Comparison of the Read and Broudy models.

The principal difference between the experimental results of Logan et alia and those of Broudy lies in the carrier mobility for current flow parallel to the bend axis. The reduced "parallel" mobility found by Broudy could be ascribed to the presence of dislocations which were not parallel to the bend axis, and then both sets of results are reasonably accommodated by the Read theory.

It is interesting to see whether Logan's results could be accommodated by the Broudy model, particularly the 'parallel' mobility result. Assuming the dislocation acceptor level to be 0.50 e.V. below the conduction band and $\theta = 0.30$ (values used by Broudy), ϵ and ϕ were calculated from Logan's data by Broudy's method. For Logan's specimen one obtains $\epsilon = 0.37$ and $\phi = 0.45$ at 77°K. Using these values, $\sigma_{\parallel}/\sigma_0$ was calculated from (4.35) and, combining with the experimental $R_{\parallel}/R_0$ one obtains

$$(R\sigma)_{\parallel}/(R\sigma)_0 = 0.7 \quad \text{at} \quad 77°K$$

This is probably within experimental error of Logan's value of unity. Thus, considering Logan's and Broudy's conductivity results only, neither set of experimental measurements enables one to discriminate between the two theoretical models.

4.1.3. Summary - dislocations in n-type germanium.

We can draw the following conclusions from the work reviewed in Sections 4.1.1. and 4.1.2.

1) The measurements indicate that dislocations act as acceptor centres in n-type germanium.

2) When analysed on the Read model, the Hall coefficient data give a dislocation acceptor level at about 0.2 e.V. below the conduction band. The dislocation densities deduced are about an order of

magnitude greater than those calculated from the bend radius, and values of $\sigma_\perp/\sigma_o$ are predicted which are in good agreement with experimental ones. The Read model predicts unchanged mobilities in 'parallel' samples, but the reduced mobilities observed in Broudy's samples could be explained in terms of non-parallel dislocations.

3) When analysed on the Broudy model, the Hall coefficient data give a dislocation acceptor level at about 0.5 e.V. below the conduction band. Dislocation densities are about a factor of seven greater than those calculated from the bend radius, and values of $\sigma_{//}/\sigma_o$ are in good agreement with experimental values. The derivation of $\sigma_{//}/\sigma_\perp$ given by Broudy is not rigorous, and predicted values give poor agreement with measurements.

Since it has been shown that the data can be analysed successfully on either model, it remains to compare the two models. Since the Broudy model predicts more reasonable dislocation densities than the Read model, and also accommodates the reduced parallel mobilities, it is concluded that the Broudy model is the more appropriate to these results.

4.2. p-type germanium.

As mentioned in Section 4.1.1., Pearson, Read and

Morin (1953) deformed 15 ohm-cm p-type germanium and observed no change in Hall coefficient and conductivity. This led to the deduction that the energy level of the dislocation-acceptors was above the middle of the energy gap.

Hobstetter and Renton (1962) deformed 5 ohm-cm p-type germanium by tensile deformation and observed changes in the Hall coefficient. Above a certain temperature (called the 'inversion temperature') the Hall coefficient was smaller than the undeformed value, while below this temperature it was greater than the undeformed value. This apparent donor action at low temperatures and acceptor action at high temperatures was analysed in terms of point defects, associating donor centres with interstitials and acceptor centres with vacancies. Hobstetter and Renton did not consider that dislocations could have been responsible in view of the evidence of Pearson, Read and Morin, but there was no independent evidence, such as the study of annealing behaviour, to confirm that point defects rather than dislocations were responsible for the electrical changes.

Bliek (1964) observed changes in the electrical properties of 50 ohm-cm p-type germanium after plastic compression. The form of the Hall coefficient results was very similar to that obtained by Hobstetter and

Renton, having an apparent 'inversion temperature'. Bliek explained his results assuming that dislocations and impurity acceptors can cancel each other's activity by mutual interaction. If the dislocation acceptor level is higher than the impurity acceptor level, the dislocation acceptors will be inactive at low temperatures. Also, some chemical acceptors will have been rendered inactive by interaction with dislocations. There is therefore an apparent donor action at low temperatures. Above a certain temperature, those dislocation acceptors which have not been annulled by impurities will become effective and thus at higher temperatures a net acceptor action will be measured. Thus an 'inversion' can be produced without invoking the creation of donors by deformation. At any temperature, therefore, the total number of holes is the sum of the 'effective' chemical acceptors and the dislocation acceptors

$$p = N_{ca} + N_s f \qquad \ldots\ldots (4.38)$$

where N_{ca} = effective chem acceptors/cm^3

N_s = No. of dislocation acceptor sites/cm^3

f = occupation fraction of dislocation acceptors.

In order to compare the measurements with the theoretical equation (4.38), the Hall coefficient

measurements were used to obtain $\rho(f)$ curves for each specimen in the following way.

The occupation probability was calculated using Fermi statistics taking into account electron spins. Bliek pointed out that each unpaired electron in the unoccupied dangling-bonds could have either a positive or a negative spin. The occupied dangling bonds, however, could have only one arrangement (two electrons with anti-parallel spins). He suggested, therefore, that if N electrons are arranged on M sites, the total number of configurations is equal to the number of ways of arranging N electrons on M sites multiplied by the number of ways of arranging the spins of $(M - N)$ unpaired electrons.

i.e. Number of configurations $= \dfrac{M!}{N!\ M-N!} \times 2^{M-N}$

$= \dfrac{M!}{Mf!\ M(1-f)!} \times 2^{M(1-f)}$

Bliek then recalculated the configurational entropy and obtained the following expression for f by the method used by Read when calculating his Fermi approximation (Section 4.1.1.)

$$\mathcal{E}^* = E_F - E_D + kT \ln\left(\frac{1-f}{2f}\right) \qquad \ldots\ldots (4.39)$$

where $\mathcal{E}^*(f) = \dfrac{d}{df} f\,\mathcal{E}_s(f)$

and $\mathcal{E}_s(f)$ = electrostatic energy per added electron.

We will refer to (4.39) as Bliek's 'Fermi' approximation, and this expression may be compared with Read's Fermi approximation (4.11). The calculation of the electrostatic energy proceeds differently for p-type material since there are no excess donors around the dislocation to ionise and form the space charge cylinder. Instead, Bliek postulated a shielding of the Coulomb field by free holes. This leads to a screened Coulomb potential

$$V(r) = \frac{q}{\kappa_o \kappa_r r} e^{-\gamma r}$$

where q = electronic charge

$\kappa_o \kappa_r$ = dielectric constants

r = distance from accepted electron

and γ = 'screening' parameter.

Using this model, Bliek derived ε^* and obtained

$$\varepsilon^* = -2f E_B \ln\left(1 - e^{-\gamma_c/f}\right) + \frac{E_B \gamma_c e^{-\gamma_c/f}}{1 - e^{-\gamma_c/f}} \quad \ldots\ldots (4.40)$$

where $E_B = \frac{q^2}{\kappa_o \kappa_r c}$.

The Fermi energy was calculated in the usual way in terms of the hole concentration p. Conversely, p could be expressed in terms of the Fermi energy, E_F. Choosing certain values of γ_c and E_D, relations (4.39) and (4.40) were solved to obtain E_F in terms of f. Thus $p(E_F)$ and $E_F(f)$ were known, and from these relations $p(f)$ isotherms were calculated for various values of temperature. Finally, assuming that

$\langle r \rangle = \mu_H / \mu R_{Hq}$ holds for deformed material, the experimental results were plotted on these isotherms. Now, relation (4.38) gives the theoretical $r(f)$ expression. The experimental $r(f)$ curves only obeyed this relation when

$$\gamma_c = 0.1$$

and $E_D = 0.115 e.V.$ above the valence band. These values were applicable to results for all specimens except those which had been very heavily deformed. Bliek explained the results on heavily deformed specimens in terms of double vacancies and showed that, after annealing for one hour at 750°C, the electrical properties could be explained in terms of dislocation acceptors as with the lightly deformed samples. Bliek concluded that these values of γ_c and E_D were the correct ones.

Using relation (4.38), values of N_s and N_{ca} were obtained by graphical solution. The values of N_s obtained were compared with those calculated from etch-pit densities, that is, $\rho_{Etch-Pit}/c$ where c was taken as 4 Å. For all specimens the density of dislocation acceptor sites calculated from etch-pit densities was about twice that calculated from the electrical measurements, but several factors could account for this discrepancy. As these specimens were deformed by plastic compression one would not expect all the dislocations to

be of edge orientation, and, since $C \rightarrow \infty$ for screw dislocations, the value of C was probably underestimated. Also some dislocation acceptors may have been annulled by impurity atoms. The screening parameter γ has been derived by Brooks (1955) as

$$\gamma^2 \simeq \frac{4\pi q^2 p}{\kappa k T}$$

with $p = 10^{14}/cm^3$, $\kappa = 16$, and $T = 77^\circ K$

$$\gamma = 4.13 \times 10^4 \ cm^{-1},$$

and $$\gamma_c = 0.001652.$$

Thus Bliek's value of γ_c is nearly two orders of magnitude higher than the theoretical value. If $\gamma_c \sim 10^{-3}$ were used in the analysis of the experimental results, the spacing of occupied acceptors would increase, and the number of acceptor sites calculated from the electrical measurements would be much greater than the number calculated from the etch-pit densities.

Bliek's assumption that the expression

$$R_H = \frac{\mu_H}{\mu \langle p \rangle q}$$ holds for deformed material is

questionable since the Bliek model for p-type material corresponds with the Broudy, rather than the Read, situation for n-type material. The charged dislocation in Bliek's model is screened by free holes so that the material consists of two conducting regions rather than one conducting and one insulating region. However, Broudy's analysis cannot be applied directly

unless a parallel array of dislocations is introduced, as, for example, in a bent sample.

4.3. The effect of dislocations on the properties of minority carriers.

Wertheim and Pearson (1957) measured carrier lifetime in plastically bent samples of p- and n-type germanium by the pulsed van de Graaff method. They found that the introduction of about 10^7 dislocations/cm^2 reduced the lifetime of 2.2 ohm-cm p-type germanium from about 10^{-4} sec to 10^{-7} sec at room temperature. The authors explained their results in terms of a dislocation energy level approximately at the centre of the forbidden gap.

Bell and Hogarth (1957) showed that the diffusion length of minority carriers, as measured by the travelling light spot method, was anisotropic in p-type silicon and in p- and n-type germanium crystals containing parallel arrays of edge dislocations. The diffusion length measured parallel to the array was greater than that measured perpendicular to the array. Bell and Hogarth explained their results assuming that there was a potential barrier to minority carriers surrounding each dislocation, tending to keep them away from the low lifetime dislocation region. This model

suggested that anisotropies would be more marked for crystals in which the dislocations were highly polygonised than for crystals with a random array. When interpreting their results, Bell and Hogarth assumed the diffusion constant, D, to be constant and suggested that the anisotropy observed in the diffusion length, L, resided in the carrier lifetime τ. However, Arthur et al. (1958) measured D by the simultaneous measurement of phase and amplitude in the travelling light spot experiment. They found that, in n-type germanium, D was not isotropic. In p-type germanium, however, D was isotropic and thus all the anisotropy appeared to reside in τ.

At high electric fields the drift mobility of holes in n-type germanium was found to be anisotropic, but no similar effect occurred in p-type material. Arthur et al. explained their results by assuming that a dislocation line in n-type material may be considered as a thread of p-type material, if sufficient dislocation acceptor sites are occupied. As a p-type region represents a potential minimum for holes, injected carriers will be captured by the dislocations where they will become majority carriers. When an injected hole is captured by a dislocation, a space-charge signal is propagated down the line with a velocity dependent on the losses in the line so that another hole is emitted a finite time later at some distance from the point of

capture. In this manner the diffusion of holes along a dislocation can be enhanced without any corresponding increase in hole mobility. In p-type material, Arthur et al. suggested that the dislocations will accept electrons, the negatively charged line repelling minority carriers (electrons), and providing a mechanism (similar to that of Bell and Hogarth) by which τ may be anisotropic. No anisotropy of D would therefore be expected in p-type material.

A quantitative discussion of the anisotropic effects has been given by Gibson and Paige (1958), who modified Read's model of dislocation-acceptors to include a free hole contribution to the space charge. Read considered dislocations in low resistivity n-type germanium at low temperatures and was thus able to neglect the contribution of free holes to the space charge. The experiments of Arthur et al., however, were performed on high resistivity n-type germanium at room temperature and thus it was necessary to consider the contribution of free holes. In Gibson and Paige's model, a dislocation in n-type material forms an 'inversion-cylinder' of p-type material, while a dislocation in p-type material forms a p^+ cylinder. Direct experimental evidence for the existence of inversion cylinders in one of the crystals used by Arthur et al. (1958) has been presented by Hogarth and Baynham (1958) who observed p-type

rectification at dislocation walls in n-type germanium. Gibson and Paige (1958) estimated the energy level of the dislocation-acceptors, using the fact that anisotropic effects had been observed in 12 ohm-cm p-type germanium. To explain these effects in p-type material, Bell and Hogarth (1957) assumed there was a potential barrier to minority carriers surrounding the dislocation. Gibson and Paige suggested that the ratio of the mean separation between ionised acceptors to the average distance between electrons trapped at dislocation sites must be equal to or greater than unity if there is to be an effective barrier. Using this criterion, Gibson and Paige estimated the dislocation acceptor level (by Fermi statistics) as not more than 0.4 e.V. from the top of the valence band. This is significantly less than the value of 0.5 e.V. given by Logan et al.(1959).

4.4. General conclusions from the study of dislocations in germanium.

The measurements of Bliek (1964) described in Section 4.2 indicated that dislocations act as acceptor centres in p-type material. Although there are weaknesses in the quantitative analysis, the results clearly indicate that the dislocation acceptor level lies below the Fermi level in p-type germanium, i.e. below the middle of the forbidden gap. The p-type measurements

therefore suggest that the Broudy analysis is appropriate for dislocations in n-type material since, unlike the Read model, this indicated a dislocation acceptor level below the centre of the forbidden gap. The anisotropic properties of minority carriers, described in Section 4.3, support this conclusion since these measurements also indicated an acceptor level which was significantly below that given by Logan et al.(1959).

CHAPTER 5.

ELECTRICAL PROPERTIES OF DISLOCATIONS IN INDIUM ANTIMONIDE.

5.1. Effect of dislocations on the Hall coefficient.

Haasen (1957) suggested that, because of the difference in core structure of In- and Sb-dislocations, they might have different tendencies for trapping conduction electrons.

Gatos, Finn and Lavine (1961) performed experiments designed to distinguish between the effects of the different dislocation types. Specimens oriented for double slip were bent to produce an excess of In- or Sb-dislocations. After In-bending an increase in Hall coefficient was observed and it was deduced that acceptor centres were introduced by the dislocations. After Sb-bending, the Hall coefficient increased except under certain conditions. When specimens of $N_D - N_A \sim 1 \times 10^{15}$ cm^{-3} were bent to a radius of more than 20 cms there was a decrease in the Hall coefficient, and even then the effect was not reproducible. Gatos believed that the increase in Hall coefficient was not associated with Sb-dislocations but with other (unspecified) effects of bending.

Gatos concluded from these somewhat ambiguous

experimental results that Sb-dislocations act as donor centres and In-dislocations act as acceptor centres. However, the unspecified effects of bending which were assumed to be responsible for the increase in Hall coefficient in the Sb-bent samples could presumably have been responsible for the increase in Hall coefficient in the In-bent samples also. Furthermore, the conditions given for donor action in Sb-bent samples (i.e. a high concentration of donors and thus a high Fermi level) are conditions under which one would least expect donors to be ionised. For these reasons, therefore, and because of the lack of reproducibility of these results, it seems likely that many of the effects observed by Gatos et alia were not associated with dislocations but with point defect or impurity centres.

The deductions made by Gatos et al. that Sb-dislocations acted as donors and In-dislocations as acceptors, are consistent with the model of dislocations in indium antimonide proposed by Gatos et al.(1960 a). In this model the In-dislocation has triply bonded In-atoms at the edge of its extra half plane. They suggested that the In-atom contributes one electron to each satisfied bond and thus there are no electrons available for the fourth dangling bond. They predicted from this model that In-dislocations should act as acceptor centres. However, in the bulk material the

In-atom clearly does not contribute one electron to each bond since it has three electrons available for four bonds. In a similar way, Gatos et al. assumed that the Sb-atom at the edge of the extra-half-plane contributes one electron to each satisfied bond and has two electrons available for the fourth 'dangling-bond'. Gatos et al. predicted that the Sb-dislocations should act as donor centres. However, it is again clear that the Sb-atom in the bulk material will not contribute one electron to each bond since it has five electrons for four bonds. Thus, the model of Gatos et al. would appear to be a great oversimplification.

Holt (1960) pointed out the above objections to the Gatos model. In his view each dangling bond from an Sb-atom must contain on average $1\frac{1}{4}$ electrons and not 2 as assumed by Gatos. Similarly each bond from an In-atom contains $\frac{3}{4}$ electron and not zero as assumed by Gatos. Holt also pointed out that on the Gatos model the crystal would have a net electrical dipole moment directed along $<111>$ due to the unsatisfied bonds at the surface. Holt introduced a resonance idea to overcome this difficulty. It was suggested that an In-dangling bond is made up by resonance between zero-electron and one-electron tetrahedral orbitals in the ratio of one to three, and similarly for the Sb-dangling bonds. He also took account of the small degree of ionicity of

bonding. Holt's model predicts the following electrical behaviour of dislocations.

The In-dislocation has three one-electron dangling bonds, each constituting an acceptor level, to each zero-electron dangling bond which gives rise to two acceptor levels. One of the latter is probably near the valence band. The Sb-dislocation has three one-electron bonds, constituting acceptor levels, to each two-electron bond which gives rise to two donor levels, one of which is probably very near the conduction band. Thus Holt's theory predicts that the behaviour of the dislocations will depend on the position of the Fermi-level relative to the acceptor and donor levels of the dangling bonds. However, in n-type material it is probable that In-dislocations will act as acceptors. The behaviour of Sb-dislocations will depend on the relative position of their acceptor and donor levels.

In a reply to Holt's objection, Gatos (1961) suggested that the net dipole moment will not extend throughout the crystal, but, at the worst, will induce a space charge at the surface only. Gatos therefore believed the objection to be unfounded.

Duga (1962) measured the electrical effects of bending indium antimonide, but did not distinguish between In- and Sb-bending. The geometry of bending

was not given unambiguously but the possible geometry suggests that at least two slip systems were favoured. The Hall coefficient was increased after bending, indicating an addition of acceptor centres. Hall coefficient data were analysed in the same way as Logan (1959), that is, using the relation

$$R_H(\text{deformed}) = \frac{1}{\langle n \rangle q}$$

The energy level of the dislocation acceptors was then deduced from the temperature dependence of ϵ, where

$$\langle n \rangle = n(1 - \epsilon)$$

The details of the method were not given, but from his analysis Duga obtained $E_D \simeq 0.14$ e.V. below the conduction band.

Broudy (1963) made similar measurements on samples bent in a double slip orientation, without regard to crystal polarity. The Hall coefficient was increased after bending and Broudy found that the results could be analysed in terms of his two-region model developed for germanium. With regard to this model Broudy pointed out that, because of the high mobility in indium antimonide, the mean free path of electrons is very large. Using a simple acoustical scattering model, the mean free path at 77°K is about 2×10^{-4}cm. Thus, at only modest

dislocation densities the mean free path is comparable to the spacing of dislocations. On the Broudy model, most of the material will be in Region 2, that is, within one mean free path of the space charge tubes.

Thus, in indium antimonide, it is to be expected that the Broudy model will predict very much lower dislocation densities than the Read model, provided total overlap of ϕ regions does not occur. However, even on the Broudy model, the electrical measurements of Broudy gave a theoretical dislocation density of $1 - 2 \times 10^7$ cm^{-2}, whereas the dislocation density calculated from the bend radius is about 1×10^6 cm^{-2}. Broudy was not able to deduce a dislocation-acceptor level because of wide scatter in his experimental results.

Summary of the effects of dislocations on the Hall coefficient of indium antimonide.

Measurements on indium antimonide are summarised in Table 5.1. Acceptor behaviour of dislocations was inferred in all cases except in the Sb-bent specimens of Gatos when donor behaviour was inferred. This case will be included in the discussion of the magnitude of the effects since the same trends are observed in this specimen. Carrier concentrations of deformed specimens have been calculated by the relation $\langle n \rangle = 1/R_H q$ Now, from (4.17), $\frac{n - \langle n \rangle}{\rho/c} = f$, and so values of

Table 5.1: Summary of previous work on InSb. Measurements relate to 77°K.

Author	Deformation	Radius of Bend	n (cm^{-3})	$\langle n \rangle$ (cm^{-3})	μ_o ($cm^2 V^{-1} sec^{-1}$)	$\mu_\perp$ ($cm^2 V^{-1} sec^{-1}$)	$\frac{n-\langle n \rangle}{\rho/c}$
Gatos et al. (1961)	Double slip, 300°C in air In-bent	15 cm	1.5×10^{15}	8.2×10^{14}	2.2×10^{5}	8.6×10^{4}	10.7
"	As above but Sb-bent	8 cm	3.9×10^{15}	1.0×10^{16}	1.7×10^{5}	5.6×10^{4}	51.2 *
Duga (1962)	Multiple slip, majority dislocation not identified (300°C in air)	200 cm	4.8×10^{14}	2.5×10^{14}	2.6×10^{5}	1.8×10^{5}	44.2
"	"	15 cm	2.6×10^{15}	1.04×10^{15}	2.2×10^{5}	9.3×10^{4}	24.4
Broudy (1963)	Double slip, 305°C, majority dislocation not identified	25 cm	6.9×10^{14}	5.7×10^{14}	3.6×10^{5}	2.0×10^{5}	3.3

* This relates to donor action. Last figure is $\frac{\langle n \rangle - n}{\rho/c}$.

$\frac{n-\langle n\rangle}{\rho/c}$ were calculated to compare with the theoretical value of f. To compute these values of $\frac{n-\langle n\rangle}{\rho/c}$, the dislocation densities were calculated by substituting the measured radii in (2.12), for in none of these experiments were the etch-pit densities given. Assuming a dislocation energy level lying near the valence band, one can calculate the maximum possible value of f, the occupation fraction of dislocation-acceptors, from Read's Fermi approximation (relation (4.11)). At $77^{\circ}K$, for material with $N_D - N_A = 1 \times 10^{14}/cm^3$ this value is $f = 0.091$. As pointed out by Duga, the values of $\frac{n-\langle n\rangle}{\rho/c}$ are all at least an order of magnitude greater than this maximum theoretical value. The discrepancy is also much larger than in the case of germanium (Table 4.2). It therefore seems unlikely that underestimation of dislocation densities could account for this discrepancy. The Broudy model could, in principle, account for these high values of $\frac{n-\langle n\rangle}{\rho/c}$ but it is probable that the diffuse scattering cylinders would have to overlap to a large extent, and the mobility in these diffuse scattering regions would have to be very low, in order to account for the observed electrical effects in terms of the dislocation density indicated by the bend radius. In Broudy's results (which could only be explained on the Read model if the dislocation density were a factor of 30 greater than that calculated from the bend radius) the

dislocation density calculated on the Broudy model was a factor of ten greater than the value calculated from the bend radius, and the results of Duga and Gatos et al. would give larger discrepancies. It appears, therefore, that either a new model is needed to accommodate the results in Table 5.1. or that centres other than dislocation centres were responsible. The presence of point defects seems likely since all specimens were deformed in double or multiple slip. Impurities might also have been important in the experiments of Duga and Gatos et al. since the deformation was carried out in air.

5.2. Effect of dislocations on conductivity.

Duga (1962) made conductivity measurements on specimens bent to radii of 15 cms to 200 cms. From these bend radii Duga calculated theoretical dislocation densities of 2×10^{6} cm^{-2} to 1×10^{5} cm^{-2} but, as discussed in Section 2.3.1., it is not clear how these values were calculated. The carrier mobility parallel to the [112] bend axis was stated to be equal to the mobility of the undeformed specimen but no measurements were presented. This parallel mobility measurement is a very strange result in view of the fact that the dislocation lines could not have been parallel to the bend axis in any of the possible slip planes. Duga suggested that the

dislocations produced by multiple slip interacted to produce a set of zig-zagged dislocations extending parallel to the bend axis, but it seems extremely unlikely that this would occur.

Duga suggested that the unaltered 'parallel' mobility was in agreement with the prediction of Read's theory. He then treated the mobilities in the 'perpendicular' samples by the method of Logan et al. (1959). As a first approximation, scattering by acoustic phonons was assumed to be the only important scattering mechanism in the undeformed samples. The undeformed mean free path was thus obtained from

$$l_A = \frac{3\mu_A}{4q}\left(2\pi m^* k T\right)^{1/2} \qquad \ldots\ldots (5.1)$$

substituting the undeformed mobility for μ_A. Then, using the Read relation for the mean free path for dislocation scattering, Duga wrote

$$l_D = \frac{3}{8 R_s \rho} = \frac{3}{8}\left(\frac{\pi}{\rho \epsilon}\right)^{1/2} \qquad \ldots\ldots (5.2)$$

Duga calculated the mobility in the deformed samples from Logan's expression (4.33)

$$\mu_\perp = \mu_o \, g(\epsilon) \, F(X)$$

where $X = l_A / l_D$

where the value of ϵ was obtained from the Hall coefficient results. The dislocation density was adjusted to give the best fit with the experimental

values. Reasonably good agreement between experimental and calculated values of $\mu_\perp$ was found using dislocation densities less than a factor of two larger than those calculated from the bend radii. Although this agreement is probably much better than can reasonably be expected, Duga refined the analysis by including impurity scattering. He did this by adding reciprocal mean free times for the various scattering mechanisms

$$\frac{1}{\tau} = \frac{1}{\tau_A} + \frac{1}{\tau_D} + \frac{1}{\tau_I} \qquad \ldots\ldots (5.3)$$

where τ_A = relaxation time for acoustic scattering,

τ_I = " " " impurity scattering,

and τ_D = " " " dislocation scattering

although Read (1955) had earlier suggested that this procedure was incorrect. Using (5.3) Duga obtained the following expression for the mobility in the perpendicular sample

$$\mu_\perp = \mu_A \, g(\epsilon) \, F(x) \, K(\beta^*) \qquad \ldots\ldots (5.4)$$

where $$K(\beta^*) = \int_0^\infty \frac{x^3 e^{-x}}{x^2 + \beta^*} \, dx$$

and $$x = \frac{\text{Carrier energy}}{kT}$$

The additional term $K(\beta^*)$ represents the effect of impurity scattering in the deformed sample. β^* is given by the relation

$$\beta^* = \frac{2Q\beta}{\pi}\int_0^{\pi/2} \frac{d\varphi}{1 + X\sin\varphi} \qquad \ldots\ldots (5.5)$$

where $\beta = 6\,\frac{\mu_A}{\mu_I}$ = 6. $\frac{\text{mobility for acoustic scattering}}{\text{mobility for impurity scattering}}$

(in the undeformed sample).....(5.6)

φ = angle between electron direction and dislocation axis.

and Q is a factor which takes into account the change in the degree of impurity screening resulting from the decreased carrier concentration and is a function of n and $\langle n\rangle$. Q is given by the relation

$$Q = \frac{\beta_2}{\beta} \qquad \ldots\ldots (5.7)$$

where β and β_2 are the values of $6\mu_A/\mu_I$ in undeformed samples containing n and $\langle n\rangle$ conduction electrons respectively. (β is thus $6\mu_A/\mu_I$ in the original sample).

From the Brooks-Herring treatment of impurity scattering, Duga obtained

$$Q = \frac{\ln(1+b'') - [b''/(1+b'')]}{\ln(1+b') - [b'/(1+b')]} \qquad \ldots\ldots (5.8)$$

where $b' = \frac{6}{\pi}\,\frac{m^*\varkappa(kT)^2}{n e^2 \hbar^2}$

and $b'' = \frac{6}{\pi}\,\frac{m^*\varkappa(kT)^2}{\langle n\rangle e^2 \hbar^2}$

Now, substituting (5.7) into (5.5) and rearranging, one obtains

$$\beta^* = \beta_2 \frac{2}{\pi} \int_0^{\pi/2} \frac{d\varphi}{1 + X \sin\varphi}$$

The factor β^* thus represents combined impurity and dislocation scattering in the deformed sample.

It is important to note that the mobility of the undeformed sample, μ_o, does not occur in relation (5.4). Instead, μ_A, the mobility when only acoustic scattering exists, appears in the relation. The undeformed mobility, μ_o, is less than μ_A because of impurity scattering and is given by the relation

$$\mu_o = \mu_A \, K(\beta) \qquad \ldots\ldots (5.9)$$

Duga calculated the dislocation density by means of equation (5.5). First, he calculated β^* by several methods, for example from the ratio of weak- to the strong-field limit of the Hall coefficient of the deformed sample. Bate, Willardson and Beer (1959) showed that the strong-field limit was independent of scattering mechanism while the weak-field limit was a function of the degree of impurity scattering (and presumably the degree of dislocation scattering). Thus the ratio of the weak-to the strong-field limit could yield the effective impurity scattering parameter β^*. Then Duga rewrote (5.5) in the form

$$\frac{\beta^*(T_1)}{\beta^*(T_2)} = \frac{Q(T_1)}{Q(T_2)} \cdot \frac{\beta(T_1)}{\beta(T_2)} \cdot \frac{\nu(T_1)}{\nu(T_2)} \qquad \ldots (5.10)$$

where $\nu(T) = \int_0^{\pi/2} \frac{d\varphi}{1 + X \sin\varphi}$

In (5.10) $\frac{\beta^*(T_1)}{\beta^*(T_2)}$ was measured as described above, Q was calculated from Hall coefficient measurements on the deformed and undeformed samples, $\frac{\beta(T_1)}{\beta(T_2)} = \left(\frac{T_2}{T_1}\right)^3$ (since $\mu_A \propto T^{-3/2}$ and $\mu_I \propto T^{+3/2}$) and thus $\frac{\nu(T_1)}{\nu(T_2)}$ was calculated.

Then, since $X(T_2) \simeq X(T_1).T_1/T_2$, the dislocation scattering parameter X could be calculated, from which the dislocation density was obtained. The dislocation densities obtained by this method were lower than those calculated by the first method and were in agreement both with etch-pit measurements and with the dislocation densities which Duga had calculated from the bend radii. As discussed in Section 2.3.1. the agreement of etch-pit density with the dislocation density calculated from the bend radius suggests either an error in the calculation of the density from the bend radius or that the etch-pit technique underestimates the dislocation density.

This calculation was made on the assumption that scattering by acoustic phonons is the dominant lattice scattering mechanism. Ehrenreich (1959) has shown that polar scattering is dominant over the acoustic modes at higher temperatures and may also be important at 77°K.

The acoustic scattering formulae, therefore, may not be appropriate. The important factor in this work, however, is the wide discrepancy between the results of the Hall coefficient and mobility analyses. It was shown in Section 5.1. that, in order to accommodate the Hall coefficient results on the Read model, the dislocation density must be orders of magnitude greater than the value calculated from the bend radius. By contrast, the mobility results could be accommodated successfully with dislocation densities close to those calculated from the bend radii. This comparison indicates that the Hall coefficient changes in Duga's specimens were probably dominated by the introduction of randomly distributed centres (such as impurities or point defects) which would be expected to produce large changes in the Hall coefficient with only a relatively small reduction in mobility. However, assuming the Hall coefficient changes were due entirely to randomly distributed centres, the observed mobility changes are larger than expected. Thus dislocations probably dominated the mobility changes, but point defects or impurities probably dominated the changes in Hall coefficient.

5.3. Effect of crystal boundaries on electrical properties.

Mueller and Jacobsen (1962) prepared bicrystals in which the grain boundaries had misfit angles of 6°. According to their model, the boundaries consisted of rows of In- or Sb-dislocations. Current flow across these boundaries in n- and p-type material was studied by measuring potential profiles across the boundaries. According to their model, boundaries which accept electrons in n-type material should charge up negatively and present a barrier to current flow. Similarly, boundaries donating electrons in p-type material should act as barriers. However, donors in n-type material should not act as barriers since the local electron concentration will be increased, thus increasing the conductivity in that region to compensate for scattering by the donor centres. In these experiments In-boundaries were found to present a barrier to current flow in both n- and p-type material. Sb-boundaries acted as barriers only in p-type material. In accordance with their model, therefore, Mueller and Jacobsen deduced for In-boundaries donor behaviour in p-type material and acceptor behaviour in n-type material. For Sb-boundaries they deduced donor behaviour in p-type material and non-acceptor behaviour in n-type material. From this evidence it was deduced that In-dislocations act as donors in p-type material and acceptors in n-type material, and that Sb-dislocations act as donors in p-type material and

do not act as acceptors in n-type material. This reasoning is doubtful, however, since dislocations in a boundary could exhibit different properties from those observed when freshly introduced by deformation. It is likely that there were Coulombic interactions between occupied sites on neighbouring dislocations in the boundary, which were probably about 40 Å apart. Thus the properties of dislocations in a low angle boundary may be quite different from those of widely spaced dislocations. Also the possibility of impurity segregation to such a boundary while near the melting temperature during the growing process is much greater than that for dislocations introduced by deformation at relatively low temperatures. Furthermore, the effects observed in the potential profile measurements could have been produced by the high density of other dislocations observed near the boundary.

5.4. Summary.

The only experiments designed to distinguish the two types of dislocation (Gatos et al. 1961, Mueller and Jacobsen, 1962) produced inconclusive results regarding widely-spaced dislocations. Other experiments which did not distinguish between In-bending and Sb-bending associated dislocations with acceptor centres but the quantitative results did not agree with the Read model

for indium antimonide. The most extensive series of experiments (Duga 1962) gave results which indicate that point defects or impurities were introduced as well as dislocations.

PART II.

EXPERIMENTAL PROCEDURE, RESULTS AND DISCUSSION.

Part II is divided into four chapters. Chapter 6 describes the experimental procedure and Chapters 7 and 8 the experimental results. In Chapter 7 the results of the deformation experiments and of the investigation into the reliability of the etch-pit techniques are given, and in Chapter 8 the results concerned with the electrical effects of plastic deformation are presented. Chapters 7 and 8 also include detailed discussion of the results, but the general discussion is contained in Chapter 9. Some original computations and theoretical derivations are contained in the Appendix.

CHAPTER 6.

EXPERIMENTAL PROCEDURE.

6.1. Plastic deformation.

6.1.1. Specimen preparation.

Single crystals of indium antimonide grown by the Czochralski (1917) technique were supplied by J.B. Mullin, O. Jones, and A. Priest of R.R.E., Worcs. Carrier concentration measurements at $77^{o}K$ on specimens cut from the seed end of the crystals were made by Mullin and co-workers with the following results

Crystal	Type	Carrier concentration
C226/Ge	p-type	$N_A - N_D = 6.3 \times 10^{14}$ cm^{-3}
C229/U	n-type	$N_D - N_A = 4.4 \times 10^{13}$ cm^{-3}
C393/U/<210>	n-type	$N_D - N_A = 4 \times 10^{12}$ cm^{-3}
C412/U/<210>	n-type	$N_D - N_A = 3.5 \times 10^{12}$ cm^{-3}
C430/U/<210>	n-type	
C431/U/<210>	n-type	$N_D - N_A = 6 \times 10^{14}$ cm^{-3}
CT200	n-type	

The carrier concentration varied by at least a factor of two along the growth direction, but properties across a

diameter were very uniform. To obtain specimens which were uniform along their length, therefore, specimens were cut with their longest dimension perpendicular to the growth direction. For the specimen orientation required, crystals grown in the <210> direction were needed, but, as discussed in Section 3.1., this growth direction introduces problems of twinning. These problems were largely overcome by Mullin and co-workers who produced the above crystals mainly free from twins. Specimens containing large twins were rejected before deformation, but occasionally internal twins were not exposed at the surface. If twins were revealed by sectioning after deformation, the specimens were rejected at this stage. The size of the virgin crystals was typically about 2.5 cm in diameter and about 5 cm in length.

To obtain slip on only one of the $\{111\}$ <110> slip systems during plastic bending, samples were prepared with a slip plane and a slip direction at 45° to the neutral axis as shown in Fig.6.1. Crystals were oriented by means of the Laue back-reflection x-ray technique and sectioned with a silicon carbide slitting wheel, great care being taken to avoid cracking of specimens, since indium antimonide is very brittle at room temperature. The crystal was first cut approximately perpendicular to the growth axis into 'slices'

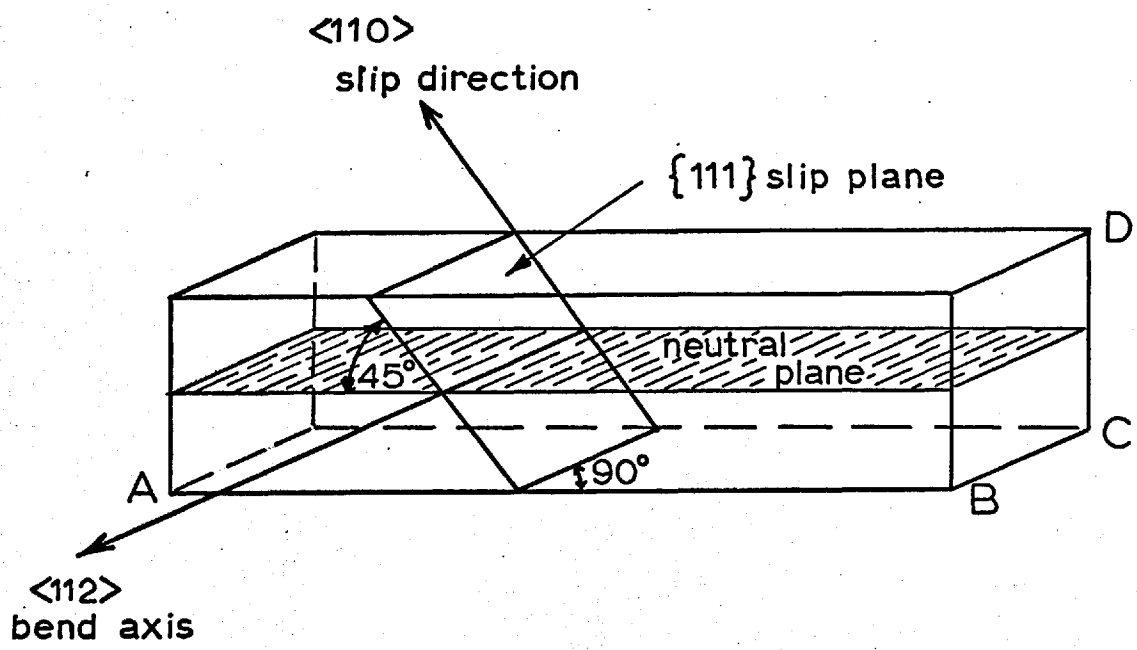

FIG. 6.1. Orientation of specimens for plastic bending.

0.25 cms thick. Specimens for electrical measurement were prepared as follows. From each 'slice' a wafer to be bent was prepared with approximate dimensions (Fig.6.1.) of AB = 2.2 cms, BC = 1.3 cms and CD = 0.25 cms. From material adjacent to this wafer in the same slice, a control sample was prepared in the shape of a bar with AB = 1.5 cms, BC = 0.2 cms, CD = 0.25 cms. The remainder of this slice was used to determine the specimen polarity and also the initial etch-pit density. The surface damage left by cutting operations was removed by etching the specimens in a mod. CP_4 solution. Specimens for deformation studies only (which were not sectioned for electrical measurement) were prepared in the shape of bars with AB = 2.2 cms, BC = 0.4 cms and CD = 0.25 cms. Specimen polarity and initial etch-pit density were measured as above.

The polar nature of the etching properties and its calibration by Warekois (1959) was utilised to determine the polarity of each sample. The obvious method would have been to section the crystal parallel to the favoured slip plane (as shown in Fig.6.2(a)) and to etch both halves with a mod. CP_4 etch. If the 'A' face (Fig.6.2(a)) showed etch-pits (due to grown-in dislocations) then it would be identified as a $\{\bar{1}\bar{1}\bar{1}\}$ face and the stacking sequence of $\{111\}$ planes as shown in Fig.6.2(b) would be deduced. Thus, bending in the

FIG. 6.2.a. Etching of 'A' face reveals pits.

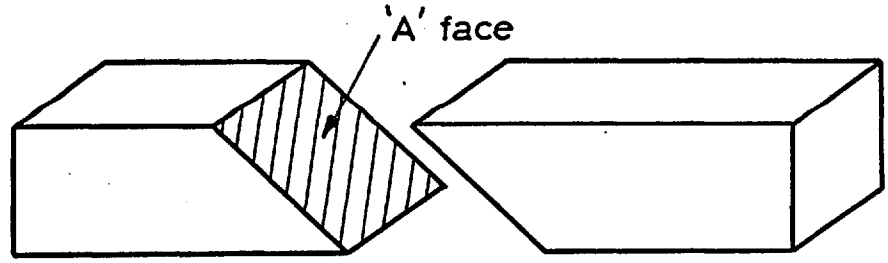

FIG. 6.2.b. Deduced stacking sequence of {111} planes.

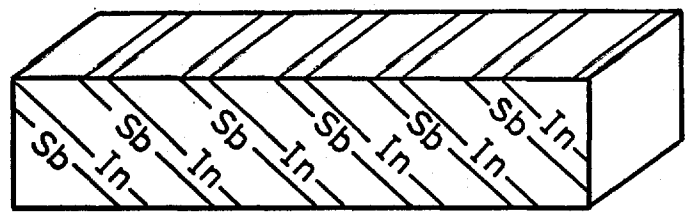

FIG. 6.2.c. Crystal bent to produce excess In-dislocations.

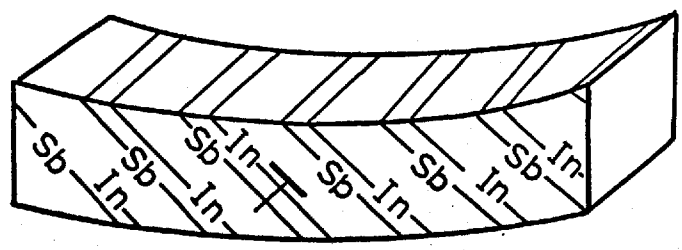

direction shown in Fig.6.2(c) would have produced an excess of In-dislocations. Conversely, if the 'A' face did not produce etch-pits (and the opposite face did produce etch-pits) the 'A' face would be identified as a $\{111\}$ face and the bending moment shown in Fig.6.2(c) would have produced an excess of Sb-dislocations.

The actual method used was a slight modification of this technique. On account of the $\bar{4}$ rotation-inversion axes along the $<100>$ directions, pairs of identical $\{111\}$ planes subtend an angle of 109° whilst pairs of unlike faces subtend an angle of 70° (Fig.6.3). Now, in the orientation of these specimens there was an octahedral face (face 'B') nearly perpendicular to the bend axis, as shown in Fig.6.4(a). The 'B' and 'A' faces subtend 70° and therefore must be unlike faces. The method followed was to section face 'B' and, by etching with mod. CP_4, to identify this face. The bending direction to introduce an excess of the required type of dislocation was then deduced from the polarity of this face. For example, if etch-pits formed on face 'B', it would be identified as a $\{\bar{1}\bar{1}\bar{1}\}$ face. From this it would be deduced that the 'A' face, if sectioned as in Fig.6.2(a), would not have revealed etch-pits and would be a $\{111\}$ face. Thus the stacking sequence shown in Fig.6.4(b) would be deduced, and the bending moment shown in Fig.6.4(c) would have produced an excess

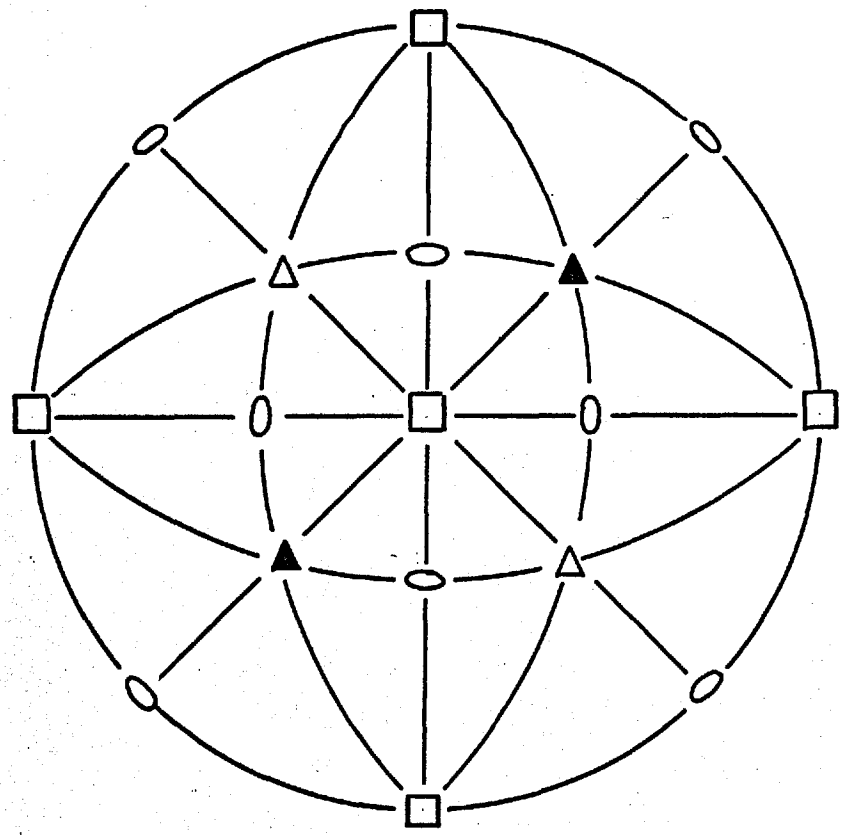

FIG. 6.3. (100) Stereographic projection for indium antimonide showing polarity of <111> directions.

FIG. 6.4.a. Etching of 'B' face reveals pits.

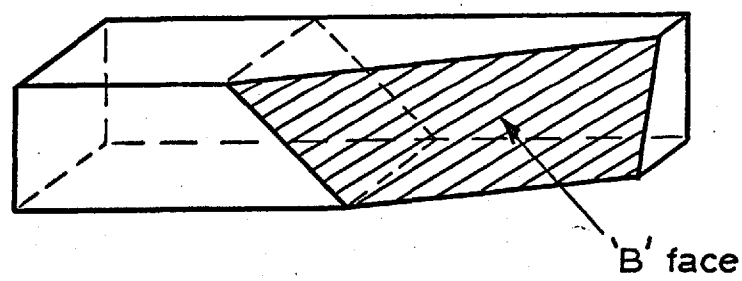

FIG. 6.4.b. Deduced stacking sequence of {111} planes.

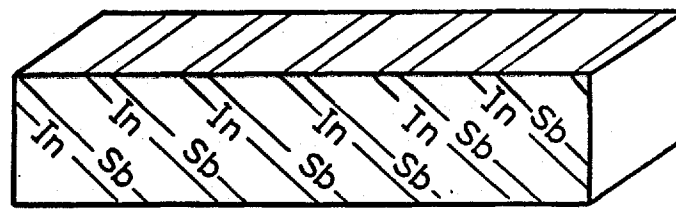

FIG. 6.4.c. Crystal bent to produce excess Sb-dislocations.

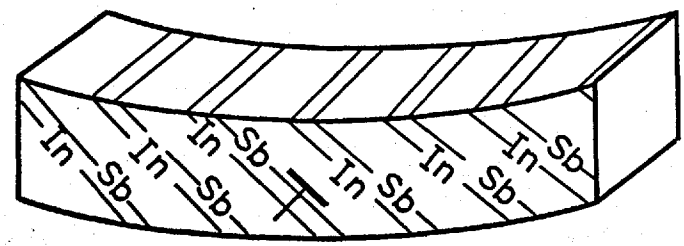

of Sb-dislocations.

In the following chapters, bending to introduce an excess of In-dislocations will be termed 'In-bending', and bending to introduce an excess of Sb-dislocations will be termed 'Sb-bending'.

6.1.2. Three-point bending technique.

The specimens used in the initial investigation had been plastically bent by R. Latkowski. Latkowski used a three-point bending jig in which the sample was supported on two knife edges while its centre was depressed at a constant rate by a third quartz knife edge connected to a motor driven lead screw. Specimens were deformed at 360°C in a reducing atmosphere, and the glide strain rate in the outermost fibres of the specimen was about 1.5×10^{-5} sec^{-1}. In each bending experiment a control sample was placed near to the one being deformed so that the two samples underwent the same heat treatment. The load to sustain the imposed deformation rate was measured via the deflection of a calibrated spring; this made the straining jig relatively 'soft' so that one would not have expected to observe any yield points. A typical graph of shear stress (resolved in the favoured slip plane and slip direction) versus glide strain is shown in Fig.6.5. The feature to which attention is called is the long region of constant load where most of

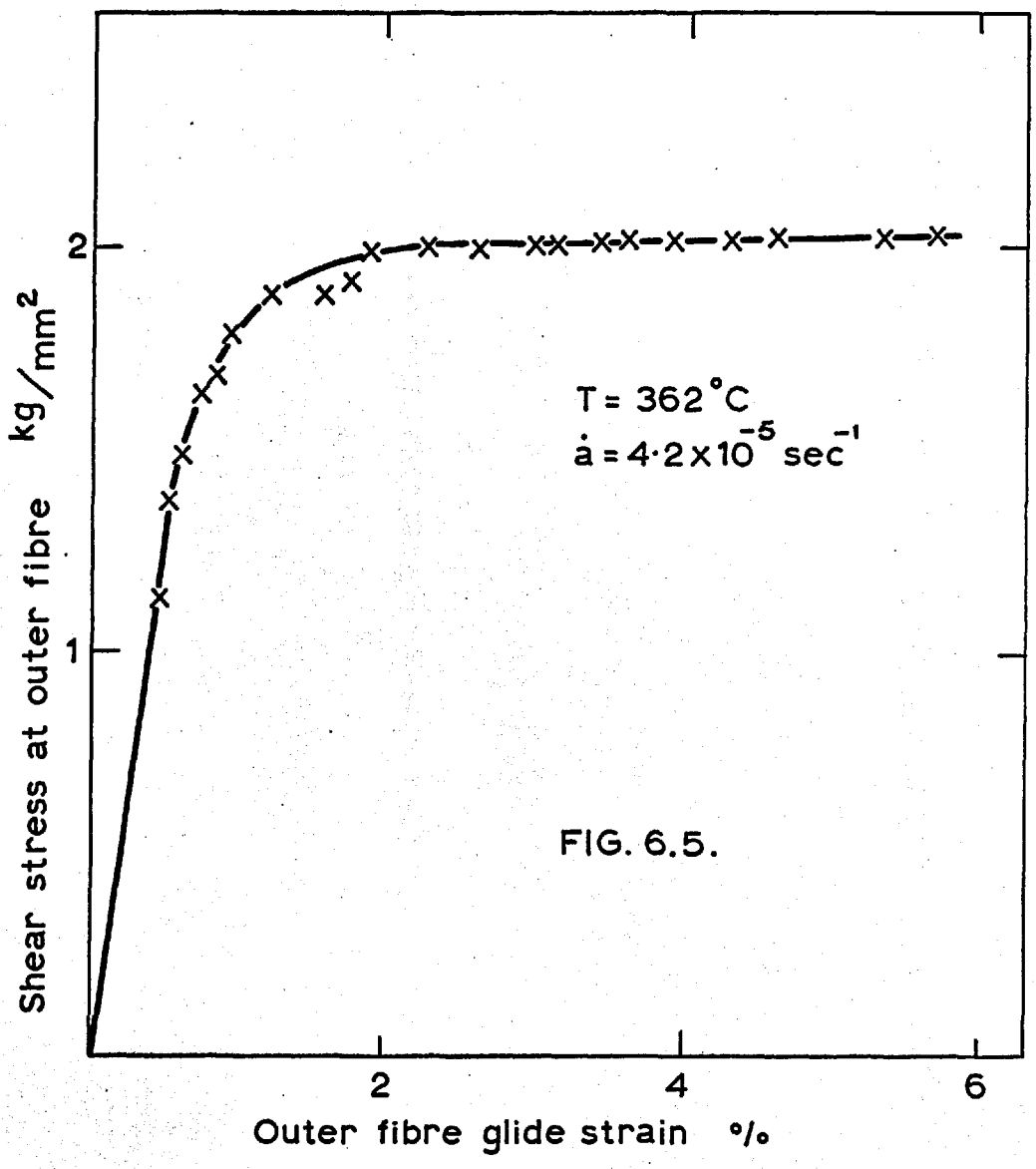
Shear stress at outer fibre kg/mm²
2
1
T = 362°C
ȧ = 4·2×10⁻⁵ sec⁻¹
2
4
6
Outer fibre glide strain %

FIG. 6.5.

the plastic strain occurred. This behaviour is characteristic of specimens undergoing slip on only one set of slip planes with no interference from dislocations on other systems (Bell and Bonfield 1964).

6.1.3. Four-point bending technique.

In subsequent deformation experiments (performed by the author) four-point bending was employed. The bending jig, shown in Fig.6.6, was constructed from En.24 steel. The relative motion of the two pairs of knife edges was guided by rods fixed in the lower block which slid easily in the holes in the upper block. This loose fit allowed both inner knife edges to rest on specimens whose upper and lower surfaces were not accurately parallel. The load was applied to the upper block 'B' via a flattened steel ball which fitted into a recess in 'B' (Fig.6.6.). This steel ball preserved the freedom of the upper block to move laterally. The knife edges were driven together by a compression cage fitted to an Instron machine (model TM-M-L).

The load was applied to the upper compression plate (Fig.6.7.) by a cross-head moving downwards at a constant rate. The load was measured by means of a tensile load cell and a load versus time plot was obtained on a potentiometric recorder. The compression cage was surrounded by a resistance furnace, introduced

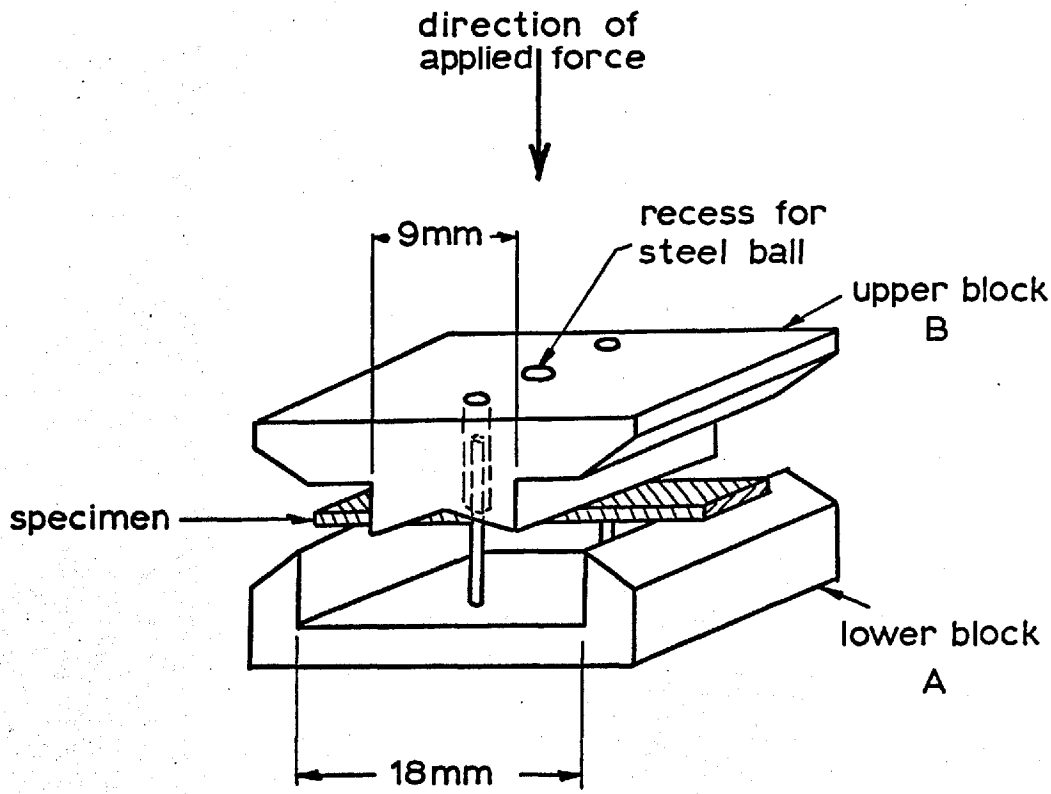

FIG. 6.6. The four-point bending jig.

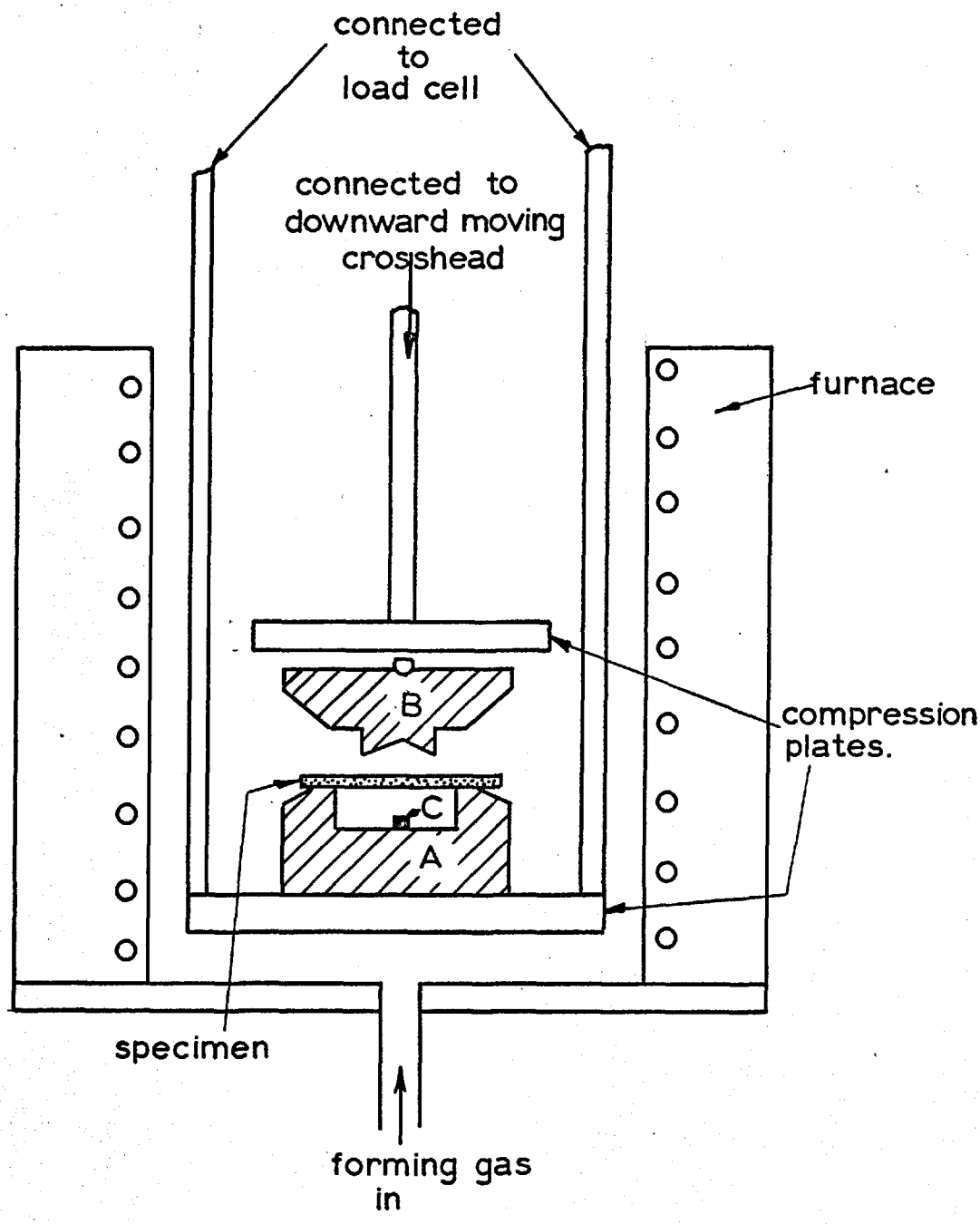

FIG.6.7. Assembled bending apparatus.

from below. This furnace was powered via an 8 amp. Variac fed from a constant voltage transformer. The temperature was measured by two thermocouples positioned near to the specimen. Variations along the length of the specimen were less than $1^{\circ}C$, and fluctuations during the course of the experiment were of the same order. Control specimens were placed in close proximity (C in Fig.6.7) where the temperature was within $2^{\circ}C$ of the specimen temperature.

Before testing, the load cell was calibrated with standard loads. A reducing gas (90% N_2, 10% H_2) was passed through the furnace for 30 minutes to displace air. The furnace was then heated up to the desired temperature and allowed to equilibrate. A small load was applied by slow downward movement of the crosshead. With the crosshead stationary the variation of the load with time was observed. When the variation in load (due to temperature variations) became small, the bending was commenced. All four-point bending experiments were performed with a rate of crosshead motion of 5×10^{-4} cm/min. In order to bend specimens to a prescribed curvature, preliminary experiments were conducted to correlate crosshead movement with final curvature. The bending experiments were typically of 2 hour duration.

The load and displacement measurements were converted to stress and strain using the relations of

Timoshenko and Goodier (1951) for the elastic deformation of beams in bending, and thus the results should apply only to the elastic part of the deformation.

The longitudinal stress, p, between the inner knife edges is given by

$$p = \frac{M}{I} y$$

where M is the bending moment

I is the moment of inertia

and y is the distance from the neutral axis.

If F is the applied force, $2B$ the span of the outer knife edges and $2A$ the span of the inner knife edges

$$M = \frac{F}{2}(B - A)$$

and

$$I = \frac{1}{12} b d^3$$

where b = beam width

and d = beam depth (perpendicular to the neutral axis)

Then the outer fibre stress is given by

$$p = \frac{F}{2}(B-A)\frac{12}{b d^3}\frac{d}{2}$$

$$\therefore p = \frac{3F(B-A)}{b d^2}$$

Resolving this stress in the slip direction, and in the slip plane we obtain

$$S = \frac{p}{2} = \frac{3F(B-A)}{2 b d^2} \qquad \ldots\ (6.1)$$

The equation for strain in the outer fibre of the central portion of the beam has been given by Bruneau and Pratt (1962) (again for elastic deformation) as

$$\gamma = \frac{d}{2R} = \frac{d\,D}{2\{A(B-A)+(B-A)^2/3 + d^2/3\}}$$

where D is the displacement of the inner knife edges relative to the outer knife edges.

The glide strain (a) is 2γ, (Schmid and Boas, 1950) for γ up to 10%, thus,

$$a = \frac{d\,D}{\{A(B-A) + (B-A)^2/3 + d^2/3\}} \quad \ldots\ldots (6.2)$$

The potentiometric recorder gave a record of the variation of the load with time. Knowing the speed of movement of the crosshead (5×10^{-4} cm/min.), this could be converted to a graph of load versus crosshead movement. The displacement, D, corresponding to plastic deformation of the specimen was determined by counting the number of divisions from the elastic region to the point. The glide strain was then determined from (6.2) and the resolved shear stress was calculated from the load by (6.1). Graphs of shear stress versus glide strain were thus obtained from the measured load versus deflection graphs.

6.2. Curvature Measurement.

6.2.1. Shape curvature.

After bending, specimens were mounted in a Vickers Projection Microscope adapted for transmitted light, and the silhouette of each bent specimen could be focussed on the viewing screen. The specimen was adjusted until the bend axis was parallel to the direction of the light beam, and photographic plates were exposed to record the silhouette of each specimen. Specimens were found to have uniform curvature in the centre section, corresponding to the region between the inner knife edges. Between the inner and outer knife edges the curvature was not uniform. Radii of curvature of the centre sections of the specimens were measured from the photographic plates, by comparison with arcs of known curvature. The error in the radius measured by this technique was estimated as $\pm 5\%$.

6.2.2. Lattice curvature.

Radii of curvature were also measured by a Laue back reflection x-ray technique. Bent specimens (L in Fig.6.8) were mounted on a movable table with their concave surface uppermost. This table could be moved horizontally in one direction by means of a micrometer screw. The specimens were mounted with the bend axis perpendicular to the direction of motion as shown

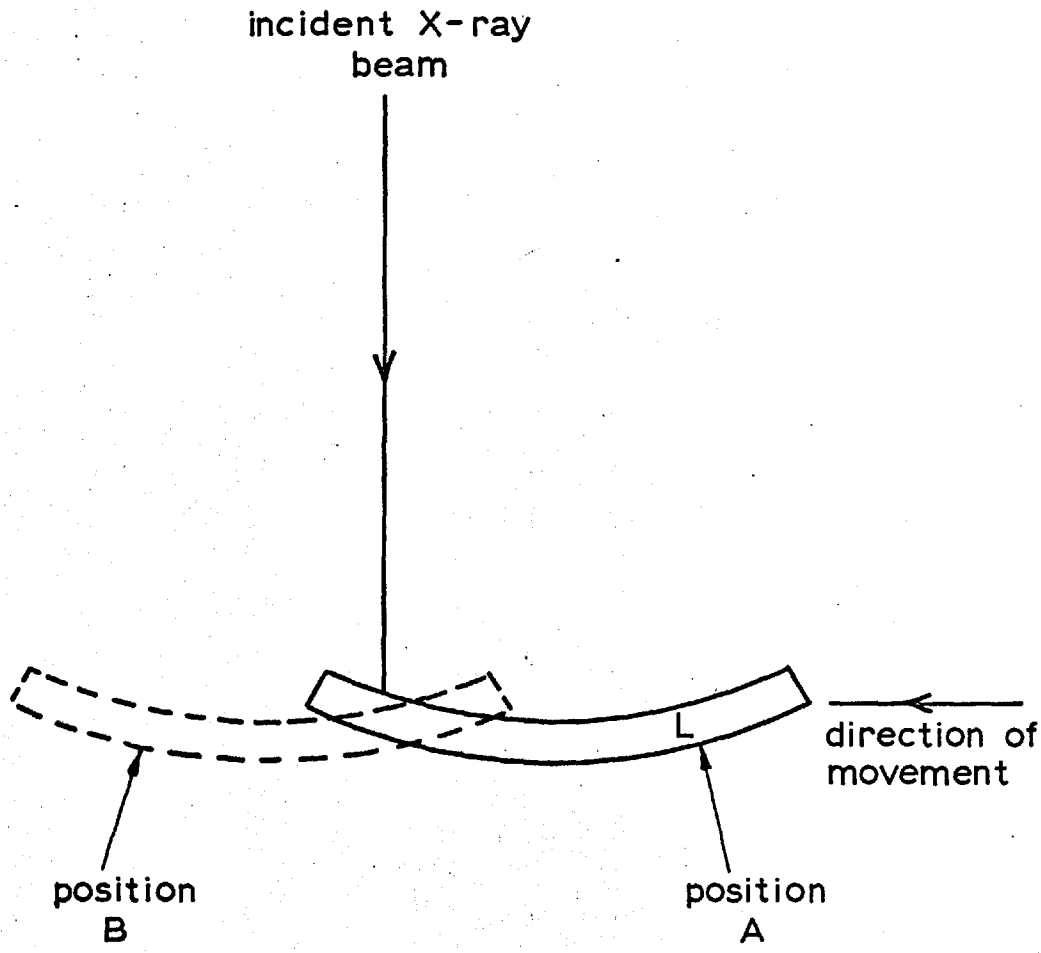

FIG. 6.8. Determination of curvature by X-ray technique.

(Fig.6.8). Laue back-reflection x-ray photographs were taken at several points along the bent bar, using the same film for all exposures. Between each exposure the specimen was moved by a measured distance as shown in Fig.6.8. From the rotation of crystallographic directions from, say, position A to position B , the radius of curvature was calculated. The angular rotation was measured either directly or, where applicable, by the technique of Cahn, Bear and Bell (1953). If $2x$ is the distance between position A and position B , and 2θ is the angular rotation, the radius of curvature (R) is given by

$$\frac{x}{R} = \sin\theta$$

Graphs of x versus $\sin\theta$ were plotted, and these approximated to a straight line between the inner knife edges. Thus, this technique also indicated a uniform curvature in the centre region, the radius being determined from the slope of the x versus $\sin\theta$ graph. The total error in R measured by this technique was estimated as $\pm 10\%$. The radius of curvature obtained from the shape curvature was compared with that obtained from the lattice curvature. The results of this comparison are given in Section 7.2.

6.3. Etch-pit techniques.

The bent samples were sectioned to expose face 'B'

(of Fig.6.4(a)) and the direction of bend was identified by the technique described in Section 6.1.1. This type of sectioning was used since edge dislocations lying on the primary slip plane should intersect this 'B' surface at a steep angle. Certain specimens were also sectioned parallel to the primary slip plane. Etching on one of the two faces exposed in this way should reveal dislocations produced by non-primary slip. The effects of the following etchants were studied.

1) Modified CP_4 etch: 2 parts HNO_3, 1 part HF, 1 acetic acid.

2) Butylamine etch: mod CP_4 etch + 0.5% butylamine.

3) H_2O_2 etch: 1 part H_2O_2, 1 part HF, 8 parts H_2O, + 0.4% butyl-thiobutane.

Lavine, Gatos and Finn (1961) suggested that the mod. CP_4 etch reveals In-dislocations on $\{\bar{1}\bar{1}\bar{1}\}$ surfaces, the butylamine etch reveals In- and Sb-dislocations on both $\{\bar{1}\bar{1}\bar{1}\}$ and $\{111\}$ surfaces, and that the H_2O_2 etch reveals only Sb-dislocations on both $\{\bar{1}\bar{1}\bar{1}\}$ and $\{111\}$ surfaces. However, in the present experiments, no reproducible etch-pits on $\{111\}$ surfaces were obtained with any of these three etchants. Thus, all etch-pit measurements given will refer to pits on $\{\bar{1}\bar{1}\bar{1}\}$ surfaces. The etch-pits were observed by oblique-

illumination microscopy, and the number of pits in a given area was counted to obtain the etch-pit density in that area. Etch-pit densities on one of the two faces exposed by sectioning parallel to the 'B' face (Fig.6.4a) were converted to densities on $\{112\}$ (perpendicular to the bend axis) by dividing by $\cos 19^{\circ} = 0.946$ (since densities on $\{112\}$ should be directly comparable with the dislocation densities predicted from the bend radii). Densities were measured in a large number of areas in each specimen, the magnification being chosen such that about 200 pits were counted in each area. Errors of observation were estimated as $\pm 2\%$.

6.4. Electrical Measurements.

6.4.1. Specimen Preparation.

After the three-point bending, L-shaped specimens were prepared from the bent samples. The portion M of the bent wafer (Fig.6.9(a)) was removed by sectioning with a silicon-carbide slitting wheel, and the portion N was removed by grinding with carborundum powder. These L-shaped specimens had one limb parallel to, and the other limb perpendicular to the bend axis, and current contacts were attached (by a technique described below) such that current would flow as shown in Fig.6.9(b). If the dislocations lay parallel to the

FIG. 6.9. Measurement of three-point bent samples.

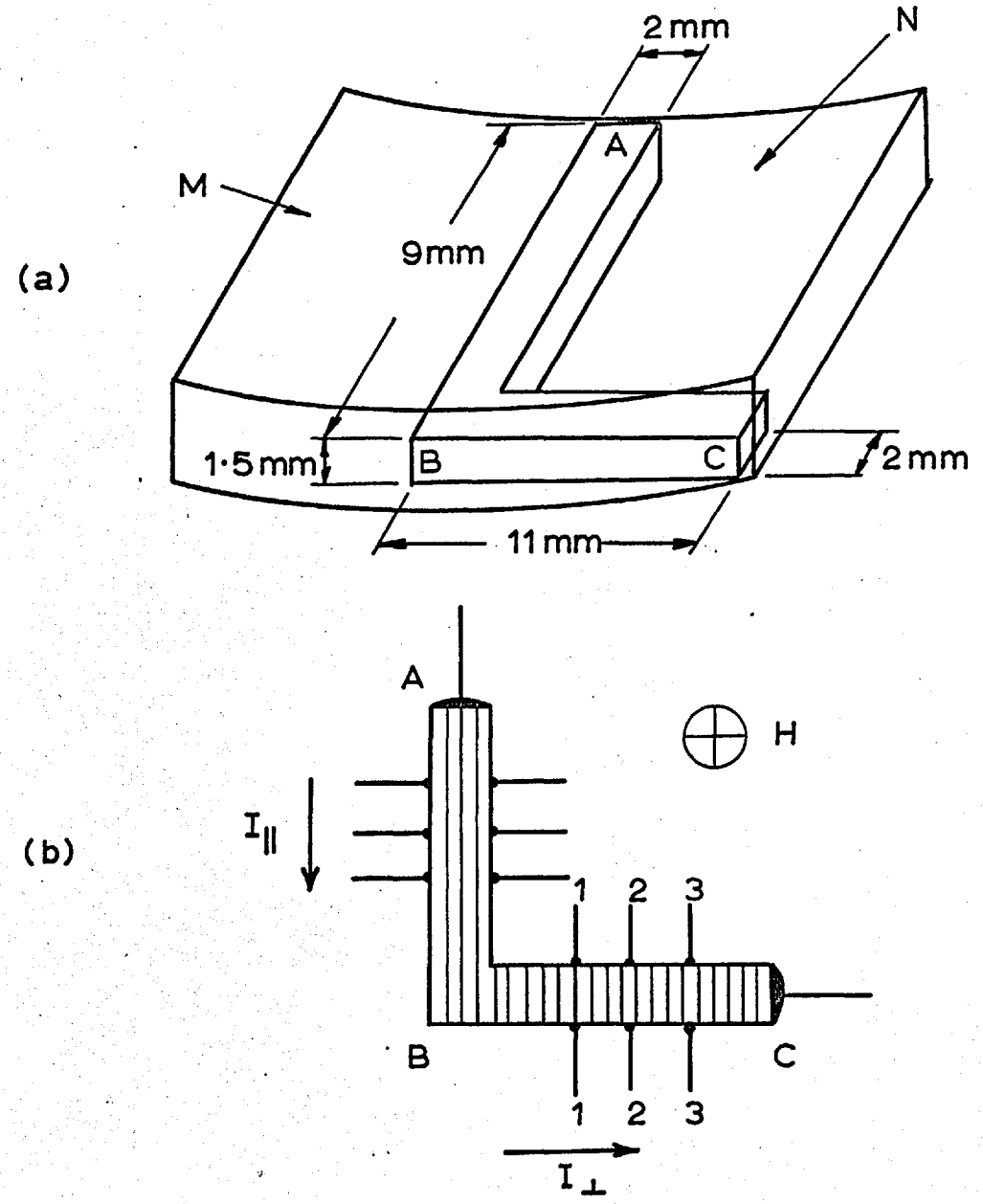

bend axis (as observed by Patel, 1958) the current would flow parallel to the dislocations in one limb and perpendicular to the dislocations in the other limb.

Because the electrical properties (and dislocation density) of three-point bent samples were found to be non-uniform, four-point bending was adopted. This type of bending produced a region, between the inner knife edges, where electrical properties were uniform. Four-point bent samples were sectioned with a silicon carbide slitting wheel to obtain two specimens, one lying parallel to, and the other perpendicular to the bend axis, as shown in Fig.6.10. The 'parallel' specimen was cut in a central position between the inner knife edges.

All the specimens were ground with 600 mesh Carborundum and etched with mod. CP_4 etch to remove surface damage. Finally they were rinsed alternately with benzene and distilled water until clean surfaces were obtained. The use of benzene was found to be of great importance in facilitating the subsequent soldering process. Platinum current leads (0.2 mm diameter) and several fine platinum potential leads (0.05 mm diameter) were attached with Indium solder using a micromanipulator and stereoscopic microscope. The potential probes had a contact diameter of about 0.3 mm and a resistance at $80^{\circ}K$ of about 10 - 20 ohms. Control specimens were

FIG. 6.10. Measurement of four-point bent samples.

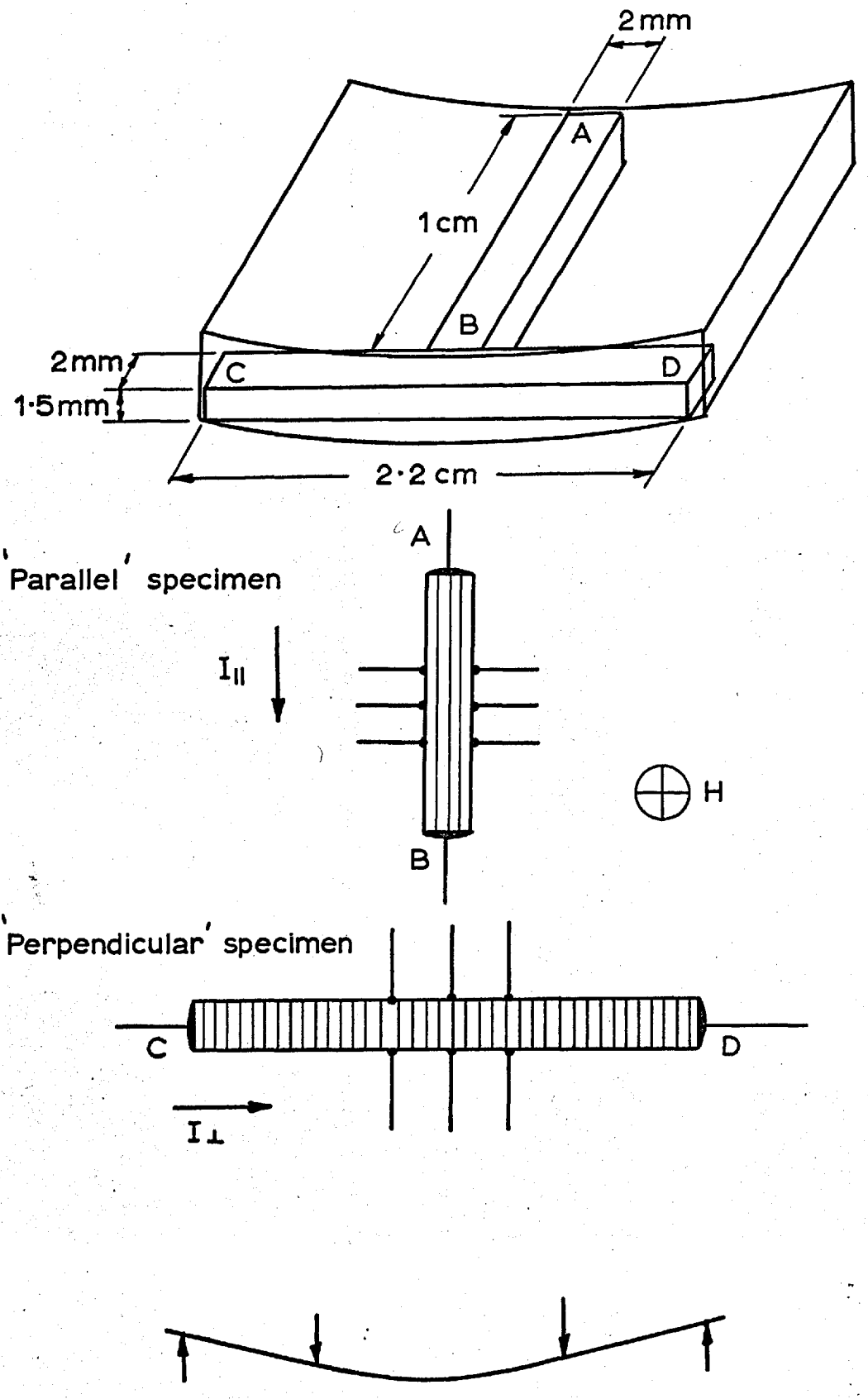

prepared for measurement in a similar way. The final arrangement of the L-shaped sample prepared for measurement is shown in Fig.6.9 and Fig.6.10 shows the four-point bent samples prepared for measurement.

6.4.2. Hall coefficient and conductivity measurement .

The Hall coefficient and electrical conductivity of both control and deformed specimens were measured by a standard D.C. technique. Magnetic fields of about 1000 gauss were provided by an electromagnet which was calibrated regularly with a search coil and fluxmeter. Each specimen, S in Fig.6.11., was mounted inside a cryostat which enabled measurements to be made from room temperature down to 80°K. The cryostat (Fig.6.11) consisted of an outer Dewar vessel containing liquid nitrogen and an inner vessel through which dry gas (90% N_2, 10% H_2) was passed to avoid condensation on the specimen (S). Temperatures between room temperature and 80°K were obtained as follows. With the whole apparatus at room temperature a small volume of liquid nitrogen was placed in the Dewar vessel. As the liquid nitrogen evaporated the temperature of the specimen fell to a certain minimum temperature T_1 and then rose when all the liquid nitrogen had evaporated. The specimen temperature was within 1°C of the minimum temperature T_1 for at least 40 seconds and Hall coefficient and conductivity measurements were made

FIG. 6.11. Low temperature measurement.

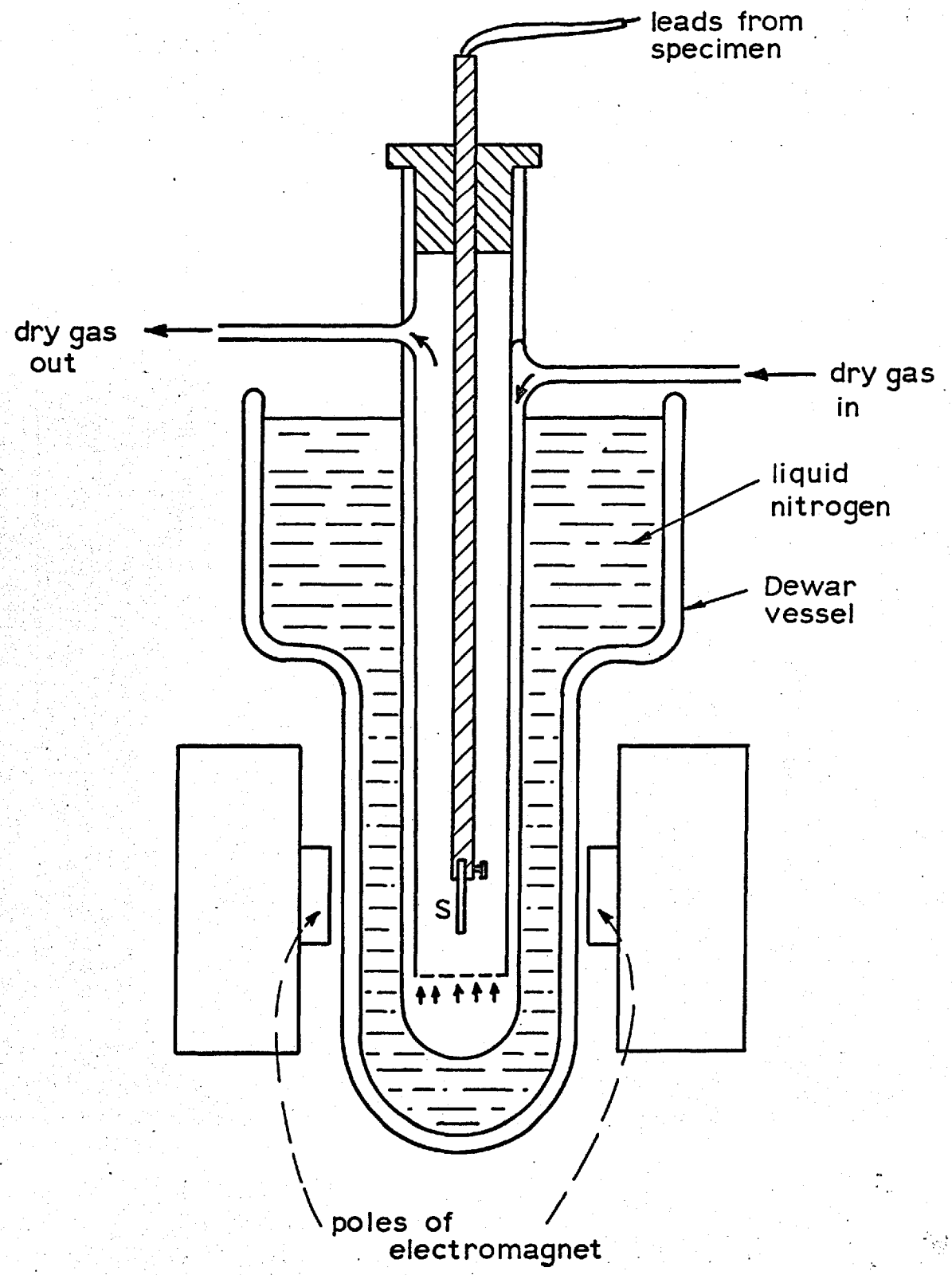

in this period. Measurements at lower temperatures were obtained in the same way, using larger quantities of liquid nitrogen. The specimen temperature was measured by means of an iron constantan thermocouple which was soldered to one of the current contacts to ensure good thermal contact with the specimen.

Fig.6.12 shows the basic circuit for Hall coefficient and conductivity measurement. The current through the specimen (I amps) was measured with a milliammeter and the potential (V_{XY} volts) between two probes X and Y was measured with a potentiometer. If the potential V_{AD} is measured, the Hall coefficient is given by

$$R_H = \frac{V_{AD}\, d}{I\, H} \times 10^8 \quad cm^3/Coulomb$$

with d in cms , H in gauss.

Measuring potential V_{AC} (in the absence of a magnetic field) the conductivity is given by

$$\sigma = \frac{I\, l_{AC}}{V_{AC}\, b\, d} \quad (ohm-cm)^{-1}$$

with l_{AC}, b and d in cms.

The Hall coefficient and conductivity were always measured for at least three values of the current (I) (usually of order 10 mA. at room temperature and of order 200 μA at liquid nitrogen temperature). For conductivity measurement, current reversal was carried out and the average of the two potential measurements was taken.

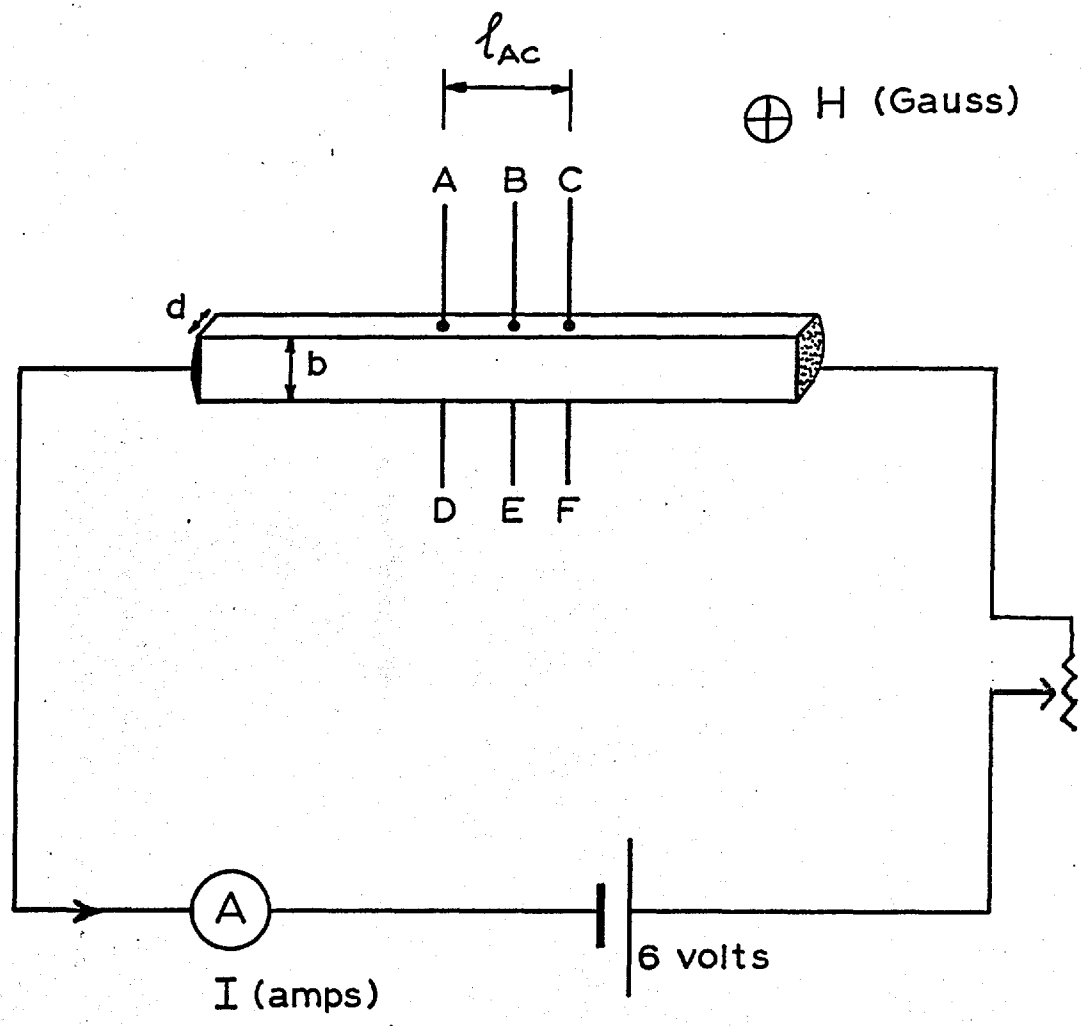

FIG. 6.12. Measurement of Hall coefficient and conductivity.

For the Hall coefficient, field reversal was carried out for each direction of the current, and the average of the four readings was taken. The potentiometer was made reversible to facilitate measurement of reversed potentials. The differences obtained on reversal were not large, about 10% for Hall voltages and 5% for conductivity measurements. Each specimen was remeasured several times to determine reproducibility. The total error in the Hall coefficients is estimated as $\pm$12% and in the electrical conductivities as $\pm$19%.

CHAPTER 7.

EXPERIMENTAL RESULTS - PLASTIC BENDING.

7.1. The dynamics of the deformation process.

Stress-strain data were recorded for the plastic bending of four series of specimens. Two series of specimens were bent at 360°C to introduce in the one case an excess of In-dislocations, and in the other case an excess of Sb-dislocations. Similarly, two series of specimens were bent at 270°C. This section refers to deformation by four-point bending only, since the three-point bending experiments had been performed previously by R.Latkowski, as described in Section 6.1.2.

Typical stress-strain curves are shown in Fig.7.1. The curves for bending at both temperatures showed well defined yield points, as observed by other workers using tensile deformation. There appears to be no other record of yield points in the bending deformation of indium antimonide, although 'delay times' have been observed in constant-load bending tests (Allen 1957, Peissker et al. 1961). Yield points in constant strain rate tests, and 'delay times' in constant-load tests of indium antimonide are commonly associated with the Johnston-Gilman dislocation velocity mechanism. After the elastic extension the specimen began to deform plastically under an

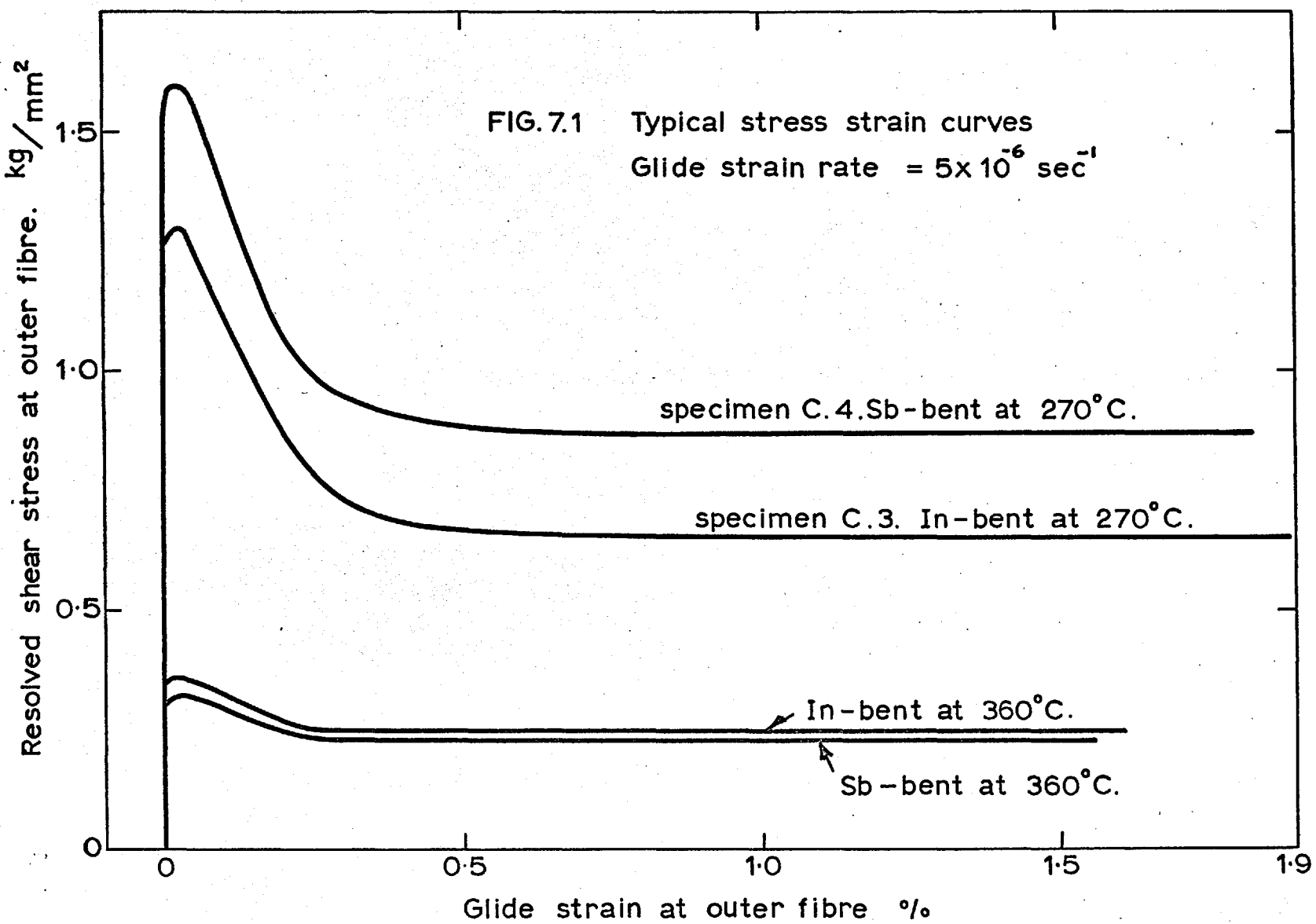
FIG. 7.1 Typical stress strain curves
Glide strain rate = 5x10⁻⁶ sec⁻¹
Resolved shear stress at outer fibre. kg/mm²
1·5
1·0
0·5
0
specimen C.4.Sb-bent at 270°C.
specimen C.3. In-bent at 270°C.
In-bent at 360°C.
Sb-bent at 360°C.
0
0·5
1·0
1·5
1·9
Glide strain at outer fibre %

increasing load until the upper yield stress (at about 0.003% glide strain at the outer fibre) after which the stress dropped rapidly until the lower yield stress was reached (at about 0.7% glide strain). In most cases, flow continued at a constant stress.

It was important to produce slip on only one set of slip planes in these deformation experiments, since the dislocation interactions occurring during multiple slip could produce large numbers of point defects, whose electrical effects would greatly complicate the interpretation of the electrical measurements. In order to determine how many slip planes were active, therefore, an etching technique was employed which estimated the number of dislocations introduced on slip planes other than the primary one (the plane oriented at 45° to the neutral plane). After bending, specimens were sectioned parallel to both 'A' and 'B' $\{111\}$ faces (Figs.6.2 and 6.4). Most etch-pits on one of the two faces exposed by sectioning parallel to the 'B' face were aligned either along the trace of the primary slip plane or perpendicular to it, as shown in Fig.7.2(a), and these pits were associated with dislocations produced by primary slip which were lying either in slip bands or in polygon walls. The density of these pits will be termed the 'B' etch-pit density. Etch-pits on one of the two faces exposed by sectioning parallel to the 'A' face, however, revealed

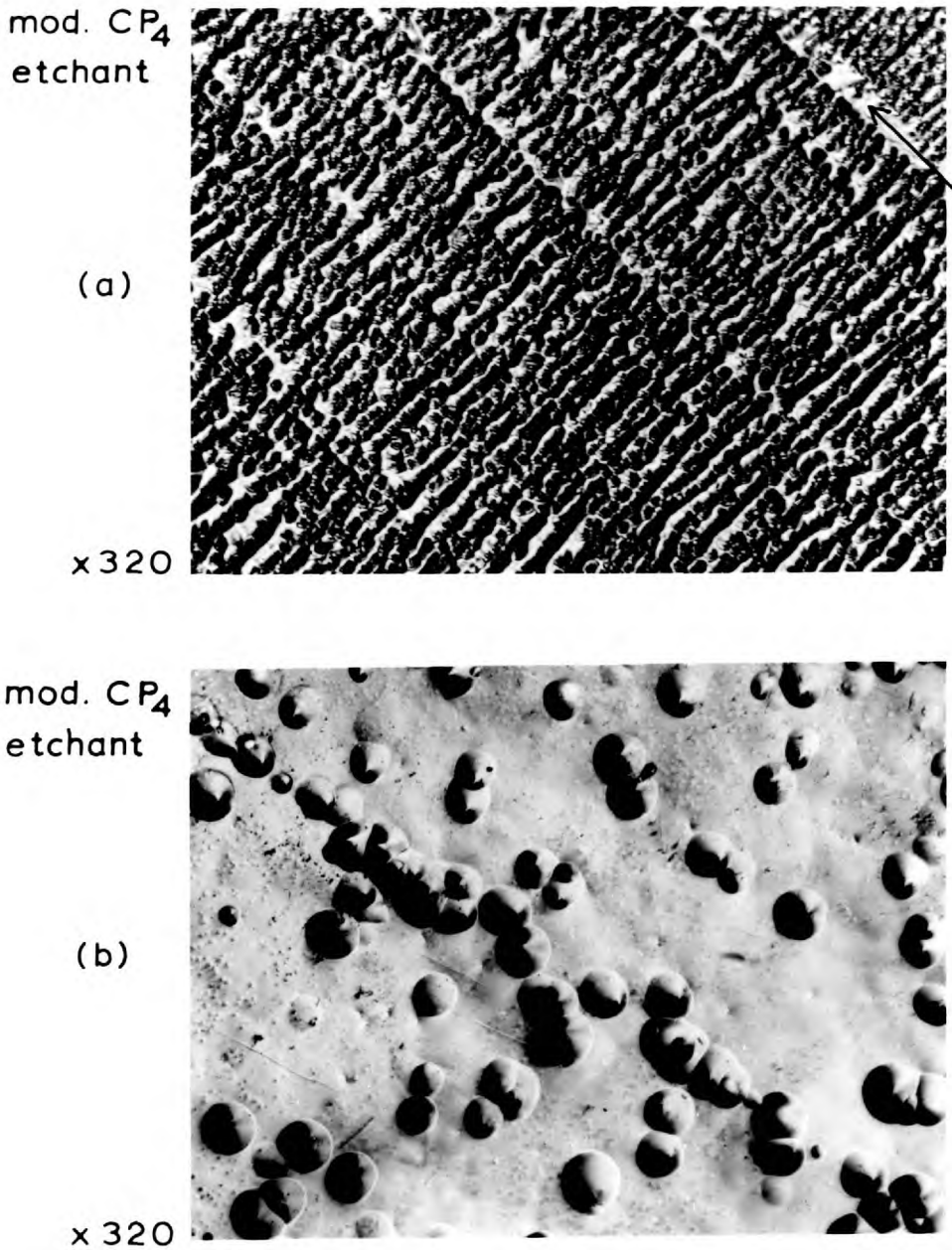

FIG. 7.2. In-bent specimen deformed at 360°C to 10 cm. radius. Etch-pits on face exposed by sectioning parallel to the 'B' face shown in (a), and parallel to the 'A' face in (b).

dislocations introduced on any slip plane other than the primary one, as shown in Fig.7.2(b). The density of these pits will be termed the 'A' etch-pit density.

The ratio of the 'A' etch-pit density to the 'B' etch-pit density (using the mod. CP_4 etch in each case) was therefore taken to be the proportion of dislocations introduced by non-primary slip. In most cases this ratio was less than $^1/_{20}$, indicating a predominance of primary slip. For some specimens, however, this ratio was larger than $^1/_{20}$ and these samples were rejected at this stage. These specimens had invariably shown an appreciable work-hardening rate after the yield drop, and often were found to contain growth twins. There was much evidence to suggest that multiple slip in these specimens was initiated by twins initially present in the material. Specimens free of twins showed single slip and an absence of work hardening after the yield drop.

The effect of temperature on the stress-strain curves is shown in Fig.7.1. As observed by previous workers, the upper and lower yield stresses were very temperature dependent, and increased by a factor of about 3 on lowering the temperature from 360°C to 270°C.

In view of the results of Peissker et al., it is interesting to compare the stress-strain curves for In- and Sb-bending. There is a certain amount of evidence

that the lower yield stress is more reproducible than the upper yield stress, since it is less sensitive to initial dislocation density (Bell and Bonfield, 1964). The lower yield stresses for In- and Sb-bending will therefore be compared. For bending at 360°C, the lower yield stresses for In- and Sb-bending were not significantly different. However, for bending at 270°C the lower yield stress for Sb-bending was significantly greater than that for In-bending as shown, for example, by the specimens C3 and C4 whose stress-strain curves are shown in Fig.7.1.

Table 7.1 gives values of the lower yield stress for a series of specimens bent at 270°C. Specimens C1 to C8 were all taken from crystal CT200, while specimens E1 to E4 were taken from crystal C412. Considering each crystal in isolation, the lower yield stress for Sb-bending was always greater than that for In-bending. The values were not reproducible from crystal to crystal but this is not surprising since the two crystals had different initial dislocation densities. For specimens C1 to C8 the values of the lower yield stress were

$S_{ly} = 0.621 \pm 0.05$ kg/mm^2 for In-bending, and

$S_{ly} = 0.868 \pm 0.09$ kg/mm^2 for Sb-bending

and for specimens E1 to E4 the values of the lower yield stress were

$S_{ly} = 0.460 \pm 0.015$ kg/mm^2 for In-bending, and

Table 7.1: Lower yield stresses of specimens bent at 270°C.

In-bent specimens		Sb-bent specimens	
Specimen No.	S_{ly} (kg/mm^2)	Specimen No.	S_{ly} (kg/mm^2)
C.1	0.6566	C.2	0.850
C.3	0.650	C.4	0.87
C.5	0.605	C.6	0.950
C.7	0.572	C.8	0.801
E.1	0.475	E.2	0.562
E.3	0.445	E.4	0.543

S_{ly} = 0.552 ± 0.010 kg/$_{mm}2$ for Sb-bending.

Thus, for specimens C1 to C8, the lower yield stress for Sb-bending was about 1.4 times that for In-bending, and for specimens E1 to E4 the corresponding factor was about 1.2. The etch-pit densities of these specimens were measured both before and after bending. The initial etch-pit density (with mod. CP_4 etchant) of specimens from crystal CT200 was 2.1×10^3 cm^{-2}, while that of specimens from C412 was 1.6×10^4 cm^{-2}. Thus, for a given bending direction, specimens with an initial dislocation density of 2.1×10^3 cm^{-2} gave a higher value of the lower yield stress than those with an initial density of 1.6×10^4 cm^{-2}. A similar trend was observed by Bell and Bonfield (1964) who explained it in terms of the dislocation density at the lower yield point. They found that specimens with an initial dislocation density of 1×10^3 cm^{-2} contained 7×10^6 cm^{-2} dislocations at the lower yield point, whereas those with an initial density of 5×10^2 cm^{-2} contained 1×10^7 cm^{-2} dislocations at the lower yield point.

Fig.7.3 shows the 'B' etch-pit density (converted to the density on $\{112\}$) of specimens which had been bent at 270°C, as a function of distance perpendicular to the neutral plane (the etchant being mod. CP_4). The Sb-bent samples had a very low density of pits at the neutral axis which did not increase appreciably as the curvature increased. No evidence for polygonisation was found in these samples and etch-pits were either aligned along the

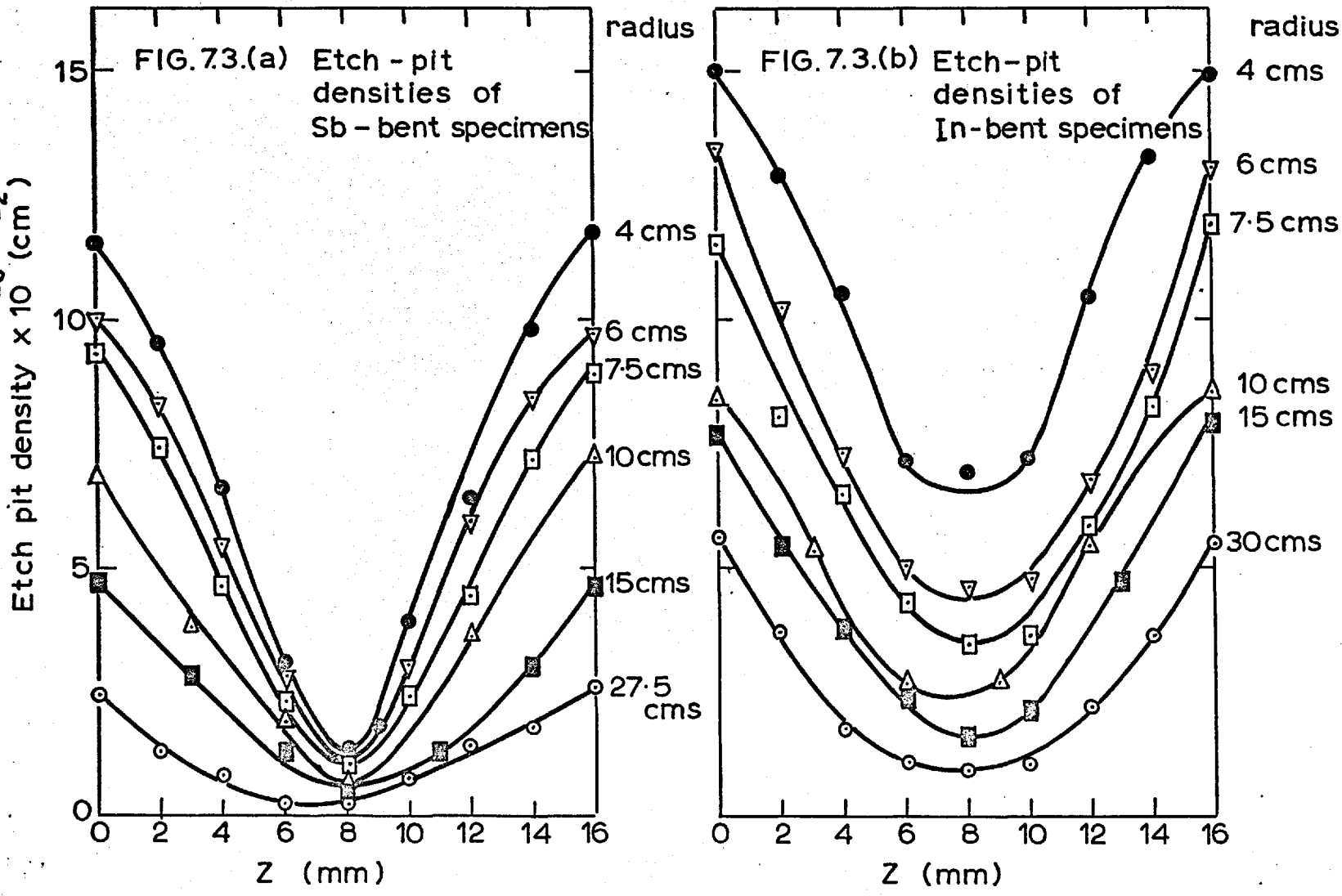
FIG. 7.3.(a) Etch - pit densities of Sb - bent specimens
radius
4 cms
6 cms
7·5 cms
10 cms
15 cms
27·5 cms
Etch pit density x 10^-6 (cm^-2)
Z (mm)
FIG. 7.3.(b) Etch-pit densities of In-bent specimens
radius
4 cms
6 cms
7·5 cms
10 cms
15 cms
30 cms
Z (mm)

trace of the primary slip plane, or randomly distributed. The In-bent samples, however, had a higher density of pits near the neutral axis which did increase as the curvature increased. The pits were aligned perpendicular to the trace of the primary slip plane, indicating a polygonised distribution of dislocations, particularly in the region around the neutral axis.

Similar comments also apply to the etch-pit distribution revealed by the butylamine etchant, the distribution of etch-pits being the same as for the mod. CP_4 etchant. In order to make deductions about the generation and movement of the different dislocations, however, it was first necessary to investigate the reliability of etchants in revealing dislocations.

7.2. Investigation of the reliability of the etch-pit technique.

In Section 2.3.1 the Nye relation

$$\rho_{MAJ} - \rho_{MIN} = \frac{1}{R\,b\cos\omega} \qquad \ldots\ldots (2.12)$$

was introduced. Now, if a bent crystal were annealed at a temperature near the melting point, one would expect minority sign dislocations to annihilate with majority sign dislocations, until none of the minority sign remained. Equation (2.12) could then be written

$$\rho_{MAJ} = \frac{1}{R\,b\cos\omega} \qquad \ldots\ldots (7.1)$$

Thus, bent and annealed crystals provide a sensitive test of whether or not etching reagents are specific to one type of dislocation. For example, if an Sb-bent (and annealed) crystal contained only Sb-dislocations, an etchant specific to In-dislocations should produce no pits, while an etchant specific to Sb-dislocations should produce the theoretical density given by (7.1).

7.2.1. Three-point bending.

In a three-point bend test the specimen does not assume a uniform curvature, but rather takes on the profile shown in Fig.6.9(c). At the position of the central knife edge the curvature of the specimen is a maximum, and it decreases to a minimum near the outer knife edges. The etch-pit density showed a similar trend with a maximum density near the inner knife edge, decreasing to values little different from that of the virgin crystal near the outer knife edges. Because of this variation in curvature, it was impossible to test equation (2.12) rigorously. However, some useful qualitative results were obtained on specimens bent at 360°C. Specimens were sectioned parallel to face 'B' (nearly perpendicular to the bend axis) for etching. The results are shown in Figs.8.1 and 8.2 in which the etch-pit density (with two etchants) is plotted against distance parallel to the neutral plane.

In both In-bent and Sb-bent samples the butylamine

etch-pit density was greater than the CP_4 etch-pit density. Furthermore, the difference between the butylamine density and the CP_4 density was greater in Sb-bent samples than in In-bent samples. These observations are qualitatively consistent with the predicted behaviour of these etchants, i.e. that the butylamine etchant reveals both In- and Sb-dislocations, and the CP_4 etchant reveals only In-dislocations. For a quantitative test of these etchants, four-point bending was adopted.

7.2.2. Four-point bending.

After four-point bending, specimens had a uniform curvature in the region between the inner knife edges. In this region the etch-pit density was uniform along any direction parallel to the neutral plane. This uniformity of properties enabled a more critical test of (2.12) to be carried out. All specimens were sectioned parallel to face 'B' (Fig.6.4) for etching, and etch-pit densities were converted to densities on $\{112\}$ by the method described in Section 6.3.

Four point bending experiments were first carried out at a high temperature ($360^{\circ}C$) and a low strain rate (5×10^{-6} sec^{-1}). In this case the etch-pit distribution in the bent samples was uniform (to within 15%) in a direction perpendicular to the neutral plane, and, as the etch-pit density did not vary appreciably along a

direction parallel to the neutral plane (in the central region), these samples were very uniform on a macroscopic scale. This macroscopic distribution was very suitable for electrical measurements and this procedure was adopted for preparing the electrical specimens. On a microscopic scale, however, the pits were aligned in discrete walls perpendicular to the slip plane as shown in Fig.7.2(a).

One would expect that the residual elastic stresses were low in these samples since they showed a macroscopically uniform etch-pit density. It is probably reasonable, therefore, to apply the Nye relation (7.1) (valid only in the absence of macroscopic elastic stresses). Now the etch-pit densities measured on these samples (using the mod. CP_4 etchant) were larger than predicted by (7.1) suggesting that some 'minority' sign dislocations were present. However, annealing treatments, even very close to the melting point, produced no significant change in etch-pit density. This behaviour is thought to be associated with the stable, polygonised arrangement of the dislocations, as revealed by the etch-pits.

In contrast, bending at low temperatures resulted in structures which did respond to annealing. For this reason a series of low temperature bending experiments

with subsequent anneals was carried out in order to calibrate the etchants. Specimens were bent at 270°C to radii from 4 cm to 30 cm, and annealed within 10°C of the melting point for 7 days. The radii of curvature were measured after bending by the two techniques described in Section 6.2, the silhouette technique measuring the curvature of the specimen profile, and the X-ray technique measuring lattice curvature. The latter technique was employed because it is conceivable that the change in shape on bending is not an accurate measure of the lattice curvature and hence of the theoretical dislocation density. However, results obtained by the two techniques agreed within the experimental errors involved. Measurements of the radii after annealing indicated that no change had taken place.

Fig.7.4 shows the etch-pit densities in one In-bent and one Sb-bent sample as a function of the distance perpendicular to the neutral plane, before and after annealing. The mod. CP_4 etchant and the butylamine etchant were each used in turn. The theoretical dislocation densities predicted by (7.1) are shown by broken lines.

The as-bent samples showed a characteristic distribution of etch-pits. For both etchants the pit density was a minimum at the neutral axis and a maximum at the top and bottom surfaces, as one would expect

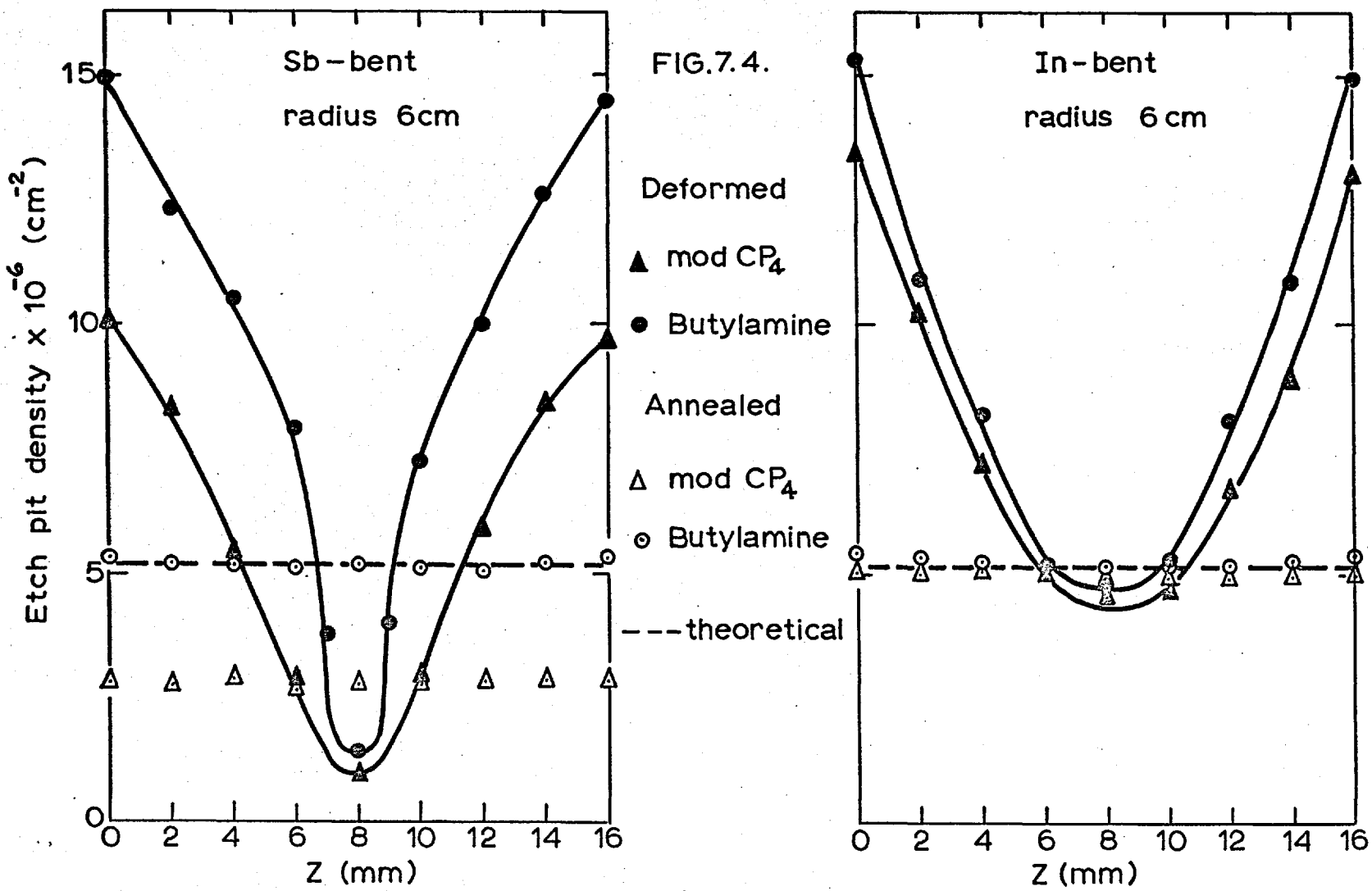
Sb-bent
radius 6cm
In-bent
radius 6 cm
Etch pit density x 10^{-6} (cm^{-2})
Z (mm)
Deformed
mod CP_4
Butylamine
Annealed
mod CP_4
Butylamine
---theoretical

FIG.7.4.

qualitatively from the stresses exerted during bending. It is noted that, for both as-bent samples, the butylamine etchant revealed more pits than the mod. CP_4 etchant. The difference between the butylamine density and the CP_4 density, however, was much greater for Sb-bending than for In-bending and again this is qualitatively consistent with their predicted behaviour. The average density obtained with the butylamine etch in both cases was greater than the theoretical value.

After annealing, the average etch-pit density was reduced. This was presumably due to annihilation of opposite sign dislocations. The high density in the outside regions fell to produce a fairly constant distribution across each specimen and etch-pits were aligned in polygon walls perpendicular to the slip plane.

For the annealed In-bent specimen, both etchants gave etch-pit densities which were close to the theoretical dislocation density. For the annealed Sb-bent sample, however, the butylamine density was close to the theoretical value while the mod. CP_4 density was about half this number. These trends were typical of specimens deformed to other radii and annealed, as shown by the collected results in Fig.7.5.

The micrographs in Fig.7.6 show typical areas of the annealed In-bent sample and the annealed Sb-bent

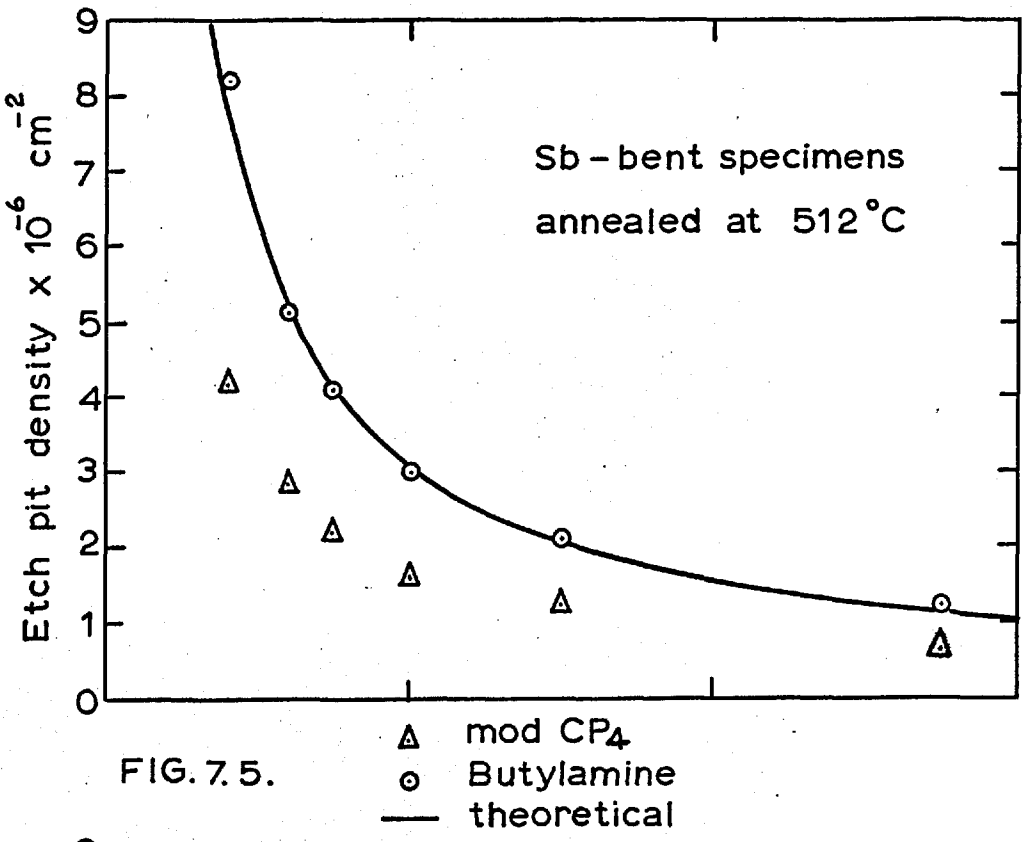
Etch pit density x 10^{-6} cm^{-2}
0
1
2
3
4
5
6
7
8
9
Sb – bent specimens
annealed at 512 °C
mod CP4
Butylamine
theoretical

FIG. 7.5.

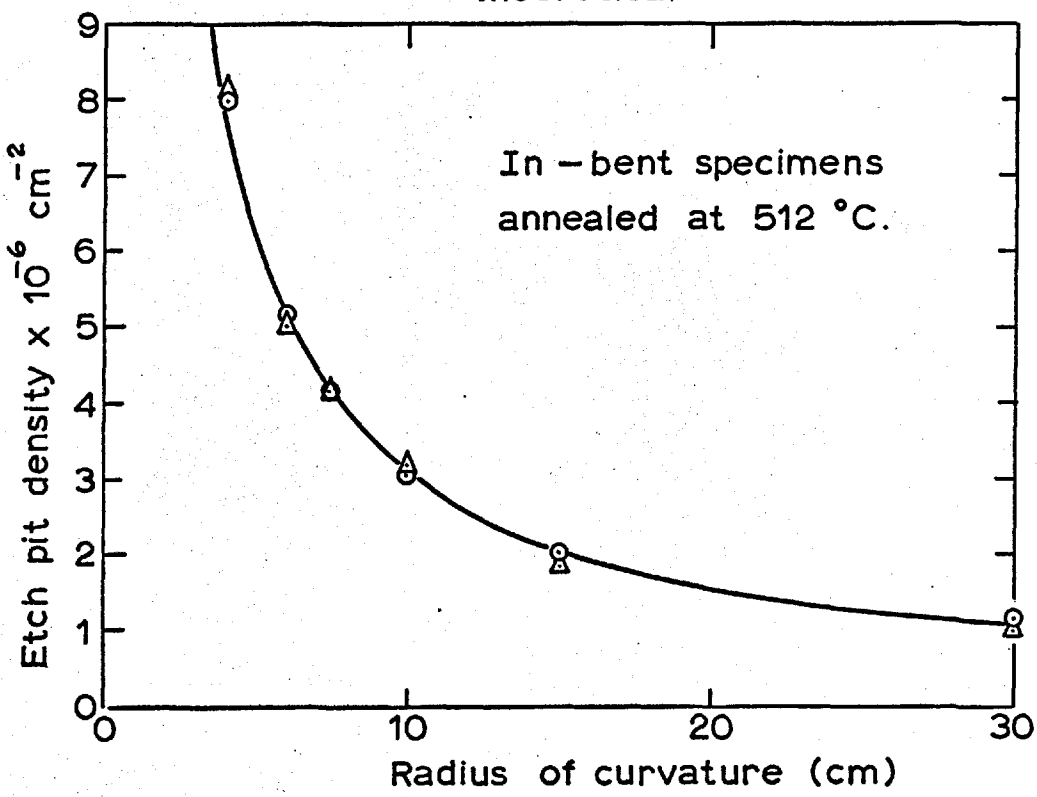
Etch pit density x 10^{-6} cm^{-2}
0
1
2
3
4
5
6
7
8
9
In – bent specimens
annealed at 512 °C.
0
10
20
30
Radius of curvature (cm)

mod. CP_4 etchant

Butylamine etchant

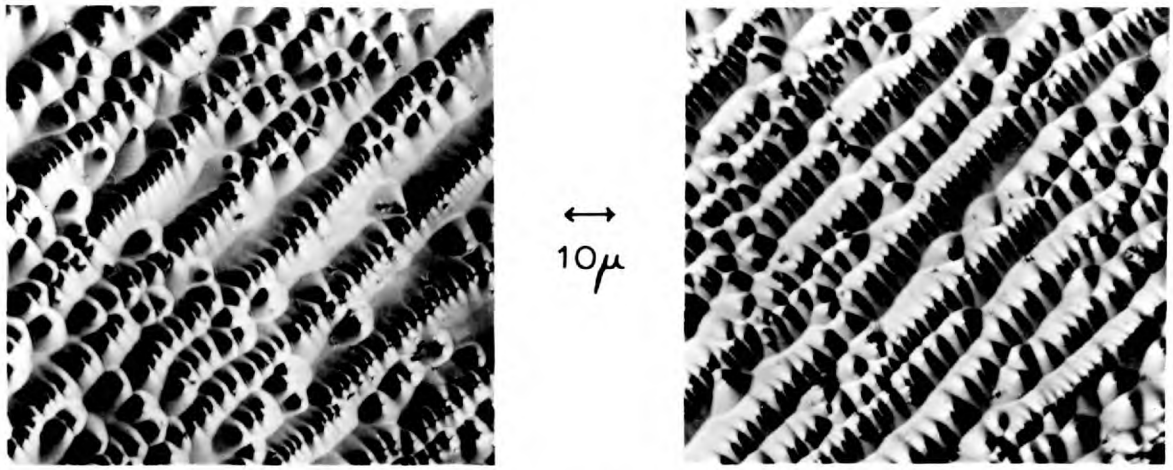

In-bent specimen

mod. CP_4 etchant

Butylamine etchant

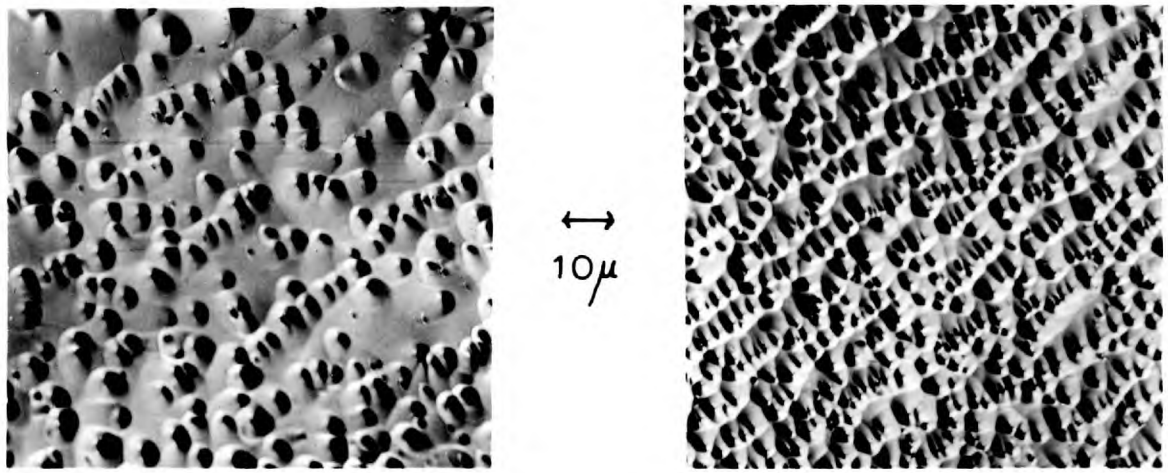

Sb-bent specimen

FIG. 7.6. Etch-pit densities of annealed specimens. Both specimens were bent to a radius of 6 cm., and annealed at 515°C for 7 days.

sample after etching with each etchant. Fig.7.6 shows that the In-bent samples have a greater tendency to polygonise on annealing than the Sb-bent samples. A similar trend was observed in the samples bent at 360°C.

Further annealing treatments did not alter the etch-pit densities of these samples significantly.

In considering these results it is simplest first to assume that no minority sign dislocations remained after annealing. It follows then that the butylamine etch revealed both In-dislocations and Sb-dislocations with equal efficiency, since the theoretical density was revealed in annealed In-bent and annealed Sb-bent samples. The CP_4 etch must have revealed In-dislocations, since the theoretical density was revealed in annealed In-bent samples, but it does not seem to be entirely specific to In-dislocations since it gave values about half that predicted from the curvature in annealed Sb-bent samples. The simplest deduction is that the CP_4 etch reveals all the In-dislocations present and about a half of the Sb-dislocations when no In-dislocations are present.

If a significant fraction of minority sign dislocations were present in the annealed samples the conclusions would be different. In this case the butylamine etch could not have revealed all the dislocations present, but it seems likely that it revealed an equal proportion

of each type. Also the CP_4 etch could not have revealed all the In-dislocations present in the annealed In-bent sample, but, although its efficiency in revealing In-dislocations could not have been 100%, its efficiency in revealing Sb-dislocations would have been appreciably lower than 50%.

The former interpretation seems far more satisfactory and will be used as the basis for estimating dislocation densities. This interpretation suggests that the butylamine etch is the more reliable, revealing both types of dislocation.

The H_2O_2 etch, thought by Gatos to reveal only Sb-dislocations, was found in annealed samples to reveal about one half the number revealed by the CP_4 etch, regardless of the sign of bending. This indicates that the H_2O_2 etch is not specific to Sb-dislocations, and in fact appears to be more specific to In-dislocations.

7.3. Interpretation of etch-pit measurements on bent samples.

The 'calibration' of the etching reagents by measurements on annealed samples enables the etch-pit results on deformed samples to be interpreted in more detail.

The results for deformation at 270°C indicated a

higher yield stress for Sb-bending than for In-bending. This is qualitatively consistent with the trend observed by Peissker et al. in creep measurements which indicated that Sb-dislocations were less mobile than In-dislocations. The etch-pit measurements in Fig.7.4 suggest that, in Sb-bent samples, the dislocations introduced by bending are situated mainly near the outer surfaces, whereas in In-bent samples the dislocations penetrate into the neutral axis region. Now, in a bending experiment the first dislocation sources to operate must be at or near the surfaces, and dislocations of the sign required to accommodate the curvature will move towards the neutral axis from these sources. The stress will fall off as the neutral axis is approached, and so the closest distance of approach of the dislocations to the neutral axis will give an indication of the stress to move the dislocations. In specimens bent to the same lattice curvature, the etch-pit measurements showed that the dislocations approached much closer to the neutral axis on In-bending than on Sb-bending even though the applied load was greater in the latter case. Now only majority sign dislocations are moved towards the neutral axis and thus we may infer that the stress to move In-dislocations is less than the stress to move Sb-dislocations. The stress-strain data and the etch-pit measurements are therefore consistent with the theory that In-dislocations

are more mobile than Sb-dislocations. It is not clear, however, what part the different tendencies for polygonisation play in the deformation process. The greater tendency of In-dislocations to polygonise may play a part in the reduction of the yield stress in In-bent samples.

If the mobilities of Sb- and In-dislocations differ, the etch-pit results on the as-bent specimens of Venables and Broudy (1958) could be explained in terms of different distributions of dislocations rather than the selectivity of their etchant. The more pronounced neutral axis observed in Sb-bent samples could be due to the low mobility of Sb-dislocations rather than to the etchant being selective to In-dislocations. Similar comments apply to the bent samples etched by Lavine et al. (1961) who only examined the region near the neutral axis.

The 'calibration' of the etchants used in the present experiments can be used further to calculate the relative densities of In- and Sb-dislocations in the samples bent at 360°C. Adopting the conclusions of Section 7.2 we can write

$$\rho_{But} = \rho_{In} + \rho_{Sb}$$

$$\text{and } \rho_{CP_4} = \rho_{In} + \tfrac{1}{2}\rho_{Sb}$$

$$\therefore \rho_{Sb} = 2\rho_{But} - 2\rho_{CP_4} \quad \ldots\ldots (7.2)$$

$$\text{and } \rho_{In} = 2\rho_{CP_4} - \rho_{But} \quad \ldots\ldots (7.3)$$

Thus ρ_{Sb} and ρ_{In} were calculated by (7.2) and (7.3) from the etch-pit densities obtained with both etchants. Table 7.2 lists values of ρ_{In} and ρ_{Sb} calculated in this way. In the case of In-bent samples, ρ_{In} is about a factor of 3 to 4 greater than ρ_{Sb}, while in Sb-bent samples ρ_{Sb} is a factor of 2 to 3 greater than ρ_{In}. The excess density of majority dislocations was then obtained by subtraction. Now the Nye relation (2.12) gives the excess density of majority dislocations in the absence of macroscopic elastic stresses, and thus strictly can only be applied to specimens which have been annealed. However, since the specimens bent at 360°C showed a uniform etch-pit distribution, the residual elastic stresses must have been low and it is probably reasonable to apply the Nye relation. Table 7.2 shows that the excess density of majority dislocations predicted by (2.12) is in fair agreement with that calculated from etch-pit measurements, and this gives confidence in the assumptions needed for the interpretation of the etch-pit measurements.

Assuming that the interpretation given in Table 7.2 is correct, the conclusion is that the bent specimens contain significant numbers of minority sign dislocations. Now, dislocation sources at the surface should produce only majority sign dislocations, since a bending stress moves minority sign dislocations away from the neutral

Table 7.2: Interpretation of etch-pit measurements on samples bent at 360°C.

In-bent specimens

Specimen No.	ρ_{CP4} (cm^{-2})	ρ_{But} (cm^{-2})	ρ_{Sb} (cm^{-2})	ρ_{In} (cm^{-2})	R (cm)	ρ_{theor} ($1/Rb\cos\omega$) (cm^{-2})	$\rho_{In}-\rho_{Sb}$ (cm^{-2})
6	5.2×10^{6}	5.82×10^{6}	1.24×10^{6}	4.58×10^{6}	10.0	3.09×10^{6}	3.34×10^{6}
3	2.9×10^{7}	3.30×10^{7}	8.0×10^{6}	2.5×10^{7}	2.5	1.24×10^{7}	1.7×10^{7}
1	1.25×10^{6}	1.40×10^{6}	0.30×10^{6}	1.10×10^{6}	30.0	1.06×10^{6}	0.8×10^{6}
11	6.3×10^{5}	7.25×10^{5}	1.90×10^{5}	5.25×10^{5}	>50	$<6.2\times10^{5}$	3.35×10^{5}
12	2.5×10^{6}	2.88×10^{6}	0.76×10^{6}	2.12×10^{6}	22.0	1.40×10^{6}	1.36×10^{6}
2	2.8×10^{6}	3.18×10^{6}	0.76×10^{6}	2.32×10^{6}	20.0	1.55×10^{6}	1.56×10^{6}
10	1.2×10^{7}	1.35×10^{7}	3.0×10^{6}	1.05×10^{7}	4.0	7.75×10^{6}	7.5×10^{6}

Sb-bent specimens

Specimen No.	ρ_{CP4}	ρ_{But}	ρ_{Sb}	ρ_{In}	R	ρ_{theor}	$\rho_{Sb}-\rho_{In}$
4	1.1×10^{6}	1.71×10^{6}	1.21×10^{6}	0.50×10^{6}	30.0	1.06×10^{6}	0.71×10^{6}
5	9.00×10^{6}	1.45×10^{7}	1.10×10^{7}	0.35×10^{7}	4.0	7.75×10^{6}	7.5×10^{6}
8	2.0×10^{6}	3.1×10^{6}	2.2×10^{6}	0.9×10^{6}	22.0	1.40×10^{6}	1.30×10^{6}
7	1.30×10^{6}	2.02×10^{6}	1.44×10^{6}	0.58×10^{6}	30.0	1.06×10^{6}	0.86×10^{6}
13	3.26×10^{6}	5.05×10^{6}	3.58×10^{6}	1.47×10^{6}	13.0	2.38×10^{6}	2.11×10^{6}
14	4.68×10^{6}	7.27×10^{6}	5.18×10^{6}	2.09×10^{6}	10.0	3.09×10^{6}	3.09×10^{6}
9	6.18×10^{6}	9.6×10^{6}	6.84×10^{6}	2.76×10^{6}	6.5	4.75×10^{6}	4.08×10^{6}

axis and towards the surface. Thus it is necessary to invoke internal sources of some kind to account for the present results. One would expect very few sources to be active near the neutral axis where the stress is low, and, since only majority sign dislocations are moved towards this region, one would expect the proportion of minority sign dislocations near the neutral axis to be lower than near the top and bottom surfaces. However, in the samples bent at 360°C, the etch-pit results indicated that the proportion of minority sign dislocations did not vary appreciably in a direction perpendicular to the neutral axis. For example, in the Sb-bent specimen 14 (Table 7.2) the etch-pit densities at the neutral axis were $\rho_{CP_4} = 4.41 \times 10^6$ cm^{-2} and $\rho_{But} = 6.81 \times 10^6$ cm^{-2}. At the top surface the etch-pit densities were $\rho_{CP_4} = 5.01 \times 10^6$ cm^{-2}, and $\rho_{But} = 7.70 \times 10^6$ cm^{-2}. Calculating ρ_{In} and ρ_{Sb} by equations (7.2) and (7.3) one finds that $\rho_{Sb}/\rho_{In} = 2.38$ at the neutral axis and $\rho_{Sb}/\rho_{In} = 2.32$ at the top surface. The reason for this behaviour is not clear, but it is possible that dislocation climb is responsible for the uniform distribution of minority dislocations.

CHAPTER 8.

ELECTRICAL MEASUREMENTS.

8.1. Specimens deformed by three-point bending.

Two series of specimens were deformed at 360°C to produce in the one series an excess of In-dislocations and in the other an excess of Sb-dislocations. Electrical conductivity and Hall coefficient measurements were made on the bent samples and on undeformed control samples. Bent samples were sectioned parallel to face 'B' (Fig.6.4) for etch-pit measurements.

8.1.1. Measurements at room temperature.

At room temperature, the conductivity and Hall coefficients of all the deformed samples were equal to the values in the corresponding control samples. All were n-type with a Hall coefficient equal to the intrinsic value, i.e. 390 cm^3/Coulomb. This indicates that the deformation produced no change in the carrier concentration at this temperature. The conductivities were all equal to the intrinsic conductivity (200 ohm-cm^{-1}) which, taken with the Hall coefficient measurements, indicate that the electron mobility at this temperature was unchanged after bending. At 80°K, however, deformed specimens showed properties markedly different from those of the control samples, and these results are detailed below.

8.1.2. Measurements at 80°K.

n-type material.

Three specimens were bent to produce an excess of In-dislocations and one was bent to produce an excess of Sb-dislocations. For all In-bent samples, electrical measurements were made on an L-shaped specimen cut from one half of each bent wafer as shown in Fig.6.9. Two L-shaped samples were prepared from the Sb-bent wafer, one from either side of the bend axis. In all cases the 'parallel' limb 'AB' showed uniform electrical properties, in that Hall coefficient and conductivity measurements made at different points along the limb were closely reproducible. The other limb, however, showed non-uniform properties. Hall coefficient measurements at one end (B) always approximated to those of the parallel limb AB, and at the other end (C) to those of the control specimen. This variation in properties was paralleled by a variation in dislocation density along the limb, since etchants revealed a high etch-pit density near the position of the central knife edge (i.e. near B), and this decreased to a value little different from that of the virgin crystal near the outer knife edges (i.e. near C).

We will first consider the 'parallel' limbs (AB):

In-bending produced an increase in the Hall

coefficient of each specimen, and the material remained n-type after deformation. In the case of Sb-bent specimens the material was converted to p-type at 80°K. These results indicate in both cases that acceptor centres had been introduced. In Table 8.1 the Hall coefficients and conductivities of control and 'parallel' samples are listed, together with etch-pit densities in the deformed samples (measured as close as possible to the bend-axis). The results were analysed on the Read model, and $\langle n \rangle$, the average carrier concentration in the n-type 'parallel' samples, was calculated from the Hall coefficient by the relation $\langle n \rangle = \frac{1}{R_{\parallel} q}$

The carrier concentration in p-type 'parallel' samples was calculated from the Hall coefficient by the relation

$$\langle p \rangle = \frac{1}{R_{\parallel} q} \qquad \ldots\ldots (8.1)$$

A similar relation was used by Bliek (1964) when analysing results on deformed p-type germanium. It must be noted, however, that (8.1) has not been derived rigorously and hole concentrations calculated by this expression are liable to be in error.

Table 8.2 gives the carrier concentrations and mobilities ($R_H \sigma$) calculated from the Hall coefficient and conductivity measurements. For In-bent specimens the increase in acceptor concentration, $n - \langle n \rangle$, was roughly

Table 8.1: Three-point bending of originally n-type material. Hall coefficient and conductivity measurements at 80°K.

In-bent specimens

Specimen No.	ρ_{CP_4} (cm^{-2})	ρ_{But} (cm^{-2})	R_o cm^3/Coul.	$R_{//}$ cm^3/Coul.	σ_o $(\Omega\text{-cm})^{-1}$	$\sigma_{//}$ $(\Omega\text{-cm})^{-1}$
D.2	4.9×10^6	6.9×10^6	8.0×10^4	5.34×10^5	6.87	0.34
D.5	8.5×10^6	1.25×10^7	5.43×10^4	1.84×10^5	10.5	0.72
D.4	1.05×10^7	1.40×10^7	5.29×10^4	2.75×10^5	10.3	0.64

Sb-bent specimens

Specimen No.	ρ_{CP_4}	ρ_{But}	R_o (n-type)	$R_{//}$ (p-type)	σ_o (n-type)	$\sigma_{//}$ (p-type
D.3	7.3×10^6	1.71×10^7	6.82×10^4	8.81×10^3	8.22	0.784
D.3a	3.5×10^6	1.05×10^7	6.82×10^4	1.63×10^4	8.22	0.355

Table 8.2: Three-point bending of originally n-type material.

'Read' interpretation of measurements at 80°K.

In-bent specimens

Specimen No.	ρ_{CP_4} (cm^{-2})	ρ_{But} (cm^{-2})	n (cm^{-3})	$\langle n \rangle$ 'Parallel' Limb	$\frac{n-\langle n \rangle}{\rho_{But}/c}$	μ_o $cm^2/V.sec$	$\mu_{//}$ $cm^2/V.sec$
D.2	4.9×10^{6}	6.9×10^{6}	7.81×10^{13}	1.17×10^{13}	0.385	5.49×10^{5}	1.82×10^{5}
D.5	8.5×10^{6}	12.5×10^{6}	1.15×10^{14}	3.4×10^{13}	0.259	5.74×10^{5}	1.32×10^{5}
D.4	10.5×10^{6}	14.0×10^{6}	1.18×10^{14}	2.27×10^{13}	0.273	5.49×10^{5}	1.71×10^{5}

Sb-bent specimens

Specimen No.	ρ_{CP_4}	ρ_{But}	n	$\langle n \rangle$ 'Parallel' Limb	$\frac{n+\langle n \rangle}{\rho_{But}/c}$	μ_o (n-type)	$\mu_{//}$ (p-type)
D.3	7.3×10^{6}	17.1×10^{6}	9.16×10^{13}	7.1×10^{14}	1.87	5.61×10^{5}	6.90×10^{3}
D.3a	3.5×10^{6}	10.5×10^{6}	9.16×10^{13}	3.83×10^{14}	1.81	5.61×10^{5}	5.78×10^{3}

proportional to the etch-pit density. The same trend was found in Sb-bent samples, but the numbers of acceptors introduced (per cm^3) were an order of magnitude higher than those for In-bent samples of comparable etch-pit density. In the In-bent samples (which remained n-type) the mobility in the 'parallel' limbs was reduced by up to a factor of 4 compared with the control specimens.

In the 'perpendicular' limbs the Hall coefficient varied along their length as shown in Figs.8.1 and 8.2. Also shown are values of the increase in acceptor concentration (calculated by the method described above) and, for comparison, the etch-pit density measured along the perpendicular direction is plotted below. It is seen that changes in carrier concentration are proportional to the local etch-pit density. Because of the variation in carrier concentration along the limbs BC it was practically impossible to obtain an accurate measurement of Hall mobility. An approximate value was obtained from the product of the conductivity measurement at probes 1 and 3 (Fig.6.9) and the Hall coefficient at probes 2 - 2. In the In-bent specimens the Hall mobilities calculated in this way were all less than 1.0×10^5 cm^2 V^{-1} sec^{-1}, i.e. about a factor of 2 less than the mobility with current flow parallel to the dislocations, and a factor of about 8 less than the mobility in the undeformed control specimens.

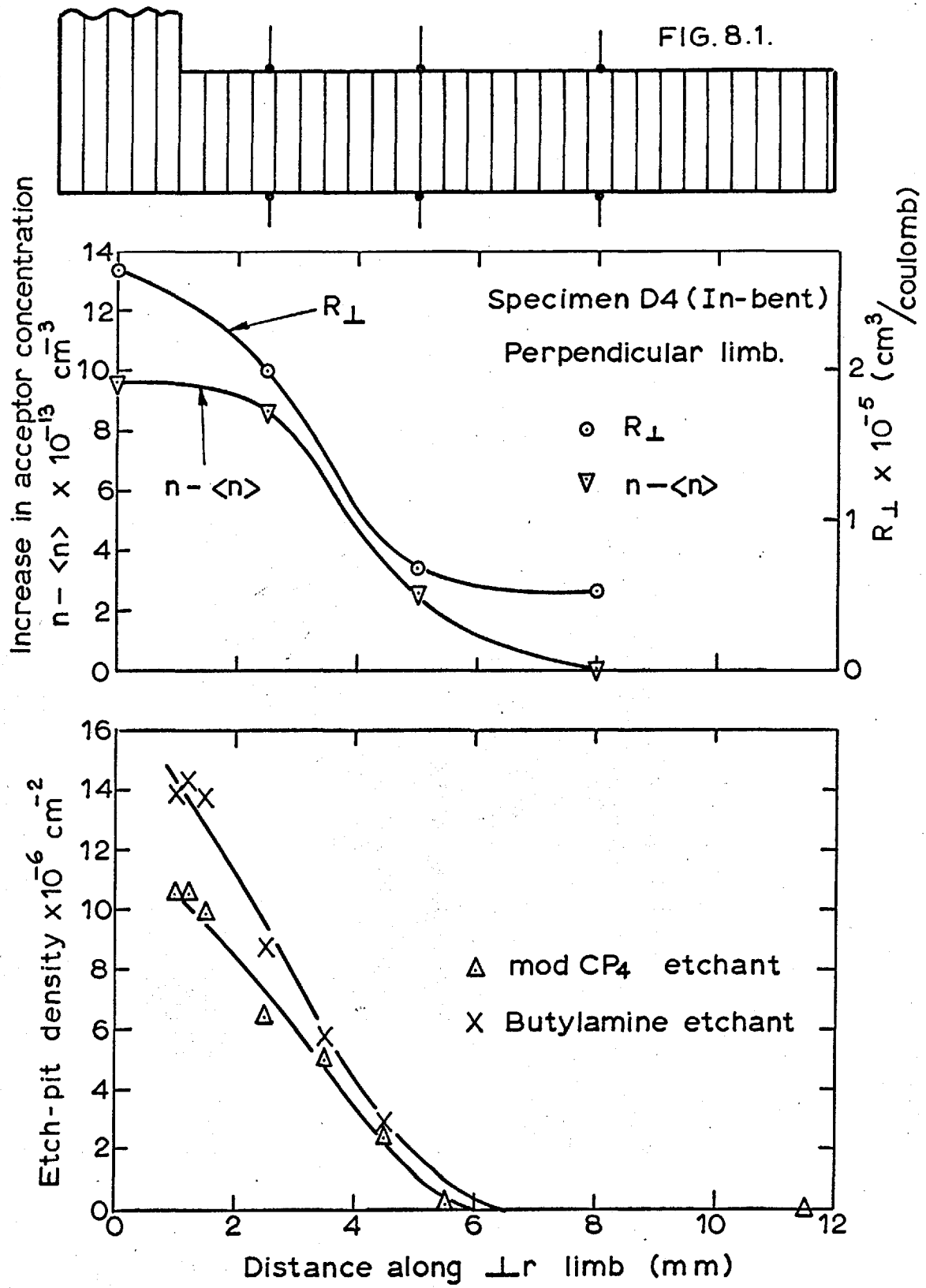
FIG. 8.1.
Specimen D4 (In-bent)
Perpendicular limb.
$R_\perp$
$n - \langle n \rangle$
Increase in acceptor concentration
$n - \langle n \rangle \times 10^{-13}$ cm^{-3}
$R_\perp \times 10^{-5}$ (cm^3/coulomb)
Etch-pit density $\times 10^{-6}$ cm^{-2}
mod CP_4 etchant
Butylamine etchant
Distance along $\perp r$ limb (mm)

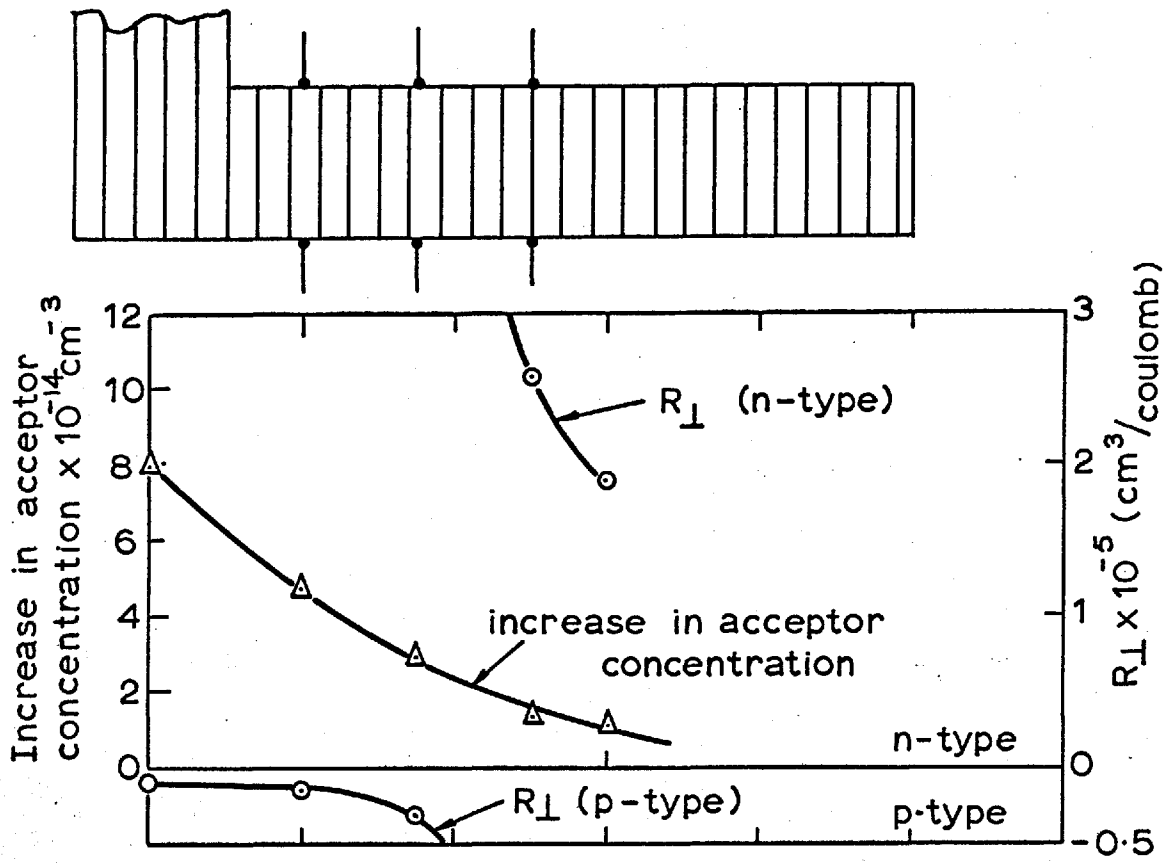

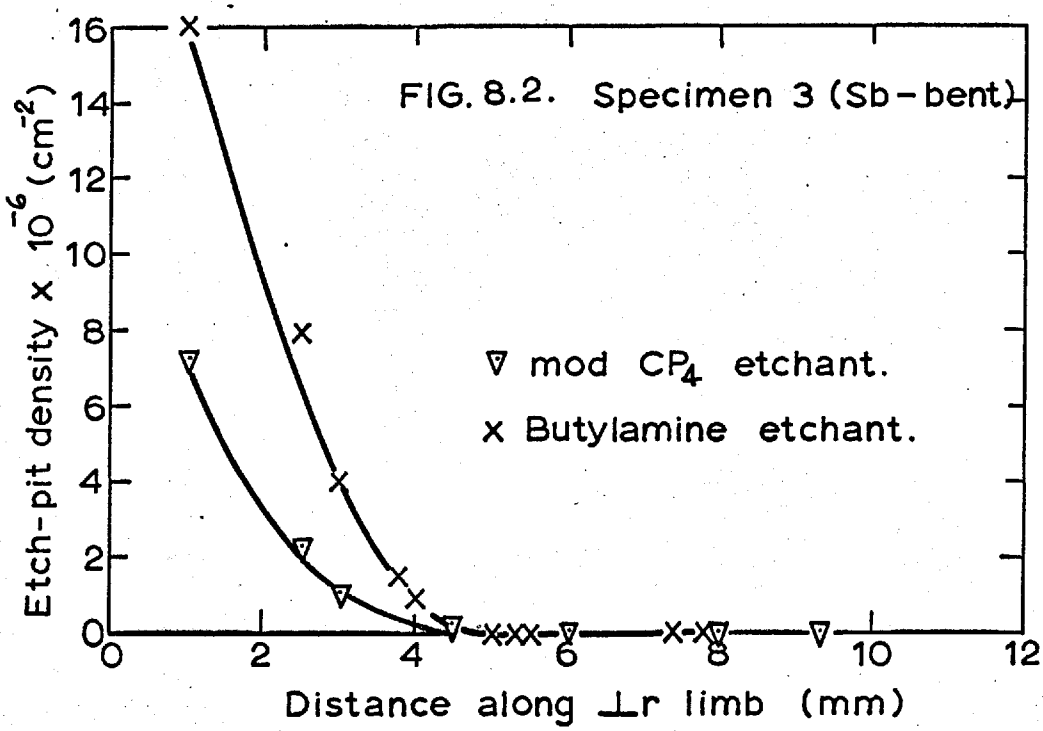

FIG. 8.2. Specimen 3 (Sb-bent)

The Sb-bent samples were all converted to p-type by the bending. They showed an anisotropy in the hole mobility of about a factor of 2.

p-type material.

Two wafers were bent to produce an excess of In-dislocations, and two to produce an excess of Sb-dislocations. L-shaped specimens were cut from the wafers for electrical measurements. The properties of the 'parallel' limbs AB were again found to be uniform along their length. Table 8.3 shows Hall coefficient and conductivity measurements for the 'parallel' limbs and control samples at 80°K. The dislocation densities in the parallel limbs were estimated by etch-pit counts made as close as possible to the bend axis. These values are also listed in the table.

Indium bending produced a decrease in the Hall coefficient of the p-type samples, indicating an introduction of acceptor centres. Sb-bending, however, produced in the one specimen a small increase in the Hall coefficient (indicating an introduction of donor centres) and in the other no measurable change in Hall coefficient.

Carrier concentrations of deformed p-type specimens were calculated from the Hall coefficients by (8.1). Table 8.4 lists values of carrier concentration and mobility ($R_H\sigma$) calculated from the Hall coefficient and

Table 8.3: Three-point bending of originally p-type material.

Hall coefficient and conductivity measurements at 80°K.

In-bent specimens

Specimen No.	ρ_{CP_4} (cm^{-2})	ρ_{But} (cm^{-2})	R_o ($cm^3/Coul$)	$R_{//}$ ($cm^3/Coul$)	σ_o $(\Omega cm)^{-1}$	$\sigma_{//}$ $(\Omega cm)^{-1}$
A.1	1.93×10^6	2.3×10^6	9.25×10^3	6.58×10^3	0.761	1.28
A.2	3.9×10^6	4.9×10^6	1.45×10^4	5.85×10^3	0.582	0.99

Sb-bent specimens

Specimen No.	ρ_{CP_4}	ρ_{But}	R_o	$R_{//}$	σ_o	$\sigma_{//}$
A.4	6.15×10^6	1.64×10^7	1.22×10^4	1.62×10^4	0.85	0.41
A.5	4.8×10^6	8.2×10^6	1.17×10^4	1.17×10^4	0.80	0.50

Table 8.4: Three-point bending of originally p-type material

Interpretation of measurements at 80°K.

In-bent specimens

Specimen No.	ρ_{CP_4} (cm^{-2})	ρ_{But} (cm^{-2})	p (cm^{-3})	'Parallel' Limb $\langle p \rangle$ (cm^{-3})	$\frac{\langle p \rangle - p}{\rho_{But}/c}$	μ_o $cm^2/V.sec$	$\mu_{\parallel}$ ($R_{\parallel}\sigma_{\parallel}$) $cm^2/V.sec$
A.1	1.93×10^6	2.3×10^6	6.67×10^{14}	9.51×10^{14}	4.93	7.04×10^3	8.45×10^3
A.2	3.9×10^6	4.9×10^6	4.30×10^{14}	10.65×10^{14}	5.18	8.45×10^3	5.78×10^3

Sb-bent specimens

Specimen No.	ρ_{CP_4}	ρ_{But}	p	$\langle p \rangle$	$\frac{p - \langle p \rangle}{\rho_{But}/c}$	μ_o	$\mu_{\parallel}$ ($R_{\parallel}\sigma_{\parallel}$)
A.4	6.15×10^6	16.4×10^6	5.11×10^{14}	3.86×10^{14}	0.305	1.03×10^4	6.69×10^3
A.5	4.8×10^6	8.2×10^6	5.34×10^{14}	5.34×10^{14}	0	0.944×10^4 (9.44×10^3)	5.85×10^3

conductivity measurements. It is seen that a very large density of acceptor centres (of order 5×10^{14} cm^{-3}) was introduced by In-bending. In-bending produced no significant change in Hall mobility in these 'parallel'limbs, but in both Sb-bent samples where the change in Hall coefficient was small there was a significant drop in Hall mobility.

8.1.3. Discussion of three-point bending results.

The results may be summarised as follows:

Indium bending introduced acceptor centres into both n- and p-type materials.

Antimony bending introduced acceptor centres into material originally n-type, to the extent that the material was converted to p-type. However, specimens which were originally p-type showed no evidence of acceptor introduction, and results for one specimen indicated the introduction of a small number of donor centres.

All of these results can be accommodated qualitatively by the scheme of energy levels shown in Fig.8.3. The low-lying acceptor level of the indium dislocation is ionised in both n- and p-type material. The dual role of the Sb-dislocation is due to a high acceptor level and a low lying donor level. In p-type material (doped with germanium) the Fermi level at $80^{o}K$ will be very close to the valence band and the Sb-donor centres will be ionised

FIG.8.3. Scheme of energy levels of dislocation – acceptors and donors.

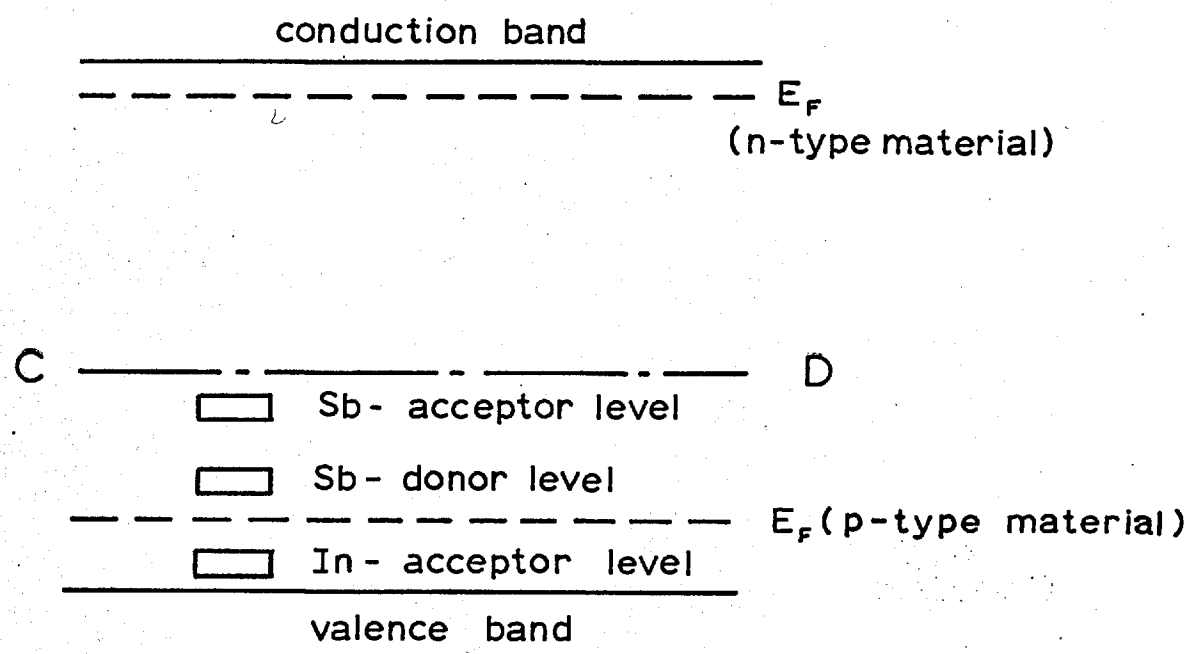

C D = Fermi level in material originally n-type which has been Sb bent and converted to p- type.

but not the Sb-acceptor centres. However, in n-type material the Fermi level at 80°K will be very close to the conduction band and the Sb-acceptor centres will be ionised but not the donor centres. In the material originally n-type, and converted to p-type by Sb-bending, the Fermi level at 80°K may be in the position CD which, although below the centre of the gap, is high enough that the Sb acceptor centres are still ionised. This energy level diagram accounts for these results qualitatively, but it is instructive to consider them quantitatively.

Assuming Read's theory to be applicable, values of the occupation fraction, f, for each sign of bending, may be calculated from the values given in Table 8.1. since rearrangement of (4.17) gives:

$$f = \frac{n - \langle n \rangle}{\rho / c}$$

Substituting the butylamine etch-pit density for ρ, values of $\frac{n - \langle n \rangle}{\rho / c}$ were calculated and are shown in Table 8.2. For originally n-type material, In-bending gives values for f of about 0.3, while Sb-bending gives values of about 1.8. Applying Read's theory to InSb, a rough calculation on the Fermi approximation (equation (4.11)) shows that the maximum theoretical value of f possible at 80°K is about 0.091. This value was obtained for the maximum value of $E_F - E_D$, the separation of the

Fermi and dislocation-acceptor levels, by setting this quantity at 0.23 e.V, the magnitude of the band gap. Thus, in the case of In-bending of n-type material, the experimental value of f is about a factor of 3 larger than the maximum theoretical value, and in Sb-bent samples the corresponding discrepancy is a factor of 18. It is possible that the discrepancy in the In-bent samples is due to an underestimation of the true dislocation density by the etch-pit technique, but it is unlikely that this could account for the large discrepancy found in the case of the Sb-bent samples.

There are other considerations which throw further doubt on the validity of Read's theory for describing dislocation-acceptors in InSb. Calculations for p-type material on Bliek's model, even using an artificially low screening length, result in values of f at 80°K of less than 0.1. It is therefore difficult to understand why In-bending should introduce over an order of magnitude more acceptors into p-type material than into n-type material, for comparable etch-pit densities. In general, one would expect an acceptor centre to be more fully occupied in n-type material than in p-type material. Also it is difficult to understand why Sb-bending of originally n-type material should introduce more acceptors than In-bending. If the Sb acceptor level is higher than the In acceptor level the reverse would be expected.

Thus this scheme of energy levels, while being qualitatively satisfactory, is questionable when examined quantitatively. In order to make a detailed quantitative study of n-type material, four-point bending was adopted for the following reasons. Firstly, four-point bending produces a region of uniform dislocation density, enabling Hall mobility measurements to be made on 'perpendicular' samples. Secondly, etch-pit densities can be correlated more accurately with electrical measurements, since neither are sensitive to position within the uniform area. Thirdly, there is more confidence in the analysis of Hall coefficients and conductivities of macroscopically uniform materials.

8.2. Four-point bending of n-type material.

Two series of specimens were bent to introduce in the one case an excess of In-dislocations, and in the other an excess of Sb-dislocations. Electrical measurements were made both before and after the deformation. Undeformed 'control' samples were measured before and after the deformation, and in all cases no significant change in Hall coefficient or conductivity was detected. In each bending experiment a 'deformed control' specimen (a sample which had previously been bent at 360°C) was also kept close to the one being deformed. This 'deformed control' specimen was measured before and after

the heat treatment and in all cases no significant change in the Hall coefficient or conductivity was detected. After bending, the deformed samples were sectioned parallel to face 'B' (Fig.6.4) for etch-pit measurements.

At room temperature, the Hall coefficient and conductivity of deformed samples were equal to those of the undeformed 'control' samples. The measurements at 80°K are detailed below.

8.2.1. Measurements at 80°K.

In-bent samples.

Table 8.5 shows the electrical measurements at 80°K for undeformed control samples, bent samples and the etch-pit densities of the deformed samples. We shall consider first the samples which remained n-type after deformation. The Hall coefficient of each deformed sample was greater than that of the corresponding control sample and qualitatively this indicates an introduction of acceptor centres. The Hall coefficients of 'parallel' and 'perpendicular' samples were equal (within experimental error), but in all cases $\sigma_{\perp} < \sigma_{//}$. Thus, the mobility was lower in the 'perpendicular' sample than in the 'parallel' sample.

One sample (15) was converted to p-type by the deformation. Since the dimension BC (Fig.6.1) of this specimen was only 0.5 cms, no 'parallel' sample could be

Table 8.5: Hall coefficient and conductivity measurements at 80°K on undeformed control samples (R_o, σ_o), 'parallel' samples ($R_{//}, \sigma_{//}$) and perpendicular samples ($R_\perp, \sigma_\perp$), and their etch-pit densities (ρ_{But}).

In-bent specimens.

Specimen No.	ρ_{But} cm^{-2}	R_o (n-type) $cm^3/Coul.$	$R_\perp = R_{//}$ (n-type) $cm^3/Coul.$	σ_o $(\Omega cm)^{-1}$	$\sigma_{//}$ $(\Omega cm)^{-1}$	$\sigma_\perp$ $(\Omega cm)^{-1}$
6	5.82×10^6	8.80×10^4	3.56×10^5	6.36	1.38	0.44
3	3.30×10^7	1.1×10^4	2.25×10^4	38.2	17.19	5.97
1	1.4×10^6	6.61×10^4	7.38×10^4	8.58	7.59	6.05
11	7.25×10^5	7.45×10^4	7.84×10^4	7.58	6.79	6.15
12	2.88×10^6	8.82×10^4	1.23×10^5	5.33	3.51	2.52
2	3.18×10^6	1.34×10^5	3.05×10^5	3.55	1.43	0.639
10	1.35×10^7	5.3×10^4	2.74×10^5	9.56	1.15	0.42
	ρ_{But}	R_o (n-type)	$R_\perp$ (p-type)	σ_o (n-type)		$\sigma_\perp$ (p-type)
15	2.67×10^7	7.50×10^4	5.21×10^4	7.60		0.112

Sb-bent specimens

	ρ_{But}	R_o (n-type)	$R_\perp = R_{//}$ (n-type)	σ_o (n-type)	$\sigma_{//}$ (n-type)	$\sigma_\perp$ (n-type)
4	1.71×10^6	5.81×10^4	1.35×10^5	10.2	3.98	1.88
5	1.45×10^7	9.00×10^3	3.99×10^4	45.6	8.16	2.44
8	3.1×10^6	3.36×10^4	6.945×10^4	16.55	6.70	2.88
7	2.02×10^6	4.28×10^4	7.27×10^4	12.3	6.22	3.08
13	5.05×10^6	1.04×10^4	1.427×10^4	37.8	24.8	15.56
14	7.27×10^6	8.62×10^3	1.147×10^4	47.9	32.6	20.05
9	9.6×10^6	6.65×10^3	8.954×10^3	52.34	35.0	22.34

cut from it, and the results given in Table 8.5 are confined to measurements on the 'perpendicular' sample.

Sb-bent samples.

Detailed results are given in Table 8.5.. All specimens were n-type after deformation and the Hall coefficient results indicated an introduction of acceptor centres. The conductivities also showed trends similar to those of In-bent samples.

8.2.2. Measurements from 80°K to 295°K.

In the case of two In-bent samples and two Sb-bent samples, the Hall coefficients of both control and deformed samples were measured over the full range of temperature from 80°K to 295°K. These results are plotted in Figs.8.4 to 8.7. In the intrinsic range of temperature the R_H versus T curves for the control and deformed samples were superposed, as shown in Fig.8.4. Some of the intrinsic range of temperature is omitted in Figs. 8.5. to 8.7 in order to show the extrinsic range in more detail, but the same trends in the intrinsic range as observed in Fig.8.4 were found in these samples.

In the extrinsic range, the undeformed control specimens showed a temperature independent Hall coefficient as observed by previous workers. For the deformed specimens, however, the Hall coefficient increased as the temperature fell. This increase in Hall

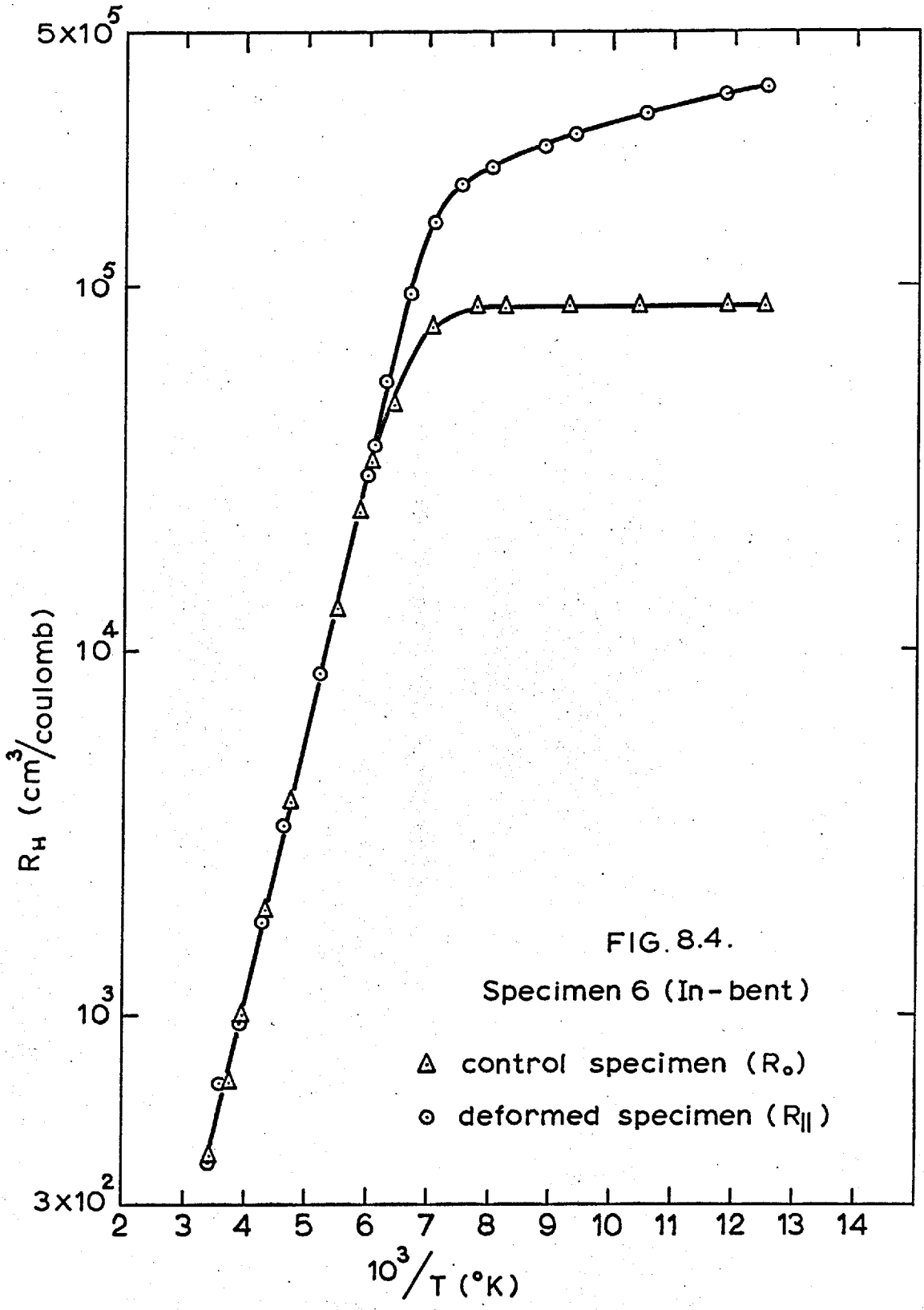
5x10^5
10^5
10^4
10^3
3x10^2
R_H (cm^3/coulomb)
2
3
4
5
6
7
8
9
10
11
12
13
14
10^3/T (°K)
Specimen 6 (In-bent)
control specimen (R_o)
deformed specimen (R_||)

FIG. 8.4.

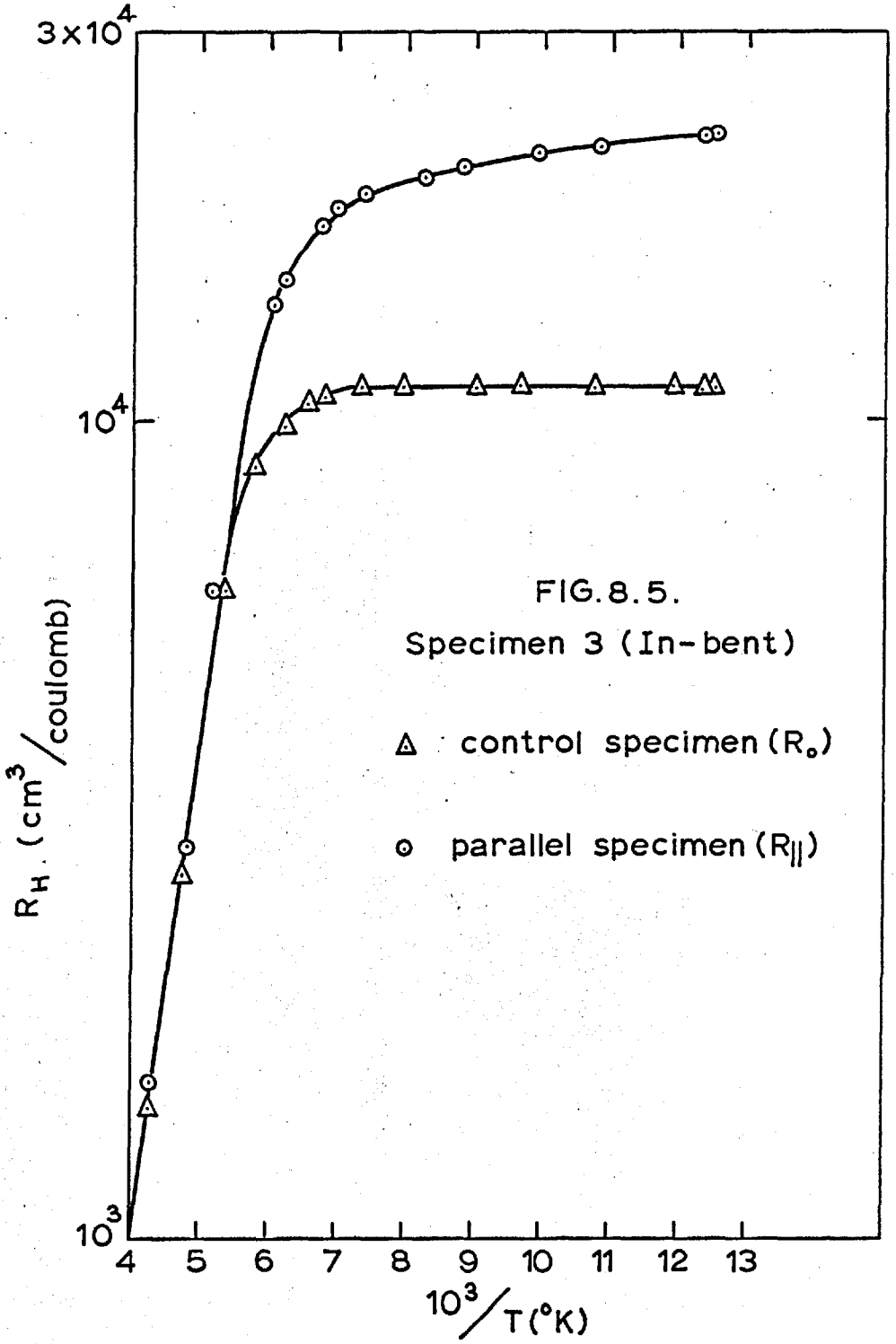

FIG. 8.5.
Specimen 3 (In-bent)

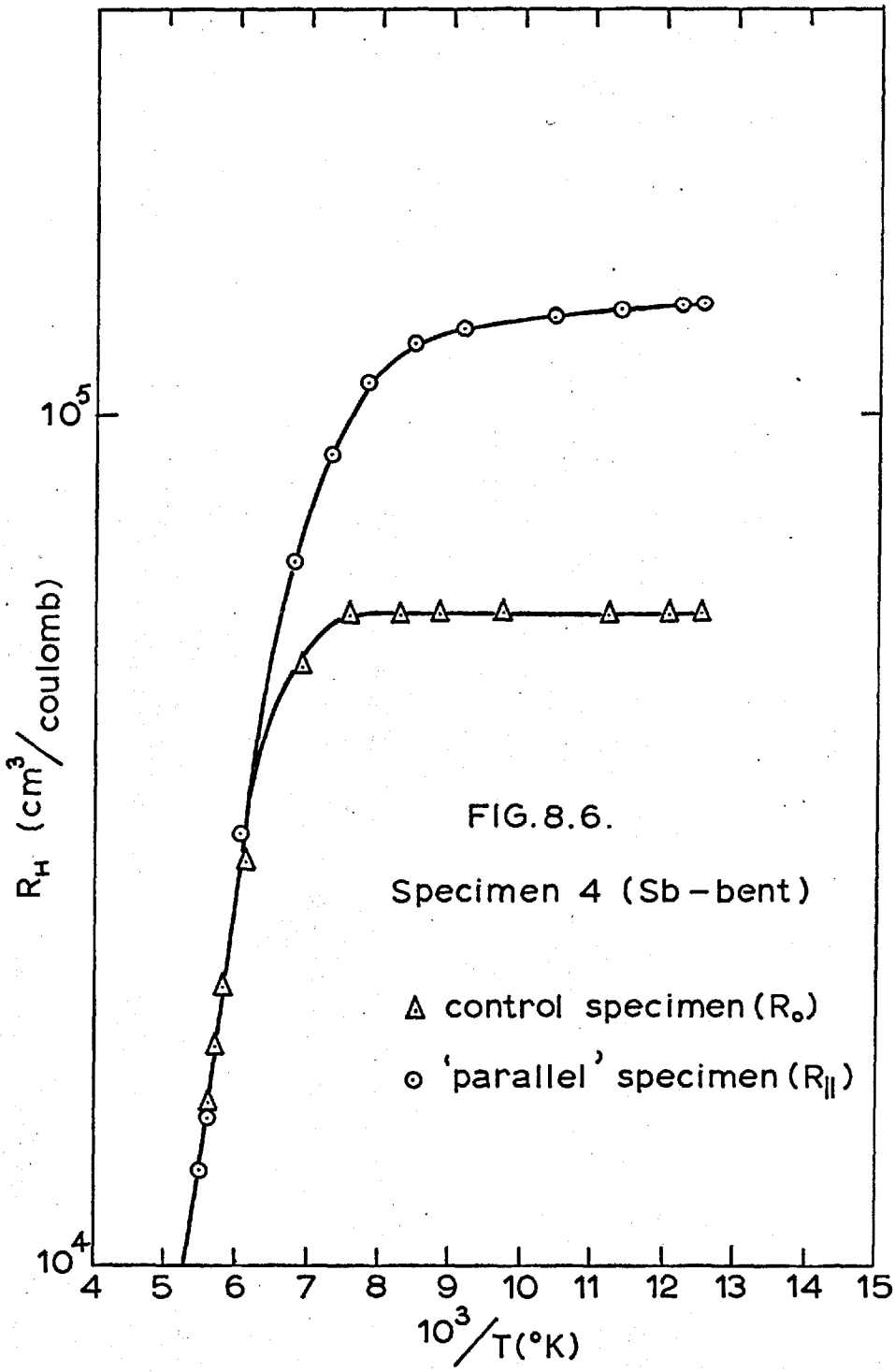
10^5
10^4
R_H (cm^3/coulomb)
4 5 6 7 8 9 10 11 12 13 14 15
$10^3/T(°K)$
FIG. 8.6.
Specimen 4 (Sb – bent)
△ control specimen (R_o)
⊙ 'parallel' specimen ($R_{||}$)

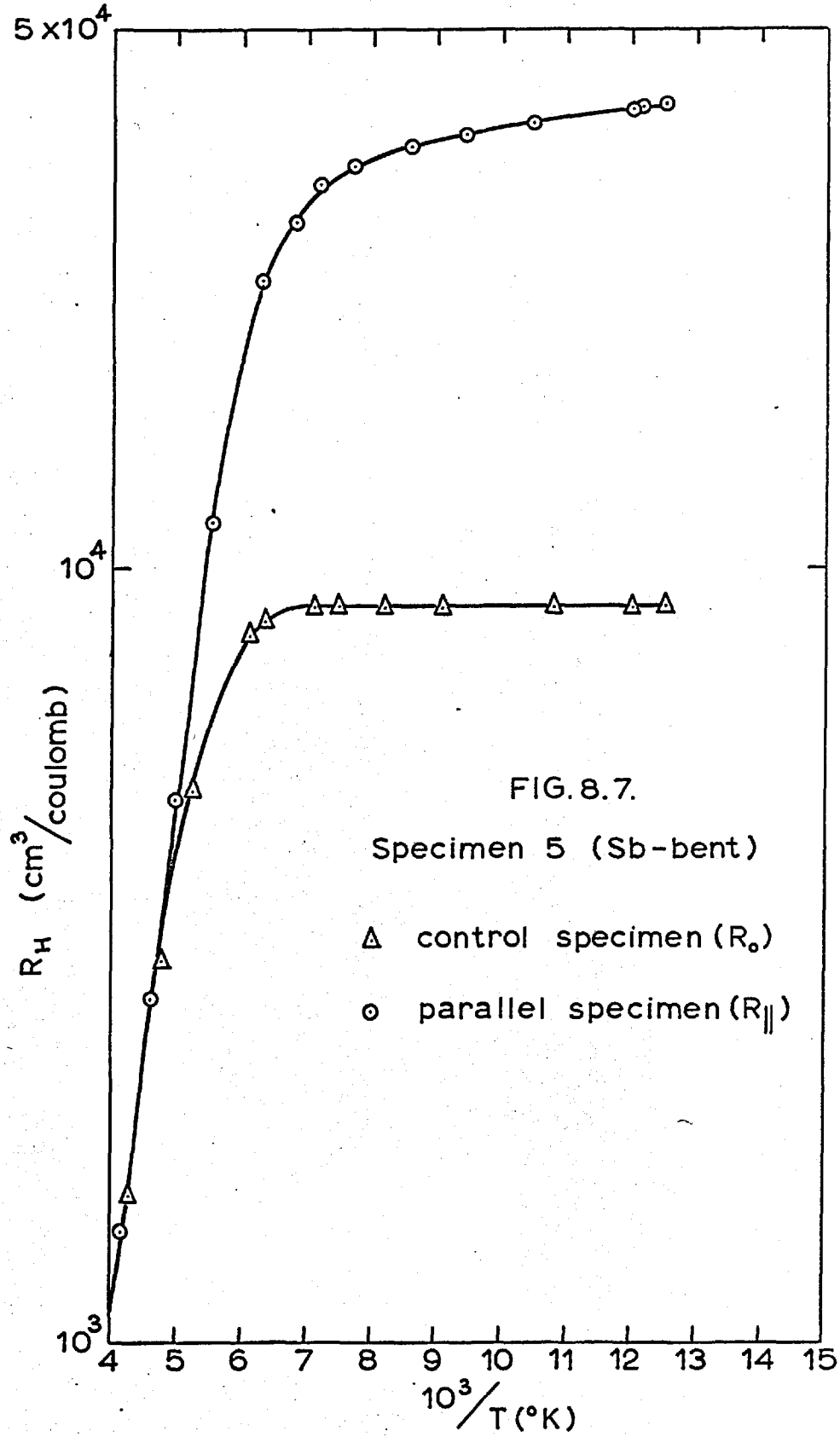
5 x 10^4
10^4
10^3
R_H (cm^3/coulomb)
4
5
6
7
8
9
10
11
12
13
14
15
10^3/T (°K)
FIG. 8.7.
Specimen 5 (Sb-bent)
control specimen (R_o)
parallel specimen (R_||)

coefficient is normally associated with the deionisation of centres whose energy level lies within the forbidden gap. If these centres are, say, widely spaced impurity acceptors, the interaction between accepted electrons is negligible and the occupation of the centres is governed by Fermi statistics. In this case the position of the energy level can usually be obtained directly from the slope of the Hall coefficient versus temperature curve. However, if these centres are dislocation acceptors, the electrostatic interaction between the accepted electrons must be considered, and a more lengthy procedure must be followed to determine the dislocation acceptor level. For the reasons outlined in Section 9.2. we will analyse these results in terms of dislocation-acceptors.

In order to determine the scattering mechanism (or mechanisms) operating at a particular temperature, it was necessary to measure the Hall mobility of the control samples over this range of temperature ($80^{\circ}K$ - $295^{\circ}K$). The conductivity of these four specimens was measured as a function of temperature and is shown in Fig.8.8. The Hall mobility ($R_H\sigma$) at each temperature was calculated and is plotted in Fig.8.9. Straight lines corresponding to a $T^{-1.5}$ and $T^{-1.6}$ temperature dependence are included for comparison. It is clear that, above about $200^{\circ}K$, the mobility was approximately proportional to $T^{-1.6}$ as noted by previous workers.

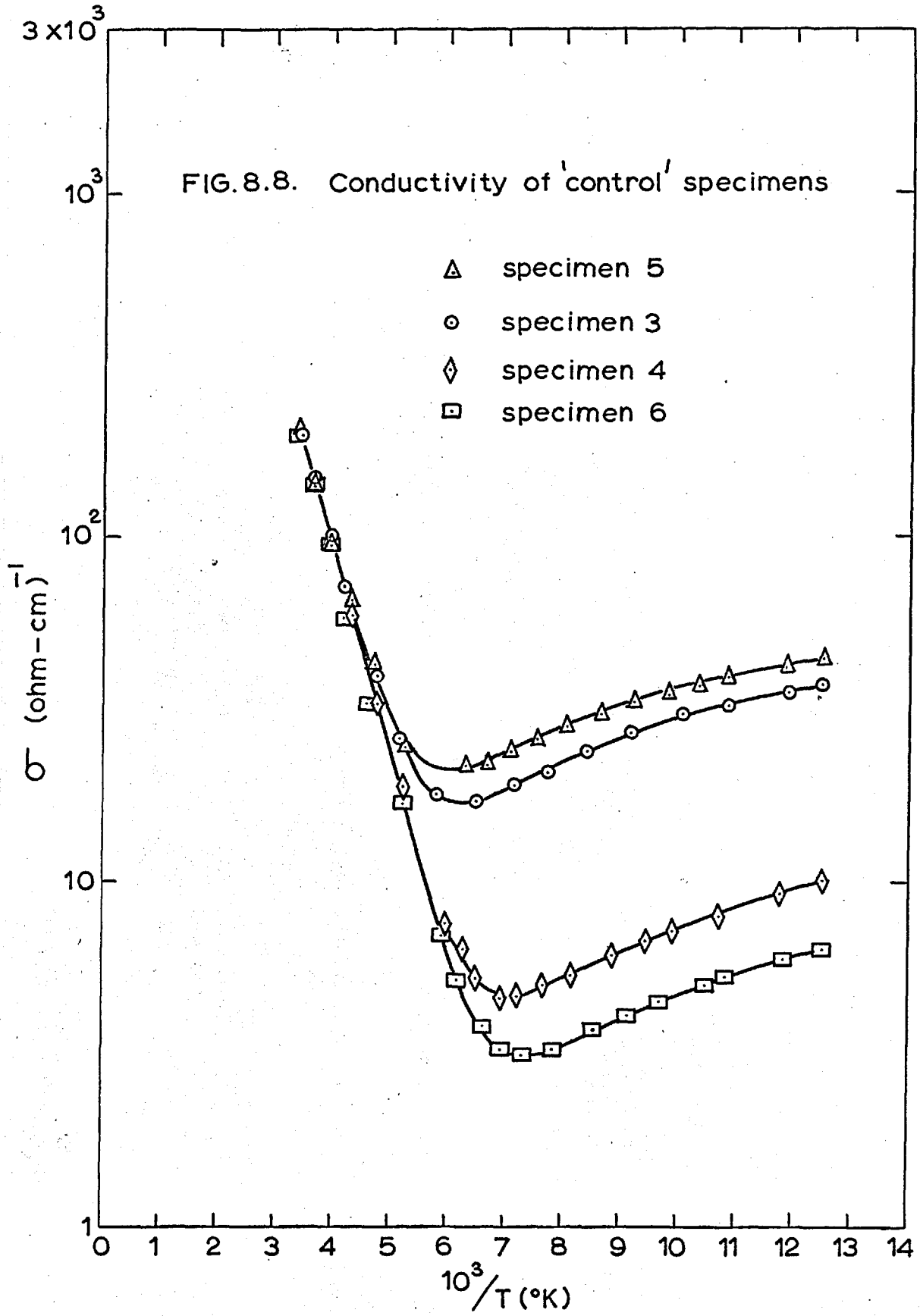

FIG. 8.8. Conductivity of 'control' specimens

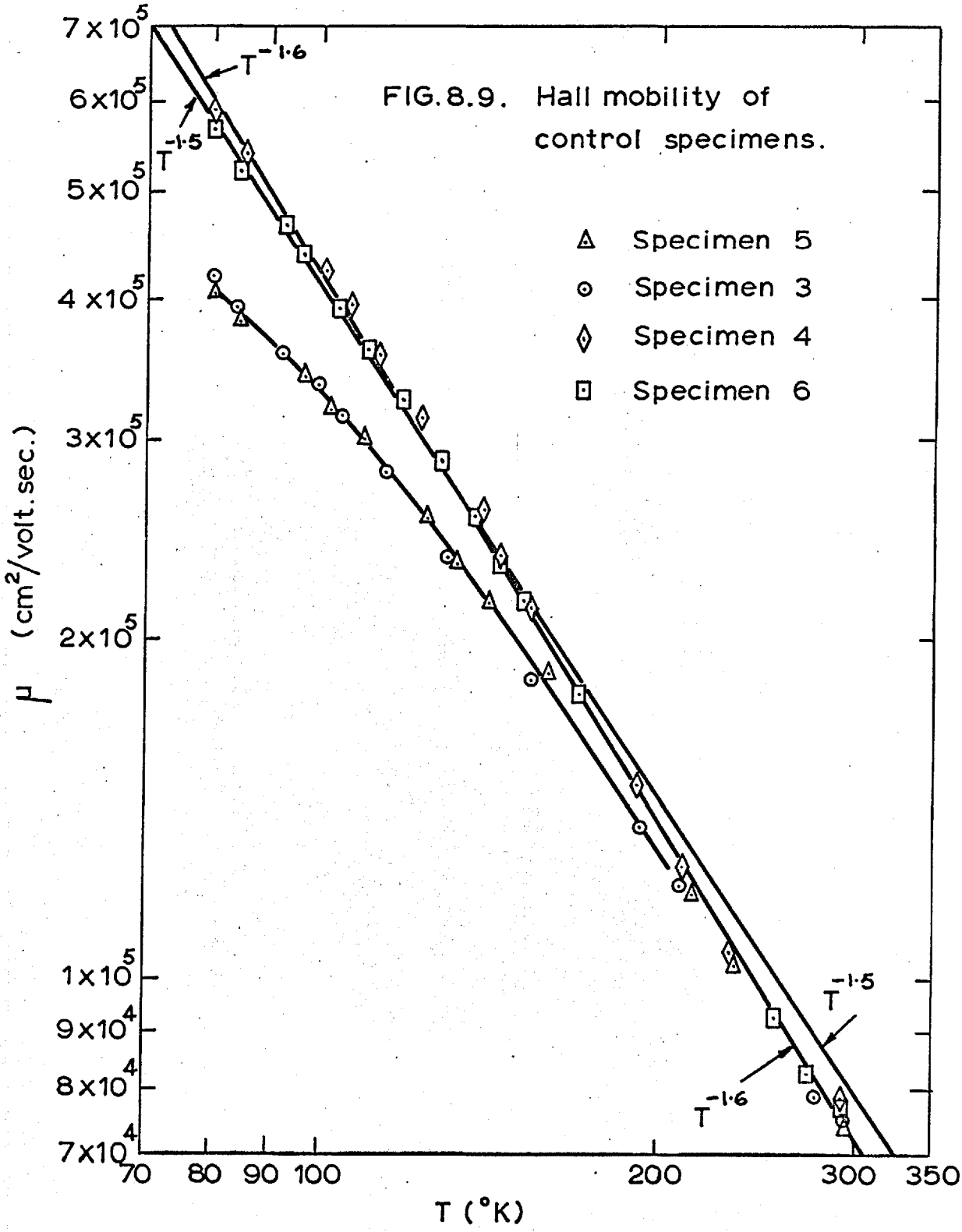

FIG. 8.9. Hall mobility of control specimens.

In the case of specimens 6 and 5, the Hall coefficient was measured as a function of magnetic field, for magnetic field strengths from 500 gauss to 1500 gauss. Throughout this range of field strengths the Hall coefficient of each sample (deformed and undeformed) at 80°K differed from its value at 1000 gauss by not more than 8%. (A similar behaviour was found by Bate, Willardson and Beer (1959) for undeformed samples). At room temperature the Hall coefficient of deformed and undeformed samples was independent of magnetic field strength (as observed by Hilsum and Barrie (1958) for undeformed samples).

8.3. 'Read' Interpretation.

8.3.1. Analysis of measurements at 80°K.

The results were first analysed on the Read model, using the method of Logan et al (1959). The carrier concentration of n-type 'parallel' and 'perpendicular' samples, $\langle n \rangle$, was calculated directly from the Hall coefficients given in Table 8.5 using the relation

$$\langle n \rangle = \frac{1}{R_{\parallel} q} = \frac{1}{R_{\perp} q}$$

[The experimental observation that $R_{\parallel} = R_{\perp}$ is in agreement with the prediction of Logan et al.]

The carrier concentration in the p-type 'perpendicular' sample of specimen 15 was calculated from the Hall coefficient by the relation $\langle p \rangle = \frac{1}{R_1 q}$. As noted in Section 8.1.2, there is no theoretical derivation of this relation. The carrier concentration in each control sample, n, was calculated from its Hall coefficient, R_o, by the relation $n = \frac{r}{R_o q}$. As discussed in Section 3.4, the parameter r was assumed to be unity since no value has been derived theoretically for this range of temperature.

Values of the net change in carrier concentration at 80°K, $n - \langle n \rangle$ or $n + \langle p \rangle$, were therefore calculated from the Hall coefficients of control and deformed specimens. The results, given in Table 8.6, indicated some correlation between $n - \langle n \rangle$ (or $n + \langle p \rangle$) and the etch-pit density, and Fig. 8.10 shows a plot of $n - \langle n \rangle$ (and $n + \langle p \rangle$) versus ρ_{But} for In-bent and Sb-bent samples. Results of the three-point bending experiments are included for comparison. Within experimental error, the results for Sb-bent samples lie on a straight line of slope = 3.85×10^7 cm^{-1}, while the In-bent results lie on a straight line of slope = 0.816×10^7 cm^{-1}. The results suggest that Sb-dislocations provide greater than four times more acceptor centres per unit length than In-dislocations. An estimate of the occupation fraction for each sign of bending can be calculated from these slopes, since

Table 8.6: 'Read' Interpretation of measurements at 80°K.

In-bent specimens.

Specimen No.	ρ_{But} (cm^{-2})	n (cm^{-3})	$\langle n \rangle$ (cm^{-3})	$n - \langle n \rangle$ (cm^{-3})	μ_o ($cm^2 V^{-1} sec^{-1}$)	$\mu_{\parallel}$ ($cm^2 V^{-1} sec^{-1}$)	$\mu_{\perp}$ ($cm^2 V^{-1} sec^{-1}$)
6	5.82×10^{6}	7.11×10^{13}	1.75×10^{13}	5.36×10^{13}	5.6×10^{5}	4.92×10^{5}	1.58×10^{5}
3	3.30×10^{7}	5.68×10^{14}	2.78×10^{14}	2.90×10^{14}	4.2×10^{5}	3.88×10^{5}	1.34×10^{5}
1	1.4×10^{6}	9.45×10^{13}	8.47×10^{13}	0.98×10^{13}	5.67×10^{5}	5.60×10^{5}	4.47×10^{5}
11	7.25×10^{5}	8.39×10^{13}	7.97×10^{13}	0.42×10^{13}	5.65×10^{5}	5.32×10^{5}	4.82×10^{5}
12	2.88×10^{6}	7.09×10^{13}	5.08×10^{13}	2.01×10^{13}	4.70×10^{5}	4.32×10^{5}	3.10×10^{5}
2	3.18×10^{6}	4.66×10^{13}	2.61×10^{13}	2.05×10^{13}	4.76×10^{5}	4.37×10^{5}	1.95×10^{5}
10	1.35×10^{7}	1.18×10^{14}	2.28×10^{13}	9.52×10^{13}	5.07×10^{5}	3.15×10^{5}	1.15×10^{5}
	ρ_{But} (cm^{-2})	n (cm^{-3})	$\langle p \rangle$ (cm^{-3})	$n + \langle p \rangle$ (cm^{-3})	μ_o(n-type) (cm^2/V sec.)		$\mu_{\perp}$(p-type) (cm^2/V sec)
15	2.67×10^{7}	8.33×10^{13}	1.20×10^{14}	2.03×10^{14}	5.7×10^{5}		5.83×10^{3}

Sb-bent specimens

	ρ_{But}	n	$\langle n \rangle$	$n - \langle n \rangle$	μ_o	$\mu_{\parallel}$	$\mu_{\perp}$
4	1.71×10^{6}	1.075×10^{14}	4.63×10^{13}	6.12×10^{13}	5.9×10^{5}	5.37×10^{5}	2.55×10^{5}
5	1.45×10^{7}	6.94×10^{14}	1.57×10^{14}	5.37×10^{14}	4.1×10^{5}	3.26×10^{5}	0.972×10^{5}
8	3.1×10^{6}	1.86×10^{14}	9.00×10^{13}	9.6×10^{13}	5.56×10^{5}	4.65×10^{5}	2.00×10^{5}
7	2.02×10^{6}	1.46×10^{14}	8.60×10^{13}	6.0×10^{13}	5.26×10^{5}	4.52×10^{5}	2.24×10^{5}
13	5.05×10^{6}	6.00×10^{14}	4.38×10^{14}	1.62×10^{14}	3.93×10^{5}	3.54×10^{5}	2.22×10^{5}
14	7.27×10^{6}	7.25×10^{14}	5.45×10^{14}	1.80×10^{14}	4.13×10^{5}	3.74×10^{5}	2.3×10^{5}
9	9.6×10^{6}	9.40×10^{14}	6.98×10^{14}	2.42×10^{14}	3.48×10^{5}	3.13×10^{5}	2.0×10^{5}

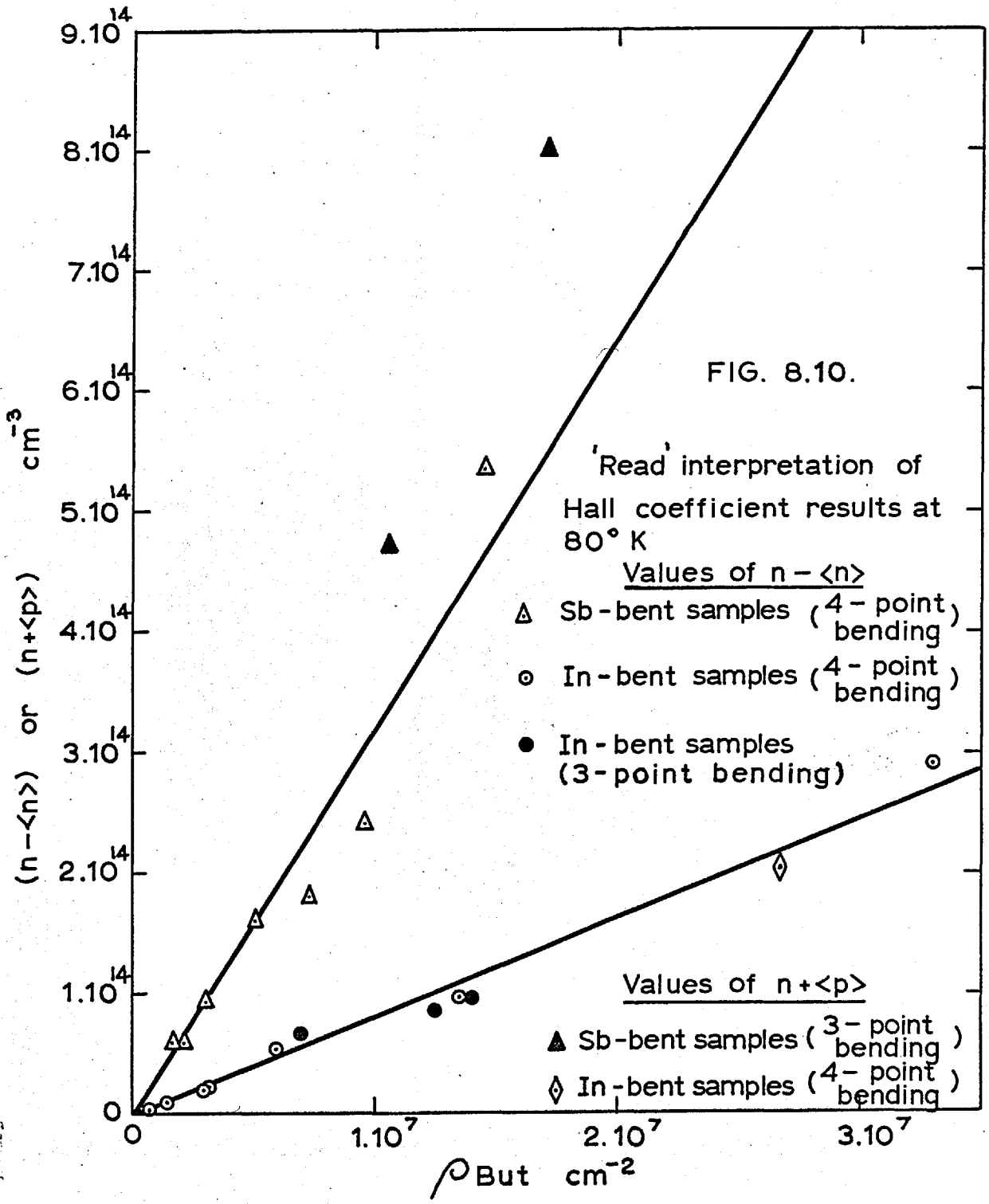
9.10^14
8.10^14
7.10^14
6.10^14
5.10^14
4.10^14
3.10^14
2.10^14
1.10^14
0
(n−<n>) or (n+<p>) cm^-3
0
1.10^7
2.10^7
3.10^7
ρBut cm^-2
'Read' interpretation of Hall coefficient results at 80° K
Values of n − <n>
Sb-bent samples (4-point bending)
In-bent samples (4-point bending)
In-bent samples (3-point bending)
Values of n + <p>
Sb-bent samples (3-point bending)
In-bent samples (4-point bending)

FIG. 8.10.

rearrangement of (4.17) gives

$$n - \langle n \rangle = \frac{f}{c}\rho$$

Setting the slopes of $n - \langle n \rangle$ (or $n + \langle p \rangle$) versus ρ_{But} equal to f/c we obtain

$$f_{In} = 0.33$$

and $$f_{Sb} = 1.54$$

We recall that on Read's theory the maximum theoretical value of f in indium antimonide at 80°K is about 0.091. Again it is possible that the discrepancy in the In-bent samples is due to an underestimation of the true dislocation density by the etch-pit technique, but it is unlikely that this could account for the large discrepancy in the Sb-bent samples.

Turning next to the mobility measurements, Read's theory predicts that $\mu_{//} = \mu_o$. The present results show that in most cases $\mu_{//}$ was significantly less than μ_o (the undeformed mobility). This result is not in agreement with Read's theory. However, Read assumed that all dislocations ran parallel to the bend axis, and if some dislocations lay in other directions they would scatter electrons and reduce $\mu_{//}$. Thus, this result in itself does not contradict Read's theory. Read also predicted that $\mu_\perp < \mu_{//}$ because of scattering and distortion of current streamlines in the 'perpendicular'

specimen. The present results are all in agreement with this prediction.

8.3.2. Analysis of measurements from 80°K to 295°K and estimation of dislocation-acceptor levels.

As a further test of Read's theory the analysis was applied to the temperature dependence of the Hall coefficient shown in Figs. 8.4 to 8.7.

Calculation of theoretical $f(T)$ curves.

A family of theoretical $f(T)$ curves was computed for each specimen using Read's Fermi approximation (4.11), Read's Minimum Energy approximation (4.9), and Blick's Fermi approximation (4.39). (The expression (4.8) for ε^* was used in conjunction with Blick's expression (4.39) since n-type material only was considered in this analysis). The calculations were performed with the aid of the University of London 'Atlas' Computer. The detailed programme is given in Appendix 1. An outline of the method will be given here.

Read's Minimum Energy approximation (4.9) can be expressed in the following form

$$(E_c - E_D) - (E_c - E_F) = \varepsilon_0 f \{3 \ln(f/f_c) - 0.232\} \quad \ldots\ldots (8.2)$$

where $f_c = c\pi^{1/3}(N_D - N_A)^{1/3}$

$\varepsilon_0 = q^2/\varkappa c$

and E_c = energy at bottom of conduction band.

The calculation of the Fermi level ($E_c - E_F$) is much simplified if the electron gas is assumed to be non degenerate. To assess the feasibility of using this simplification the Fermi energy was calculated for each specimen (a) by the general expression for arbitrary degeneracy, and (b) by the non-degenerate approximation. It was found that, in the range of temperature to be considered, the error incurred by using the non-degenerate expression was less than 5% for all specimens. The Fermi level was therefore calculated by the non-degenerate expression for a saturated extrinsic semiconductor, i.e.

$$E_c - E_F = kT \ln\left\{\frac{2(2\pi m^* kT/h^2)^{3/2}}{(N_D - N_A)}\right\}$$

Thus, substituting this value of ($E_c - E_F$) into (8.2) together with the values $c = 4\text{Å}$, $\varkappa = 16$, $m^* = 0.013\, m_o$ and the measured value of $(N_D - N_A)$, we obtain an equation relating f, T and $(E_c - E_D)$. At certain chosen values of $(E_c - E_D)$, f was calculated as a function of temperature. A numerical method was necessary since f is contained in equation (8.2) as an implicit function. A typical family of curves is shown in Fig.8.11 (for specimen 3). Similar sets of curves were computed for Read's 'Fermi' approximation (4.11) and Bliek's 'Fermi' approximation (4.39). One of each of these curves is shown in Fig.8.11 for comparison.

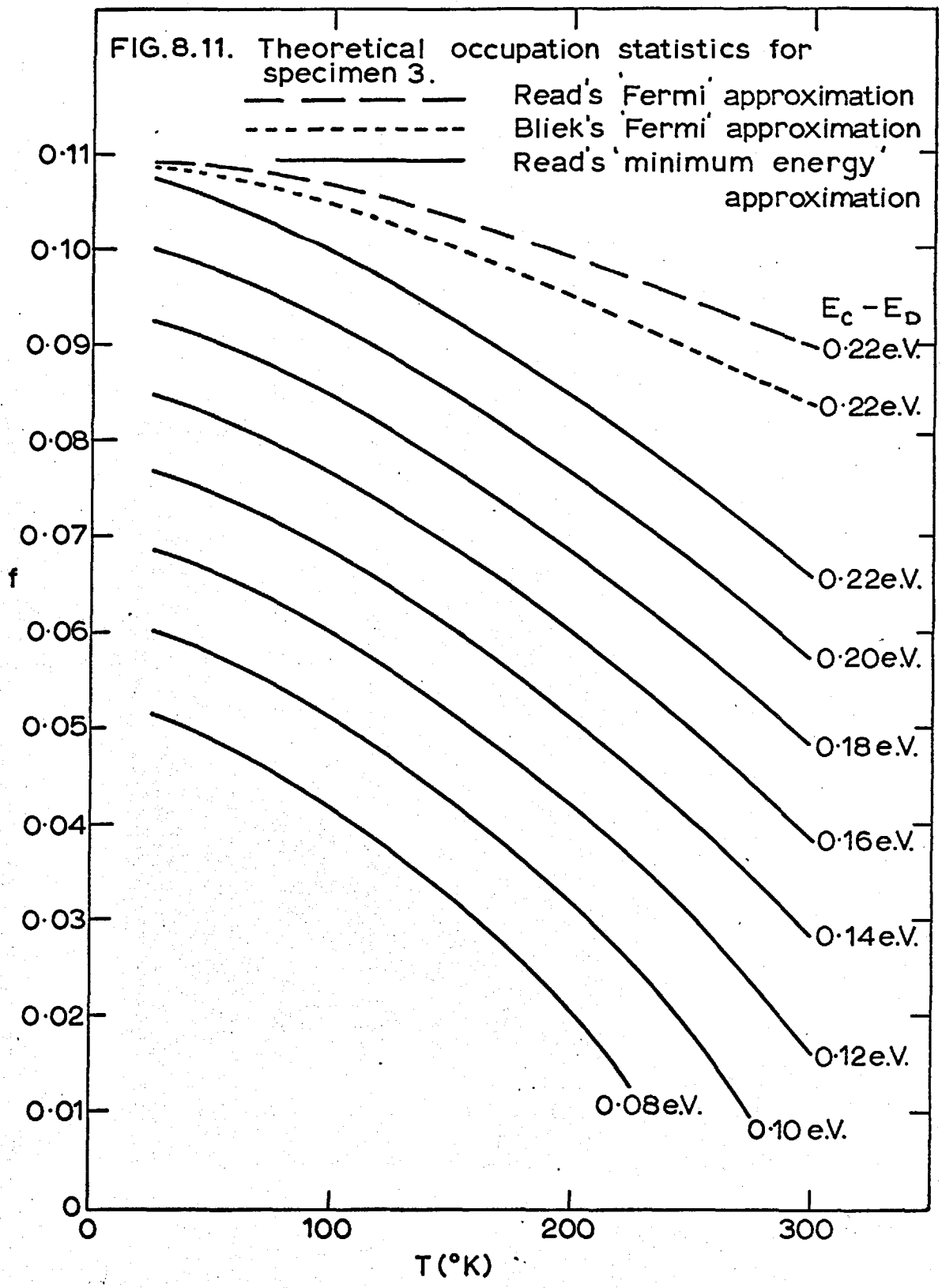

FIG.8.11. Theoretical occupation statistics for specimen 3.

Analysis of Hall Coefficient results.

Following the method of Logan (1959) the basic relation (4.17) was rewritten in the form

$$\epsilon(T) = \lambda f(T) \qquad \ldots\ldots (8.3)$$

where $\lambda = \rho / c (N_D - N_A)$

Equation (8.3) was then used to interpret the results in the following way. As an example of the method we will consider specimen 3.

(i) Values of ϵ ($= 1 - R_o/R_{II}$) were calculated from the Hall coefficients of the control and 'parallel' samples. These values are plotted against temperature in Fig.8.12 (for specimen 3).

(ii) Theoretical $f(T)$ curves were calculated by the method described above, for certain values of $(E_c - E_D)$ (the dislocation-acceptor level). Considering, say, the $f(T)$ curve calculated by the 'Minimum Energy' approximation for $E_c - E_D$ = 0.12 e.V., the value of f (75°K) was obtained as 0.0634.

(iii) Using the value of f (75°K) from (ii) and the value of ϵ(75°K) extrapolated from the experimental results, λ was calculated using the expression (8.3)

(iv) With this value of λ and the $f(T)$ curve corresponding to $E_c - E_D$ = 0.12 e.V., ϵ values were

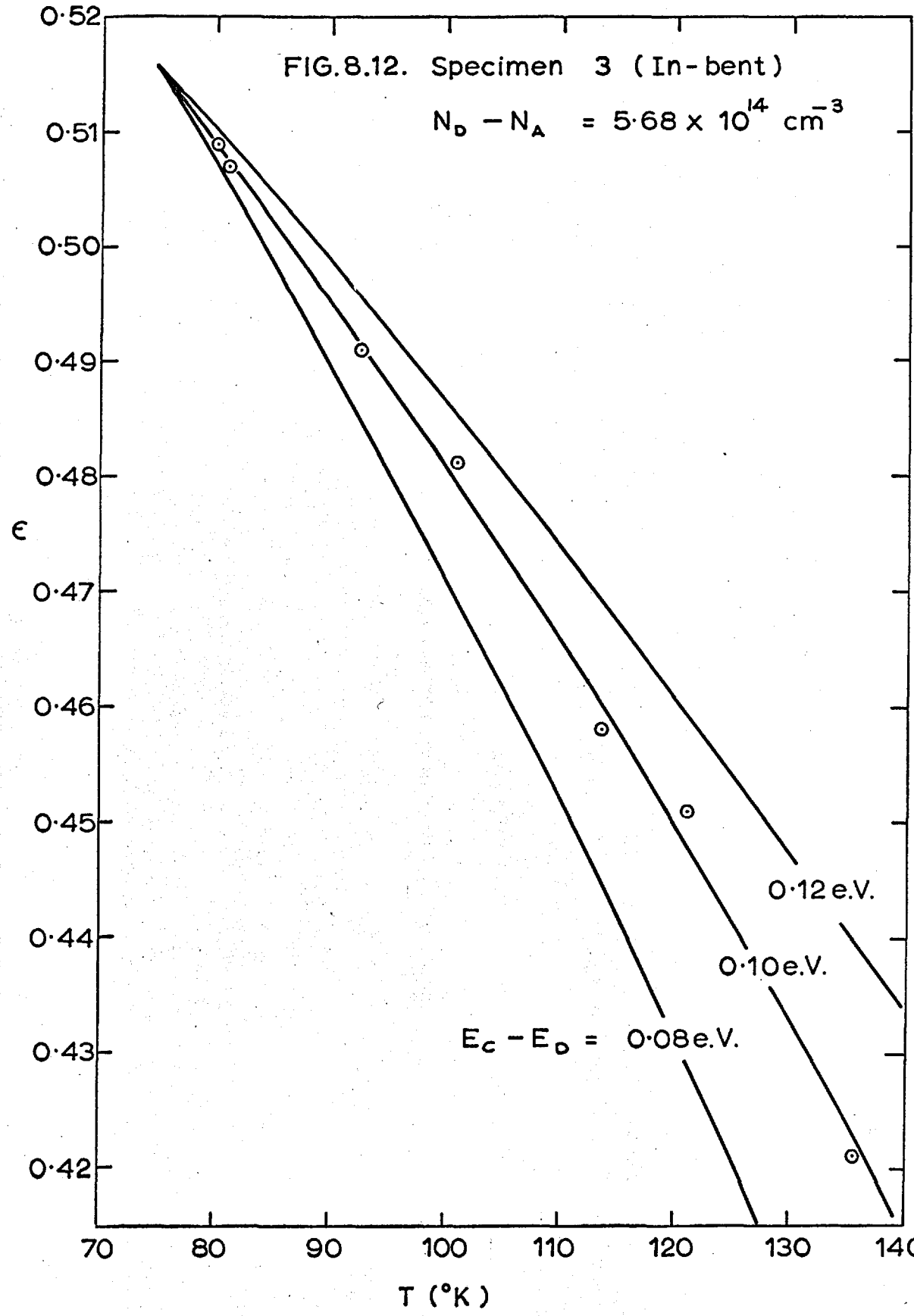
FIG. 8.12. Specimen 3 (In-bent)
$N_D - N_A = 5{\cdot}68 \times 10^{14}$ cm^{-3}
0·52
0·51
0·50
0·49
0·48
0·47
0·46
0·45
0·44
0·43
0·42
ϵ
0·12 e.V.
0·10 e.V.
$E_C - E_D$ = 0·08 e.V.
70
80
90
100
110
120
130
140
T (°K)

calculated over the whole range of temperature. This theoretical $\epsilon(T)$ curve shown in Fig.8.12 and labelled $E_c - E_D$ = 0.12 e.V. has a shallower slope than that of the experimental values, so the procedure (i) to (iv) was repeated using other values of $(E_c - E_D)$ until a good fit between theory and experiment was obtained with $E_c - E_D$ = 0.10 e.V.

From the value of λ used to calculate the theoretical curve for $E_c - E_D$ = 0.10 e.V. the dislocation density was calculated from the relation

$$\rho = \lambda c (N_D - N_A)$$

The temperature dependence of the Hall coefficient for all the specimens measured could be accommodated using $f(T)$ curves calculated by Read's 'Minimum Energy' approximation. The quality of the fits obtained is shown in Figs. 8.12 to 8.15, whilst in Table 8.7 the acceptor levels and dislocation densities deduced are listed. The latter are compared with the measured etch-pit densities. For In-bent samples the theoretical dislocation density is about seven times the etch-pit density, while for Sb-bent samples the corresponding factor is about fifteen.

If the $f(T)$ curves were calculated using Bliek's 'Fermi' approximation a fit could be obtained for the two Sb-bent samples using an acceptor level near the

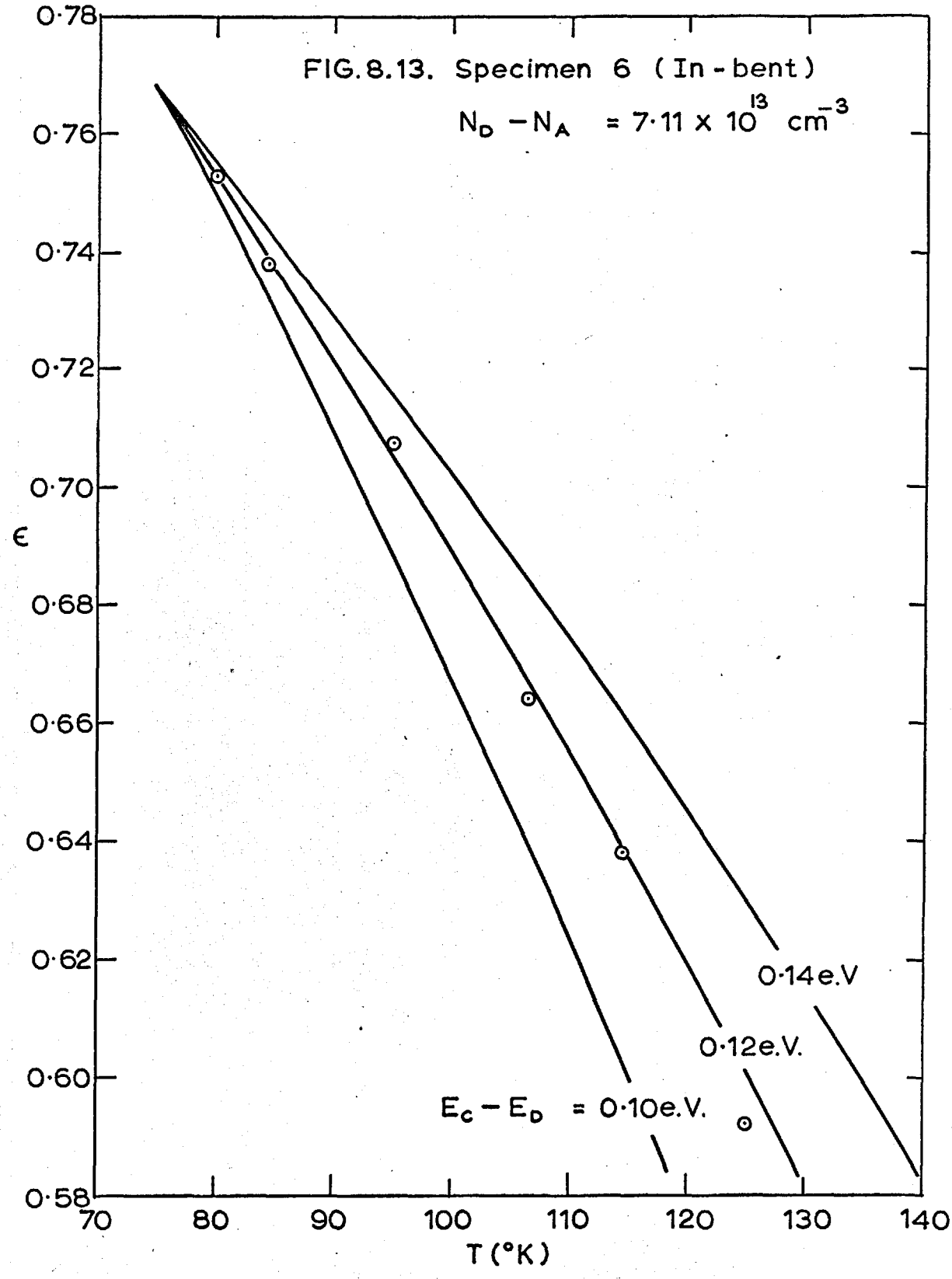

FIG. 8.13. Specimen 6 (In-bent)

$N_D - N_A = 7{\cdot}11 \times 10^{13}$ cm^{-3}

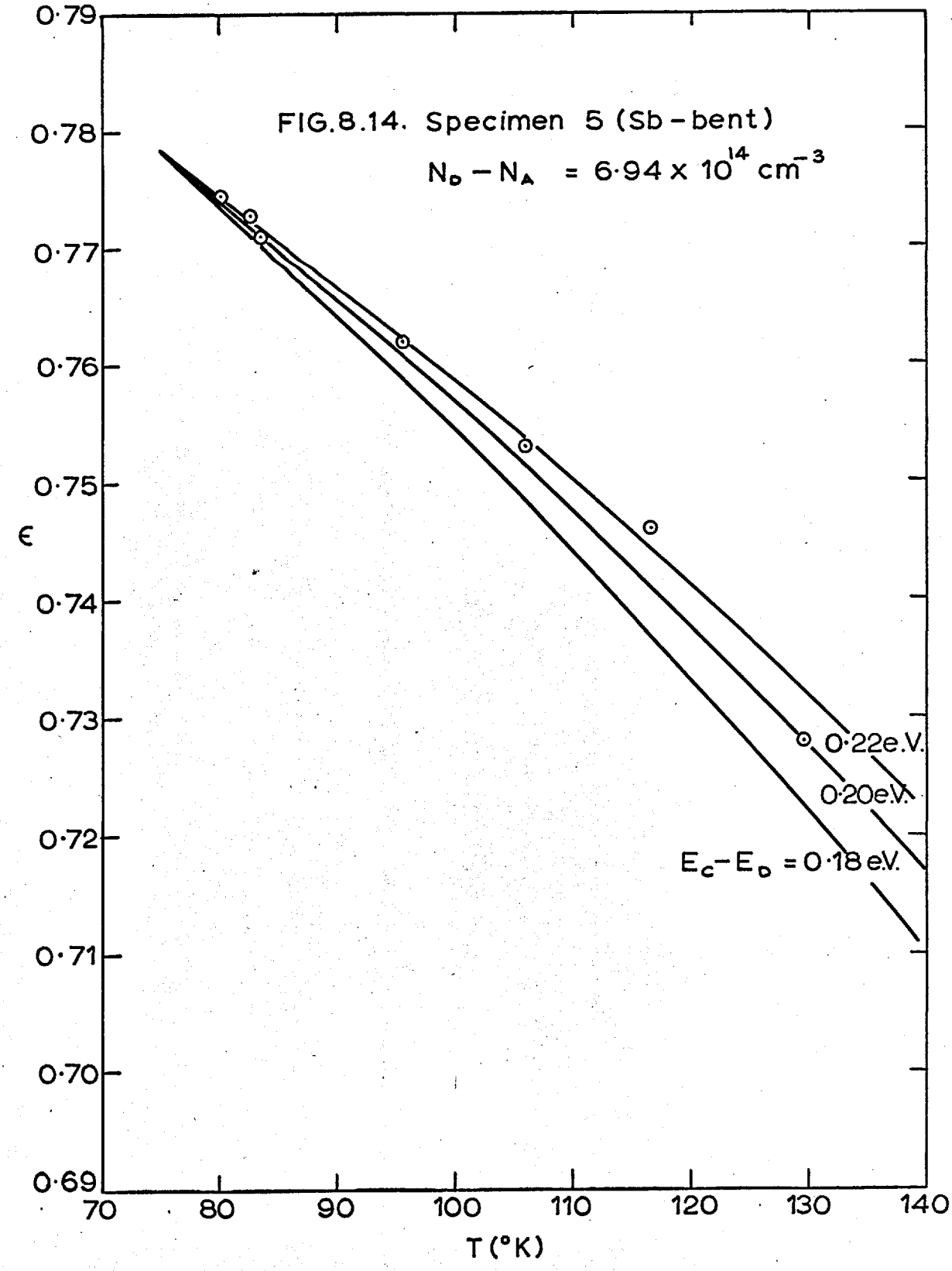
FIG.8.14. Specimen 5 (Sb-bent)
$N_D - N_A = 6{\cdot}94 \times 10^{14}\ cm^{-3}$
0·22e.V.
0·20e.V.
$E_c - E_D = 0{\cdot}18$ eV.
ϵ
T (°K)
0·79
0·78
0·77
0·76
0·75
0·74
0·73
0·72
0·71
0·70
0·69
70
80
90
100
110
120
130
140

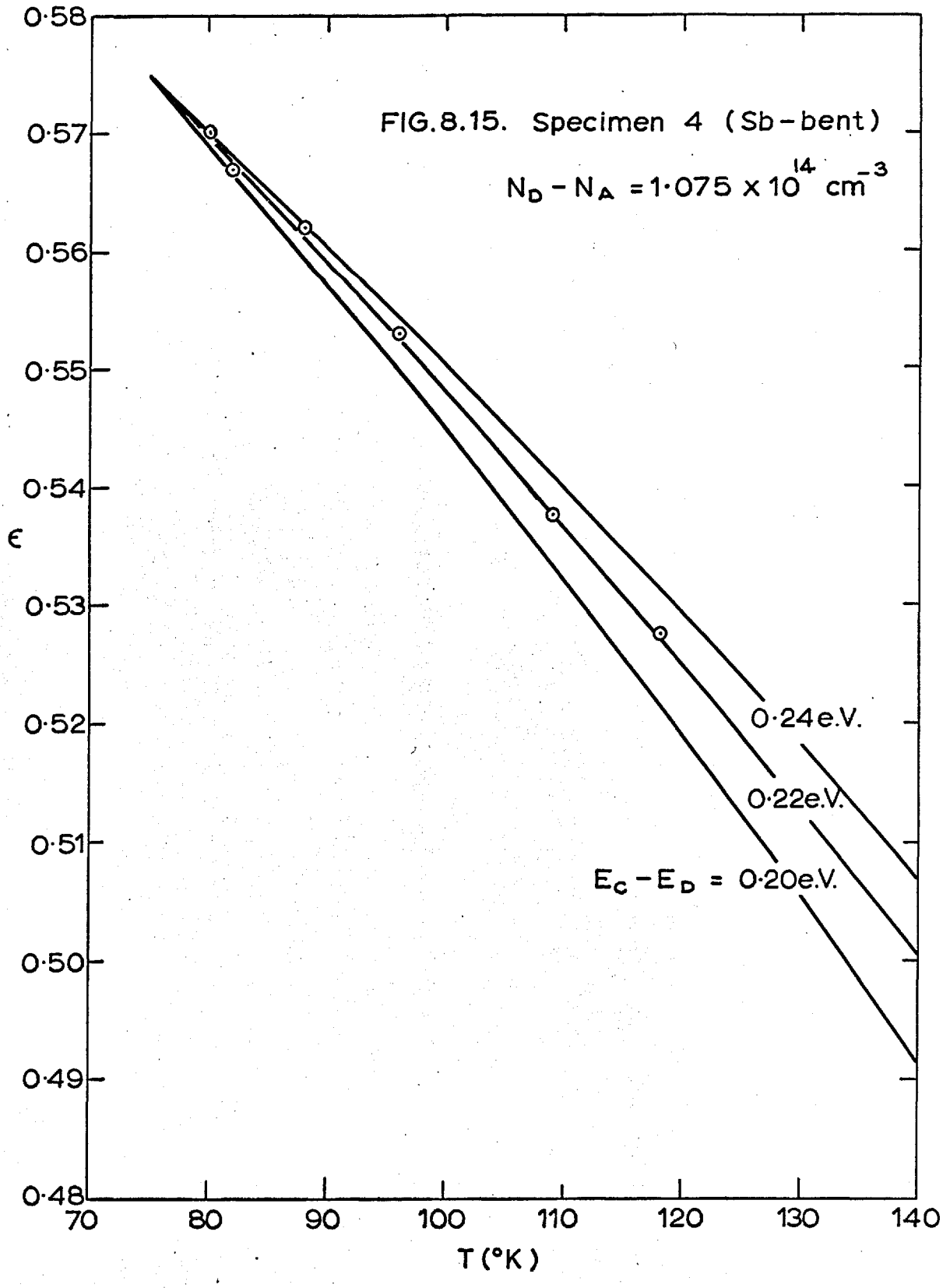

FIG.8.15. Specimen 4 (Sb-bent)

$N_D - N_A = 1{\cdot}075 \times 10^{14}$ cm^{-3}

Table 8.7: 'Read' Interpretation.

Specimen No.	Polarity	$E_c - E_D$ e.V.	Dislocation Density (cm^{-2})		$\mu_\perp$ $cm^2/V.sec.$	
			Theoretical	Etch-pit (ρBut)	Theoretical	Experimental
6	In-bent	0.12 e.V.	4.49×10^7	5.82×10^6	1.24×10^5	1.58×10^5
3	In-bent	0.10 e.V.	2.14×10^8	3.30×10^7	0.966×10^5	1.34×10^5
4	Sb-bent	0.22 e.V.	2.86×10^7	1.71×10^6	1.89×10^5	2.55×10^5
5	Sb-bent	0.20 e.V. -0.22 e.V.	2.06×10^8	1.45×10^7	0.644×10^5	0.972×10^5

conduction band. No fit was possible for the In-bent samples.

If Read's 'Fermi' approximation were used, a fit could be obtained for neither the In-bent nor the Sb-bent samples.

Comparison of mobility measurements with the predictions of Read's Model.

Read's model was further used to predict the electron mobility in the perpendicular samples from the experimental values of the Hall coefficients of 'parallel' and 'perpendicular' samples and the Hall coefficient and conductivity of the control samples. Now, the analysis depends on the dominant scattering mechanisms in the undeformed samples and thus these mechanisms must be determined before calculating the effects of dislocations. The theoretical derivation of Duga (1962) assumed acoustic scattering to be the dominant lattice scattering mechanism, and therefore this was also assumed for these present calculations although, as discussed in Section 3.4, this assumption may not be correct.

Firstly, the temperature dependence of the carrier mobility in the control samples was examined to determine the degree of ionised impurity scattering β, which is defined by the relation (5.6). The determination of β is given in detail in Appendix 2, Section (1), and typical

values are listed in Table A.1. In the case of samples 5 and 3, the temperature dependence of the carrier mobility in the control samples (Fig.8.9) deviated considerably from the $T^{-1.5}$ law of acoustic scattering below 200°K. Thus ionised impurity scattering is presumably important in these control specimens (as reflected in the values of β of 1.5 and 0.92 for specimens 5 and 3 respectively at 80°K) and ionised impurity scattering had to be considered in the calculation of the mobilities in 'perpendicular' samples.

Duga obtained the following expression for $\mu_\perp$ (as described in Section 5.2).

$$\mu_\perp = \mu_A \, g(\epsilon) \, F(X) \, K(\beta^*) \qquad \ldots\ldots (5.4)$$

The four parameters on the right hand side of (5.4) were obtained as follows.

The mobility μ_A was obtained from the measured mobility of control specimens in which impurity scattering was not important. β (equation (5.6)) was calculated for each control specimen by the method described in Appendix 2(1). Referring to equation (5.9), if $K(\beta) \rightarrow 1$ then the measured mobility μ_o is equal to μ_A. This situation existed for control specimens 6 and 4 and thus μ_A was taken as the measured mobility of these specimens.

The calculation of ϵ from the Hall coefficient measurements was detailed above. $g(\epsilon)$ was then

interpolated from the graph plotted by Read (1955).

The mean free path for acoustic scattering, l_A, was calculated from μ_A by (5.1) and the mean free path for dislocation scattering, l_D, was calculated from (5.2) in which the value of ρ resulting from the Hall coefficient analysis was used. After calculating $X = l_A/l_D$ the function $F(X)$ was interpolated from Logan's calculated values.

β^* was calculated from (5.5) using the value of β determined from the temperature dependence of the control mobility (by the method of Appendix 2(1)). The parameter Q was calculated from the Hall coefficient results, and the integral in (5.5) was solved* to obtain

$$\int_0^{\pi/2} \frac{d\varphi}{1 + X \sin\varphi} = \frac{\sec\alpha}{X} \log \frac{\sin\frac{1}{2}\alpha}{\cos(-\frac{1}{2}\alpha)}$$

where $\alpha = \sin^{-1}\left(\frac{1}{X}\right)$

Thus β^* was calculated from the values of β, Q and X. Finally $K(\beta^*)$ was obtained by interpolation from the tabulated values of Beer et al. (1957)

---

*This integral was solved by Peirce (1910), who obtained

$$\int_0^{\pi/2} \frac{d\varphi}{1 + X \sin\varphi} = \left[\frac{\sec\alpha}{X} \log \frac{\sin\frac{1}{2}(\alpha+\varphi)}{\cos\frac{1}{2}(\varphi-\alpha)} \right]_0^{\pi/2}$$

$$= \frac{\sec\alpha}{X} \log \frac{\sin\frac{1}{2}\alpha}{\cos(-\frac{1}{2}\alpha)}$$

where $\alpha = \sin^{-1}\left(\frac{1}{X}\right)$

For specimens 6 and 4 the value of β^* was very small and $K(\beta^*)$ was practically unity (within 1%). Thus, in these cases the simplified expression of Logan, (4.33), which does not consider impurity scattering, could have been used.

The computed values of $\mu_\perp(80^\circ K)$ are shown in Table 8.7. in which they are compared with the experimental values. The theoretical values are consistently less than the experimental values by about 30%, but this difference is within the experimental error in the measured values of mobility.

8.3.3. Summary of Read analysis.

The results can be accommodated on the Read model assuming that the underestimation of dislocation density by the etch-pit technique is large enough to accommodate the discrepancies given in Table 8.7. It must also be assumed that the dislocations do not all lie parallel to the bend axis to explain the reduced mobilities in the 'parallel' samples. The fact that the theoretical values of $\mu_\perp$ are consistently lower than the experimental ones can be explained also in terms of non-parallel dislocations. Any dislocations running perpendicular to the bend axis would increase $\mu_\perp$ while decreasing $\mu_{//}$. Thus on this basis the trends in $\mu_\perp$ and $\mu_{//}$ are self-consistent. The scheme of energy levels for the

dislocation-acceptors calculated by this analysis is shown in Fig.8.16.

Assuming that this scheme of energy levels is correct, the analysis can be extended to calculate theoretical values for all other specimens which were measured at 80°K only. It is probably not reasonable to extend the Hall coefficient analysis to specimens 14 and 9, since the electron gas is degenerate in these specimens. However, the values must represent a fair approximation. The values of $\mu_\perp$ were calculated assuming that $K(\beta^*) = 1$ except in the case of specimens 13, 14 and 9 where values of β were taken from specimen 5 to calculate β^*. These values are probably the best approximations which could be made in the absence of measured values of β. The results of the analysis are shown in Table 8.8 in which theoretical values of dislocation density and $\mu_\perp(80^\circ K)$ are compared with experimental values. The trends observed in the previous samples are found in these specimens, and in some cases the agreement between experiment and theory is closer than in the first four samples.

8.4. 'Broudy' Interpretation.

The 'Broudy' model seems appropriate to these results for two reasons. Firstly, it would accommodate the reduced 'parallel' mobilities by the assumption of

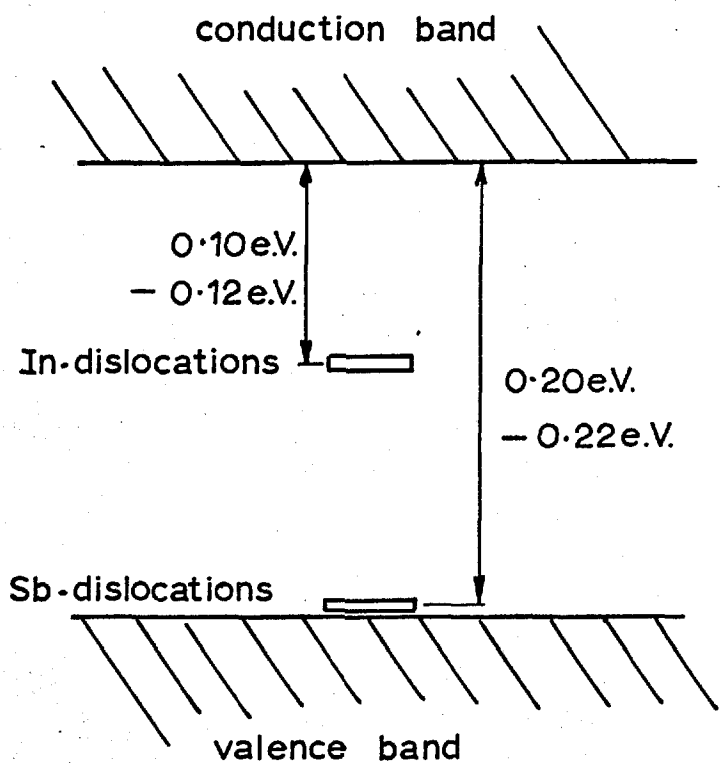

FIG. 8.16 Dislocation acceptor levels on Read analysis.

Table 8.8: 'Read' Interpretation; comparison of theory and experiment. Theoretical values calculated assuming $E_c - E_D$ = 0.12e.V. for In-disl^{ns} and 0.20e.V. for Sb-disl^{ns}

In-bent specimens

Specimen No.	$f(80^\circ K)$ $E_c - E_D$ = 0.12e.V.	$\rho_{theor.}$ (cm^{-2}) (From R_H)	ρ_{But} (cm^{-2})	$\frac{\rho_{theor}}{\rho_{But}}$	$\mu_\perp$(theor) $\left(\frac{cm^2}{Volt\ sec.}\right)$	$\mu_\perp$(expt) $\left(\frac{cm^2}{Volt\ sec.}\right)$	$\frac{\mu_\perp(expt)}{\mu_\perp(theor)}$
1	0.0486	8.067×10^6	1.4×10^6	5.75	4.02×10^5	4.47×10^5	1.11
11	0.0477	3.523×10^6	7.25×10^5	4.87	4.93×10^5	4.82×10^5	0.98
12	0.0466	1.726×10^7	2.88×10^6	6.00	2.37×10^5	3.10×10^5	1.31
2	0.0439	1.868×10^7	3.18×10^6	5.88	1.57×10^5	1.95×10^5	1.25
10	0.0502	7.585×10^7	1.35×10^7	5.62	0.78×10^5	1.15×10^5	1.47
	Sb-bent specimens						
	$E_c - E_D$ = 0.20e.V.						
8	0.0836	4.594×10^7	3.1×10^6	14.8	1.38×10^5	2.00×10^5	1.45
7	0.0815	2.945×10^7	2.02×10^6	14.6	1.77×10^5	2.24×10^5	1.27
13	0.0954	6.793×10^7	5.05×10^6	13.4	1.60×10^5	2.22×10^5	1.38
14	0.0974	7.393×10^7	7.27×10^6	10.4	1.69×10^5	2.3×10^5	1.36
9	0.1004	9.642×10^7	9.6×10^6	10.0	1.44×10^5	2.0×10^5	1.39

non-specular scattering at dislocations, and secondly, it would reduce the large discrepancies between theoretical and experimental dislocation densities found in the Read analysis.

In order to apply the model, the mean free path in undeformed indium antimonide must be known as a function of temperature.

8.4.1. Calculation of the mean free path.

The calculation of the mean free path from the carrier mobility depends on the dominant scattering mechanism (or mechanisms). Since it is uncertain in indium antimonide whether acoustic scattering or polar scattering is the more important lattice scattering mechanism at 80°K, both were considered. In some specimens ionised impurity scattering was also important and therefore mixed acoustic and impurity scattering, and mixed polar and impurity scattering, were considered. The detailed calculation of mean free paths is given in Appendix 3, and values at 80°K are presented in Table 8.9. In this table, $\frac{2}{\sqrt{\pi}} I(\beta)$ is the ratio of the mean free path for mixed acoustic and impurity scattering $(\bar{l})$ to the mean free path for acoustic scattering only (l_A). In the case of specimens 4 and 6, $\frac{2}{\sqrt{\pi}} I(\beta) \simeq 0.9$ and thus an error of only about 10% would have resulted from neglecting impurity scattering. The values of $\bar{l}$

Table 8.9: Calculation of the mean free path at 80°K.

Specimen No.	Acoustic + Impurity Scattering			Polar + Impurity Scattering		
	β	$\frac{2}{\sqrt{\pi}} I(\beta)$	$\bar{l}$ (cm.)	η	$L(\eta)$	$\bar{l}$ (cm.)
5	1.5	0.47	1.176×10^{-4}	1.75	0.525	1.115×10^{-4}
4	0.016	0.94	2.353×10^{-4}	0.120	0.900	1.912×10^{-4}
3	0.92	0.55	1.377×10^{-4}	1.121	0.605	1.285×10^{-4}
6	0.041	0.891	2.231×10^{-4}	0.171	0.87	1.847×10^{-4}

obtained for acoustic plus impurity scattering are in all cases slightly larger than those for polar plus impurity scattering. At the most this amounts to a difference of about 20%.

8.4.2. Application of Broudy model to results.

The mean free path values shown in Table 8.9 are of the same order of magnitude as the spacing between dislocations in the bent samples. The possibility of overlap of the ϕ regions around individual dislocations will therefore have to be considered. However, first we will assume no overlap and apply the Broudy theory in its original form.

No overlap of ϕ regions.

Broudy obtained equations (4.25) and (4.27) relating the unknown parameters ϵ, ϕ, f and θ to the measured R_0/R_{11}. Writing (4.27) in the form $\phi = K_1\epsilon$ these equations were combined giving a quadratic expression in ϵ, which was solved for ϵ to give

$$\epsilon = \frac{2L_1 - (R_0/R_{11})M_1 - \sqrt{(R_0/R_{11})^2 M_1^2 - 4(R_0/R_{11})K_1\theta L_1(1-\theta)}}{2L_1^2} \quad \ldots\ldots (8.4)$$

where

$$K_1 = \frac{\pi c(N_D - N_A)}{f}\left\{l^2 + 2l\sqrt{\frac{f}{c\pi(N_D - N_A)}}\right\}. \quad (8.5)$$

$$L_1 = K_1(1-\theta) + 1$$

and

$$M_1 = K_1(1-\theta^2) + 1$$

The original equation (4.23) can be rewritten as

$$R_o/R_{//} = \frac{(1-\epsilon L_1)^2}{(1-\epsilon M_1)} \qquad \ldots\ldots (8.6)$$

which is equivalent to (8.4).

Broudy's procedure for applying his model to the results was not used, since it involved a comparison of one theoretical quantity with a quantity which was a combination of theoretical and measured quantities. Instead, the following procedure, which enables a theoretical quantity to be compared directly with an experimental one, was adopted.

Initially a value for θ was assumed in order to solve for the other unknowns. It was found, by varying θ, that a real solution of equation (8.4) could only be obtained with $\theta < 0.1$. This point will be discussed more fully later, but for the rest of the analysis θ was assumed to be 0.05. Having assumed θ, and having calculated the mean free path by equation (A.11) or (A.20)(initially (A.11) was used), equation (8.4) gives ϵ in terms of f and $R_o/R_{//}$, and (8.6) gives $R_o/R_{//}$ in terms of f and ϵ, all other parameters being known.

One value of the dislocation energy level, $E_c - E_D$ was chosen, and hence a value for f at a particular temperature, say 80°K, was calculated as before by Read's

Minimum Energy Approximation (4.9). Then, using the experimental value of $R_o/R_{//}$ at $80^\circ K$, $\epsilon\,(80^\circ K)$ was calculated by equation (8.4). Next λ was calculated from $\epsilon\,(80^\circ K)$ and $f\,(80^\circ K)$. With this value of λ, ϵ was calculated for other temperatures from the values of f at those temperatures (calculated by Read's Minimum Energy approximation for the chosen $(E_c - E_D)$ value) by the relation (8.3).

Then using equation (8.6), $\left(R_o/R_{//}\right)$ was calculated over the whole range of temperature from the $f\,(T)$ and $\epsilon(T)$ values. This $R_o/R_{//}(T)$ curve is a purely theoretical curve, except for the use of $R_o/R_{//}\ (80^\circ K)$ to obtain λ.

This theoretical $R_o/R_{//}\ (T)$ curve did not fit the experimental points, and so another value of the dislocation acceptor level, $E_c - E_D$, was chosen. However, repetition of the procedure for the whole range of dislocation energy levels within the gap did not produce a fit between theory and experiment. The fit was closest when the dislocation acceptor level was near the valence band, but even then the slope of the theoretical $R_o/R_{//}\ (T)$ curve was steeper than the experimental curve. Since there was no problem in obtaining a fit on the Read model (Section 8.3) the difficulty here must be ascribed to the rapid variation of ϕ with T. The variation of

ϕ with temperature would be less rapid if neighbouring ϕ regions overlapped (as is likely in these samples) and thus it is thought that a model which included overlap of ϕ regions might accommodate the experimental results.

Overlap of ϕ regions.

Etch-pit measurements on these samples indicated that the dislocations were arranged in a polygonised array, the spacing of neighbouring dislocations in the polygon walls being about 0.5 - 2μ, and the distance between polygon walls about 5 - 10μ. Now, since the space charge cylinders are probably about 0.5μ in diameter (for a typical value of f), and the mean free path is about 1 - 2μ in length, the ϕ regions of two dislocations will overlap if they are less than 2.5 - 4.5μ apart. Thus, overlap is very likely to occur between neighbouring dislocations in the polygon walls but unlikely to occur between neighbouring polygon walls. The model was therefore modified to include these observations. As a first approximation, the model shown in Fig.8.17 was adopted. Here the specimen consists of sheets of ϕ material, of thickness ($2l + 2R_s$) in the centre of which are the space charge cylinders $2R_s$ in diameter. These layers of ϕ regions are separated from each other by material in which the mobility is unaltered from the control mobility. This model will be a good

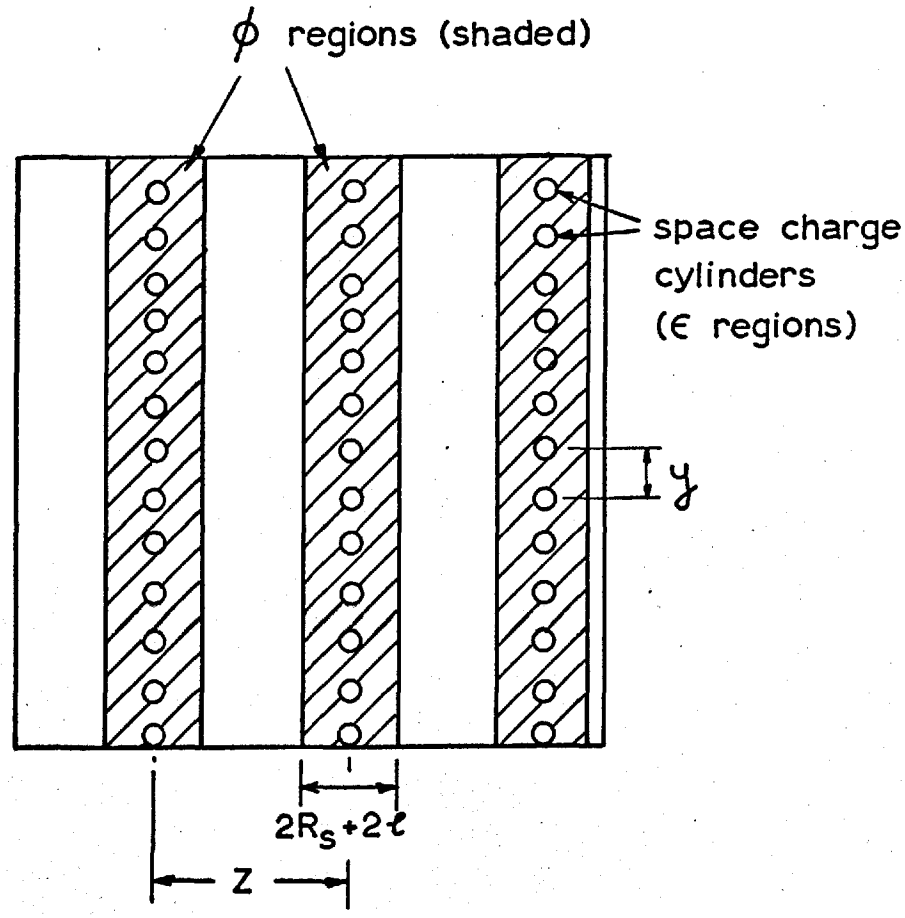

FIG. 8.17. Broudy model modified to include overlap of ϕ regions in polygon walls.

approximation if $(2l + 2R_s) \gg y$, where y is the spacing of dislocations in the polygon walls.

In the unit area shown in Fig.8.17 the fraction occupied by the $(\phi + \epsilon)$ regions of one wall is $(2R_s + 2l)$. If z is the distance between the centres of neighbouring walls, then the number of walls in unit area shown = $1/z$

$\therefore$ Total area occupied by $\phi + \epsilon$ regions = $(2R_s + 2l)/z$. With a simple parallel array of dislocations, the volume fraction $\phi + \epsilon$ is also $(2R_s + 2l)/z$.

$$\therefore \phi = 2(R_s + l)/z - \epsilon$$

$$= 2(R_s + l)\rho y - \epsilon \quad \left(\text{Since } \rho = \frac{1}{zy}\right) \quad (8.7)$$

Now, from (4.17)

$$\rho = \frac{\epsilon c (N_D - N_A)}{f}$$

$$\therefore \phi = \frac{\epsilon c (N_D - N_A)}{f} 2y \{R_s + l\} - \epsilon$$

$$= \epsilon \left[\frac{2yc (N_D - N_A)}{f} \{R_s + l\} - 1 \right]$$

Substituting

$$R_s = \sqrt{\frac{f}{c\pi (N_D - N_A)}}$$

we obtain finally

$$\phi = K_1' \epsilon \quad \ldots\ldots (8.8)$$

where

$$K_1' = \frac{2yc (N_D - N_A)}{f} \left\{ \sqrt{\frac{f}{c\pi (N_D - N_A)}} + l \right\} - 1 \quad (8.8a)$$

Equation (8.8a) is the counterpart of (8.5) in the case of no overlap. Equations (8.4) and (8.6) may be used in the case of overlap of ϕ regions if K_1' (as given by 8.8a) is used in place of K_1. Thus the analysis can be carried through as before except in one particular:

In the Broudy analysis the dislocation density is treated as an unknown to be determined from the electrical measurements. Having introduced the possibility of a non-random distribution of dislocations we have introduced two unknowns, y and z, in place of the one ρ. We will overcome this problem by inserting the value of y obtained from a photomicrograph of the etch-pits in the particular specimen concerned.

The reason for inserting the measured value of y rather than that of z is as follows. Since $l \gg R_s$, the ϕ regions must occupy much more volume than the ϵ regions. Thus, if the value of z were inserted, the number of walls per unit volume would be known and $(\phi + \epsilon)$ would be practically predetermined since l is not adjustable and a change in R_s (through change in $E_c - E_D$) makes very little difference to $(\phi + \epsilon)$. However, if y were inserted, $(\phi + \epsilon)$ would not be predetermined since the number of walls per unit volume would still be a variable. For this reason the spacing, y, (from the etch-pit spacing) was inserted.

Applying the analysis as described above for the case of no-overlap, a fit was obtained between theoretical and experimental R_o/R_{II} (T) curves. Fig.8.18 shows a typical set of theoretical curves together with the experimental values for specimen 5. In this case reasonable agreement was obtained for $E_c - E_D = 0.04$ e.V.

Hall coefficient versus temperature data for four specimens, two indium bent and two antimony bent, were analysed in this way. Table 8.10 lists the values of the dislocation acceptor level and of the dislocation density which were derived. The two In-bent samples agreed very well, as did the two Sb-bent ones. The In- and Sb-dislocation acceptor levels were obtained as 0.06 and 0.04 e.V. respectively. The dislocation densities deduced for the In-bent samples were only 10 - 20% greater than the butylamine etch-pit densities; for Sb-bent samples the discrepancy was in the same direction but larger, a factor of about 5/2.

With the information on the dislocation energy level and dislocation distributions derived above, the conductivity ratios σ_{II}/σ_o and $\sigma_\perp/\sigma_{II}$ at 80°K were obtained from the Broudy relations (4.35) and (4.37) using equation (8.8) to calculate ϕ, and setting Θ equal to 0.05 as before. Table 8.11 shows the values of f, ϵ and ϕ computed for each specimen at 80°K, and compares theoretical and experimental values of σ_{II}/σ_o, $\sigma_\perp/\sigma_{II}$

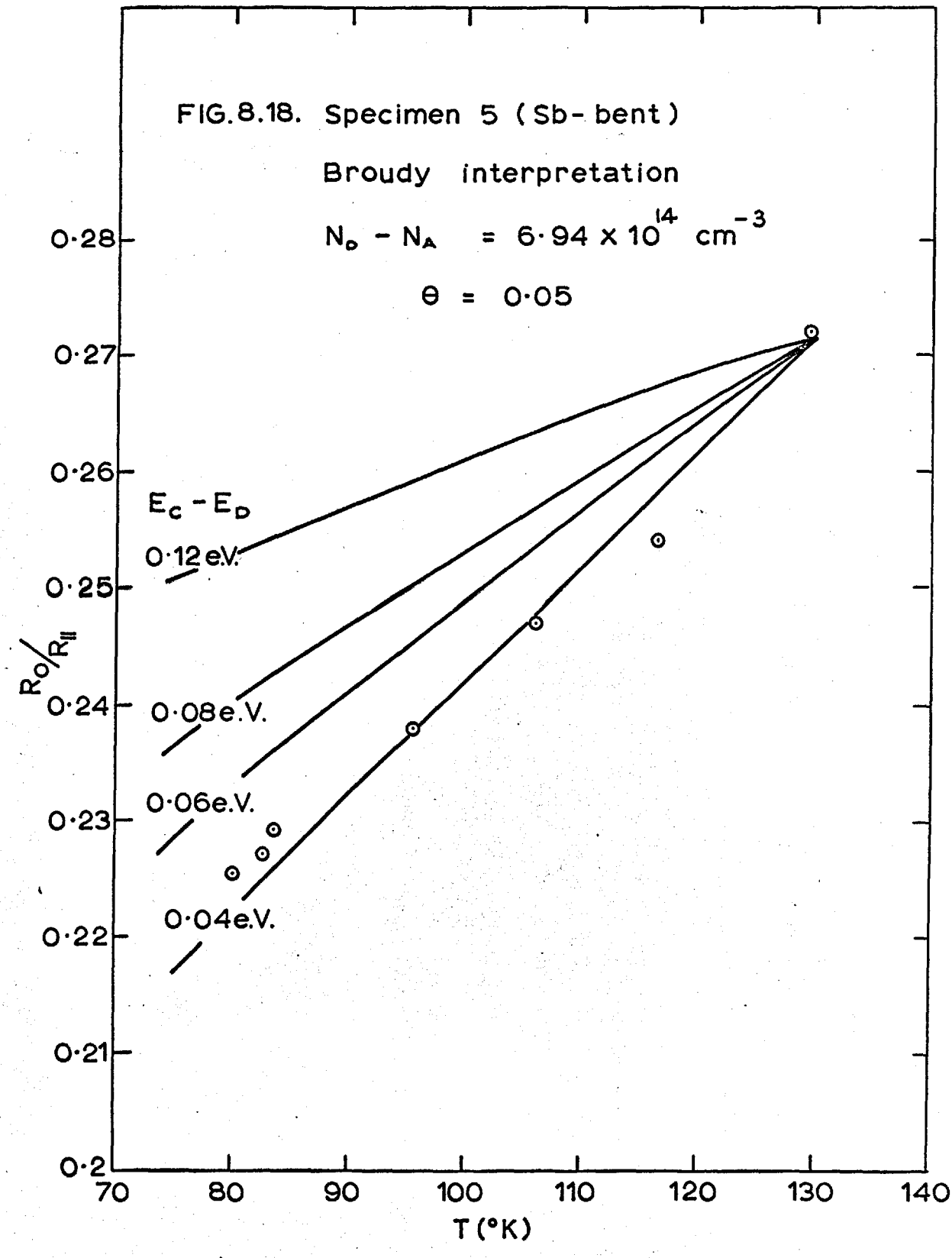
FIG. 8.18. Specimen 5 (Sb-bent)
Broudy interpretation
$N_D - N_A = 6{\cdot}94 \times 10^{14}$ cm^{-3}
$\theta = 0{\cdot}05$
$E_C - E_D$
0·12 e.V.
0·08 e.V.
0·06 e.V.
0·04 e.V.
R_O/R_{II}
0·28
0·27
0·26
0·25
0·24
0·23
0·22
0·21
0·2
70
80
90
100
110
120
130
140
T (°K)

Table 8.10: Broudy Interpretation of $R_o/R_{//}$ (T) Measurements.

Specimen No.	Polarity	$E_c - E_D$ e.V.	Dislocation Density (cm^{-2})	
			Theoretical	Etch-Pit Density (Butylamine etch)
5	Sb-bent	0.04 e.V.	3.42×10^7	1.44×10^7
4	Sb-bent	0.04 e.V.	4.05×10^6	1.71×10^6
3	In-bent	0.06 e.V.	3.56×10^7	3.30×10^7
6	In-bent	0.06 e.V.	7.48×10^6	5.82×10^6

Table 8.11: Broudy Interpretation (Acoustic + impurity scattering) at 80°K.

Specimen No.	Polarity	f (80°K)	ϵ (80°K)	ϕ (80°K)	$R_o/R_{//}$ (80°K)		$\sigma_{//}/\sigma_o$ (80°K)		$\sigma_\perp/\sigma_{//}$ (80°K)	
					Theor$^{tl.}$	Exp$^{tl.}$	Theor$^{tl.}$	Exp$^{tl.}$	Theor^{tl}	Exp$^{tl.}$
5	Sb-bent	0.0252	0.03104	0.8407	0.2225	0.2255	0.171	0.179	0.546	0.299
4	Sb-bent	0.0127	0.01195	0.6145	0.435	0.430	0.400	0.390	0.624	0.472
3	In-bent	0.0351	0.05501	0.5046	0.4911	0.491	0.466	0.450	0.652	0.347
6	In-bent	0.0206	0.05417	0.766	0.262	0.247	0.218	0.217	0.560	0.320

(and $R_0/R_{//}$). There is good agreement between theoretical and experimental values of $\sigma_{//}/\sigma_0$, but poor agreement for $\sigma_\perp/\sigma_{//}$. The latter is not surprising since the expression (4.37) was not rigorously derived by Broudy. Furthermore, one would expect an overestimation of $\sigma_\perp/\sigma_{//}$ for large values of $(\epsilon+\phi)$, since the original Juretschke relation $\sigma_\perp/\sigma_{//} = 1/(1+\epsilon)$ overestimates $\sigma_\perp/\sigma_{//}$ for large values of ϵ (as discussed in Section 4.1.2).

Tables 8.10 and 8.11 refer to the analysis carried out assuming acoustic scattering to be the lattice scattering mechanism. A similar analysis was carried out assuming polar scattering to be the lattice scattering mechanism. The resultant energy levels were the same as those obtained for acoustic scattering and the dislocation densities deduced were within a factor of two of those obtained previously. The values of $\sigma_{//}/\sigma_0$ were still within experimental error of the observed values. These results are not surprising since the mean free path for acoustic scattering is close to that for polar scattering (as shown in the calculated values of Table 8.9) and the temperature dependence as given by equations (A.8) and (A.18) is identical.

8.4.3. Summary of Broudy analysis.

It was noted above that there was a maximum

value of the parameter Θ which could be used, above which no real solution to equation (8.4) could be obtained. It is interesting to consider why Θ has a maximum value.

In the Broudy analysis, one calculates a dislocation density from the Hall coefficient changes brought about by the bending. This dislocation density depends on the value of Θ used. For example, a high value of Θ (say 0.7) means that the ϕ regions are relatively ineffective in increasing the Hall coefficient and consequently a high dislocation density is needed to explain the Hall coefficient change. With this high dislocation density, however, the ϕ regions of neighbouring polygon walls overlap such that equation (8.7) is not valid. Since (8.7) was used in formulating (8.4), the latter equation is not valid either.

A low value of Θ (say 0.05), however, means that the ϕ regions are much more effective in increasing the Hall coefficient and consequently a smaller dislocation density results. Since the dislocation density is smaller, the ϕ regions of neighbouring polygon walls do not overlap and equation (8.4) is valid.

It is clear, therefore, that there exists a maximum value of Θ which, in these experiments, was about 0.1. The value of Θ used in the analysis (0.05) was chosen arbitrarily between the limits of 0 and 0.1,

but variation of θ within these limits did not alter the resultant energy level ($E_c - E_D$) significantly. The theoretical dislocation density is, of course, changed when θ is varied, but as θ is so small the maximum change in ρ was a factor of two.

Values of ϵ and ϕ given in Table 8.11 show that the ϕ regions are very much larger than the ϵ regions. This is because the mean free path is very much longer than the radius of the space charge cylinders, the latter being especially small because of the high energy levels of the dislocation-acceptors. For example, in specimen 5 at 80°K, the ϕ regions occupy 84% of the material while the ϵ regions occupy only 3.1%. Because of the dominance of the ϕ regions it is important to use accurate values of the mean free path to calculate their size. The close agreement between the mean free path values calculated using the two lattice scattering mechanisms gives confidence that the values are not seriously in error.

Unlike the Read analysis, an experimental error enters into the slope of the theoretical $R_o/R_{//}$ (T) curve. The experimental error in β, the degree of impurity scattering, enters the expression for $R_o/R_{//}$ through the mean free path, and since β varies with temperature, an error in β will alter the resultant

slope of the $R_o/R_{//}$ (T) curve. However, in the case of specimens 6 and 4, the contribution of β is negligible and so the result is not dependent upon errors in β. Since the analyses of specimens 3 and 5, in which β is significant, confirmed the energy levels calculated for specimens 6 and 4 we may infer that the actual errors in β did not introduce a large error into the result.

In the curve-fitting technique described in this section, it is not obvious that the resultant energy level will be independent of the temperature at which theoretical and experimental $R_o/R_{//}$ values are matched (to calculate λ). However, it was found that matching at a second temperature produced the same energy level as before, and a dislocation density which was within 10% of that obtained previously.

Thus the Broudy model, when modified to include overlap of ϕ regions within polygon walls of dislocations, can accommodate the temperature dependence of the Hall coefficient of deformed samples. This model predicts values of dislocation density and conductivity which are in good agreement with the measured values, and gives the scheme of energy levels for dislocation acceptors shown in Fig.8.19. Comparing the Broudy scheme of levels in Fig.8.19 with the Read scheme in Fig.8.16, it appears that the Broudy analysis inverts the levels,

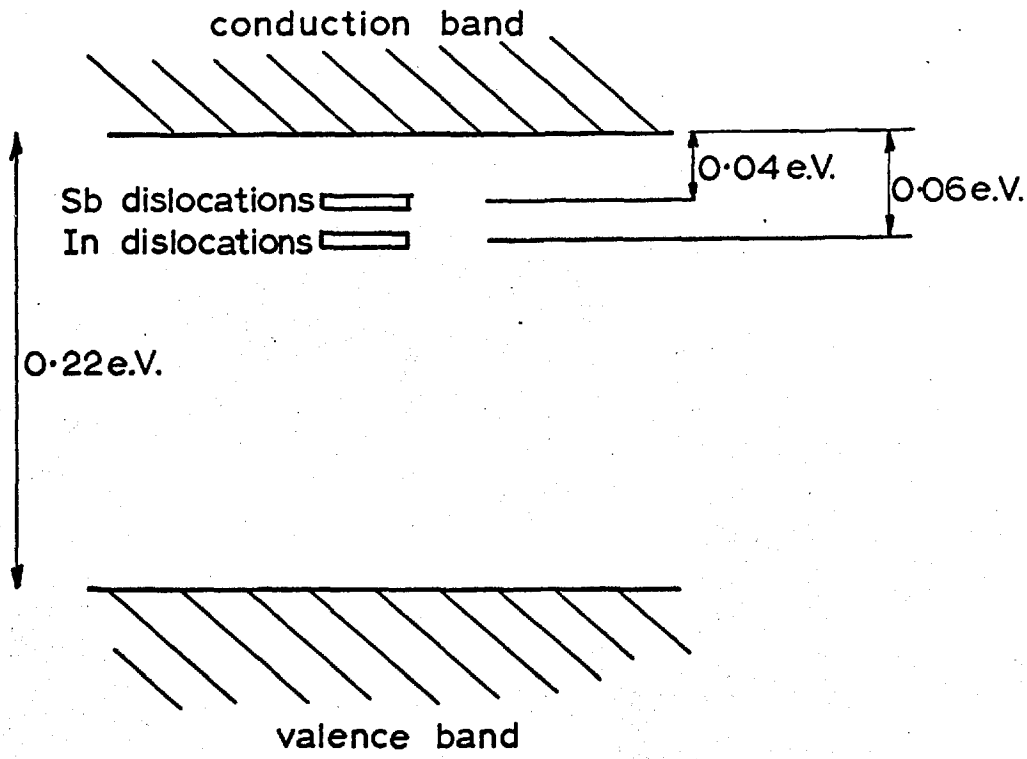

FIG. 8.19. Dislocation-acceptor levels on Broudy analysis.

the Sb-level being higher in the forbidden gap than the In-level. However, the difference of 0.02 e.V. between the levels in the Broudy scheme is not significant and the levels are so close that it is not possible to state which is higher in the forbidden gap.

CHAPTER 9

DISCUSSION

9.1. The Mechanics and Dynamics of Plastic Bending

In this series of experiments plastic bending was used primarily as a means to an end, the end being the introduction of an excess of In- or Sb- dislocations into samples of indium antimonide. However, the movement of dislocations during plastic bending is of interest in itself, and the analysis of Section 8.4. indicates that the electrical effects of plastic bending are extremely dependent upon the distribution of dislocations produced by this type of deformation.

9.1.1. The Dislocation Structure as Revealed by Etching

The etching experiments described in Section 7.2. confirm the conclusions made by Venables and Broudy (1958) that in indium antimonide dislocations of one sign etch more rapidly than those of the opposite sign, in certain etching reagents. The results show that the CP_4 etch attacks In-dislocations preferentially and also a fraction (probably about half) of the antimony ones, while the butylamine etch shows up both the indium and the antimony dislocations. This is the first quantitative test of the behaviour of these etchants.

Interpretation of the etch-pit measurements on samples bent at 360°C produced the result that these samples contained one third as many minority dislocations as majority dislocations. It is therefore worth while discussing the dislocation dynamics which might give rise to such a small majority to minority ratio.

It is interesting to compare the present results with those of Livingston (1962, 1963) on copper, this being the only other case where an etch which can discriminate between dislocations of opposite sign has been developed. Livingston found that, in copper crystals bent at room temperature, about 95% of the dislocations were of the majority sign. He explained this result in terms of the dominant role of surface sources, since only majority sign dislocations should move towards the neutral axis under a bending stress. To account for the present results which indicate large numbers of minority dislocations, it is necessary to invoke internal sources. Peissker, Haasen and Alexander (1961) first suggested that surface sources were not important in indium antimonide. They deduced this from a study of the effect of varying specimen dimensions on the creep properties. In these present experiments the initial dislocation density was only $10^3 - 10^4$ / cm^2, and thus it seems unlikely that the minority sign dislocations issued from internal

Frank-Read sources. The double cross-glide multiplication mechanism, which produces internal sources, is thought not to be important in diamond and sphalerite structure materials. The phenomenon of slip-band broadening, which was first seen in lithium fluoride and discussed in terms of propagation by double cross-glide, does not occur in germanium or silicon, and Dew-Hughes (1961) suggested that the absence of cross-slip in germanium might account for some of the differences between its behaviour and that of lithium fluoride. However, Holt and Crawford (private communication) have observed elementary structure in the slip-line pattern of germanium; this is sometimes taken as evidence for double cross-slip. On the other hand, Alexander and Haasen (1961) found evidence for the deviation of slip-lines by the climb of edge dislocations but not by the cross-slip of screws. If the propagation of slip were dependent on the climb of edge segments one would expect the yielding behaviour to be very temperature sensitive, which it is in these materials.

It is also interesting to consider whether the sharply polygonised dislocation structures obtained in specimens bent at 360°C were a result of glide processes alone, or a combination of glide and climb. For copper, Livingston was able to show that 'glide polygonisation', in which edge dislocations of like sign

stick in minimum energy positions when they attempt to pass on parallel slip planes, can occur at temperatures well below those necessary for climb. The mechanism of polygonisation at 360°C in indium antimonide, however, is not so clear. Duga and Maringer (1960) reported that this material does not polygonise after deformation even when heated within a few degrees of the melting point. However, the present results indicate that this is true only for specimens deformed by multiple slip. The samples bent at 270°C in single slip showed little or no tendency to polygonisation, but after annealing close to the melting point it was very marked (Vogel, 1956, found similar effects in germanium). The annealing temperature was quite critical and had to be above 500°C for polygonisation to occur. Specimens were sharply polygonised after bending at 360°C, a rather low temperature compared with that found necessary to produce climb polygonisation on annealing. Furthermore, the small applied stress (a consequence of the small applied strain rate) would favour the formation of polygon walls by a glide process. Nevertheless, following the previous arguments, it seems very likely that climb played a part in the transfer of slip from one plane to another, and possibly, therefore, in the formation of polygon walls, too.

9.1.2. The Differences Between In-bending and Sb-bending

The measurements of lower yield stresses for bending at 270°C indicated that the mobilities of In- and Sb-dislocations were different. The results suggested that In-dislocations were more mobile than Sb-dislocations, a deduction also made by Peissker et al. (1961) from creep measurements. It is interesting to compare the magnitude of the effects observed in the two types of experiments.

Peissker et al. described their experimental results by the empirical expression

$$\dot{a}_w = C_1 S^{3.3} \exp(-U/kT) \qquad (9.1.)$$

where $\dot{a}_w$ = constant creep rate (in steady state creep) and U = 0.88 ± 0.02 eV (U for Sb-bending was about 1-2% higher than for In-bending).

[Equation (9.1.) is of the same form as (2.11.) which was derived by Haasen.]

Consider two specimens bent in opposite directions under creep conditions at the same stress and temperature. We will calculate an expression for $d\dot{a}_w$, the difference between the constant creep rate of the In-bent specimen and that of the Sb-bent specimen.

Taking logarithms in (9.1.)

$$\log \dot{a}_w = \log C_1 + 3.3 \log S - U/kT$$

and differentiating,

$$\frac{d\dot{a}_w}{\dot{a}_w} = \frac{dC_1}{C_1} - \frac{dU}{kT} \qquad (9.2.)$$

(since S is the same for both specimens).
Now, Peissker's experiments gave $\frac{d\dot{a}_w}{\dot{a}_w} = 0.5$ (where $\dot{a}_w$ refers to Sb-bending) and thus the corresponding differences in U and C_1 are given by

$$\frac{dC_1}{C_1} - \frac{dU}{kT} = 0.5$$

Consider, now, two specimens bent in opposite directions under constant strain rate conditions at the same temperature and strain rate. We will calculate an expression for dS_{ly}, the difference between the lower yield stress of the In-bent specimen and that of the Sb-bent specimen. Now the lower yield stress in a constant strain rate experiment corresponds to steady state creep in the static test, since in both the stress and strain rate are constant. Thus, as described in Section 2.2., the lower yield stress S_{ly} follows by inversion of (9.1.), i.e.

$$S_{ly}^{3.3} = \frac{\dot{a}}{C_1} \exp (U/kT) \qquad (9.3.)$$

Taking logarithms in (9.3.)

$$3.3 \log S_{ly} = \log \dot{a} - \log C_1 + U/kT$$

and differentiating

$$3.3\,\frac{dS_{1y}}{S_{1y}} = -\frac{dC_1}{C_1} + \frac{dU}{kT} \qquad (9.4.)$$

(since á is the same for both specimens)

Peissker's experiments gave $\frac{dC_1}{C_1} - \frac{dU}{kT} = 0.5$ and, substituting this value in (9.4.) we obtain

$$3.3\,\frac{dS_{1y}}{S_{1y}} = -0.5$$

or $$\frac{dS_{1y}}{S_{1y}} = -0.15$$

(where S_{1y} refers to Sb-bending).

Thus the creep measurements of Peissker et al. predict that, in the constant strain rate test, the lower yield stress for Sb-bending should be greater than that for In-bending by an amount dS_{1y}, where $\frac{dS_{1y}}{S_{1y}} = 0.15$.

In the present results we obtained

$$\frac{dS_{1y}}{S_{1y}} \simeq 0.25 \ ,$$

a value rather larger than that predicted from Peissker's results. This discrepancy, however, is within experimental scatter which was large in both series of experiments. Furthermore, other factors could account for the difference between the two sets of

results. For example, if the density or distribution of dislocations in Peissker's specimens during steady state creep were different from that in the present specimens at the lower yield, one would not expect the two sets of results to be equivalent. Such a difference in density or distribution of dislocations could have arisen from a difference in initial dislocation density or from the difference in the modes of deformation.

Peissker et al. concluded from their creep studies that In-dislocations move more readily than Sb-dislocations. Whilst this seems a reasonable deduction from their observed differences in creep rate, or from the present differences in flow stress for oppositely bent samples, the line of argument is not a simple one for it is now clear that there is always a significant fraction of minority sign dislocations. Also it does not follow necessarily that In-dislocations move in the slip plane more readily than Sb-dislocations. It is possible that different tendencies for climb could explain the observations.

The possibility that In-dislocations and Sb-dislocations have different tendencies for climb was suggested by the present annealing experiments on samples which had been deformed at 270°C. These

experiments indicated that In-dislocations polygonised by climb more readily than Sb-dislocations. Now the climb of edge dislocations could be a means of relieving stress concentrations in piled up groups. If the In-dislocations relieved stresses in this way while Sb-dislocations still remained in piled-up groups one would expect significant differences in the lower yield stress for In- and Sb- bending. If this climb mechanism were responsible for the differences between In-bending and Sb-bending one would expect the differences to be less marked at higher temperatures where Sb-dislocations also begin to polygonise (as observed in samples bent at 360°C). This prediction was confirmed in the present measurements but not in those of Peissker et al.

It is not unreasonable, theoretically, for In- and Sb-dislocations to have different tendencies for climb. Although both types of dislocation must climb by the movement of double vacancies or interstitials (to ensure that the dislocation half plane terminates at the widely spaced pair of planes), it is possible that double defects would prefer to annihilate at one type of dislocation rather than another. For example, if the formation energy of jogs in In- and Sb-dislocations were different, one would expect more jogs to occur in one type of dislocation and hence

that type would climb more readily.

Finally, although it seems reasonable that In- and Sb-dislocations should have different mobilities in glide by virtue of the difference in core structure, it seems an oversimplification to describe the movement of, say, an In-dislocation in terms of diffusion of In-atoms only, since, on Haasen's model the 'rupture' which diffuses as the dislocation moves is a broken bond between an In and an Sb atom. In fact the results of Peissker et al. were not in quantitative agreement with the diffusion model. It seems possible, therefore, that some other mechanism such as the climb mechanism described above, may be responsible for the differences between In- and Sb-bending.

9.2. The Electrical Effects of Plastic Bending: Consideration of Point Defects and Impurities.

In Chapter 8 the observed effects of plastic bending were interpreted on the basis that dislocations were responsible for all changes in electrical properties. This procedure will here be justified by showing that other possibilities can, with some confidence, be ruled out.

Considering only deformation of n-type material (since comparatively few experiments were performed

on p-type material) it must first be considered whether these results do show the introduction of acceptors by bending, since it is conceivable that the Hall coefficient could be increased simply by the introduction of low mobility regions within the sample. However, in certain cases n-type specimens were converted to p-type by the bending, and thus we must conclude that acceptors were introduced.

In Chapter 8 it was shown that if the measured etch-pit densities were used to estimate the dislocation densities in bent samples, then the changes in the Hall coefficient were rather larger than one would expect on the simple Read model. This prompts one to consider the possibility that the observed effects were due to impurities or point defects.

We will first consider the possibility of impurity (chemical) acceptors being responsible for the observed changes. The undeformed and deformed control samples did not show any evidence for impurity contamination after the heat treatment and we may conclude that, even in the presence of a static dislocation density of about $10^6/cm^2$, impurity pick up was not serious at this temperature. However, this does not rule out all impurity effects since it is possible that impurities could be dragged in during the bending by the gliding

dislocations. The results could not be explained by a random distribution of impurities since this would produce an isotropic conductivity in the deformed samples. It is possible, however, that the impurities could segregate preferentially along the dislocation lines and thus give rise to anisotropic conductivities. Thus, the impurity postulate is sufficiently flexible as to permit an explanation of almost any effect and yet it is difficult to test critically. Although the results do not rule out the possibility of impurities being partly responsible for the observed effects, it is felt that most mechanisms of contamination can be ruled out by the measurements on control samples.

Secondly we will consider the possibility of point-defects being responsible for the observed changes. It is well known that point defects can be produced by the interaction of dislocations moving on intersecting slip planes. However, great care was taken to produce slip on a single set of planes to minimise point-defect production, and etch-pit evidence has been presented which indicates that only a small number of dislocations were introduced by non-primary slip. Furthermore the deformed control specimens showed no evidence for annealable centres after heat treatment at 360°C (the deformation temperature). It was intended to check

the presence of point-defects more thoroughly by annealing close to the melting point, but the results were inconclusive due to the rapid pick up of impurities at this high temperature.

There are some indications in the literature of the mobility of point defects at 360°C. Electron and neutron irradiation experiments (Aukerman 1959, Eisen 1961, Cleland and Crawford 1954) have indicated that radiation-produced point defects anneal out rapidly at 360°C. These defects were thought to be single defects. Plastic deformation, on the other hand, is expected to produce double defects which may have quite different annealing kinetics. However, with dislocation densities of order 10^6 cm^{-2}, point defects would need to diffuse only a short distance to reach a sink. It is thought, therefore, that point defects are not important in the present results.

A further indication that the centres introduced by deformation are not randomly distributed (as impurities or point defects) is afforded by the temperature dependence of the Hall coefficient of deformed samples. The slopes in the extrinsic range were very shallow (see, for example, Figure 8.6.) and, when analysed in terms of randomly distributed centres, the measurements indicate an acceptor level at about 0.002 eV

- 0.004 eV below the conduction band. This acceptor level does not correspond to any known impurity level in indium antimonide, since all known impurity acceptor levels lie in the lower half of the band gap (Table 3.1.). Also this level does not correspond to any point defect level estimated from experiments on irradiated material. The energy level obtained from the present measurements, when analysed in terms of randomly introduced centres, varied from specimen to specimen. In contrast, the energy levels determined from an analysis of the results in terms of dislocation centres, were very similar for a given bending direction.

Perhaps the strongest indication that the centres introduced by deformation were not impurities or point defects lies im the magnitude of the change in electron mobility brought about by bending n-type samples. If impurity centres alone were responsible then more than 10^{16} impurities/cm^3 would be needed (if randomly distributed) to produce the observed mobility in the 'perpendicular' samples (which was, in some cases, less than one third of the mobility in the control samples). Since the Hall coefficient measurements indicated the introduction of only about 10^{14} centres/cm^3, it is clear that the centres were not randomly distributed.

9.3. Interpretation of the Electrical Effects in Terms Of Dislocations

Having considered all other possibilities we conclude that it is most probable that dislocations were responsible for the electrical changes observed. We now consider possible models of dislocation-acceptors.

It has been shown in Chapter 8 that the simple Read model appears to be inadequate for at least some of the present results since more acceptor centres were found than predicted by the theory. Mueller and Jacobson (1962), discussing their experiments on indium antimonide crystals containing a small angle boundary, introduced a modification to the Read model. They assumed that closely spaced dislocations in a boundary give rise to local bands of electron energy levels instead of a single level. However, this modification makes a difference of only a factor of two to the number of states per unit length of dislocation, and the occupation fraction (which they did not consider) would be less than for widely spaced dislocations because of the additional Coulombic interaction between occupied sites on neighbouring dislocations. In a polygon wall where the dislocations were about 1 micron apart this additional interaction would be very small.

Shockley (1953) originally proposed that at the

bottom of the dislocation half-plane there might be a one-dimensional band of "edge states" and that under certain conditions this might become a one-dimensional degenerate-electron-gas conductor. This model is clearly unsuitable for the present results on n-type material where the conductivity was always reduced by deformation.

Arthur, Gibson, Granville and Paige (1958) and subsequently Gibson and Paige (1958), when discussing their results concerning minority carrier behaviour in n-type germanium specimens containing parallel arrays of dislocations, suggested that the dislocation may be considered as a thread of p-type material embedded in the crystal. Now, Gibson and Paige were concerned with high resistivity germanium at room temperature where the density of intrinsic carriers was comparable with the density of extrinsic electrons and hence with the density of ionised donors. Then it is likely that the (intrinsic) free holes may make a significant contribution to the space charge, since they will be attracted by the row of accepted electrons. In this way, a cylinder of p-type material may form around the dislocation. In indium antimonide at $80^{\circ}K$, however, the density of (intrinsic) free holes in a sample containing 10^{14} electrons/cm^3 is only $\sim 10^6 cm^{-3}$ (since $n_i^2 \simeq 10^{20}/cm^3$)

i.e. many orders of magnitude less than the density of ionised donors. Thus it is unlikely that p-type cylinders would form at 80°K. However, at about 150°K, where the material is near intrinsic, this model might be appropriate.

The model of Bliek (1964) developed for p-type material considers the screening of accepted electrons by free holes alone. A comprehensive theory of the occupation of dislocation-acceptors in n-type material would have to consider screening by free holes and ionised donors. Time did not permit the development of such a theory.

The modification of the Read model introduced by Broudy seemed very appropriate for the present results since it predicts larger increases in the Hall coefficient than the Read model (for the same density of dislocations) and also predicts reduced parallel mobilities in agreement with the measurements. For these reasons, therefore, the Broudy model was applied to the results as well as the simple Read model, and the outcome of these analyses will now be considered.

The electrical measurements on samples bent by three-point and four-point bending may be summarised as follows.

Both In-bending and Sb-bending of n-type material introduced acceptor centres. This result was obtained in seventeen n-type specimens deformed by either three-point or four-point bending.

In-bending of p-type material introduced acceptor centres while Sb-bending of p-type material either had no effect or introduced a small number of donor centres. Only four p-type specimens were deformed (by three-point bending).

The temperature dependence of the Hall coefficient of n-type samples was analysed on the Read and Broudy models, which gave the schemes of energy levels shown in Figures 8.16. and 8.19. respectively. These schemes of levels (particularly the Broudy scheme) could accommodate qualitatively the observed effects of Sb-bending on p-type material if an additional Sb-donor level were postulated. However, neither scheme of levels accommodates the observed effect of In-bending on p-type material since both schemes place the In-acceptor level above the Fermi level in p-type material at $80^{\circ}K$, and thus predict that In-dislocations will not act as acceptors in p-type material at that temperature. The qualitative results concerning In-bending of p-type material seem unambiguous since large effects were observed, but, taken by themselves, these particular

results would be very difficult to explain quantitatively even if the In-acceptor level were near the valence band. As discussed in Section 8.1.3. one would not expect acceptors to be more fully occupied in p-type material than in n-type material, but the numbers of acceptors introduced into these two In-bent p-type samples were very much greater than observed in n-type samples bent to the same radius (and very much greater than the number predicted by Bliek's theory).

Only two p-type samples were In-bent and these were deformed by three-point bending. This reduces confidence in the results since the specimens were not macroscopically as uniform as the four-point bent samples. Thus, while noting that the qualitative effects of In-bending on p-type material are not in agreement with the models developed from the study of n-type material, we will not dwell on the difficulty any longer but will confine the following discussion to the effect of dislocations in n-type material, bearing in mind the need for a more detailed experimental study of p-type specimens.

9.4. Detailed Consideration of the Results on n-type Material

Both In- and Sb-bending introduced acceptor centres

into n-type material. For a given sign of bending the number of acceptor centres introduced per unit length of dislocation (as calculated on Read's theory) was found to be approximately the same for three-point and four-point bending. The only discrepancy between the two series of experiments was in the electron mobilities in 'parallel' samples. The mobilities in the 'parallel' limbs of three-point bent samples were very much lower than the mobilities in 'parallel' samples from four-point bent specimens of comparable etch-pit density. A possible reason for this difference might be that the dislocations were not in such a parallel array in the three-point bent samples as they were in the four-point bent samples, perhaps because of the different stress distributions during bending.

9.4.1. Consideration of Minority Sign Dislocations

It was concluded from the etch-pit measurements that significant numbers of minority sign dislocations were present in samples bent at 360°C. In order to simplify the analysis in Chapter 8 the electrical measurements were analysed on the assumption that no minority sign dislocations were present. However, the Read theory may be extended to account for the presence of both In- and Sb-dislocations in the same sample, assuming that each type of dislocation is associated

with its own energy level, and that both acceptor levels lie below the Fermi level in n-type material. If the different sign dislocations are far enough apart that no electrostatic interaction occurs between them, the two arrays of acceptor centres will have quite independent occupation statistics. It is thus possible to calculate $f(T)$ curves for each type of dislocation, knowing its acceptor level.

If a specimen, A, contains $\rho_{In(A)}$ In-dislocations/cm^2 and $\rho_{Sb(A)}$ Sb-dislocations/cm^2, the fraction of sites occupied being $f_{In(A)}$ and $f_{Sb(A)}$ respectively, then we may write

$$\epsilon_{(A)} = \frac{f_{In(A)}\rho_{In(A)} + f_{Sb(A)}\rho_{Sb(A)}}{c\,(N_D - N_A)_{(A)}}$$

Now, considering two specimens A and B, with similar initial carrier concentrations and similar positions of the Fermi level, then $f_{In(A)} = f_{In(B)}$ $(= f_{In})$ and $f_{Sb(A)} = f_{Sb(B)}$ $(= f_{Sb})$. Also, interpretation of the etch pit measurements indicated that, for In-bent samples,

$$\rho_{In} = 3 \text{ or } 4 \times \rho_{Sb} \ ,$$

and for Sb-bent samples,

$$\rho_{Sb} = 2 \text{ or } 3 \times \rho_{In} .$$

As a first approximation we will assume that, for both directions of bend, the majority dislocation density is a factor of three times the minority dislocation density. Thus, if the subscript (A) refers to an In-bent sample and (B) to an Sb-bent one,

$$\epsilon_{(A)} = \frac{\rho_{In(A)} \left(f_{In} + \tfrac{1}{3} f_{Sb} \right)}{c \left(N_D - N_A \right)_{(A)}}$$

$$\epsilon_{(B)} = \frac{\rho_{Sb(B)} \left(\tfrac{1}{3} f_{In} + f_{Sb} \right)}{c \left(N_D - N_A \right)_{(B)}}$$

or $$\epsilon_{(A)} = \lambda_{(A)} \left(f_{In} + \tfrac{1}{3} f_{Sb} \right) \qquad (9.5.)$$

and $$\epsilon_{(B)} = \lambda_{(B)} \left(\tfrac{1}{3} f_{In} + f_{Sb} \right) \qquad (9.6.)$$

where $$\lambda_{(A)} = \frac{\rho_{In(A)}}{c \left(N_D - N_A \right)_{(A)}}$$

and $$\lambda_{(B)} = \frac{\rho_{Sb(B)}}{c \left(N_D - N_A \right)_{(B)}}$$

Equations (9.5.) and (9.6.) were then used to determine energy levels from the temperature dependence of the Hall coefficient of two specimens A and B. Specimens 3 and 5 were selected as they fulfilled the requirement of having similar initial carrier concentrations. The procedure used was an extension of the method used in the initial Read analysis (Section 8.3.). Energy levels were assigned to In- and Sb-dislocations and $f_{In}(T)$ and $f_{Sb}(T)$ curves were calculated. Then, using (9.5.) and (9.6.), experimental values of $\epsilon_{(A)}$ and $\epsilon_{(B)}$ at one temperature were used to determine $\lambda_{(A)}$ and $\lambda_{(B)}$, from which theoretical $\epsilon_{(A)}(T)$ and $\epsilon_{(B)}(T)$ curves were constructed. Different combinations of energy levels were tried and curves for two combinations are shown in Figure 9.1. The combination $(E_c - E_D)_{In}$ = 0.06 eV and $(E_c - E_D)_{Sb}$ = 0.24 eV gave fair agreement for both specimens. Trial of other values showed that no other combination of energy levels would produce agreement between experiment and theory.

The values of $\lambda_{(A)}$ and $\lambda_{(B)}$ used to calculate the theoretical curves corresponding to $(E_c - E_D)_{In}$ = 0.06 eV and $(E_c - E_D)_{Sb}$ = 0.24 eV were used to calculate the densities of In- and Sb-dislocations in the two samples, by the relations,

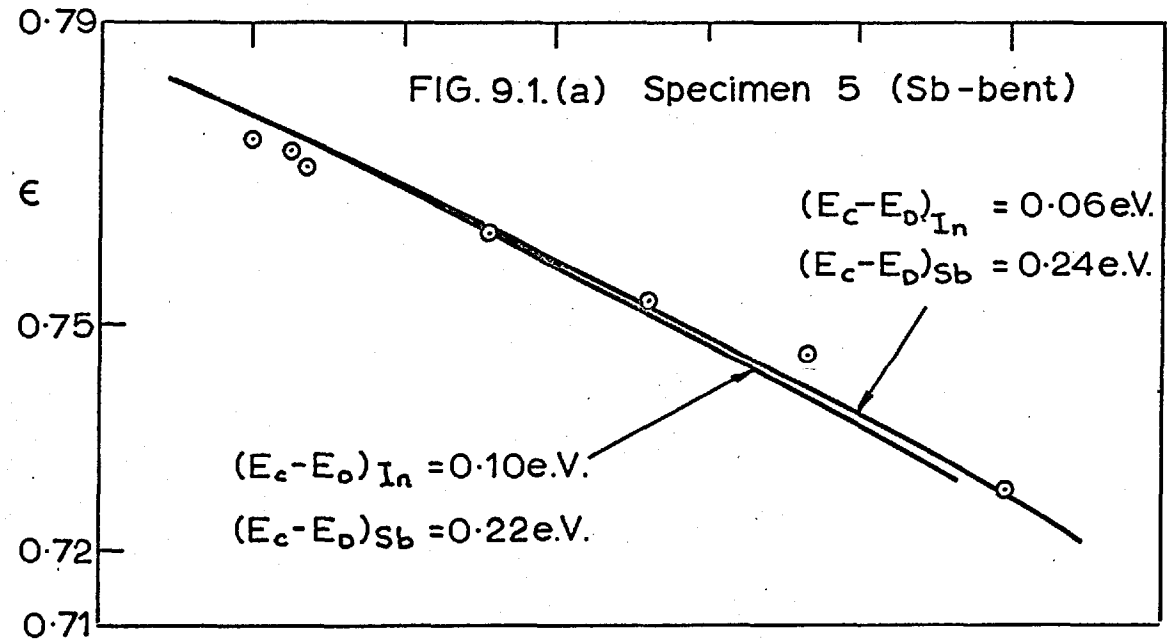
0·79
0·75
0·72
0·71
ϵ
FIG. 9.1.(a) Specimen 5 (Sb-bent)
$(E_c-E_D)_{In}$ = 0·06e.V.
$(E_c-E_D)_{Sb}$ = 0·24e.V.
$(E_c-E_D)_{In}$ = 0·10e.V.
$(E_c-E_D)_{Sb}$ = 0·22e.V.

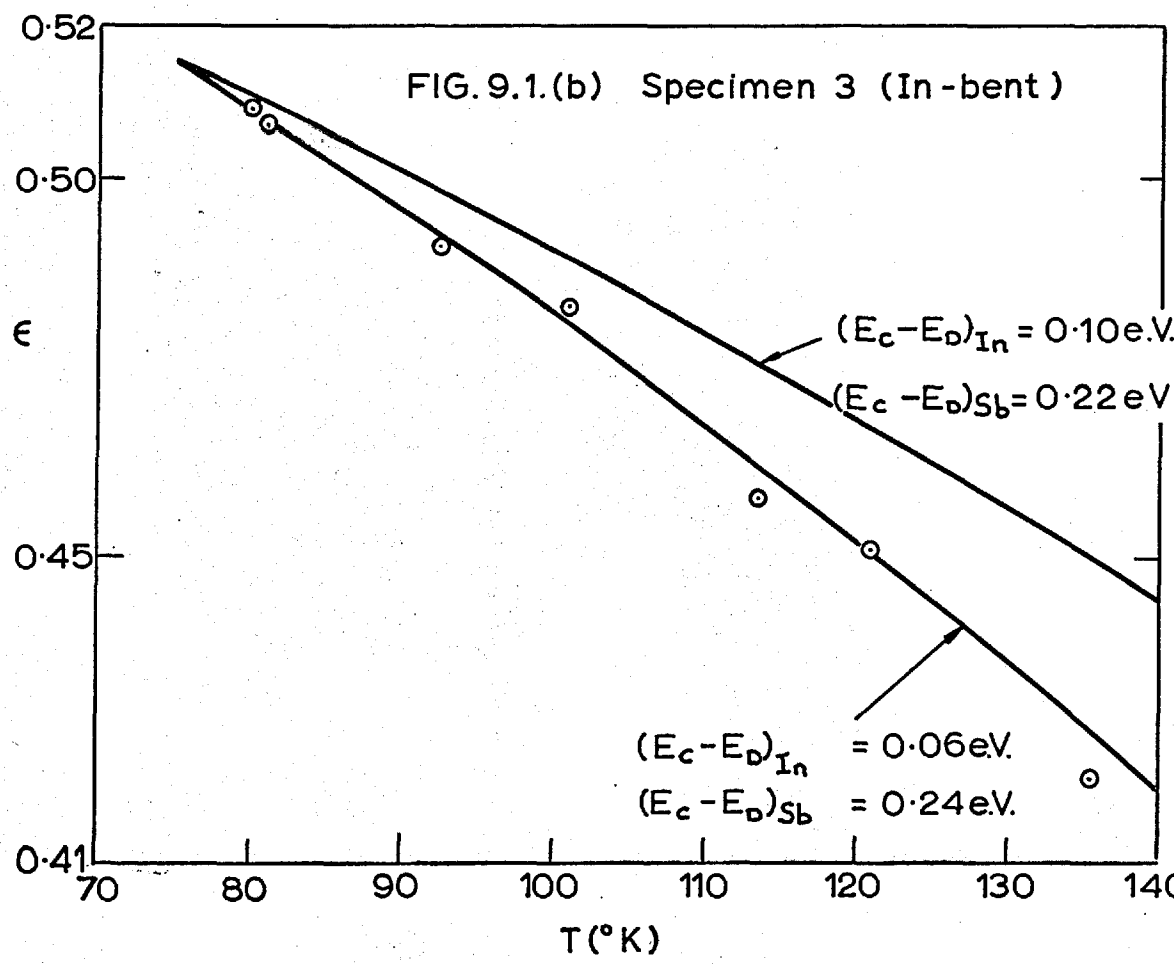
0·52
0·50
0·45
0·41
ϵ
FIG. 9.1.(b) Specimen 3 (In-bent)
$(E_c-E_D)_{In}$ = 0·10e.V.
$(E_c-E_D)_{Sb}$ = 0·22 eV
$(E_c-E_D)_{In}$ = 0·06e.V.
$(E_c-E_D)_{Sb}$ = 0·24e.V.
70
80
90
100
110
120
130
140
T(°K)

$$\rho_{In(A)} = \lambda_{(A)} C \left(N_D - N_A\right)_{(A)}$$

$$\rho_{Sb(B)} = \lambda_{(B)} C \left(N_D - N_A\right)_{(B)}$$

Table 9.1. compares these theoretical values with the values deduced from etch-pit measurements. The discrepancies between theoretical and experimental values are approximately the same as those found in the original Read analysis. The total density of dislocations $(\rho_{In} + \rho_{Sb})$ deduced from this interpretation, is within 10% of the dislocation density deduced previously. Furthermore, the energy levels have not been altered drastically by considering minority sign dislocations, since the In- level has been moved upwards by only 0.04 eV and the Sb-acceptor level has been moved downwards by only 0.02 eV (the latter change may not be significant as this would move the Sb-level into the valence band. In fact the levels $(E_C - E_D)_{In}$ = 0.06 eV and $(E_C - E_D)_{Sb}$ = 0.22 eV give reasonable agreement between theory and experiment, but better agreement is obtained if the Sb-level is moved towards the valence band).

It is reasonable to deduce that a consideration of minority dislocations in the Broudy interpretation would also have little effect on the energy levels deduced

Table 9.1. Read Analysis Considering Presence of Minority Dislocations, for Dislocation Acceptor Levels of $(E_C - E_D)_{In} = 0.06$ eV, $(E_C - E_D)_{Sb} = 0.24$ eV.

Specimen No.	Polarity	ρ_{Sb} (cm^{-2})		ρ_{In} (cm^{-2})	
		Theoretical	Etch-Pit	Theoretical	Etch-Pit
5	Sb-bent	1.64×10^8	1.10×10^7	5.46×10^7	3.5×10^6
3	In-bent	5.04×10^7	8.0×10^6	1.51×10^8	2.5×10^7

previously. In the Broudy model the two dislocation acceptor levels were only 0.02 eV apart on the previous analysis, because the dominance of the ϕ regions reduces the difference between the In-level and the Sb-level. Consequently it is unlikely that a second order effect, such as that of minority dislocations, would increase the resultant difference in levels appreciably.

9.4.2. Comparison of Read and Broudy Interpretations

It has been shown that the electrical measurements on deformed indium antimonide specimens can be accommodated on the Read model, but the analysis predicts dislocation densities which are larger than expected. The modification introduced by the Broudy model reduces this discrepancy in dislocation density but the resultant energy levels are very different from those on the Read model, and still do not fully explain the results on p-type material. It is interesting to consider why the two models give widely different dislocation-acceptor levels.

It will now be shown that the dislocation level which one deduces using either model is determined both by $d\epsilon/dT$ and by the absolute value of ϵ. On the Broudy model, the following approximate expressions for these two quantities can be written

$$\epsilon = \left(1 - R_o/R_{II}\right) - \phi(1-\theta)^2 \qquad (9.7.)$$

$$\frac{d\epsilon}{dT} = \frac{d}{dT}\left(1 - R_o/R_{II}\right) - (1-\theta)^2 \frac{d\phi}{dT} \qquad (9.8.)$$

In other words ϵ turns out less than $(1 - R_o/R_{II})$ (which gives ϵ on the Read model) and $d\epsilon/dT$ less than $d/dT\ (1 - R_o/R_{II})$ (which gives $d\epsilon/dT$ on the Read model).

In indium antimonide the value of ϵ which one deduces from measurements of R_o/R_{II} turns out to be very small since ϕ is very large (due to the long mean free path of electrons). Also, on the partial-overlap model developed in Chapter 8, $d\phi/dT$ is smaller than on the no-overlap model, and thus $d\epsilon/dT$ turns out larger on the partial-overlap model. This small value of ϵ and large value of $d\epsilon/dT$ are responsible for the upward displacement of the energy levels on the Broudy interpretation. For example, in Figure 9.2.(a), since ϵ is small, and $d\epsilon/dT$ large, the $\epsilon(T)$ curve cuts the T-axis at T_2. Now a theoretical $f(T)$ curve at the correct energy level for this $\epsilon(T)$ curve must satisfy the relation,

$$\epsilon(T) = \lambda_1 f(T)$$

FIG.9.2. Comparison of energy level determination on Read and Broudy models.

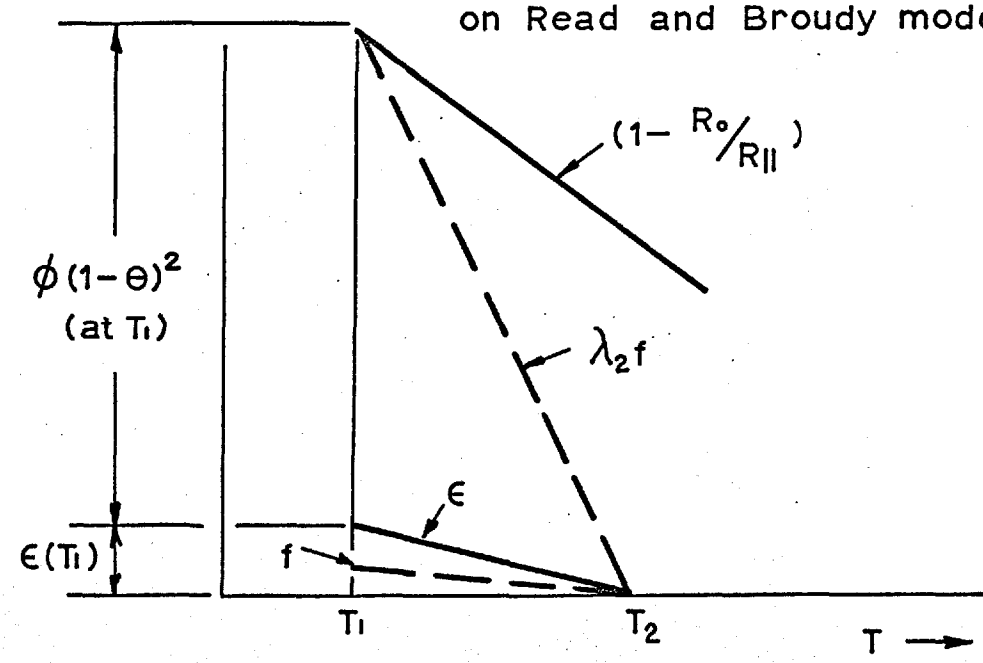

(a) Indium Antimonide.

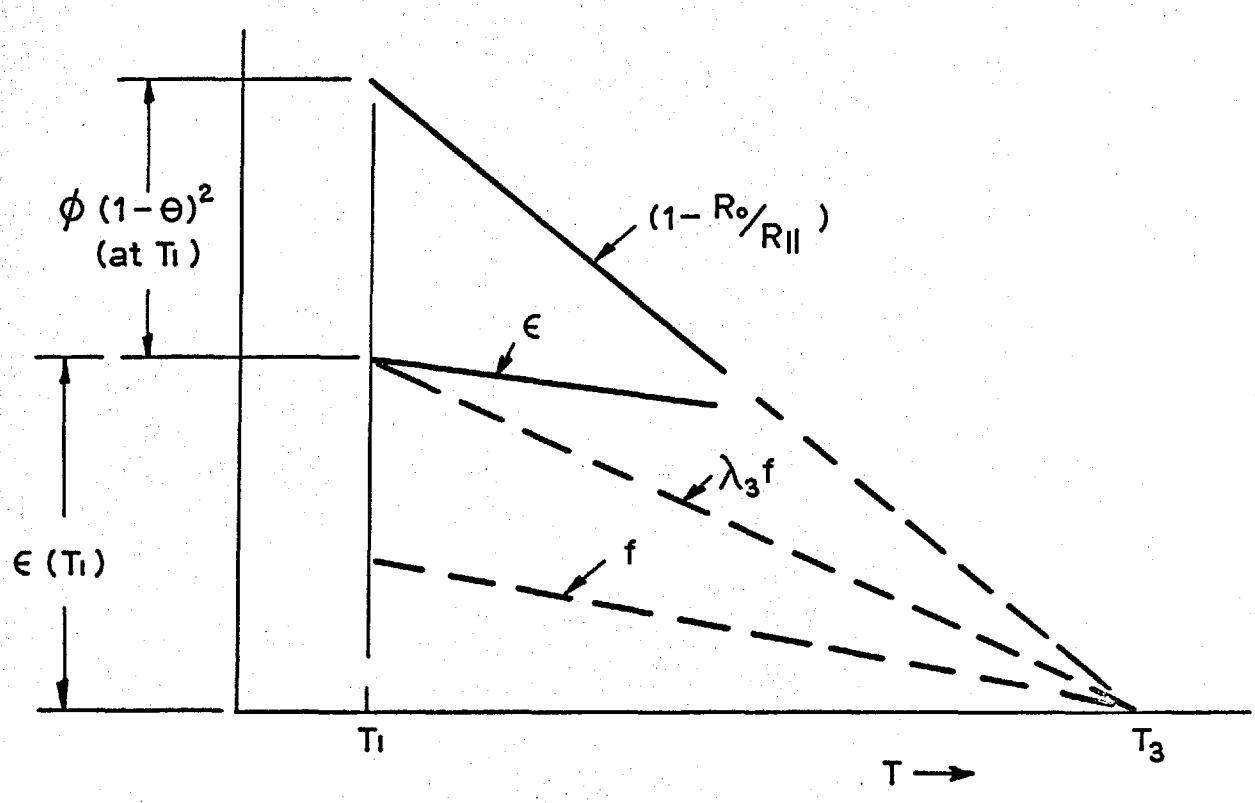

(b) Germanium.

Since $\epsilon(T_2) = 0, f(T_2) = 0$, i.e. the $f(T)$ curve must also cut the T-axis at T_2 (as shown in Fig. 9.2.(a)).

On the Read model the same energy level is tested by constructing a theoretical $\epsilon(T)$ curve to compare with the $(1 - R_o/R_{//})$ curve. First λ_2 is determined where

$$\lambda_2 = \frac{(1 - R_o/R_{//}) \text{ at } T_1}{f(T_1)}$$

and then the theoretical $\epsilon(T)$ curve is calculated by the relation $\epsilon(T) = \lambda_2 f(T)$. Now this $\epsilon(T)$ curve will also cut the T-axis at T_2, since, for the energy level being tested, $f(T_2) = 0$. The theoretical $\epsilon(T)$ curve also passes through the point $(1 - R_o/R_{//})$ at T_1 (as shown in Fig. 9.2.(a)) and is much steeper than the $(1 - R_o/R_{//})$ curve. Thus an $f(T)$ curve needed to fit the $(1 - R_o/R_{//})$ curve must correspond to a lower energy level in the forbidden gap since this will give a larger value of $f(T_1)$, a smaller value of λ and consequently a shallower $\epsilon(T)$ curve than before. Thus the Read model requires an energy level which is lower in the forbidden gap than the Broudy model.

In the no-overlap model used by Broudy when analysing his germanium results, ϕ is more rapidly varying with temperature than in the partial overlap model developed in Chapter 8 for indium antimonide,

i.e. for germanium $d\phi/dT$ is large and from (9.8.), $d\epsilon/dT$ is small. Thus the slope of the $\epsilon(T)$ curve is much shallower than that of the $(1 - R_o/R_{//})$ curve. This small value of $d\epsilon/dT$ is responsible for the downward displacement of the energy levels on the unmodified Broudy model.

Referring to Fig. 9.2.(b), the $(1 - R_o/R_{//})$ curve is extrapolated to cut the T-axis at T_3. Now, on the Read model, an $f(T)$ curve at the correct energy level must satisfy the relation $(1 - R_o/R_{//}) = \lambda f(T)$ and this $f(T)$ curve must also cut the T-axis at T_3, as shown in Fig. 9.2.(b).

On the Broudy model the same energy level is tested by constructing a $\lambda_3 f(T)$ curve to compare with the $\epsilon(T)$ curve. First λ_3 is determined where

$$\lambda_3 = \frac{\epsilon(T_1)}{f(T_1)}$$

and then the $\lambda_3 f(T)$ curve is calculated from the $f(T)$ curve used before. This $\lambda_3 f(T)$ curve will also cut the T-axis at T_3 since, for the energy level being tested, $f(T_3) = 0$. This curve will also pass through the point $\epsilon(T_1)$ and is much steeper than the $\epsilon(T)$ curve, as shown in Fig. 9.2.(b). Thus by reasoning in the same way as above it can be seen that the Broudy model requires an energy level which is

lower in the forbidden gap than the Read model, when analysing the germanium results in this way. A similar effect occurs when analysing the indium antimonide results on the no-overlap model, since $d\phi/dT$ is large and the small value of $d\epsilon/dT$ produces a similar downward displacement of the energy levels.

The Read and Broudy models gave rise to widely different energy levels when applied to the present results, for the reasons outlined above. It is therefore important to discuss the relative merits of these two theories.

The Read model has the advantage of being very simple, with few adjustable parameters, but this theory predicted dislocation densities which were larger than the etch-pit densities. In the case of the Sb-bent samples this discrepancy was outside the estimated limit of accuracy of the etch-pit technique.

The Broudy model is a more complex theory with more adjustable parameters. A particular difficulty with this theory when applied to indium antimonide is the large value of the mean free path, which introduces the possibility of overlap of neighbouring ϕ regions. This possibility makes the analysis very sensitive to the detailed arrangement of dislocations in the sample. For example, it has been noted that, if we

assumed a random arrangement of dislocations with no overlap of ϕ regions, no solutions could be obtained, the fit being closest for an energy level near the valence band. Thus the modification introduced by assuming overlap in the polygon walls is a drastic one, moving the levels up to positions near the conduction band. It appears therefore, that a model which assumes a smaller degree of overlap than envisaged in our model would result in levels which were lower in the forbidden gap. Now the etch pit measurements suggest that the dislocations in these samples were more randomly distributed than in the polygonised model of Fig. 8.17. A more random distribution would involve a smaller degree of overlap than in the model of Fig. 8.17., and the lower levels which would result from this more random model could possibly explain fully the results on p-type material.

In this light it is interesting to consider why the agreement between theoretical and experimental dislocation densities is better for In-bending than for Sb-bending. Although both theoretical predictions are within the estimated error of the etch-pit density, there appears to be a real difference between In- and Sb-bending. A possible reason could be that the Sb-dislocations were more randomly distributed

than the In-dislocations, as indicated by etch-pit measurements. More overlap of ϕ-regions would occur in the sharply polygonised arrangement of In-dislocations than in the more random array of Sb-dislocations, and thus, in the Sb-bent samples the ϕ-regions would occupy more volume (per dislocation) than in the In-bent samples. Thus, one might expect the more randomly arranged Sb-dislocations to be more effective in increasing the Hall coefficient of deformed material, and an analysis which assumed the same distribution for In- and Sb- dislocations would predict higher dislocation densities for Sb-dislocations than for In-dislocations. Following previous arguments it can be seen that an analysis taking into account the more random arrangement of the Sb-dislocations would give a lower energy level than that for the more sharply polygonised In-dislocations. Thus it is suggested that the marked differences in the electrical properties of In- and Sb-dislocations may be due to differences in dislocation distribution rather than to differences in energy levels.

The Broudy analysis is also very dependent on the size of the ϕ-regions, since $\phi >> \epsilon$. Thus, any errors in the computation of the mean free path will be reflected in the final results. Despite these unsatisfactory points concerning the Broudy model,

however, it has been shown that good agreement between calculated and measured values of dislocation density and conductivity can be obtained on this basis, the calculated values having been obtained from analysis of the Hall coefficient results. There is confidence in the values of the mean free path used, especially as the values calculated for polar scattering are close to those calculated for acoustic scattering. Also there is confidence in the general features of the overlap model, since it was suggested by the etch-pit measurements, whose reliability was established in Section 7.2. We therefore conclude that the Broudy model is the appropriate model for dislocations in n-type indium antimonide.

However, it must be emphasised that the levels deduced by the Broudy analysis are extremely sensitive to the dislocation distribution and, unless the correct distribution is used, the dislocation levels cannot be calculated with any certainty.

The only parameter in the Broudy analysis whose value is not independently known is θ, which must be less than 0.1 for the analysis. Although no theoretical treatment of non-specular scattering at dislocations has appeared in the literature, it is felt that this value of θ is rather lower than would be

expected, even if the space charge tubes were quite 'rough'. However, this analysis would only accommodate higher values of θ if the model of Fig. 8.17. were modified to accommodate higher dislocation densities. This modification would involve more overlap of ϕ-regions than envisaged on the model of Fig. 8.17. By analogy with the effect of changing from a no-overlap model to a model of overlap in the polygon walls (which raises the levels to the top of the forbidden gap), it is seen that a model assuming still more overlap would raise the levels into the conduction band (the model of Fig. 8.17. could accommodate higher dislocation densities without moving the levels into the conduction band if y were smaller than that measured from the etch-pit spacing, but it seems unlikely that the values of y were appreciably smaller than those used). Thus it appears that the analysis will only give reasonable results (a level within the forbidden gap) if θ is less than 0.1. If the true value of θ is greater than 0.1 then the Broudy analysis is not applicable to the present results.

Finally we will compare the observed behaviour of dislocations in indium antimonide with the predictions of the theories of Gatos, Finn and Lavine (1961) and Holt (1960). The results are clearly at variance

with the theory of Gatos who predicted donor action for Sb-dislocations. However, as discussed in Section 5.1., this theory appears to be a great oversimplification. The theory of Holt, however, which overcomes some of the objections to Gatos's model, makes predictions which could be in agreement with the present results, since he associated acceptor levels as well as donor levels with Sb-dislocations. These results, therefore, show a clear preference for the Holt model rather than the Gatos model.

9.5. Comparison with Previous Work

Turning to previous work in this field, but confining attention in the first case to observed acceptor action in n-type indium antimonide it is seen (Table 5.1.) that in all cases the discrepancies between the number of acceptors introduced (as calculated on the Read model) and the number predicted by a dangling bond model are greater than those found in the present work. To compute these values of $\frac{n - \langle n \rangle}{\rho/c}$

in Table 5.1. the dislocation densities were calculated by substituting the measured radii of bend into (2.12.), for in none of these experiments were the etch-pit

densities given. It is likely that this procedure underestimates the true dislocation density by up to a factor of ten depending on the conditions of deformation. The discrepancies, however, are as large as a factor of 400. Thus it is unlikely that even the Broudy model, as applied to the present results, would accommodate these large discrepancies. The only results which probably could be accommodated are those obtained by Broudy (1963) in which the value of $\frac{n - \langle n \rangle}{\rho / c} = 3.3$

Broudy drew attention to substantial experimental scatter in his results, and this could possibly bring the measurements within the limits of the Broudy model as used for the present results. In only one experiment was the sign of bending identified and here (Gatos et al. 1961) the result showed a big discrepancy in the case of In-bending. The conditions of deformation (double slip at 300°C) would favour point defect production, and no attempt was made to exclude impurities as the heating was performed in air. Thus the results of Gatos et al. may be dominated by point-defect or impurity centres. The results of Duga (1962), as discussed in Section 5.2. cannot be explained in terms of dislocation acceptors only, and suggest the presence of randomly distributed centres as well as dislocation

centres.

It was concluded in Section 5.1 . that Gatos et al's observation of donor action in n-type indium antimonide was not due to dislocation centres. This conclusion is reinforced by the quantitative considerations: even if every dangling bond donated one electron (which is unlikely from electrostatic energy considerations), the number of donors would still be a factor of 50 less than that observed experimentally.

Summarising, the previous work has yielded results which differ from the predictions of the simplest theory by more than the present results. It is suggested that most of the effects observed previously were due to point-defect or impurity centres.

9.6. Suggestions for Further Work

1. The implications of the deformation experiments with regard to the differences between In-bending and Sb-bending suggest some further experiments. It would be very interesting to study the expansion of a single dislocation loop such that the mobility of the In- and Sb- segments could be measured directly. This would indicate whether the two types of dislocations do have different mobilities in glide. This experiment could be performed using an etch-pit technique or perhaps

an X-ray technique, such as that developed by Lang (1959), which can distinguish In- and Sb-dislocations. It would also be interesting to study the yield point in indium antimonide and the way in which slip propagates at the beginning of deformation.

2. The annealing experiments described in Section 7.2. suggest that annealing could give useful information concerning the interpretation of the electrical measurements, provided that impurities could be excluded effectively. Firstly, specimens could be annealed to reduce the density of minority sign dislocations. This treatment would considerably simplify the interpretation of the results. Secondly, annealing treatments could give information about annealable centres like point defects which may be present in the deformed samples. It would be necessary, however, to distinguish between the electrical changes due to the elimination of minority dislocations and those due to the elimination of point defects.

3. The model of dislocation-acceptors which has been developed from the study of n-type material could be tested critically in a number of ways. A thorough study of the effect of dislocations in p-type material could confirm or deny the scheme of energy levels suggested by the n-type analysis. A quantitative analysis would

require the development of a theoretical model of dislocations in p-type material since this situation has not been treated in any detail.

4. The model could be tested by the deformation of n-type samples to produce either a very low or a very high dislocation density. If the dislocations were so closely packed that no material lay further than one mean free path from a space charge cylinder the sample should have a very low value of $\mu_{//}$, measurement of which would give an experimental value of θ to compare with that used in the analysis of Section 8.4. If, on the other hand, the dislocation density were low enough that no overlap of ϕ-regions occurred it should then be possible to accommodate the results on the unmodified Broudy model (which assumes no overlap of ϕ-regions).

5. The electrical conductivity measurements on bent samples indicated that most of the dislocations ran parallel to the bend axis. This deduction could be tested by a direct observation technique such as electron microscopy or the Lang X-ray technique.

9.7. Conclusions

1. Stress-strain curves for the plastic bending of indium antimonide showed a well defined yield point followed by a region when flow occurred at a constant

stress and single slip predominated. Bending at 270°C indicated a higher value of the lower yield stress for Sb-bending than for In-bending. This may be due either to the glide mobility of In-dislocations being greater than that for Sb-dislocations, or to the more rapid climb of the former.

2. It has been shown that etch-pit techniques give a reliable estimate of the dislocation density in indium antimonide and, from annealing of bent specimens it has been deduced that the modified CP_4 etch shows a preference for In-dislocations while the butylamine etch appears to reveal Sb- and In-dislocations with equal efficiency.

3. The electrical measurements indicate that In- and Sb-dislocations act as acceptor centres in n-type material.

4. The electrical measurements on bent n-type specimens could be accommodated on the Read model with an In-dislocation level at 0.10 - 0.12 eV below the conduction band and an Sb-dislocation level at 0.20 - 0.22 eV below the conduction band. The Read analysis predicted dislocation densities which were greater than the butylamine etch-pit densities by a factor of about seven in the case of In-bending and a factor of about fifteen in the case of Sb-bending.

5. The electrical measurements on bent n-type specimens could also be accommodated on the Broudy model when modified to include a polygonised arrangement of dislocations. This analysis predicted dislocation densities which were greater than the butylamine etch-pit densities by about 20% in the case of In-bending and by a factor of about 5/2 in the case of Sb-bending. The dislocation acceptor levels deduced were 0.04 eV below the conduction band for Sb-dislocations and 0.06 eV below the conduction band for In-dislocations, but there is considerable uncertainty in the accuracy of these levels since their position is very sensitive to the dislocation distribution used in the analysis.

APPENDIX 1

COMPUTATION OF THEORETICAL $f(T)$ CURVES

A computer programme was set up to calculate theoretical $f(T)$ curves for a range of values of the dislocation acceptor level, E_D, at each of several values of the initial carrier concentration, $(N_D - N_A)$.

As an example, the programme to calculate $f(T)$ as given by Read's 'Minimum Energy' approximation (4.9.) will be described. On this approximation, $f(T)$ is given by the expression

$$(E_c - E_D) - (E_c - E_F) = \varepsilon_o f \left\{ 3 \ln \frac{f}{f_c} - 0.232 \right\}$$

Now, we define $F(f)$ by the expression

$$F(f) = \varepsilon_o f \left\{ 3 \ln \frac{f}{f_c} - 0.232 \right\} + (E_c - E_F) - (E_c - E_D) \quad \text{(A.1.)}$$
$$= 0$$

Equation (A.1.) was solved numerically by Newton's method, which can be used to find a close approximation to a root. If f_n is an approximation to the root f of (A.1.), then a closer approximation f_{n+1} is given by

$$f_{n+1} = f_n - \frac{F(f_n)}{F'(f_n)} \qquad \text{(A.2.)}$$

Thus Newton's method was used repeatedly to obtain a value very close to the required root. Since the values of f were expected (from a rough calculation) to be about 0.10, the computer was instructed to repeat Newton's method until the change in the value of

$$f \left\{ = F(f_n) / F'(f_n) \right\}$$

was less than 0.0005. The final value computed was therefore within about $\frac{1}{2}\%$ of the required root. Part of the programme is given below (the code being Extended Mercury Autocode), together with a description of the most important instructions.

Programme	Description of Instructions.
A = 0.225	Put $\mathcal{E}_o$ = 0.225 eV in 'A' register
K = 0(1)3	
READ (AK)	Read (N_D-N_A) value into A_o register
NEWLINE	
PRINT (AK) 0,3	Print (N_D-N_A) on output chart
NEWLINE	
I = 0(1)12	
C = 0.02I ?	Put (E_c-E_D) = 0.02, 0.04....0.24 eV and print on output chart.
J = 1(1)12	
G = 25J	Put T = 25, 50....300°K.

Programme	Description of Instructions
X' = Ø LOG (AK) Z' = Ø LOG (G) W' = 29.60 + 1.5Z'-X' D = 0.00008615 GW'	Compute $E_c - E_F = kT \ln\left\{\frac{N_c}{N_D - N_A}\right\}$ and place in register D
U = Ø LOG (πAK)	
X = 0.1	Put f = 0.1 as first approximation in X register.
2) V' = Ø LOG (X)	
Z = V' + 17.03 - U/3	Put $\log_e f/f_c$ in Z register
Y = 3AXZ - 0.232 AX-C+D	Put $F(f)$ in Y register
W = 3A + 3AZ - 0.232A	Put $F'(f)$ in W register
V = Y/W	Put $F(f)/F'(f)$ in V register
X = X - V	Put new value of f in X register
JUMP 12, 0 ⩾ X	Test for f positive
V = Ø MOD (V)	
JUMP 2, V > 0.0005	Repeat calculation if change in f is > 0.0005.
12) NEWLINE	
PRINT (G) 0,3	Print T °K on output chart
PRINT (X) 0,3	Print f on output chart
PRINT (D) 0,3	Print $(E_c - E_F)$ on output chart

Programme	Description of Instructions
REPEAT	Repeat for different values of $T^{\circ}K$
NEWLINE	
REPEAT	Repeat for different values of $(E_c - E_D)$
REPEAT	Repeat for different values of $(N_D - N_A)$

Provision was also made in the programme for divergence. If successive values of f were not converging, then a sub-routine was executed which indicated this fact on the output chart, and by-passed that particular set of values.

Similar programmes were set up to compute $f(T)$ curves by Read's Fermi approximation and by Bliek's Fermi approximation, and the calculations were extended to compute $f(T)$ curves for germanium which were used in the analysis of Broudy's results (given in Chapter 4). All these computations used the same numerical method as a basis.

APPENDIX 2

DETERMINATION OF DEGREE OF IMPURITY SCATTERING

1.) Acoustic Scattering the Predominant Lattice Scattering Mechanism

The degree of impurity scattering was determined from the temperature dependence of the carrier mobility (of the control samples), by the method of Bate, Willardson and Beer (1959). Johnson and Whitesell (1953) expressed the mobility for mixed scattering (μ) in terms of the mobility when only acoustic scattering exists (μ_A), and the degree of impurity scattering

$$\beta = 6\mu_A/\mu_I$$

(where μ_I is the mobility when only impurity scattering exists) by the relation.

$$\mu = \mu_A K(\beta) \qquad \text{(A.3.)}$$

where $$K(\beta) = \int_0^\infty \frac{x^3 e^{-x}}{x^2 + \beta}\, dx$$

x = Carrier energy/kT

Values of $K(\beta)$ have been tabulated by Beer et al. (1957).

Now, we can write

$$\mu_A = m_A T^{-3/2}$$

and

$$\mu_I = m_I T^{+3/2}$$

$$\therefore \quad \mu = m_A T^{-3/2} K(s_1 T^{-3})$$

where $$s_1 = \frac{6 m_A}{m_I}$$

Thus, if μ_1 is the mobility at temperature T_1, and μ_2 is the mobility at T_2,

$$\frac{\mu_1}{\mu_2} = \left(\frac{T_1}{T_2}\right)^{-3/2} \frac{K(s_1 T_1^{-3})}{K(s_1 T_2^{-3})} \qquad \text{(A.4.)}$$

or, rearranging

$$\frac{K(s_1 T_1^{-3})}{K(s_1 T_2^{-3})} = \frac{\mu_1}{\mu_2} \left(\frac{T_1}{T_2}\right)^{3/2} \qquad \text{(A.5.)}$$

Substituting measured values of μ_1 and μ_2 at T_1 and T_2, the value of

$$\frac{\mu_1}{\mu_2}\left(\frac{T_1}{T_2}\right)^{3/2}$$

was calculated. Then, for a range of values of s_1 values of $K(s_1 T_1^{-3})/K(s_1 T_2^{-3})$ were calculated and

plotted against S_1. On this graph, at the point when

$$\frac{K(s_1, T_1^{-3})}{K(s_1, T_2^{-3})} = \frac{\mu_1}{\mu_2}\left(\frac{T_1}{T_2}\right)^{3/2}$$

the value of S_1 was noted. Then β was calculated from this value of S_1, using the relation,

$$\beta = s_1 T^{-3}$$

Typical values of β (80°K) are shown in Table A.1.

Table A.1.

Specimen No.	$N_D - N_A$ (cm^{-3})	β (80°K)
5	6.94×10^{14}	1.5
3	5.68×10^{14}	0.92
6	7.11×10^{13}	0.041
4	1.075×10^{14}	0.016

Ionised impurity scattering is therefore more important in specimens 5 and 3, than in specimens 6 and 4, as would be expected from their excess donor concentrations. This procedure for calculating the degree of impurity scattering employs only the ratios of measured mobilities at different temperatures and

thus avoids the need for absolute magnitudes of total impurity content and lattice mobilities which are required when a direct calculation of μ_A/μ_I is made. This method thus eliminates errors due to compensation effects.

2.) Polar Scattering the Predominant Lattice Scattering Mechanism

A procedure similar to that followed above was used to calculate the degree of impurity scattering. In this case there is some doubt about the temperature dependence of μ_P (the mobility when only polar scattering exists). The theoretical expression derived by Ehrenreich (1959) is too cumbersome to be used in the present analysis. We will therefore use the dependence measured by previous workers on samples with a very low impurity content, i.e.

$$\mu_P \propto T^{-1.6} \qquad \text{(A.6.)}$$

Assuming an energy independent relaxation time for polar scattering (as in Appendix 3.3.) the following expression was obtained for the mixed scattering mobility by a method analogous to that used by Johnson and Whitesell (1952)

$$\mu = \frac{4}{3\sqrt{\pi}} \mu_P \, J(\eta) \qquad \text{(A.7.)}$$

where $$J(\eta) = \int_0^\infty \frac{x^3}{\eta + x^{3/2}} e^{-x} \, dx$$

x = Carrier energy/ kT ,

and $$\eta = \frac{2^3}{\sqrt{\pi}} \frac{\mu_P}{\mu_I}$$

Ginter (1964) has tabulated $J(\eta)$ for a limited range of η values, but, as this was not adequate for the present calculations, further values were computed numerically as described in Appendix 4 . Following the procedure used in the previous section, we obtain from (A.6.) and (A.7.)

$$\frac{\mu_1}{\mu_2} = \left(\frac{T_1}{T_2}\right)^{-1.6} \frac{J(y_1 T_1^{-3.1})}{J(y_1 T_2^{-3.1})}$$

and y_1 was obtained graphically as before, substituting values of μ_1 and μ_2 at temperatures T_1 and T_2 respectively. Finally, η was calculated by the relation

$$\eta = y_1 T_1^{-3.1}$$

APPENDIX 3

CALCULATION OF THE MEAN FREE PATH

The mean free path was calculated for acoustic scattering, polar scattering, mixed acoustic and impurity scattering and mixed polar and impurity scattering and the calculated values were used in the Broudy analysis as described in Section 8.4.

1.) Acoustic Scattering

For scattering by acoustical phonons the mean free path, l_A, is given by

$$l_A = \frac{3\mu_A}{4q}\sqrt{2\pi m^* kT} \qquad (A.8.)$$

2.) Mixed Acoustic and Impurity Scattering

Johnson and Whitesell (1953) derived the mean free path for mixed acoustic and impurity scattering as a function of carrier energy, E ,

$$l(E) = \frac{l_A E^2}{E^2 + \beta(kT)^2}$$

where β was defined in Appendix 2 .

If $$x = E/kT$$

$$l(x) = \frac{l_A x^2}{x^2 + \beta} \qquad \text{(A.9.)}$$

The mean free path must now be averaged over the Maxwellian energy distribution. The average, $\bar{l}$, is given by

$$N\bar{l} = 2\int_0^\infty l(E)\, N(E) f(E)\, dE$$

where

$$N = 2\int_0^\infty N(E) f(E)\, dE$$

is the total number of electrons.

Now, for a non-degenerate electron gas

$$f(E) = A_1 e^{-E/kT}$$

and for spherical energy surfaces the density of states is given by

$$N(E) = B E^{1/2}$$

$$\therefore \quad \bar{l} = \frac{2A_1 B\int_0^\infty l(E) E^{1/2} e^{-E/kT} dE}{2A_1 B\int_0^\infty E^{1/2} e^{-E/kT} dE}$$

$$= \frac{\int_0^\infty l(x) x^{1/2} e^{-x} dx}{\int_0^\infty x^{1/2} e^{-x} dx}$$

$$= \frac{2}{\sqrt{\pi}}\int_0^\infty l(x) x^{1/2} e^{-x} dx \qquad \text{(A.10)}$$

Substituting $l(x)$ from (A.9.) in (A.10.) we obtain

$$\bar{l} = l_A \frac{2}{\sqrt{\pi}} I(\beta) \qquad \text{(A.11.)}$$

where $$I(\beta) = \int_0^\infty \frac{x^{5/2}}{x^2 + \beta} e^{-x} dx$$

The integral $I(\beta)$ was evaluated numerically by Simpson's Rule (The computer programme is given in Appendix 4). The results, for β values between 1×10^{-3} and 8×10^{2} are given in Table A.2.

Now since β was known from the temperature dependence of the carrier mobility in the undeformed samples (as described in Appendix 2.1.), the average mean free path, $\bar{l}$, could be calculated in terms of l_A by equation (A.11.). l_A was obtained from μ_A using for this quantity the measured mobility of control samples 6 or 4. The justification for this is outlined in Section 8.3.2.

3.) Polar Scattering

The calculation of the mean free path for polar scattering has not been treated in any detail in the literature. An early calculation by Frohlich and

Mott (1939) assumed an energy independent mean free time at temperatures below the Debye temperature (θ_D) which in indium antimonide is about 290°K. A detailed calculation by Howarth and Sondheimer (1953) showed that a mean free path at temperatures above θ_D could be calculated, but that at lower temperatures it was not possible to define a unique relaxation time. However, they showed that the rigorous calculation carried out without the assumption of a unique relaxation time produced the same result as that obtained using an energy independent relaxation time. Theoretical mobilities in InSb calculated by Hilsum (1957) using the latter assumption were in fair agreement with experimental values. Similarly Ginter (1964) assumed an energy independent relaxation time for polar scattering, and calculated mobilities for mixed polar and impurity scattering in CdSe and CdTe, which compared well with experimental values. In the present calculation of the mean free path for polar scattering we will also assume an energy independent relaxation time, since this appears to be the most reasonable simplifying assumption.

Thus, $$\tau_p \propto E^0$$

and $$l_p \propto E^{1/2}$$
$$= \alpha_p E^{1/2} \qquad \text{(A.12.)}$$

Following the method of Johnson and Whitesell (1953) we evaluate α_p . A. H. Wilson (1958) obtained a solution of the Boltzmann equation for electrical conduction in an isotropic material. Assuming that no temperature gradient exists, electric current flows in the x-direction, a magnetic field (H) is applied in the z-direction and that there is no current flow in the y-direction, he obtained the following expressions for the current densities j_x and j_y, from this solution of the Boltzmann equation

$$j_x = i_1 E_x - i_2 E_y$$

$$j_y = i_2 E_x + i_1 E_y = 0$$

where i_1 and i_2 are the conductivity coefficients, and E_x and E_y are the electric field intensities.
If H = 0, Wilson's expressions for the conductivity coefficients i_1 and i_2 may be written in the following form

$$i_2 = 0$$

and

$$i_1 = \frac{8\pi q^2 m^3}{3h^3} \int_0^\infty l v^3 \frac{\partial f}{\partial E} dv$$

where f is the distribution function which, for a non-degenerate electron gas may be written

$$f = \frac{nh^3}{2(2\pi mkT)^{3/2}} e^{-E/kT}$$

Thus, i_1 becomes

$$i_1 = \frac{4\pi q^2}{3} \int_0^\infty l v^3 \frac{K_0}{kT} e^{-E/kT} dv \qquad \text{(A.13.)}$$

where $K_0 = n \left\{ m/2\pi kT \right\}^{3/2}$ (A.14.)

Substituting (A.12.) in (A.13.) we obtain

$$i_1 = \frac{4\pi q^2}{3} \alpha_p \frac{K_0}{kT} \int_0^\infty E^{1/2} v^3 e^{-E/kT} dv$$

Now $E^{1/2} = \frac{m^{1/2} v}{2^{1/2}}$

$$\therefore \quad i_1 = \frac{4\pi q^2}{3} \alpha_p \frac{K_0}{kT} \frac{m^{1/2}}{2^{1/2}} \int_0^\infty v^4 e^{-E/kT} dv$$

Rearranging, we obtain

$$i_1 = \frac{4\pi q^2}{3} \alpha_p \frac{K_0}{kT} \frac{m^{1/2}}{2^{1/2}} \frac{2^{5/2}(kT)^{5/2}}{m^{5/2}} \int_0^\infty z_0^4 e^{-z_0^2} dz_0$$

where $z_0 = \frac{m^{1/2} v}{2^{1/2}(kT)^{1/2}}$

Now $$\int_0^\infty z_o^4 e^{-z_o^2} dz_o = \frac{1.3.\sqrt{\pi}}{2^3}$$

$$\therefore \quad i_1 = \frac{2\pi q^2 \alpha_p K_o (kT)^{3/2} \sqrt{\pi}}{m^2}$$

Substituting K_o from (A.14.) we obtain

$$i_1 = \frac{nq^2 \alpha_p}{2^{1/2} m^{1/2}}$$

Now $$i_1 = j_x / E_x = \sigma = nq\mu_p$$

$$\therefore \quad nq\mu_p = \frac{nq^2 \alpha_p}{2^{1/2} m^{1/2}}$$

and $$\alpha_p = \frac{\mu_p \sqrt{2m}}{q} \qquad \text{(A.15.)}$$

Substituting (A.15.) in (A.12.)

$$l_p(E) = \frac{\mu_p \sqrt{2m}}{q} E^{1/2} \qquad \text{(A.16.)}$$

or $$l_p(x) = \frac{\mu_p \sqrt{2mkT}}{q} x^{1/2} \qquad \text{(A.17.)}$$

Averaging over the energy distribution, we obtain from (A.10.) and (A.17.)

$$\bar{l} = \frac{2}{\sqrt{\pi}} \frac{\sqrt{2mkT}}{q} \mu_p \int_0^\infty x e^{-x} dx$$

and, since $\int_0^\infty x e^{-x} dx = 1$

$$\therefore \quad \bar{l} = \frac{2}{\sqrt{\pi}} \frac{\sqrt{2mkT}}{q} \mu_p \qquad \text{(A.18.)}$$

4.) Mixed Polar and Impurity Scattering

The combined mean free path, l, can be written in terms of the mean free path when only polar scattering exists, l_p, and the mean free path when only impurity scattering exists, l_I, by the relation

$$\frac{1}{l} = \frac{1}{l_I} + \frac{1}{l_p}$$

$$\therefore \quad l(E) = \frac{l_I l_p}{l_I + l_p}$$

$$= \frac{\alpha_I \alpha_p E^{5/2}}{\alpha_I E^2 + \alpha_p E^{1/2}}$$

since $l_I = \alpha_I E^2$ and $l_p = \alpha_p E^{1/2}$.

Rearranging, we obtain

$$l(E) = \frac{\alpha_p E^2}{E^{3/2} + \alpha_p/\alpha_I} .$$

Now, since

$$\alpha_I = \frac{\sqrt{\pi m}\, \mu_I}{2^{5/2} (kT)^{3/2}}$$

and α_p is given by (A.15.)

$$\alpha_p/\alpha_I = \frac{2^3}{\sqrt{\pi}} \frac{\mu_p}{\mu_I} (kT)^{3/2}$$

$$\therefore \quad l(E) = \frac{\sqrt{2m}\,\mu_p}{q} \left\{ \frac{E^2}{E^{3/2} + \frac{2^3}{\sqrt{\pi}} \frac{\mu_p}{\mu_I} (kT)^{3/2}} \right\}$$

$$\text{or} \quad l(x) = \frac{\sqrt{2mkT}\,\mu_p}{q} \left\{ \frac{x^2}{x^{3/2} + \eta} \right\} \quad \text{(A.19.)}$$

where $$\eta = \frac{2^3}{\sqrt{\pi}} \frac{\mu_p}{\mu_I}$$

The average over the distribution of energies is given by (A.10.), and we obtain from (A.19.)

$$\bar{l} = \frac{2}{\sqrt{\pi}} \frac{\sqrt{2mkT}}{q} \mu_p \, L(\eta) \quad \text{(A.20.)}$$

where $$L(\eta) = \int_0^\infty \frac{x^{5/2}}{x^{3/2} + \eta} e^{-x} dx \quad \text{(A.21.)}$$

This integral $L(\eta)$ was evaluated numerically for values of η from 1×10^{-3} to 8×10^{2} and the results are shown in Table A.3. η was calculated from the

temperature dependence of the carrier mobility, as described in Appendix 2.2., and μ_p was taken as the mobility of a specimen where $\eta \to 0$. Thus $\bar{l}$ was calculated for mixed polar and impurity scattering.

Values of the mean free path at 80°K, calculated by the methods described above, are presented in Table 8.9.

APPENDIX 4

EVALUATION OF INTEGRALS FOR THE CALCULATION OF THE MEAN FREE PATH WHEN MIXED SCATTERING OCCURS

The integrals obtained in the calculation of the mean free path for mixed scattering could not be solved analytically. A typical example of these integrals is that for mixed acoustic and impurity scattering

$$I(\beta) = \int_0^\infty \frac{x^{5/2}}{x^2 + \beta} e^{-x} dx \qquad \text{(A.22.)}$$

The integrals were calculated by a numerical method based on Simpson's rule, which states

$$\int_0^{nh} y\,dx = \tfrac{1}{3}h\left(y_0 + 4y_1 + 2y_2 + 4y_3 + \ldots 2y_{n-2} + 4y_{n-1} + y_n\right) \qquad \text{(A.23.)}$$

For the integral (A.22.) it was found that no great error resulted from a calculation using (A.23.) if the upper limit of integration, nh, was set at 20. An increase in nh to 100 made no significant difference to the result. Similarly, the number of intervals, n, was set at 200, since an increase in n gave

results which were identical to four significant figures. Thus the integral $I(\beta)$ was computed using (A.23.) where $n = 200$ and $nh = 20$. The results are shown in Table A.2. for values of β from 0.001 to 800. A similar method was used to calculate $L(\eta)$ (Appendix 3.4.) and $J(\eta)$ (Appendix 2.2.) and these results are presented in Table A.3. The integral $J(\eta)$ was used in the calculation of η as described in Appendix 2, and the integrals $L(\eta)$ and $I(\beta)$ were used to calculate mean free paths for mixed scattering as described in Appendix 3.

Table A.2. Integral Used for Calculating the Mean Free Path for Acoustic Plus Impurity Scattering.

$\beta = 6\mu_A/\mu_I$	$I(\beta) = \int_0^\infty \frac{x^{5/2}}{x^2+\beta} e^{-x} dx$
0.001	0.8781
0.003	0.8687
0.005	0.8609
0.008	0.8512
0.010	0.8456
0.030	0.8064
0.050	0.7799
0.080	0.7496
0.100	0.7330
0.300	0.6285
0.500	0.5675
0.800	0.5055
1.000	0.4747
3.000	0.3188
5.000	0.2507
8.000	0.1942
10.000	0.1701
30.000	0.07968
50.000	0.05305
80.000	0.03557
100.000	0.02922
300.000	0.01055
500.000	0.006451
800.000	0.004076

Table A.3. Integrals Used to Calculate the Mean Free Path for Polar Plus Impurity Scattering.

η	$J(\eta)$ $\left(=\int_0^\infty \frac{x^3}{x^{3/2}+\eta} e^{-x} dx\right)$	$L(\eta)$ $\left(=\int_0^\infty \frac{x^{5/2}}{x^{3/2}+\eta} e^{-x} dx\right)$
0.001	1.328	0.9986
0.003	1.327	0.9960
0.005	1.325	0.9935
0.008	1.322	0.9898
0.010	1.320	0.9875
0.030	1.304	0.9670
0.050	1.289	0.9496
0.080	1.269	0.9270
0.100	1.256	0.9136
0.300	1.155	0.8139
0.500	1.079	0.7457
0.800	0.9905	0.6705
1.000	0.9424	0.6311
3.000	0.6625	0.4192
5.000	0.5241	0.3231
8.000	0.4047	0.2439
10.000	0.3528	0.2105
30.000	0.1587	0.09112
50.000	0.1033	0.05861
80.000	0.06796	0.03826
100.000	0.05537	0.03108
300.000	0.01944	0.01082
500.000	0.01180	0.006552
800.000	0.007420	0.004117

LIST OF REFERENCES

Aerts,E., Delavignette P., Siems R. and Amelinckx S., 1962, J. Appl. Phys. 33, 3078.

Alexander H., 1961, Z. Metallkunde 52, 344.

Alexander H., and Haasen P., 1961, Acta Met. 9, 1001.

Allen J. W., 1957, Phil. Mag. 2, 1475.

Art A., Aerts E., Delavignette P. and Amelinckx S., 1963, Appl. Phys. Letters 2, 40.

Arthur J. B., Gibson A. F., Granville J. W. and Paige E. G. S., 1958, Phil. Mag. 3, 940.

Aukerman L. W., 1959, J. Appl. Phys. 30, 1239.

Bardsley W., 1959, Progress in Semiconductors, 4, 157.

Bardsley W. and Bell R. L., 1957, J. Electronics, 3, 103.

Bate R. T., Willardson R. K. and Beer A. C., 1959, J. Phys. Chem. Solids, 9, 119.

Beer A. C., Armstrong J. A. and Greenberg I. N., 1957, Phys. Rev. 107, 1506.

Bell R. L., 1957, J. Electronics, 3, 487.

Bell R. L. and Hogarth C. A., 1957, J. Electronics, 3, 455.

Bell R. L. and Bonfield W., 1964, Phil. Mag. 9, 9.

Bliek L., 1964, Dipl. Thesis (Göttingen).

Brooks H., 1955, Adv. in Electronics and Electron Physics, 7, 156.

Broudy R. M., 1963, Adv. in Physics, 12, 135.

Bruneau A. A. and Pratt P. L., 1962, Phil. Mag., 7, 1871.

Cahn R. W., 1949, J. Inst. Metals 76, 121.

Cahn R. W., Bear I. J. and Bell R. L., 1953, J. Inst. Metals 82, 481.

Carreker R. R., 1956, J. Metals 8, 111.

Chauduri A. R., Patel J. R. and Rubin L. G., 1962, J. Appl. Phys., 33, 2736.

Cleland J. W. and Crawford J. H., 1954a, Phys. Rev. 93, 894; 1954b, ibid. 94, 1410; 1954c, ibid, 95 1177.

Cottrell A. H., 1958, Dislocations and Plastic Flow in Crystals, Oxford University Press.

Czochralski J., 1917, Z. Phys. Chem. 92, 219.

Dash W. C., 1956, J. Appl. Phys. 27, 1193.

Dewald J. F., 1957, J. Electrochem. Soc. 104, 244.

Dew-Hughes D., 1961, I.B.M. J. Res. Dev. 5, 279.

Dresselhaus G., Kip A. F., Kittel C. and Wagoner G., 1955, Phys. Rev. 98, 556.

Duga J. J., 1962, J. Appl. Phys. 33, 169.

Duga J. J. and Maringer R. E., 1960, Bull. Am. Phys. Soc. 5, 375.

Ehrenreich H., 1957, J. Phys. Chem. Solids 2, 131; 1959, ibid 9, 129.

Eisen F. H., 1961, Phys. Rev. 123, 736.

Eisen F. H. and Birchenall C. E., 1957, Acta Met., 5 265.

Ellis W. C. and Greiner E. S., 1953, Phys. Rev. 92 1061.

Fan H. Y. and Gobeli G. W., 1960, Phys. Rev. Letters, 4, 546.

Frohlich H. and Mott N. F., 1939, Proc. Roy. Soc. A219, 53.

Gallagher C. J., 1952, Phys. Rev. 88, 721.

Gatos H. C., 1961, J. Appl. Phys. 32, 1232.

Gatos H. C. and Lavine M. C., 1960a, J. Electrochem. Soc. 107, 427; 1960b, J. Appl. Phys. 31, 743; 1960c, J. Phys. Chem. Solids 14, 169.

Gatos H. C., Finn M. C., and Lavine M. C., 1961, J. Appl. Phys. 32, 1174.

Gibson A. F. and Paige E. G. S., 1958, Phil. Mag. 3, 950.

Ginter J., 1964, Phys. Stat. Sol. 6, 863.

Haasen P., 1957, Acta Met. 5, 598; 1964, Faraday Soc. Conf. Gottingen.

Hendrickson A. A. and Machlin E. S., 1955, Acta Met. 3, 64.

Hibbard W. R. and Dunn C. G., 1956, Acta Met. 4, 306.

Hilsum C. and Barrie R., 1958, Proc. Phys. Soc., 71, 676.

Hilsum C. and Rose-Innes A. C., 1961, "Semiconducting III-V Compounds" (Pergamon Press).

Hilsum C., 1957, S.E.R.L. Tech. Memo No 366.

Hobstetter J. N. and Renton C. A., 1962, J. Appl. Phys. 33, 600.

Hogarth C. A. and Baynham A. C., 1958, Proc. Phys. Soc. 71, 647.

Holt D. B., 1960, J. Appl. Phys. 31, 2231; 1962, J. Phys. Chem. Solids. 23, 1353.

Hornstra J., 1958, J. Phys. Chem.Solids 5, 129.

Howarth D. J. and Sondheimer E. H., 1953, Proc. Roy. Soc. A219, 53.

Hrostowski H. J., Morin F. J., Geballe T. H. and Wheatley G. H., 1955, Phys. Rev. 100, 1672.

Hulme K. F., 1959, J. Elect. Cont. 6,397.

Hulme K. F. and Mullin J. B., 1962, Solid State Electronics, 5,211.

Johnson V. A. and Whitesell W. J., 1953, Phys. Rev. 89, 941.

Johnston W. G. and Gilman J. J., 1959, J. Appl. Phys. 30, 129.

Juretschke H. J., Landauer R. and Swanson J. A., 1956, J. Appl. Phys. 27, 838.

Koster D., Knol K. S. and Prins J. A., 1930, Z. Phys. 63, 345.

Lang A. R., 1959, Acta Crystallographica 12, 249.

Lavine M. C., Gatos H. C. and Finn M. C., 1961, J. Electrochem. Soc. 108, 974.

Livingston J. D., 1962, "Direct Observation of Imperfections in Crystals" (Interscience), p. 115; 1963, J. Austr. Inst. Metals 8, 15.

Logan R. A., Pearson G. L. and Kleinman D. A., 1959, J. Appl. Phys. 30, 885.

Maringer R. E., 1958, J. Appl. Phys. 29, 1261.

Morin F., 1954, Phys. Rev. 93, 62.

Mueller R. K. and Jacobson R. L., 1962, J. Appl. Phys. 33,2341

Nye J. F., 1953, Acta Met. 1, 153.

Patel J. R., 1956, Phys. Rev. 101, 143; 1958, J. Appl. Phys. 29, 170.

Patel J. R. and Chauduri A. R., 1962, J. Appl. Phys. 33 2223; 1963, J. Appl. Phys. 34,2788.

Pearson G. L., Read W. T. and Morin F. J., 1954, Phys. Rev. 93, 666.

Peissker E., Haasen P. and Alexander H., 1961, Phil. Mag. 7, 1279.

Peirce B. O., 1910, "A Short Table of Integrals" (Ginn and Co.).

Putley E. H., 1959, Proc. Phys. Soc. 73, 280; 1960, ibid., 76, 802.

Read W. T., 1954a, Phil Mag. 45, 775; 1954b, ibid. 45 1119; 1955, ibid. 46, 111.

Rezek J. and Rosenberg A., 1963, Private Communication.

Schafer S., Alexander H. and Haasen P., 1964, Phys. Stat. Sol. 5, 247.

Schmid E. and Boas W., 1950, Plasticity of Crystals (F. A. Hughes and Co.).

Seitz F., 1952, Phys. Rev. 88, 722.

Shockley W., 1953, Phys. Rev., 91, 228.

Siethoff H. and Alexander H., 1964, Physica Stat. Sol. 6, K165.

Stein D. F. and Low J., 1960, J. Appl. Phys. 31, 362.

Timoshenko S. and Goodier J. N., 1951, Theory of Elasticity (McGraw-Hill).

Treuting R. G., 1955, J. Metals 7, 1027.

Tweet, A. G., 1955, Phys. Rev., 99, 1245.

Venables J. D., and Broudy R. M., 1958, J. Appl. Phys. 29, 1025.

Vogel F. L., 1956, J. Metals, 8, 946.

Warekois E. P., 1959, Unpublished results quoted by Gatos and Lavine (1960a), also Lincoln Lab Quarterly Progress Report, 15th July, p. 45.

Warekois E. P., and Metzger, P. H., 1959, J. Appl. Phys. 30, 960.

Wertheim G. K. and Pearson G. L., 1957, Phys. Rev. 107, 694.

White J. G. and Roth W. C., 1959, J. Appl. Phys. 30,946.

Wilson A. H., 1958, "The Theory of Metals" (Cambridge: University Press).

GLOSSARY OF PRINCIPAL SYMBOLS

Symbol	Definition
a	Glide strain
b	Burgers Vector
c	Spacing of acceptor sites along dislocation line
d	Spacing of accepted electrons along dislocation line
D	Diffusion constant
E	Carrier energy
E_F	Fermi energy (measured from valence band)
E_D	Dislocation acceptor level (measured from valence band)
ε_s	Electrostatic energy (Read's theory)
ε^*	$d/df\,(f\varepsilon_s)$
ε_e	Electrostatic energy of row of electrons
ε_c	Electrostatic energy of space charge
ε_{ce} and ε_{ec}	Electrostatic energy of interaction of electrons and space charge
ε_o	$q^2/\varkappa c$
E_c	Energy at bottom of conduction band
E_x, E_y	Electric field in x or y directions
f	Occupation fraction
f_c	$c\,\pi^{1/3}(N_D - N_A)^{1/3}$

F — Force

$F(X)$ — $\frac{3}{2}\int_0^{\pi/2} \frac{\sin^3\varphi\, d\varphi}{1 + X \sin\varphi}$

G_e — Free energy per accepted electron

G* — Shear modulus

$g(\epsilon)$ — Distortion parameter

h — Planck's constant

$\hbar$ — $h/2\pi$

H — Magnetic Field

i_1, i_2 — Conductivity coefficients

$I(\beta)$ — $\int_0^{\infty} \frac{x^{5/2}}{x^2 + \beta} e^{-x} dx$

j_x, j_y — Current density (in x or y direction)

$J(\eta)$ — $\int_0^{\infty} \frac{x^3}{x^{3/2} + \eta} e^{-x} dx$

$\underline{k}$ — Wave vector

k — Boltzmann's constant

K_1 — ϕ/ϵ (no overlap model)

K_1' — ϕ/ϵ (overlap model)

$K(\beta)$ — $\int_0^{\infty} \frac{x^3}{x^2 + \beta} e^{-x} dx$

l — Mean free path

l_A — Mean free path for acoustic scattering

l_I — Mean free path for impurity scattering

l_P — Mean free path for polar scattering

$$L(\eta) \int_0^\infty \frac{x^{5/2}}{x^{3/2} + \eta} e^{-x} dx$$

L		Diffusion length (minority carriers)
	L_1	$K_1(1 - \theta) + 1$ (Broudy model)
m		Parameter in dislocation velocity - stress relation $\bar{v} \propto s^m$
	m_o	Electron mass
	m^*	Effective mass
	M_1	$K_1(1 - \theta^2) + 1$ (Broudy model)
n_i		Intrinsic carrier concentration
	N_D	Number of donors/cm^3
	N_A	Number of acceptors/cm^3
	N_{ca}	Number of effective chemical acceptors/cm^3
	N_S	Number of sites/cm^3
	n	Number of conduction electrons/cm^3
	$\langle n \rangle$	Average number of conduction electrons per cm^3 in deformed samples
	p	Hole concentration
	$\langle p \rangle$	Average hole concentration in deformed samples
	q	Electron charge
	R_H	Hall coefficient
	R_o	Hall coefficient of (undeformed) 'control' sample
	$R_{//}$	Hall coefficient of 'parallel' sample
	$R_\perp$	Hall coefficient of 'perpendicular' sample

R_s	Radius of space charge cylinder
R	Radius of curvature (of bent specimens)
r	Numerical factor in relation $R_H = \frac{r}{nq}$
s	Stress
S_e	Entropy per accepted electron
T	Absolute temperature
T_M	Melting temperature
t_w	Incubation (or delay) time
t	Time
U	Activation energy
U_e	Increase in energy per accepted electron
$\bar{V}$	Average dislocation velocity
x	E/kT
X	L_A/L_D
y	Spacing of dislocations in polygon walls (Fig. 8.17.)
z	Spacing of polygon walls (Fig. 8.17.)
α_o	Work hardening parameter
β	Degree of impurity scattering ($6\mu_A/\mu_I$)
β^*	Effective degree of impurity scattering in deformed sample
γ	Screening parameter
δ	Dislocation multiplication parameter
ϵ	Fraction of material in space charge cylinders (or ϵ regions)

η	$\frac{2^3}{\sqrt{\pi}} \frac{\mu_P}{\mu_I}$
θ	μ_2/μ_1 (Broudy theory)
$\varkappa$	Dielectric constant
λ	ϵ/f
μ	Carrier mobility
μ_H	Hall mobility
μ_A	Mobility for acoustic scattering
μ_I	Mobility for impurity scattering
μ_P	Mobility for polar scattering
ρ	Dislocation density
ρ_{CP_4}	Etch-pit density (mod. CP_4 etch)
ρ_{But}	Etch-pit density (butylamine etch)
σ	Conductivity
σ_0	Conductivity of (undeformed) 'control' sample
$\sigma_{//}$	Conductivity of 'parallel' sample
$\sigma_\perp$	Conductivity of 'perpendicular' sample
τ	Relaxation time
ϕ	Fraction of material in region 2 or Ø-region (Broudy's theory)
χ	Angle between Burgers Vector and dislocation line
ψ	Electrostatic potential
φ	Angle between electron direction and dislocation axis.

ω Angle between slip plane and neutral plane

ACKNOWLEDGEMENTS

The author is grateful to Professor R. L. Bell, who supervised this project, for his constant encouragement and advice; to Professor J. G. Ball for the provision of laboratory facilities; to Dr. W. Bardsley, Dr. J. B. Mullin, Dr. K. F. Hulme and colleagues at the Royal Radar Establishment for the supply of indium antimonide single crystals and for the interest they have taken in the work; to Dr. B. Donovan of Westfield College for helpful discussions concerning the material of Appendix 3; and to the Department of Scientific and Industrial Research and the Trustees of the Beit Fellowship for Scientific Research, for financial support.

Finally, the author is indebted to his wife for her encouragement throughout this work.